Carrier Transport in Undoped and Doped Films of Amorphous Arsenic Triselenide.

A thesis presented by

Alan C Sharp

(Sponsoring establishment

Dundee College of Technology,

Collaborating establishment

Dundee University)

to the CNAA

in partial fulfilment of the

requirements for the degree of

Doctor of Philosophy

June 1983.

DECLARATION

I declare that while registered as a candidate for the degree for which this thesis is presented I have not been a candidate for any other award. I further declare that except where stated the work contained in this thesis is original, and was performed by the author. The author is grateful to Dr J T Edmond of Dundee University who helped with the preparation of the bulk glass, Dr S W Provencher who provided a computer programme used in the analysis, and the Material Science department of GEC Hirst Research Centre who performed the compositional analysis.

Signed [redacted]

Alan C Sharp

ADVANCED STUDIES

In addition to the original research reported in this thesis the author followed a programme of postgraduate study. This programme included attendance at the lectures and tutorials of the Joint Scottish Universities M Sc course in the Physics and Technology of Amorphous Materials held at Dundee University during 1978-79. In addition the author attended the Chelsea Meeting on Liquid and Amorphous Semiconductors in 1978, 1979, 1980, 1981 and 1982, and participated in the Ninth International Conference on Amorphous and Liquid Semiconductors held in Grenoble in 1981.

Acknowledgements

The author wishes to express his thanks to Dr Joseph M Marshall for his inspiration and friendship during the period of this study. Thanks are also due to Dr Peter LeComber for stimulating discussions and constructive criticism throughout the project.

The assistance and co-operation of many members of the academic and technical staffs of Dundee College of Technology and the University of Dundee is gratefully acknowledged (particularly Mr J Higgins and Mr J Anderson at the college, and Dr J T Edmond of Dundee University).

A further debt of thanks is due to Mr Henry S Fortuna and Mr Lindsay Arcari, colleagues during part of the period of study, who taught me the meaning of the word 'reprobate', and whose friendship and assistance made my time at Dundee much more enjoyable.

The financial assistance provided by the Scottish Education Department which made this work possible was much appreciated.

Finally, the author would like to thank his colleagues at the GEC Research Laboratories, Hirst Research Centre for their friendship and support during the writing of this account, Mr D E H Smith and Dr D V McCaughan for their encouragement and assistance as the deadline approached, and Miss T Carter who typed part of the manuscript.

Carrier Transport in Undoped and Doped Films of Amorphous Arsenic Triselenide.

Alan C Sharp

The work reported in this thesis was carried out at the Physics Department of Dundee College of Technology between October 1978 and October 1981. The aim of the work was to examine the nature of the changes in electrical properties of amorphous chalcogenide films fabricated using different techniques, and to study the modifications to these properties produced by the introduction of impurities.

In vitreous films of arsenic triselenide, both the dark d.c. conductivity and hole drift mobility have been studied as a function of temperature and applied electric field. Measurements of the d.c. conductivity have been extended to lower temperatures than in previous studies (down to 165K as compared with 280K). A full discussion of the interpretation of these results in terms of a simple model with trap levels approximately 0.3eV, 0.4eV and 0.6eV above the valence band mobility edge is presented. A new analysis is developed from the concept of a thermally activated capture process. This analysis yields a value for the capture coefficient of the traps 0.6eV above the mobility edge of $1.1 \pm 0.5 \times 10^{-7}$ cm^3/s at 300K, which agrees very well with other estimates from transient photoconductivity measurements in the literature.

Similar measurements on evaporated arsenic triselenide are reported. These results are discussed in terms of a model similar to that proposed for the vitreous material. The densities of localised states in the mobility gap calculated on the basis of this model are one to two orders of magnitude greater than those calculated for vitreous films. The temperature dependence of the current pulse shape in evaporated films was observed to be less marked than in vitreous films.

Measurements of the d.c. conductivity and drift mobility in arsenic triselenide prepared by r.f. sputtering are reported for the first time. The behaviour of these films differed significantly from that observed for the other films. The time-of-flight current transients decayed extremely quickly making measurements difficult. Electron transits were observed in arsenic triselenide for the first time.

Films doped by co-sputtering Ni and Cu dopants were also studied. Additions of less than 2 at% produced an increase in the room temperature conductivity of 4 orders of magnitude for less than a 10% change in optical band gap. A shift in the Fermi level in heavily Ni doped films of at least 0.3eV is inferred.

CONTENTS

CHAPTER 1

This chapter will present an overview of the theory of electronic transport in amorphous semiconductors. The outline of the chapter is as follows. Section 1.1 presents a brief summary of some of the important concepts in the field of amorphous semiconductors and the differences between the band structure of amorphous and crystalline semiconductors. The next section summarizes the criteria which must be met for conventional transport theory to be applicable. The chapter then continues with a detailed exposition of the salient features of the theory of carrier transport in extended states in section 1.3, and carrier trapping and release in section 1.4. The relationship between the problem of trapping in a number of different levels and the observation of dispersive transport is the subject of section 1.5. Section 1.6 which describes carrier transport between localised states, concludes the chapter.

1.1 THE CONCEPT OF AN AMORPHOUS SEMICONDUCTOR

The great majority of everyday materials such as glass, paper and so forth do not have a crystalline structure. By this we mean that although the local chemistry in such materials provides constraints on bond length and bond angle which extend over several nearest neighbour atoms, on a larger scale the lattices of these solids do not possess translational symmetry. Thus in a non-crystalline substance, the atoms have a local environment which is very similar to that found in the crystalline state - a fact which is readily demonstrated by X-ray diffraction studies (Grigorovici (1973)). Such non-crystalline materials, because they exhibit marked short range ordering, should not be thought of as being composed of atoms or molecules arranged at random - although the long range order of the crystal is lacking.

At present there appears to be widespread agreement that if the short range order of an amorphous material is the same as that of the crystalline state, some basic features of the electronic structure of the crystal are preserved (Ioffe (1951)). One can understand this intuitively if one considers that in conventional solid state theory the tight-binding approximation uses the atomic wavefunctions of the individual isolated atoms perturbed only by the presence of the nearest neighbours - which in a material with significant short range order will be in nearly the same orientations as the crystal.

It has been known since the work of Bloch (1928) that there are universal features in the electronic structures of crystals. The most important of these are the presence of energy bands separated by forbidden gaps, the fact that the crystal momentum is a good quantum number, and the result that the electron wavefunction has the form of a plane wave modulated by a function which has the same periodicity as the lattice.

The first steps towards an understanding of the theory of the electronic structure of disordered solids were not taken until almost 20 years after the work of Bloch, when Frohlich (1947) pondered the nature of the eigenstates in the tails of the bands. It was not until

much later that Mott (1967) combined these ideas with the work of Anderson (1958) on the absence of diffusion in a three dimensional random potential to give a simple model containing the essential features common to all disordered systems.

This model can be considered as a natural extrapolation of the results for a crystalline semiconductor with the disorder treated as a small perturbation which causes the scattering of electrons after they have travelled a mean distance L known as the mean free path. The electron has a wavefunction of the Bloch type which extends through the whole lattice. If we were to introduce disorder progressively into the lattice, we would eventually reach a point where L became equal to the lattice spacing a. Obviously L cannot become less than a, so this is the limiting case. From the Heisenberg uncertainty principle,

$$\Delta k \ \Delta x \ \sim \ 1$$

so if $k = 1/a$ (a typical value) this criterion becomes

$$\frac{\Delta k}{k} = \frac{a}{\Delta x} \rightarrow 1$$

so that k is no longer a useful quantum number, and the phase of the Bloch function will change in a random way over a distance of the order of the lattice spacing. The wavefunction will still however extend throughout the lattice (figure 1).

Although the mean free path of the electrons cannot be made less than a, it is still possible to increase the disorder by introducing a random fluctuation of potential, Vo, on each lattice site (as shown in figure 2). This was the model used by Anderson in 1958 - note that the randomness is confined to the depth of the potential wells, and does not involve their spatial separation. Anderson showed that for a tight binding (narrow) band that a fundamental change occurs to the electron wavefunction when the disorder becomes so great that

$$\frac{V_o}{B} > \left[\frac{V_o}{B}\right]_{crit.} \sim 5$$

where

$$B = 2 \ z \ J$$

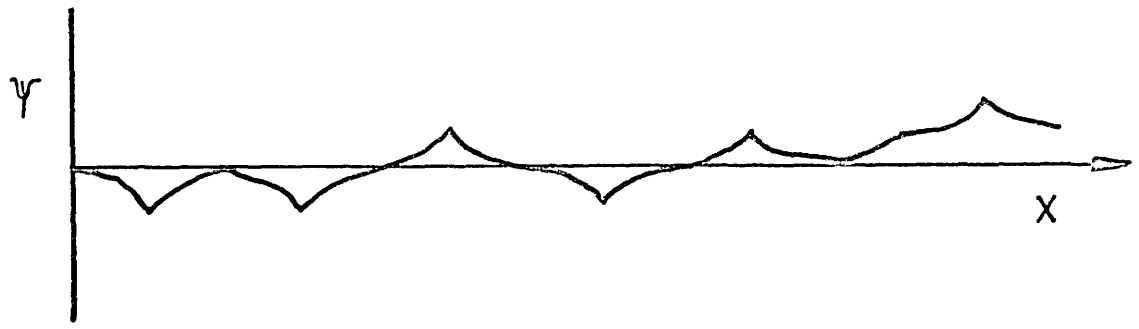

FIGURE 1

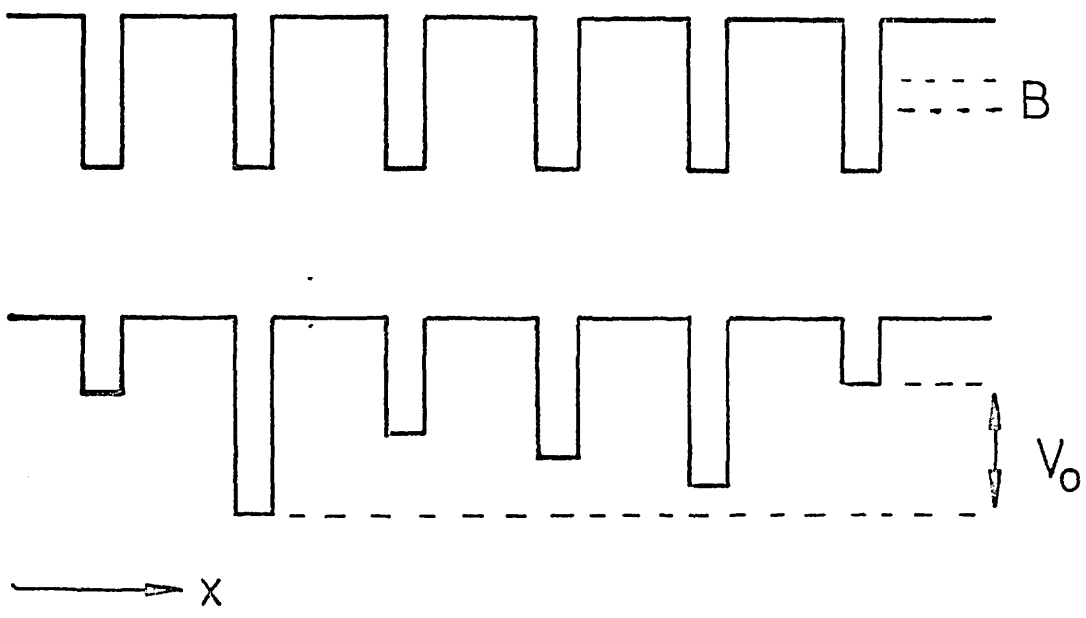

FIGURE 2

is the bandwidth of the tight binding band, J is the overlap integral, and z is the coordination number of the lattice. This fundamental change is called Anderson localisation - all electrons in the band suddenly become localised (with wavefunctions similar to that sketched in figure 3) - even although there may be significant wavefunction overlap! Figure 4 illustrates the way in which the conductivity is expected to change with increasing disorder.

More recent theoretical studies (Thouless (1974), Kramer and Weaire (1979), Economou, Cohen, Freed and Kirkpatrick (1974)) have shown that Anderson's critical value of the disorder potential Vo = 5B was too restrictive, and indicate that a value of Vo nearer 2B is all that is required.

The above discussion for a narrow band has been generalised by Mott to include the case of a wide band. Mott argued that the overlap integral in a wide band is given by

$$J \propto \exp(-2\alpha r)$$

therefore if we assume the disorder potential Vo is constant throughout the band

$$g(E) = 1/r^3 V_o$$

so that

$$r \propto g(E)^{-1/3}$$

This implies that when g(E) is small, r is large and so J becomes very small. Thus since the localisation depends on Vo/J, this will occur first where g(E) is small - that is at the edges of the band.

A band in such an idealised semiconductor is compared to a band in a typical crystal in figure 5. In the amorphous case, the bandedges are not proportional to

$$g(E) \propto (E - E_c)^{1/2}$$

as in the crystalline case, but are smeared out so that there are no singularities at the band edge. The Van - Hove singularities in the band also disappear due to strong scattering.

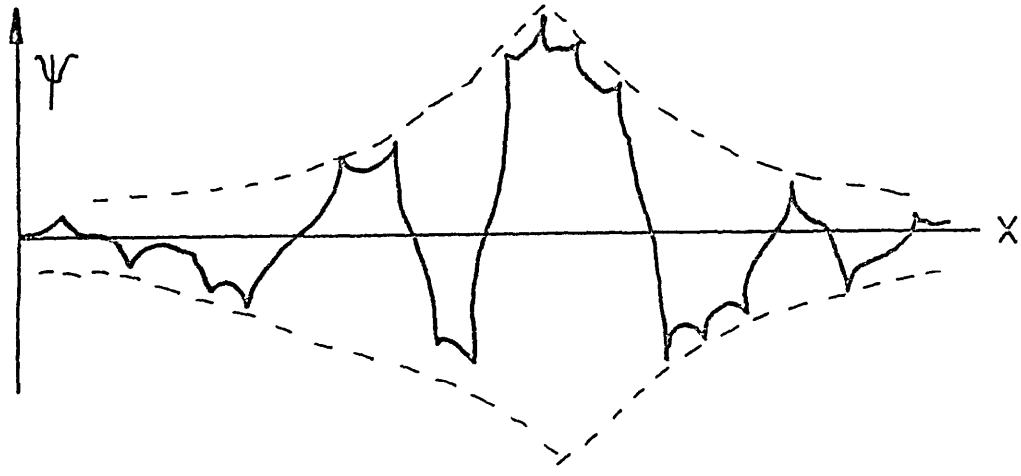

FIGURE

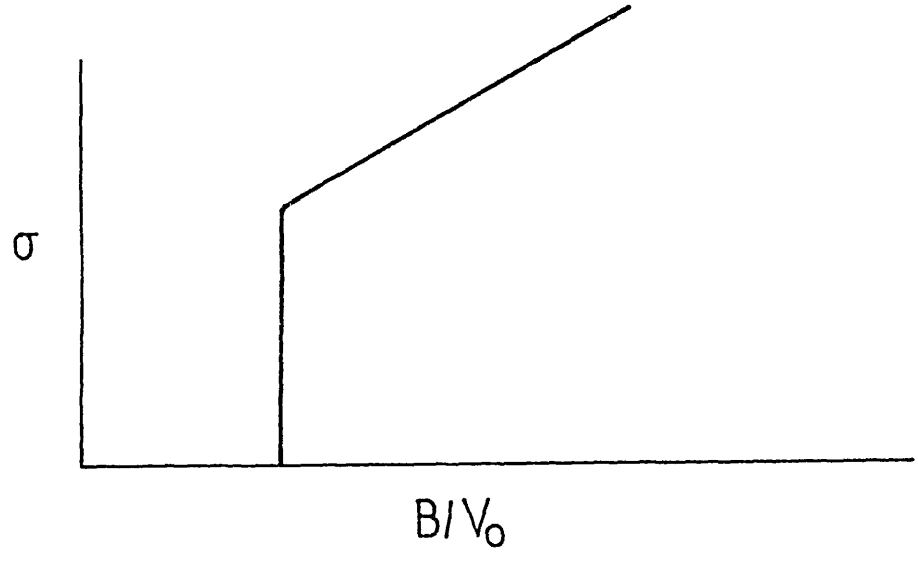

FIGURE 4

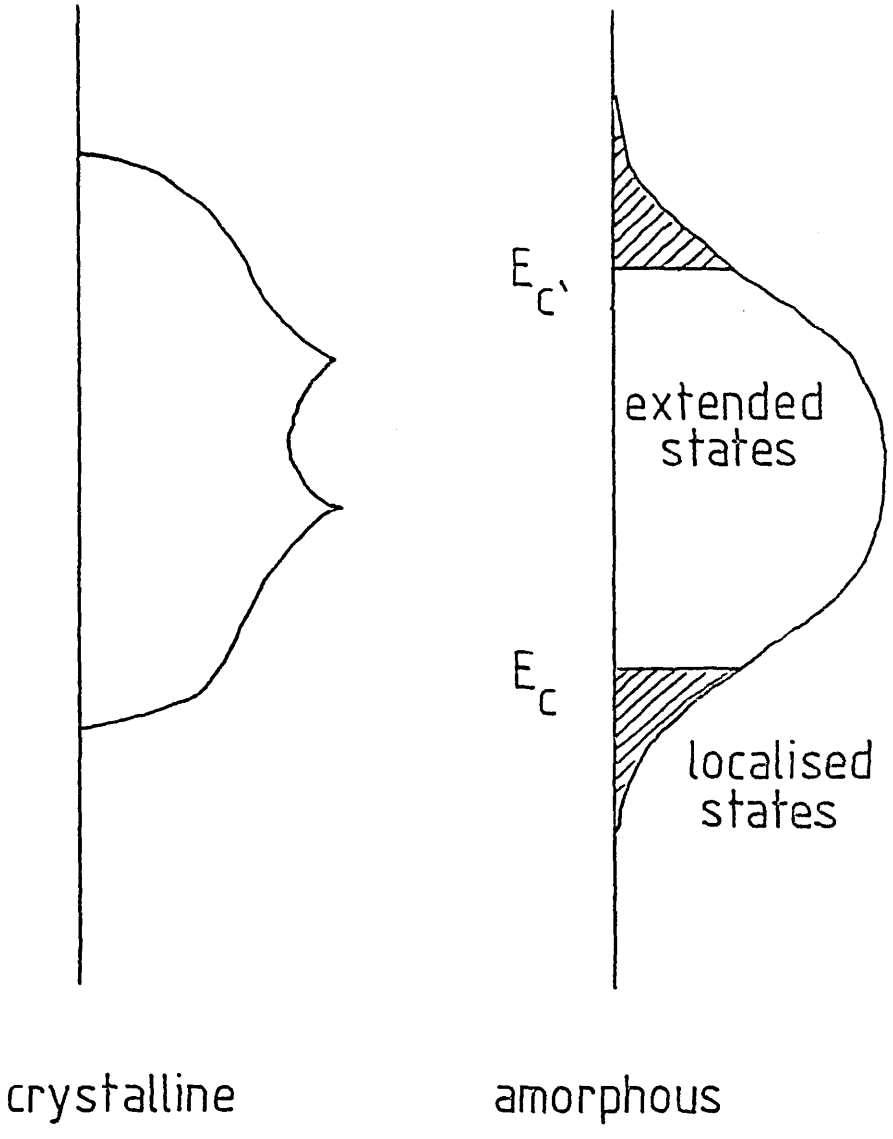

FIGURE 5 : Density of states as a function of energy.

Figure 5 shows that for Ec < E < Ec' the states remain extended with a finite phase coherence length. Below Ec, the ensemble average of the conductivity (and hence the mobility) vanishes at T = 0. Thus at Ec and Ev there will be mobility edges analogous to the band edges in conventional solid state theory, between which is a 'mobility gap' which will play a similar role to the band gap in crystalline semiconductors. Thus the energy eigenstates of electrons in amorphous semiconductors consist of extended 'band' states separated by mobility gaps containing localised band-tail and gap states.

The foregoing description of an 'ideal' amorphous semiconductor forms the basis upon which the electrical and optical properties of real amorphous semiconductors may be understood. There is a great deal of experimental evidence to support the existence of valence and conduction bands in amorphous semiconductors dating from the pioneering work of Kolomiets and co-workers in the 1950's. There is similarly a large amount of experimental evidence for the presence of mobility edges (the position of which may be temperature dependent), which has been reviewed by Mott, Pepper, Pollitt, Wallis and Adkins (1975) - although the sharpness of such edges, as well as the presence of a minimum metallic conductivity at low temperatures remain controversial.

Detailed measurements of the drift mobility, field effect, photoconductivity etc. on a variety of materials have subsequently verified the existence of fairly discrete levels or, at least, structure in the distribution of the density of states throughout the mobility gap of amorphous semiconductors. Many models have been proposed to account for this structure, and these will be described in some detail in the next chapter. For the rest of this chapter we need only assume the existence of extended band states and localised gap states.

1.2 THE BREAKDOWN OF CONVENTIONAL TRANSPORT THEORY

The Boltzmann equation formulation of transport theory is based on the idea that the electrons in a solid move freely under the influence of external fields, and that these movements are interrupted by interactions with the lattice such as phonon emission or absorption. Electrons considered in this way are represented by wave-packets using combinations of Bloch functions. These wave-packets must have a smaller extent than does the Brillouin zone in k-space, and hence must extend over several lattice constants in real space. In addition, all other space-dependent qualities (such as lattice disorder, external fields etc.) must change slowly along the length of the wave-packet. Thus, if the mean free path of the electron starts to approach the dimensions of the lattice parameter this approach breaks down, and $\underline{k}$ ceases to be a good quantum number (as in section 1.1). This is the familiar Ioffe-Regel condition which applies in the case of amorphous metals (Ioffe and Regel 1960).

There is also a restriction placed on the applicability of this approach by the use of the relaxation time approximation. When this approximation is used, the electron is considered to be accelerated like a free particle between two 'collisions'. Between these collisions it will absorb energy from the field and give it up to the lattice at the next collision. The model will thus fail when the energy absorbed from the external field becomes comparable to the width of the energy band, which is important in the case of narrow bands. This implies that there must be sufficiently weak electron-phonon coupling so that the interaction time during collisions is smaller than the time between collisions.

Another limitation on the applicability of conventional transport theory was pointed out by Frohlich and Sewell (1959), who showed that in a narrow band ($B < 2kT$) the uncertainty principle provides the condition

$$\hbar / \tau > 2J$$

and because

$$\mu = \frac{eD}{kT} = \frac{e}{kT} \frac{\tau J^2 a^2 \hbar^2}{2}$$

it follows that the mobility must be greater than a limiting value

$$\mu > \frac{ea}{\hbar} \frac{B}{kT} = 0.1 \ (B/kT) \ cm^2V^{-1} \ s^{-1}$$

In a semiconductor with a wide band ($B = 2zJ >> kT$) we can use the concept of an effective mass, so that

$$\mu = \frac{e \tau}{m^*}$$

and the uncertainty principle again provides us with the condition for the applicability of conventional theory

$$\hbar / \tau < kT$$

which in turn implies

$$\mu > (m/m^*) \ (e\hbar/kT) = (m/m^*) . \ 30 \ cm^2V^{-1}s^{-1}$$

Summarising, there are three criteria which must be met if conventional band theory and the Boltzmann equation formulation of transport theory can be applied:-

1. The absence of a disordered potential which changes abruptly over distances of the order of the lattice constant.
2. The absence of a strong electron-phonon coupling.
3. A mobility of greater than about 10 $cm^2V^{-1}s^{-1}$.

These are necessary conditions for the applicability of conventional band theory and the Boltzmann equation, but they do not tell us anything about the conduction mechanisms which will apply if these criteria are not met. In particular they do not imply that the one-electron states are localised. There are in fact two possibilities:-

1. Extended-state conduction - where k is no longer a good quantum number and the Boltzmann formulation fails. Instead the extended motion is a diffusive motion or random walk from one atom to the next. This mechanism does not require phonon assistance and

$< \sigma > \neq 0$ at $T = 0$.

2. Localisation and hopping conduction - this will occur for sufficiently low mobilities as a result of either

   1. Anderson localisation described in the previous section and/or

   2. Small polaron formation (or self-trapping), when the local electron-phonon interaction is sufficiently strong to distort the lattice and trap the electron before it moves to another site. Here $< \sigma > = 0$ at $T = 0$, and so the processes are thermally activated.

These transport mechanisms will now be discussed in greater depth.

1.3 EXTENDED STATE CONDUCTION

We have seen that for conduction near a mobility edge in an amorphous semiconductor the Boltzmann equation formulation of transport theory is unlikely to be applicable for the reasons outlined in the previous section. Instead, one must start from the more general formulation of conductivity theory developed by Kubo and subsequently simplified by Greenwood (a detailed discussion of this formalism is beyond the scope of the present work, but may be found in Madelung (1978) or Mott and Davis (1979)). For states involved in the conductivity which are several kT from the Fermi-level, the Kubo-Greenwood formula may be written as

$$\sigma = \int e\mu(E)\, n(E)\, dE \qquad -1.1$$

with

$$n(E) = g(E)\, f_o(E)$$

$$\mu(E) = \frac{\sigma_E\,(O)}{kT\, e\, g(E)}$$

The physical meaning of this formula is that the conductivity is made up of contributions from individual states, whose localisation or delocalisation is given by the value of the "mobility" $\mu(E)$. If one assumes that the Fermi-level is situated near the centre of the mobility gap, and thus sufficiently far from Ec that Boltzmann statistics can be used to describe the occupancy of states (this is to be expected in the case of arsenic triselenide) one gets

$$f(E) = \exp \{ - (E-E_f)/kT \} \qquad - 1.2$$

In the non-degenerate case and under the assumption of a constant density of states and constant mobility (Nagels (1979))

$$\sigma = e\, N(E_c)\, kT\, \mu_c \exp \{ -(E_c-E_f)/kT\} \qquad - 1.3$$

where μ_c is the average mobility. The number of electrons is given by

$$n = N(E_c)\, kT \exp \{-(E_c-E_f)/kT\} \qquad - 1.4$$

Mott (1973) showed that the above expression for the conductivity could be written

$$\sigma(E_c) = e < N(E) > \mu_c\, kT/3 \qquad - 1.5$$

and calculated the lowest value of the conductivity to be expected before the onset of an activated process - that is just at Ec. This is called the minimum metallic conductivity and is given by

$$\sigma_{min} = \text{const. } e^2/\hbar a \qquad - 1.6$$

where the constant lies between 0.025 and 0.1. Taking the constant to be 0.025 one finds for the mobility

$$\mu_c = 0.078\, e/\hbar a \quad \{<N(E)>\, kT\}^{-1} \qquad - 1.7$$

which may be simplified using the nearly-free electron model (Nagels (1979)) to

$$\mu_c = 0.078\, \frac{ea^2B}{\hbar kT} \sim 10\ cm^2V^{-1}s^{-1} \qquad - 1.8$$

taking $a = 2$ Å and $B = 5$ eV.

This value corresponds to a mean free path comparable to the inter-atomic spacing. Cohen (1970) suggested that for this reason conduction in this regime would be more properly described as a diffusive or Brownian-type motion. In this regime the mobility may be calculated from the Einstein relation given that

$$D = \frac{1}{6} \nu a^2 \qquad - 1.9$$

where ν is the jump frequency and a is the inter-atomic distance. This yields

$$\mu = \frac{1}{6} \frac{ea^2\nu}{kT} \qquad - 1.10$$

which has the same temperature dependence as equation 1.8 derived by Mott. Since

$$\mu_c \propto \frac{1}{kT}$$

One expects the expression for the conductivity to be of the form

$$\sigma = \sigma_o \exp\left[\frac{-(E_c - E_f)}{kT}\right] \qquad - 1.11$$

Optical absorption measurements made on amorphous semiconductors have shown that the band gap decreases with increasing temperature - therefore Ec-Ef should show a similar behaviour, and under the assumption of a linear temperature dependence

$$E_c - E_f = E(o) - \gamma T \qquad - 1.12$$

the expression for the conductivity becomes

$$\sigma = \sigma_o \exp(\gamma/k) \exp\left[-\frac{E(o)}{kT}\right] \qquad - 1.13$$

where E(O) is the energy separation at T=O. This may be written in the form

$$\sigma = C_o \exp\left[\frac{-E(o)}{kT}\right] \qquad - 1.14$$

where

$$C_o = eN(E_c)\, kT\, \mu_c \exp\left(\frac{\gamma}{k}\right) \qquad - 1.15$$

As seen before, the mobility is proportional to 1/T, so that the pre-exponential factor Co is temperature independent. In general σ_o may lie between 10 and 1000 Ω^{-1} cm^{-1}, in most amorphous semiconductors. In chalcogenide glasses, the temperature co-efficient of the optical gap generally lies between 4×10^{-4} and 8×10^{-4} eV K^{-1}. As the Fermi-level is situated near the middle of the gap, values of approximately half this magnitude are expected and hence values of exp (γ/k) in the range 10 - 100 seem to be most probable.

A different approach based on a 'random phase' model was used by Hindley (1970) and Friedman (1971) to calculate the mobility in the extended states near Ec or Ev. In this model a mean free path of the order of the lattice spacing is represented by a loss of phase memory of the electron wavefunction as it moves from site to site. Assuming a constant density of states at the mobility edge, they derived the following expression for the d. c. conductivity in the extended states

$$\sigma = \frac{2\pi e^2}{3\hbar a}\, za^6 J^2 \left[N(E_c)\right]^2 \exp\left\{\frac{-(E_c - E_f)}{kT}\right\} \qquad - 1.16$$

Here a is the interatomic spacing, z the co-ordination number and J the electronic transfer integral. The d.c. conductivity in the random phase model follows a simple exponential law

$$\sigma = \sigma_o \exp\left\{\frac{-(E_c - E_f)}{kT}\right\}$$

The conductivity mobility can be derived from the above equations by dividing by ne, where the electron density is given by equation 1.4. This yields

$$\mu_c = \frac{2\pi ea^2}{3\hbar}\, z \left\{\frac{J}{kT}\, a^3 JN(E_c)\right\} \qquad - 1.17$$

The mobility decreases with increasing temperature as 1/T. Inserting typical numbers, one finds a mobility of about $2 cm^2 V^{-1} s^{-1}$.

The thermopower (S) associated with conduction in extended states will now be discussed. Nagels (1979) has given a general expression for the thermopower

$$S = -\frac{k}{e} \int \frac{E - E_f}{kT} \frac{\sigma(E)}{\sigma} dE$$

If we combine this with equation 1.1 for the conductivity, and Boltzmann statistics, one may calculate the thermopower directly.

Under the assumption of a constant density of states and an energy independent mobility, the thermopower can be readily found by integrating this equation. This yields an expression of the familiar form for band conduction of electrons

$$S = -\frac{k}{e} \left[\frac{E_c - E_f}{kT} + A \right] \qquad - 1.18$$

with A = 1 (in the case of crystalline semiconductors it is well known that the kinetic term A depends on the scattering mechanism).

From the above results we see that in this regime, S and σ should have the same activation energy. Hindley has shown that a similar expression is to be expected from the random phase model of conduction.

If both electrons and holes contribute to the conductivity, then the thermopower should be the sum of the individual contributions each weighted according to the ratio of its conductivity to the total conductivity. Thus we have

$$S = \frac{S_e \sigma_e + S_h \sigma_h}{\sigma_e + \sigma_h} \qquad - 1.19$$

The above discussion has summarised the main points of the theory of conduction in the extended states of amorphous semiconductors far from Ef. In practice, however, the transport properties in this regime will often be dominated by trapping and release by localised states closer to Ef. The next section will present a summary of the main results from the theory of trapping in crystalline semiconductors which may be usefully applied to carrier transport in amorphous semiconductors.

1.4 TRAPPING AND RELEASE OF CARRIERS IN SEMICONDUCTORS

One of the easiest ways to study carrier transport in semiconductors is to investigate excess-carrier phenomena which occur when the distribution of electrons and holes in the semiconductor is perturbed perceptibly from equilibrium.

The process of generation of free charge carriers in a semiconductor requires energy to overcome the energy gaps between allowed bands or between localised states and these bands. Under normal conditions, this energy is drawn from the reservoir of thermal energy present in the solid. Electrons and holes in a solid interact very strongly with the ions of the lattice, and therefore the lattice and electron temperatures are usually identical. In consequence, heating a semiconductor will increase the numbers of electrons in the conduction band and holes in the valence band, and these 'thermally ionised' carriers will have densities corresponding to thermal equilibrium, and are usually called 'equilibrium carriers'.

Of course, there are methods other than thermal ionisation which may serve to generate free electrons and holes - for example excitation by light or by electrons or other radiations. Moreover, excess carriers may appear in a semiconductor due to 'injection' at a rectifying contact, by the application of strong electric fields (impact ionisation) and so forth (Ryvkin (1964) p1). The energy donated to the carriers by these methods of generation will in general be retained by the free carriers, while the average thermal energy of the lattice will remain practically unaffected. Consequently the thermal equilibrium between lattice and carriers is disturbed, and such carriers are usually called 'excess' or 'non-equilibrium' carriers.

The field of non-equilibrium effects in semiconductors is huge, and a full treatment of the relaxation of such non-equilibrium populations would not be appropriate here. We therefore confine our discussion to the processes which are likely to be important in describing the propagation of excess carriers in drift-mobility experiments.

In time-of-flight drift mobility experiments (a full description of which appears in chapter three) excess carriers are generated at one side of a bulk semiconductor sample. This is accomplished using either a short flash of strongly absorbed light, or a short pulse of electrons. The current transient produced by the drift of these carriers through the sample under the influence of an electric field may then be captured using an oscilloscope, and from the length of the current pulse one may calculate the drift mobility from the relation

$$\mu_d = \frac{\ell^2}{Vt_T} \qquad - 1.20$$

During their transit of the sample, the carriers may be trapped and released a number of times by localised states in the band tails or deep in the mobility gap. In the case of extended state motion, the interaction rate of free carriers with a species of traps is given by $1/\tau_T$ where τ_T is the trapping time with respect to that species. For a crystalline material (Dolazalek (1976)) the trapping time may be expressed as

$$\frac{1}{\tau_T} = N_t S v_{th} \qquad - 1.21$$

The rate is thus proportional to both the trap density Nt and the capture cross-section S, and only weakly dependent on the temperature through the thermal velocity term. In low mobility media where the carrier mean free path may be comparable to the lattice spacing, Mott and Davis (1979) have argued that a similar expression is to be expected. Chandrasekhar (1943) has studied carrier motion by diffusion in disordered systems. He found the capture coefficient σ ($=\nu_{th}S$ above) was given by

$$\sigma = 4\pi R_o D$$

where D is the diffusion coefficient and R_o the trap radius.

In contrast to the trapping rate, the release rate will be strongly temperature dependent, and will be given by

$$\frac{1}{\tau_r} = \nu_{ph} \exp\left\{ - \frac{\Delta E}{kT} \right\} \qquad - 1.22$$

where ν_{ph} is the phonon attempt-to-escape frequency and ΔE the trap depth. Note that if ΔE is small, the release rate to the band may be increased by the application of high electric fields (figure 6).

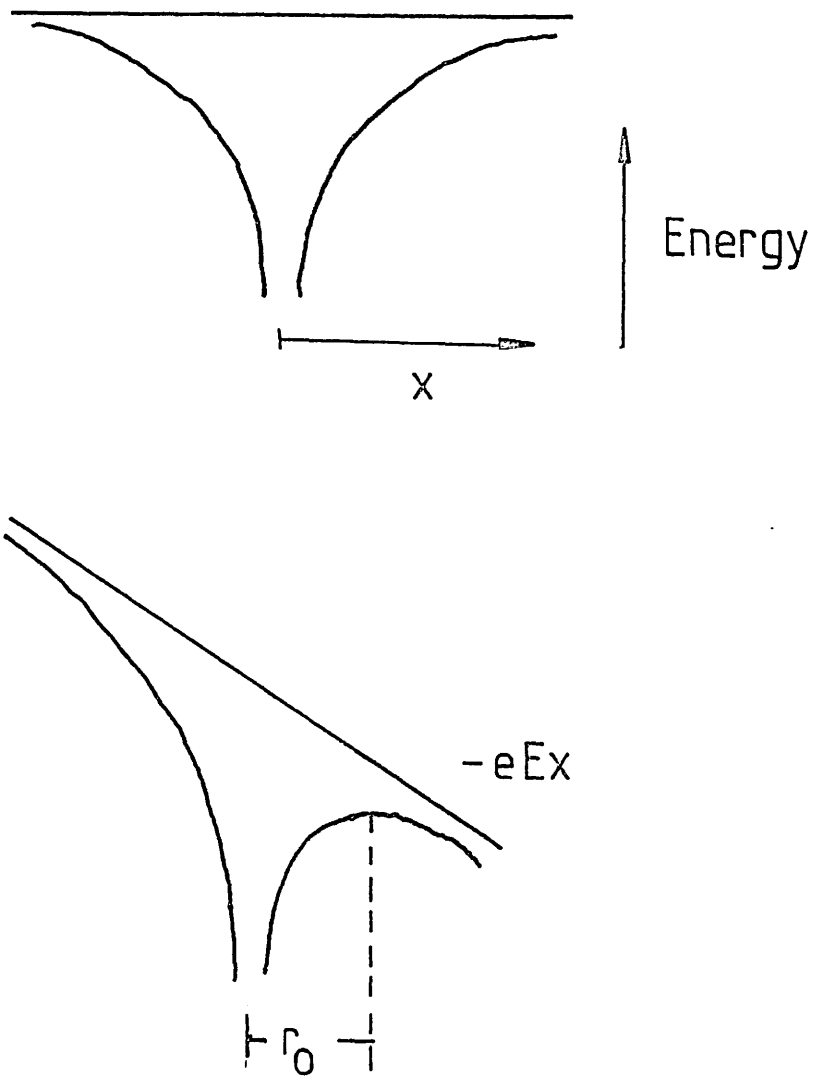

FIGURE 6

For the observed drift mobility in such an experiment to be appreciably affected by shallow trapping, a large fraction of the carriers must interact with these traps, i.e.

$$\tau_T \ll t_T$$

In addition, these carriers must spend a significant fraction of the transit time in the traps, so that

$$\tau_r \gg \tau_T$$

The effective transit time of the fraction which has suffered trapping will then be longer than the transit time in the absence of traps by a period of time proportional to the mean time lost in the traps (τ_r), so that

$$\frac{t_{eff}}{t_T} = \frac{(\tau_t + \tau_r)}{\tau_t} \qquad - 1.23$$

In view of the strong temperature dependence of the release time, t_{eff} will become longer than t_T as the temperature is lowered beyond the point at which $\tau_T = \tau_r$. If $\tau_t << t_T$, both will be very small compared with t_{eff}. This is the case of multiple trapping in which quasi-thermal equilibrium may be assumed. Here the principle of detailed balance implies

$$\frac{\tau_r}{\tau_t} = \frac{N_t}{N_c} \exp \{\Delta E/kT\} \qquad - 1.24$$

where Nc is the effective density of states at the band edge, or its equivalent in the non-crystalline case. Thus an effective mobility for multiple trapping may be defined as

$$\mu_{eff} = \frac{\mu_o}{(1 + \frac{N_t}{N_c} \exp \left\{ \frac{\Delta E}{kT} \right\})} \qquad -1.25$$

where μ_o is the microscopic mobility between trapping events. As the temperature is lowered, this expression predicts a change from temperature insensitive to activated behaviour, from which the density of traps Nt and their depth ΔE may be determined. This is possible

because $e\mu_o N_c$ is the pre-exponential factor in the dark d.c. conductivity.

The diagrams in figure 7 show the shapes of the transit pulses to be expected for transport through materials with differing trap parameters. Part (a) shows a typical transit pulse shape expected for multiple trapping as described above, where the initial equilibration of the excess carriers occurs in a time much shorter than the transit time - this is a necessary criterion for the unambiguous interpretation of such current transients. Equilibrium with band-tail localised states occurs in a time of the order of 10^{-11} - 10^{-12} seconds and can therefore be regarded as almost instantaneous. However, when several phonons have to be emitted at once the process can be much slower - such multiphonon processes are expected to be important for states deep in the mobility gap (Mott, Davis and Street (1976)). The capture cross-sections of such deep traps have been calculated by Lang and Henry (1975), who found

$$S = A \exp\left\{-\frac{\omega}{kT}\right\}$$

which with $A = 10^{-15} cm^2$ gives good agreement with optical data in GaP.

The transit pulse shape to be expected for traps with a longer trapping time but fairly short release time is shown in part (b) of figure 7. It should be noted that the time taken for the excess carriers to equilibrate will always be of the order of a few trapping times, and thus independent of the release time. Equation 1.21 implies that the trapping time will be short for traps with a sufficiently high density and/or large capture cross-section.

If there are a number of trapping levels in the gap with different densities and capture cross-sections, the analysis may become rather complicated (Schmidlin (1977)). The condition that a trap will release carriers during the passage of a pulse is

$$\nu_{ph}\, t_{eff} \exp\{-\Delta E/kT\} > 1 \qquad - 1.26$$

from equation 1.22 where t_{eff} is the duration of the pulse (the

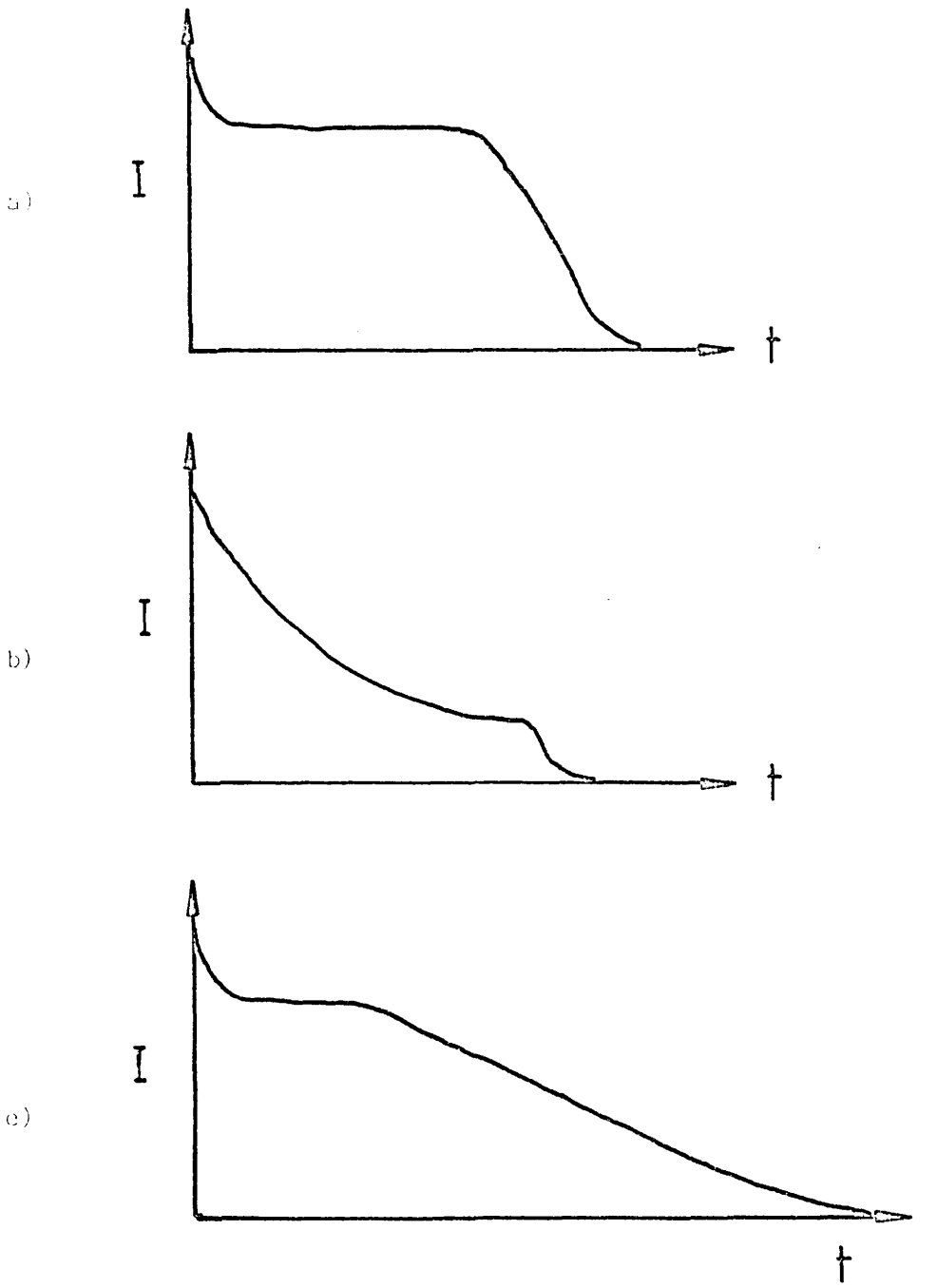

FIGURE 7 : Shape of transit pulse for a) normal multiple trapping, b) for traps with a long trapping time, and c) in the presence of deep traps with long release times.

effective transit time). Deeper traps, which will have correspondingly longer release times will lead to a tail in the carrier pulse as shown in part (c) of figure 7. Under such conditions one can still determine a time from which a meaningful drift mobility may be calculated, but one is then only probing states sufficiently close to the mobility edge to have release times shorter than the transit time.

In amorphous arsenic triselenide, the interpretation of drift mobility measurements is complicated by a significant 'spreading' or dispersion of the carrier packet as it propagates through the sample (Pfister (1974), Pfister and Scher (1977)). This property has come to be known as dispersive transport, and is now thought to be intimately related to the problem of carrier trapping and release in a material with either a wide distribution of localised states in the gap, or a number of discrete trapping levels. This will be the subject of the next section.

1.5 DISPERSIVE TRANSPORT

It has been observed that the transport of holes through samples of amorphous arsenic triselenide in time-of-flight drift-mobility experiments cannot be described by conventional Gaussian broadening of the carrier packet (Pfister and Scher (1978)). This behaviour has also been observed for electrons in crystalline arsenic triselenide by Marshall (1977). In other words, the dispersion σ of the carrier sheet and its mean displacement ℓ from the excited surface do not obey the well-known relations

$$\sigma \propto t^{\frac{1}{2}} \quad \text{and} \quad \ell \propto t$$

which are to be expected from Gaussian statistics. In fact, whereas for the case of Gaussian pulse broadening the spread of the pulse will become relatively less pronounced with time

$$\frac{\sigma}{\ell} \sim t^{-\frac{1}{2}} \qquad - 1.27$$

for dispersive transport the observed pulse broadening appears to stay constant, as shown in figure 8 - i.e.

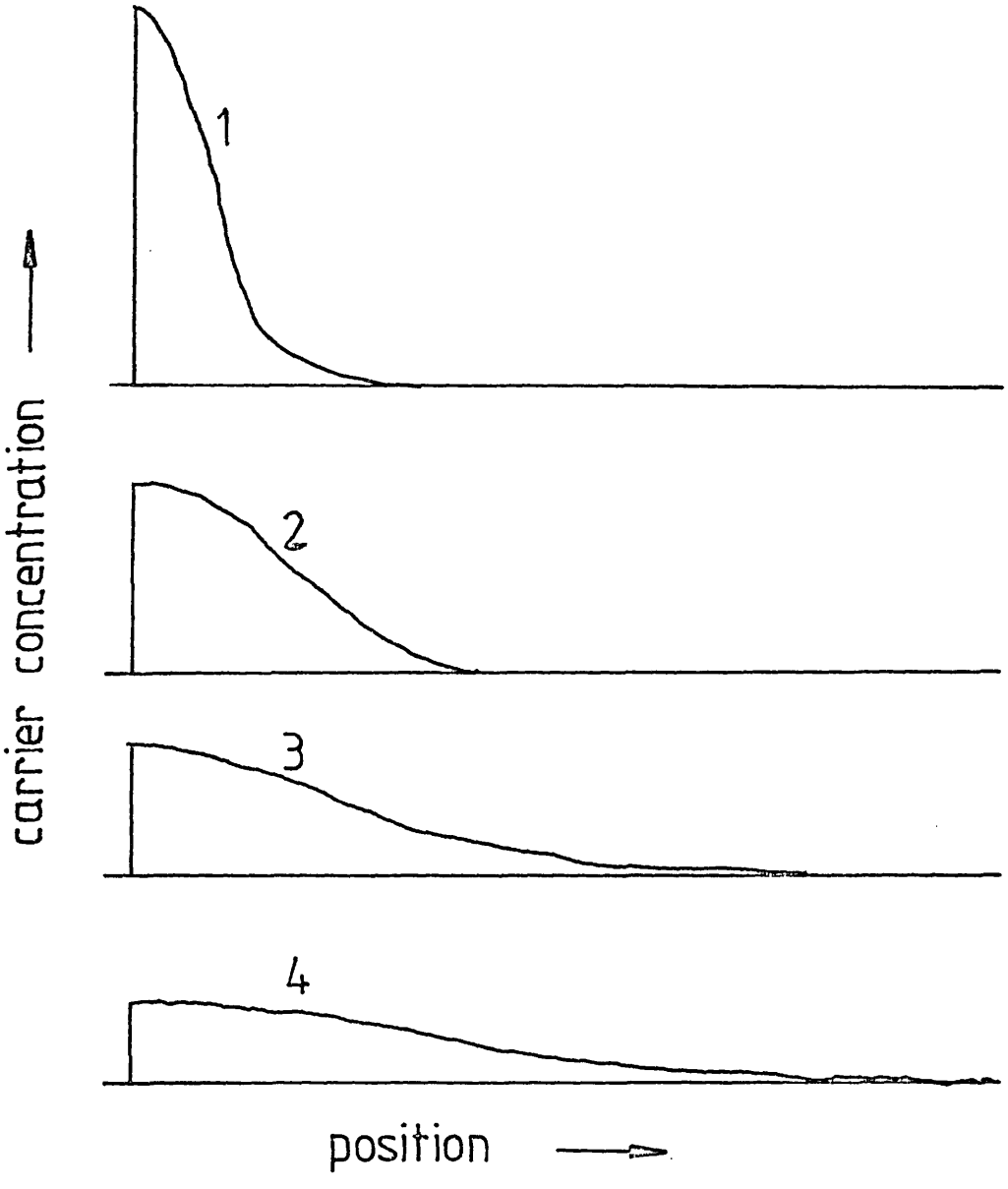

FIGURE 8 : Non-Gaussian carrier packet broadening.

$$\frac{\sigma}{\ell} = \text{const.} \qquad - 1.28$$

These experimental results led Scher and Montroll (1975) to suggest that the microscopic processes which control the hole transport in amorphous arsenic triselenide must be characterised by a very wide distribution of event times. In their analysis, Scher and Montroll considered carrier transport in such a material as a succession of carrier hops from one localised site to the next. If one follows the motion of a single carrier, a wide fluctuation of hopping times will occur as the carrier progresses from site to site. This sequence is a stochastic process with the probability to remain at a single site being the significant random variable. Scher and Montroll grouped these sites together into cells, and considered the motion from cell to cell. They considered a continuous time random walk (CTRW) on a discrete lattice of such cells, with a distribution function $\psi(s,t)$ governing the intercell events. Their main assumption was that this distribution of hopping times is so large that the maximum in the carrier concentration remains close to the excited surface region.

Under such conditions, the current transient will represent the time dependence of the arrival of carriers from the leading edge of the distribution (i.e. the fastest few percent of carriers reaching the extinction electrode). The dispersion of the carrier sheet and the mean displacement of the charge from the excited surface both increase with time in the same manner, and thus their ratio will remain constant.

The probability for a carrier to hop to the next site after arriving at a site at $t = 0$ was taken by Scher and Montroll to be

$$\psi(t) = t^{-(1+\alpha)} \qquad - 1.29$$

where $(0 < \alpha < 1)$ is a parameter depending on the hop distance, the hop energy, and the spatial extent of the localised site. When compared

with the Gaussian case this is a very weak dependence on time, which leads to a time dependence of the current behaving as

$$I \propto t^{-(1-\alpha)} \qquad t < t_T$$
$$I \propto t^{-(1+\alpha)} \qquad t > t_T \qquad - 1.30$$

Such a current transient may appear featureless on a linear current - time graph, with no obvious discontinuity of gradient or 'knee' associated with the transit time. However, if such a pulse is drawn on logarithmic axes, the above equations imply that there will be two distinct straight-line regions with gradients of $-(1-\alpha)$ before the transit time t_t, and $-(1+\alpha)$ at longer times. The gradients of the two lines of log-log graphs would thus always sum to two (see figure 9).

This theory also accounted for some other unusual features of carrier transport in arsenic triselenide - for example the observation that the shape of transit pulses did not depend strongly on the transit time through the sample, and consequently did not depend appreciably upon the applied electric field. A further prediction of this theory was that the transit time of the fastest few percent of carriers should depend superlinearly on the ratio of the sample thickness to the applied field.

This theory was applied to transit pulses in arsenic triselenide by Pfister and Scher (1977, 1978) with some success. These authors found the dispersion parameter to be about 0.5 - 0.6 and independent of temperature. A discussion of their work appears in chapter two.

The model employed by Scher and Montroll described above has, however, since been criticised by several authors (Pollak (1977 a,b), Marshall (1977 a,b), Silver and Cohen (1977)) for a variety of reasons. The major criticism is that hopping sites with very long dwell times must be considered as <u>isolated</u> sites which will consequently be avoided by the fastest carriers. Pollak has provided a criterion for the observation of dispersive transport - that the sites which have long release times must not be correspondingly difficult to enter. This criterion is clearly not met for a spatially random hopping system, as has been confirmed by Monte-Carlo computer simulation (Marshall

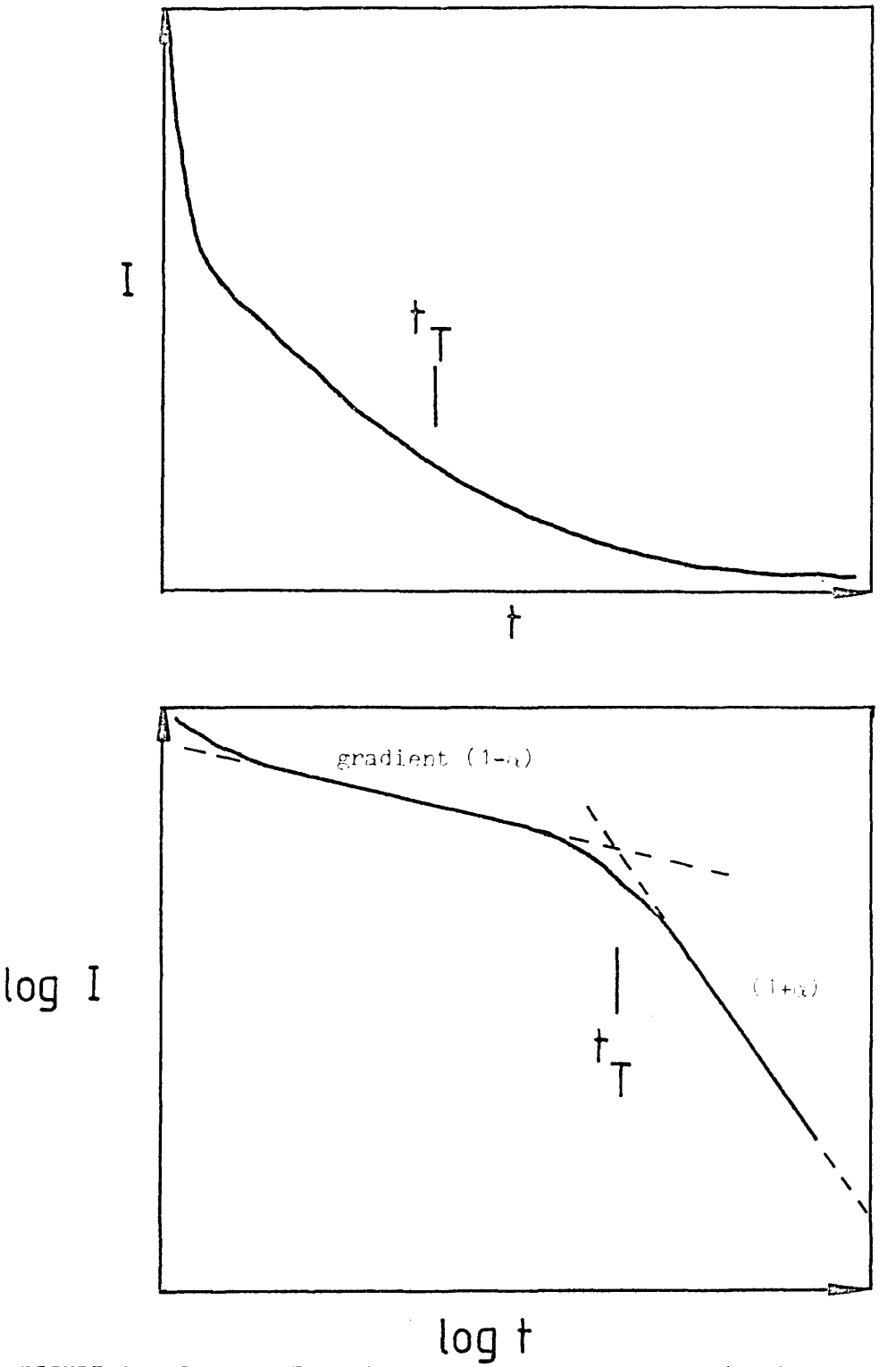

FIGURE 9 : Current Transient displayed on linear (top) and logarithmic axes.

(1978, 1981), Silver and Cohen (1977)).

The computer simulation of hopping transport has recently been extended to include hopping in a random spatial array of sites, a regular spatial array of sites with random energies, and a random spatial array with random energies (Marshall and Sharp (1980), Marshall (1981)). The array used in these model calculations was usually 7 x 7 x 50 sites, although increasing the cross-sectional area of the model specimen by more than an order of magnitude did not affect the results significantly. The main conclusions which may be drawn from these studies are as follows:-

1. The time of flight current transients observed for hopping conduction will not be highly dispersive unless a) the carriers are constrained to hop in only one or two dimensions (i.e. along long chain-like molecules) and/or b) one considers samples which are much thinner than are normally studied experimentally- so that carriers have completed less than about 10 hops and consequently have not had sufficient time to equilibrate.
2. Although not highly dispersive, the transport is anomalous in the sense that the shape of the drifting charge sheet does not conform to Fick's laws of diffusion - carrier equilibration and transit pulse dispersion are dominated by the distance which carriers have travelled through the specimen, rather than the drift time as such.
3. Dispersive transport is however to be expected for trap-limited transport mechanisms (Marshall (1977)).

This simulation work has been recently complimented by a fuller theoretical discussion (Butcher and Clark (1980, 1981), Clark and Butcher (1981)), the results of which show substantial agreement with the results summarised above.

It thus appears that hopping conduction alone cannot account for the observation of dispersive transport, and therefore the Scher-Montroll analysis cannot correspond to this transport mechanism! What transport mechanism does their analysis actually represent?

This question has been answered by the work of Schmidlin (1977) and Noolandi (1977 a,b,), which has shown that the CTRW equations derived by Scher and Montroll are formally equivalent to a set of generalised multiple trapping equations - so that essentially the observation of dispersive transport is closely related to the trapping and release of carriers which we described in the previous section. The next part of this section will be devoted to a description of Schmidlin's multiple trapping analysis, which will be seen to provide interesting physical insights into the criteria which must be satisfied to observe dispersive transport for the multiple-trapping mechanism.

Schmidlin's analysis started from the continuity equations which may be formulated in the familiar context of an electronic carrier moving through extended states with localised gap states acting as traps (as we have described in the previous section). Schmidlin showed that the same equations will apply to any mobile entity which simply stops and starts at random from a distribution of resting places. This formulation is extremely general, and in consequence one must be very careful about the definition of localised states - some will act as traps, whereas for trap-limited hopping conduction (described in more detail in the next section) some may act as transport states. In this analysis, traps are considered to be sufficiently isolated spatially so that direct transitions between them are negligible. In contrast, localised transport states (which by definition cannot occur at T = 0) are sufficiently close to each other to allow hopping from state to state. Thus the microscopic mobility would <u>decrease</u> if these states were removed at non-zero temperatures.

In the previous section we considered the release from a trap to be activated, requiring an energy ΔE (equation 1.22). In general for microscopic hopping we must also take into account a possible activation energy for capture explicitly, so that

$$\frac{1}{\tau_{ri}} = N_i S_i \; e^{\{-\Delta i/kT\}} \qquad - 1.31$$

$$\mu = \mu_o \exp\{-\Delta_\mu kT\}$$

where Δ_i and Δ_μ are possible activation energies for a capture event

and microscopic mobility respectively.

Schmidlin then investigated the degree of dispersion to be expected in the small signal case for carriers drifting through a sample with from one to seven discrete trap levels with varying trap parameters (leading to vastly different trapping and release times). His findings may be summarised as follows:-

1. The empirical transit time t_T is approximately the free transit time plus the the total resting time in all traps visited at least twice.

2. The post transit current decay is controlled by the rate of release from the slow traps which capture a carrier once or less (on average).

3. To obtain a broad dispersion of transit times (or featureless current trace) a carrier must be captured approximately once in a trap whose mean release time is approximately equal to the transit time. This Schmidlin called the critical trap criterion (CTC).

4. Superlinearity of t_T with L/E results from an increasing number of traps satisfying the CTC, or visited more than twice during the transit.

5. A power law waiting time distribution function in CTRW analyses implies a power law relation between capture and release times.

$$\tau_t \quad \propto \quad (\tau_r)^{-\alpha} \qquad - 1.32$$

6. A lower bound on the magnitude of the microscopic mobility may be determined from the transit time and the ratio of initial current to the current at the transit time, from

$$\mu = \frac{L}{t_T E} \qquad \frac{I(t \to 0)}{I(t)} \qquad - 1.33$$

7. The ratio of trap to transport state densities can be determined from trap parameters, which in turn can be determined by fits to experimental current traces using the formula

$$\frac{N_i}{N_v} = \text{const.} \quad \nu_i^{\alpha-1} \exp\{-(\alpha E_i - \Delta_i)/kT\} \qquad -.134$$

where Ni/Nv is the ratio of the density of traps to the density of transport states, Ei is the energy difference between trap and transport states, and Δ_i is a possible activation energy for a capture event. Note that this equation implies that α must be temperature dependent unless Ei is constant or

$$\Delta_i = \alpha E_i \qquad - 1.35$$

8. In general CTRW is formally equivalent to multiple trapping. These conclusions have been substantially confirmed by the computer simulation work of Fleming (1979), although he found that trap parameters could only be calculated unambiguously if transient photoconductivity or drift mobility measurements were made in conjunction with thermally stimulated current or depolarisation measurements. Fleming's simulation was not however restricted to the small signal case, and consequently is useful in ascertaining the possible effect of space charge perturbation on dispersive transits. This aspect of drift mobility experiments is discussed in greater detail in Chapter 3.

Yet another physical interpretation of dispersive transport has recently been given by Tiedje and Rose (1980). In this multiple trapping model, the progressive thermalisation of carriers in an exponential distribution of gap states gives rise to the dispersive behaviour. They assumed that all the localised states in this exponential distribution have the same capture cross-section, so that the distribution of release times is given by

$$\psi(t) = \frac{N_t(E)}{kT_c N_o} \times \frac{dE(t)}{dt} = \alpha \nu (\nu t)^{-(1+\alpha)}$$

for $t > \nu^{-1}$, where $\alpha = T/T_c$ (which is similar to the distribution considered by Scher and Montroll). Using equation 1.22 we can then define a critical trap level $E_c(t)$ such that

$$E_c(t) = kT \ln \{\nu t\}$$

Thus for electrons above $E_c(t)$, the number of trapped carriers will decrease with increasing time, whereas below $E_c(t)$ the distribution

will be essentially unchanged. The bulk of the trapped charge will occur near $E_c(t)$, and it becomes possible to treat the problem as equivalent to a single trap level problem where the depth of the level increases (and the density of traps decreases) with time. This gives

$$\mu_D(t) = \mu_o \alpha (1-\alpha) (\nu t)^{\alpha-1}$$

which reproduces the first part of the log (I) - log (t) graph since $I(t) \propto \mu_D(t)$. This equation describes the motion of the centre of gravity of the charge packet.

The application of an electric field spreads this distribution out in space without changing its energy dependence (because emmission and trapping rates are linear in electron densities). The spatial distribution of charge has been shown to assume a Gaussian shape centred at the origin for the special case of $\alpha = \frac{1}{2}$ after a large number of trapping events, although the exact distribution is not critical to the discussion. They defined the transit time to be the time taken for the centre of gravity of the charge packet to move halfway through the sample to give

$$t_T = \frac{1}{\nu} \{\nu/2(1-\alpha)\}^{1/\alpha} \{L/\mu_o E\}^{1/\alpha}$$

which has the expected field and sample thickness dependence.

For times greater than t_T, they found the current to vary as

$$I(t) \sim I_o (1-\alpha) (\nu t_T)^{2\alpha} (\nu t)^{-(\alpha+1)}$$

where $I_o = Q \mu_o E/L$, and Q is the total injected charge.

Thus this model reproduces the major features of the Scher-Montroll picture in the low temperature limit ($T < T_c$). At high temperatures ($T > T_o$), the mobility will approach the free carrier mobility because the fraction of the total change trapped in deep states approaches zero at long times. In this case

$$\mu_D \sim \mu_o (1 - T_c/T)$$

The main difference between this approach and the Scher-Montroll analysis is that the parameter $\alpha = T/T_c$ is temperature dependent

for traps, but need not be so for hopping. This approach is similar to one developed by Orenstein and Kastner, which is discussed in Chapter 2.

This chapter finishes with a short section devoted to hopping conduction.

1.6 HOPPING CONDUCTION

As we saw in section 1.2, there are two possible localisation mechanisms which may lead to carrier localisation and thermally activated transport. These mechanisms are small polaron formation and Anderson localisation. We shall now discuss the transport mechanisms expected in each case.

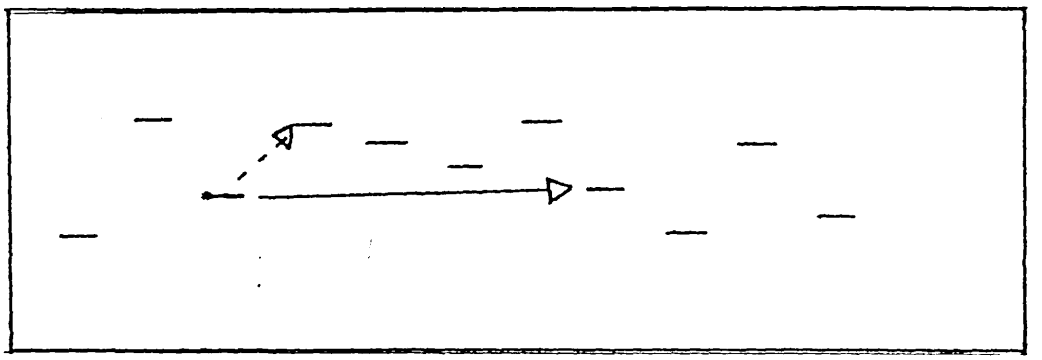

Figure 10 : Dotted line represents nearest neighbour hopping, solid line represents variable range hopping at lower temperatures.

1.6.1. Hopping Conduction in Band Tails

If carrier wavefunctions are Anderson-localised, so that $< \sigma (E) > = 0$ at $T = 0$, conduction at low temperatures will be by thermally activated processes. One way that this can happen in band tail states is by 'hopping' from one localised state to another, the wavefunction of which overlaps that of the first state. Since the two states have quantised energies, the carrier must exchange energy with a phonon each time it moves. The rate-determining step is that in which the carrier obtains energy from the phonon. Hopping of this kind was first described by Miller and Abrahams (1960) and Twose (1959) in their theories of impurity conduction in doped and compensated crystalline semiconductors. They supposed that a carrier on one occupied site would normally jump to a nearest site with energy ΔE above it, where a is the intersite seperation and

$$\Delta E \sim \frac{1}{a^3 N(E)} \qquad - 1.36$$

The hopping probability is then of the form

$$\nu_{ph} \quad \exp \quad (-2\alpha R - \Delta E/kT) \qquad - 1.37$$

where ν_{ph} depends on the strength of the interaction with the phonons, and α is a measure of the localisation of the wavefunction. If α is small , the carrier wavefunction will overlap many possible sites and a percolation theory approach may be more appropriate (Ambegaokar, Halperin and Langer 1971).

Thus hopping will lead to a thermally activated mobility

$$\mu_{hop} = \mu_o \quad \exp \quad \{-W/kT \} \qquad - 1.38$$

The pre-exponent will have the form

$$\mu_o = \frac{1}{6} \quad \nu_{ph} \quad e \, R^2/kT \qquad - 1.39$$

where ν_{ph} is the phonon frequency and R the distance covered in one hop (Nagels (1979)). For a typical phonon frequency $\nu_{ph} = 10^{13}$Hz and W = kT this yields a mobility of the order of $10^{-2} cm^2 V^{-1} s^{-1}$ at

room temperature. If we compare this value with the minimum to be expected for extended state conduction (section 1.3), we see that the mobility is expected to drop by a factor of at least 100 at the 'mobility edge'.

The contribution to the conductivity from this transport mechanism, being an integral over all available energy states, will depend on the energy distribution of the density of localised states. If one assumes that the density of states N(E) behaves as some power s of E, one obtains

$$N(E) = \frac{N(E_c)}{(\Delta E)^s} \quad (E - E_A)^s \qquad - 1.40$$

with $E = E_c - E_a$, then the conductivity due to the hopping of carriers can be easily calculated from equation 1.1 giving

$$\sigma_{hop} = \sigma_{o}hop \left[\frac{kT}{\Delta E}\right]^s C \exp\left\{\frac{-(E_A - E_F + W)}{kT}\right\} \qquad - 1.41$$

where

$$\sigma_{o\ hop} = \frac{1}{6} \mu_{ph} e^2 R^2 N(E_c) \qquad - 1.42$$

and

$$C = s! - \left[\frac{\Delta E}{kT}\right]^s \exp\left\{-\frac{\Delta E}{kT}\right\} \left[1+s\left\{\frac{kT}{\Delta E}\right\}+ S(s-1)\left\{\frac{kT}{\Delta E}\right\}^2 + \ldots\right] \qquad - 1.43$$

For the specific case of s = 1 (linear variation) the conductivity becomes

$$\sigma_{hop} = \sigma_{ohop} \frac{kT}{\Delta E} C_1 \exp\left\{-\frac{(E_A - E_F+W)}{kT}\right\} \qquad - 1.44$$

with

$$C_1 = 1 - \exp\left\{\frac{-\Delta E}{kT}\right\}\left[1 + \frac{\Delta E}{kT}\right] \qquad - 1.45$$

The thermopower built up by the carriers conducting in localised band tail states will be given by

$$S = -\frac{k}{e} \frac{\int \left[\{(E - E_f)/kT\} \exp \{-(E-E_f)/kT\} \right] N(E)\,dE}{\hbar} \qquad - 1.46$$

(Nagels 1979). If it is again assumed that the density of states behaves as some power s of E,

$$N(E) = \frac{N(E_c)}{(E_c - E_A)^s} (E - E_A)^s \qquad - 1.47$$

then one obtains

$$S = \frac{-k}{e} \frac{E_A - E_F}{kT} + \frac{C^*}{C} \qquad - 1.48$$

where C is again defined by equation 1.43 and C* by

$$C^* = \int_0^{\frac{\Delta E}{kT}} e^{-x} x^{s+1} dx \qquad - 1.49$$

Here

$$\Delta E = E_c - E_A$$

is the width of the tail, and

$$x = (E - E_A)/kT$$

The value of the term C*/C depends on the energy distribution of the density of localised states. For a linear variation of N(E), S can be represented by

$$S = -\frac{k}{e} \left[\frac{E_A - E_F}{kT} + \frac{C_1^*}{C_1} \right] \qquad - 1.50$$

with

$$C_1^* = 2 - \left[\exp(-\Delta E/kT) \{2 + 2(\Delta E/kT) + (\Delta E/kT)^2\} \right] \qquad - 1.51$$

and

$$C_1 = 1 - \exp(-\Delta E/kT)\left[1 + (\Delta E/kT)\right] \qquad - 1.52$$

If the carriers move by hopping in the localised states, the conductivity varies nearly exponentially with temperature (apart from a small temperature dependent pre-exponential term as shown by equation 1.44), and the measured activation energy is the sum of the activation energies for carrier creation and for hopping. The activation energy for hopping does not appear in the expression for S, and therefore one expects a difference of slope between the conductivity and thermopower graphs.

1.6.2 Hopping Conduction at the Fermi-level

As we have shown in section 1.3, at high temperatures one may observe extended state conduction which follows the expression

$$\sigma = \sigma_o \exp\left\{-\frac{(E_c - E_f)}{kT}\right\}$$

As the temperature is lowered, we saw in the last sub-section that band tail hopping may take place, with

$$\sigma = \sigma_o \exp\left\{-\frac{(E_A - E_f + W)}{kT}\right\}$$

At still lower temperatures, the conduction path will move into the localised states deep in the mobility gap, where we expect to obtain a conductivity of the form

$$\sigma = \sigma_o \exp\left\{-\frac{(E_x - E_f + W)}{kT}\right\}$$

where Ex is the depth of the localised states in which the conduction path may be found at a given temperature. Finally, the conduction path will reach the Fermi-level. If there is a non-zero single particle density of states at E_f, the phenomenon of variable range hopping is to be expected. The conductivity will then follow the formula

$$\sigma = A \exp \{-(Q/kT)^{\frac{1}{4}}\} \qquad - 1.53$$

(Mott 1968, 1969, Mott and Davis 1971, Ambegaoker, Halperin and Langer 1971). Here

$$Q = 1.5/\alpha^3 N(E_f) \qquad - 1.54$$

The behaviour from which this is deduced is sketched in figure 10. An electron just below the Fermi-level jumps to a state just above it, the energy required being written ΔW. The farther it jumps, the greater is the choice of states it has, and in general it will jump to a state for which ΔW is as small as possible.

Although Mott's analysis yields the behaviour observed in a number of materials, it is now believed to be in error, and the percolation approach of Ambegaoker et. al. is thought to be more rigorously correct. This approach also yields the $T^{-\frac{1}{4}}$ behaviour which is a characteristic of variable range hopping. The onset of variable range hopping is also marked by a sudden drop in the thermopower from typically 500 μV/K to 'metallic' values of about 25 μV/K.

There have been a number of experimental observations of such $T^{-\frac{1}{4}}$ behaviour in amorphous germanium, doped crystalline silicon, cerium sulphide and other materials (for a review see Mott (1974) and Mott, Pepper, Pollitt, Wallis and Adkins (1975)), although it has never been observed in the chalcogenide glasses. In general

one may deduce either the wavefunction localisation parameter, or the density of states at the Fermi-level from experimental $T^{-\frac{1}{4}}$, data. However, one always obtains a value of g(E) of about $10^{18} cm^{-3} eV^{-1}$ using this method - although other measurements on the same specimens can give wildly differing values. In addition, if one tries to fit the slope and intercept of lnσvs. $T^{-\frac{1}{4}}$ graphs to the theory self consistently, one finds densities of the order of $10^{30} cm^{-3} eV^{-1}$! It must therefore be borne in mind that some of the experimental agreement with the above theory is fortuitous, and our theoretical understanding of $T^{-\frac{1}{4}}$ behaviour leaves much to be desired.

1.6.3 Trap-Limited Hopping

As mentioned briefly in the section on dispersive transport, another possible mechanism for band tail hopping is that of trap-limited hopping. This mechanism was first proposed for electron transport in sulphur by Adams, Gibbons and Spear (1964), and developed in greater detail by Street and Gill (1966) and more recently by Schmidlin (1980).

A schematic diagram of this transport mechanism is shown in figure 12. Carriers move through shallow localised states by hopping, but are periodically trapped and released by states deep in the band gap. Street and Gill have shown that the drift mobility to be expected for this process behaves as

$$\mu_d = \frac{ea^2}{kT} P_o \frac{N_h}{N_t} \exp\left\{ - \frac{(E_T + E_P)}{kT} \right\} \qquad - 1.58$$

where a is the intersite separation, P_o a constant associated with the hopping probability, N_h is the density of hopping sites, N_t is the density of deep traps, E_t is the trap depth and E_p is the activation energy of the hopping process. The temperature dependence of the drift mobility observed for this transport mechanism in realgar (As_4Se_4) is shown in figure 11.

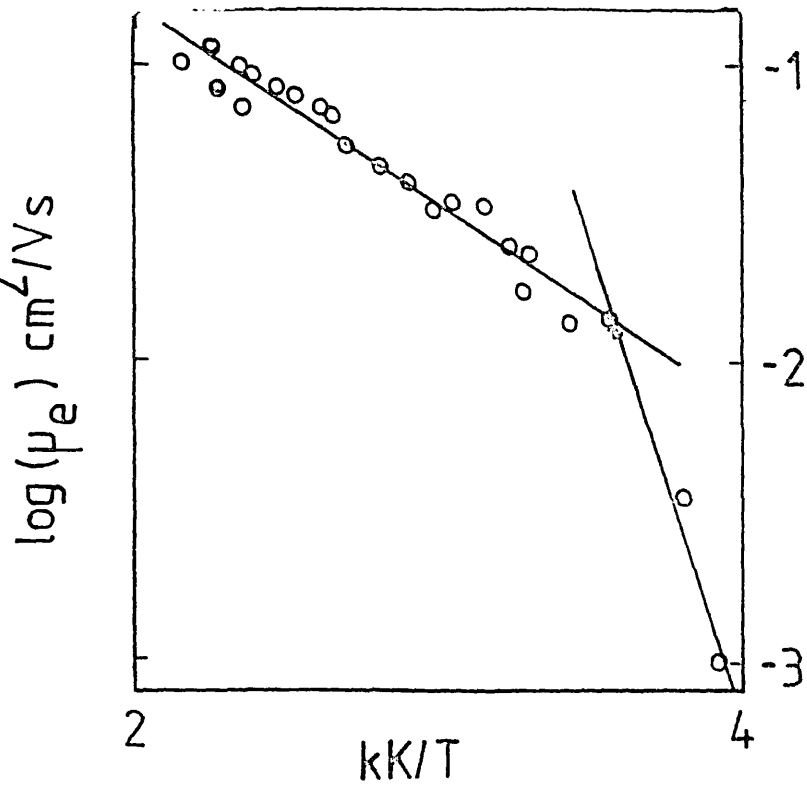

FIGURE 11 : Electron mobility in a realgar crystal.

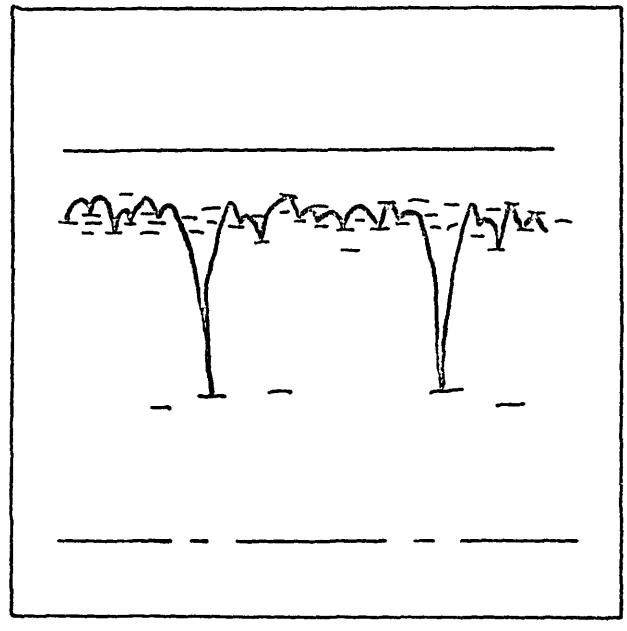

FIGURE 12 : Schematic diagram of trap-limited hopping.

1.6.4 Small Polaron Formation

In a polar solid, if an extra electron is added to a positive ion then the electrostatic forces between the electron and neighbouring charged ions will displace these ions to new equilibrium positions. As a result, the electron sees a potential well which it has created itself. If this well is sufficiently deep, the electron will occupy a bound or localised state. This process will become energetically favourable when the energy lowering due to the well is larger than the increase in strain energy due to the distortion of the lattice plus the energy which would be given out through delocalisation (about 1/2 B - see figure 13).

There is thus a criterion for the formation of a polaron which is similar to the criterion for Anderson localisation discussed in section 1.1 - namely that the band must be narrow for polaron formation. If the band is not sufficiently narrow there will be no polaron formation. The physical significance of this criterion is that the carriers in narrow bands have a much larger effective mass, and so move much more slowly. For polaron formation, the carriers must be moving sufficiently slowly for the lattice to distort and trap the carrier before it has moved to the next lattice site.

The size of a polaron may be calculated by minimizing the polaron's energy, which will be made up of the energy of the electron in the polaron well, plus the energy required to polarize the medium (Mott 1974). The polaron is called a small polaron when its radius is of the order of the lattice constant so that

$$r_p = \tfrac{1}{2}\left[\frac{\pi}{6N}\right]^{1/3} \qquad - 1.59$$

where N is the number of sites per unit volume. Its energy is given by W_p where

$$W_p = \tfrac{1}{2}\ e^2/K_p r_p \qquad - 1.60$$

and

$$\frac{1}{K_p} = \frac{1}{K_\infty} - \frac{1}{K}$$

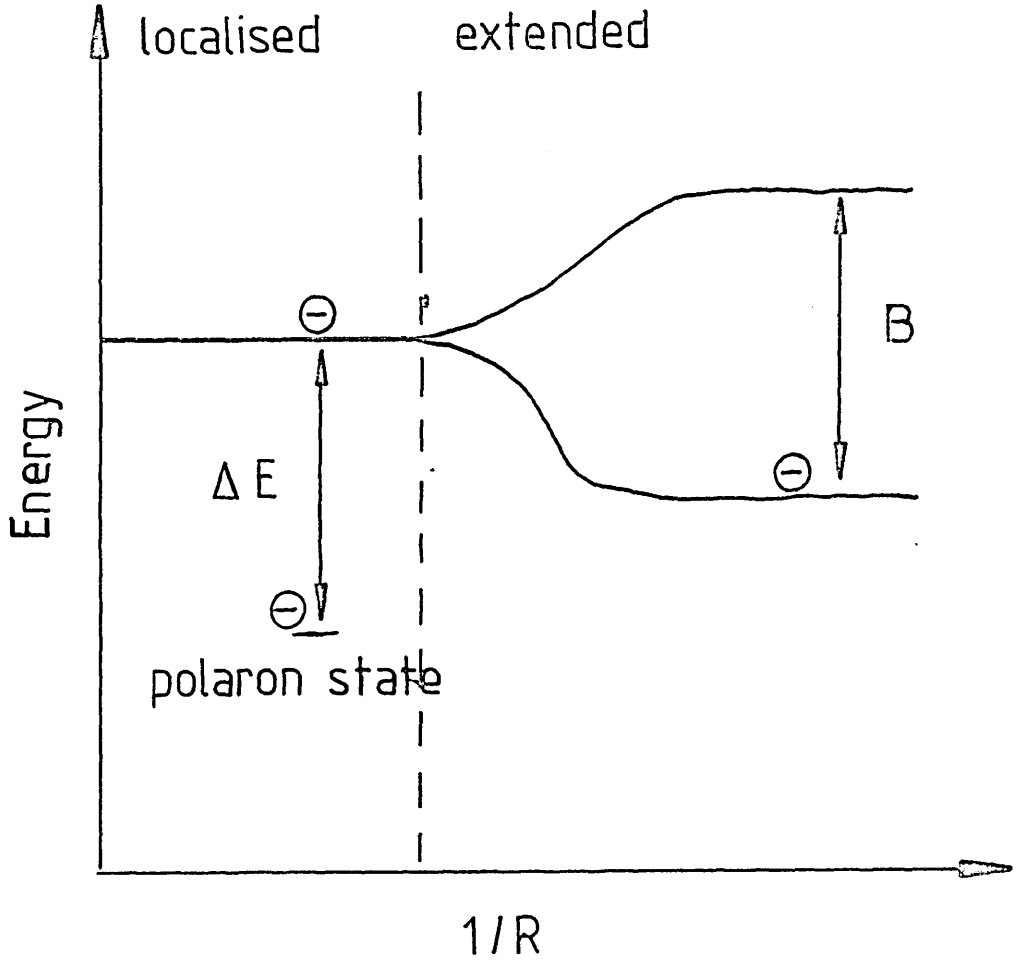

FIGURE 13 : Energy diagram for polaron formation.

where K_∞ and K are the high frequency and static dielectric constants respectively.

Most theoretical studies of the motion of small polarons use a simple model called the Molecular Crystal Model (Holstein 1959, Holstein and Friedman 1968, Emin 1973, Spear 1974) in which a single excess carrier is placed in an ordered array of deformable diatomic molecules (see figure 14), and may only move by 'hopping' to the next site if the deformation on two adjacent molecules are equal. This is sometimes known as a 'coincidence event'. For the small polaron, one may distinguish two different regimes:-

a) At high temperatures ($T > \frac{1}{2}\ \theta_D$), the polaron will move from site to site by thermally activated hopping. Here one may distinguish two different cases, namely

1. Adiabatic Case - where the electron hops backwards and forwards many times during the period of time that the two sites have equal potential depths. Here the carrier will have a high probability of moving to the next site.
2. Non-adiabatic Case- in which the electron cannot follow the lattice vibrations and the time required for an electron to hop is large compared to the duration of a coincidence event. In this case the carrier will have many coincidence events before it hops, and so the probability for transfer will be much lower than in the adiabatic case.

b) At lower temperatures ($T < \frac{1}{2}\ \theta_D$), the carrier moves from site to site without the aid of thermal activation, the zero-point energy $1/2\ \hbar\omega$ taking the place of thermal vibrations (Holstein 1959). This corresponds to polaron band motion with an enhanced effective mass (Mott 1974).

In the high temperature regime, one may use the Einstein relation to obtain the mobility and conductivity from the diffusion coefficient - which can be written as the product of the hopping probability P and the square of the interatomic distance a (Nagels 1979) so that

$$\sigma = (ne^2a^2/kT)P \qquad - 1.61$$

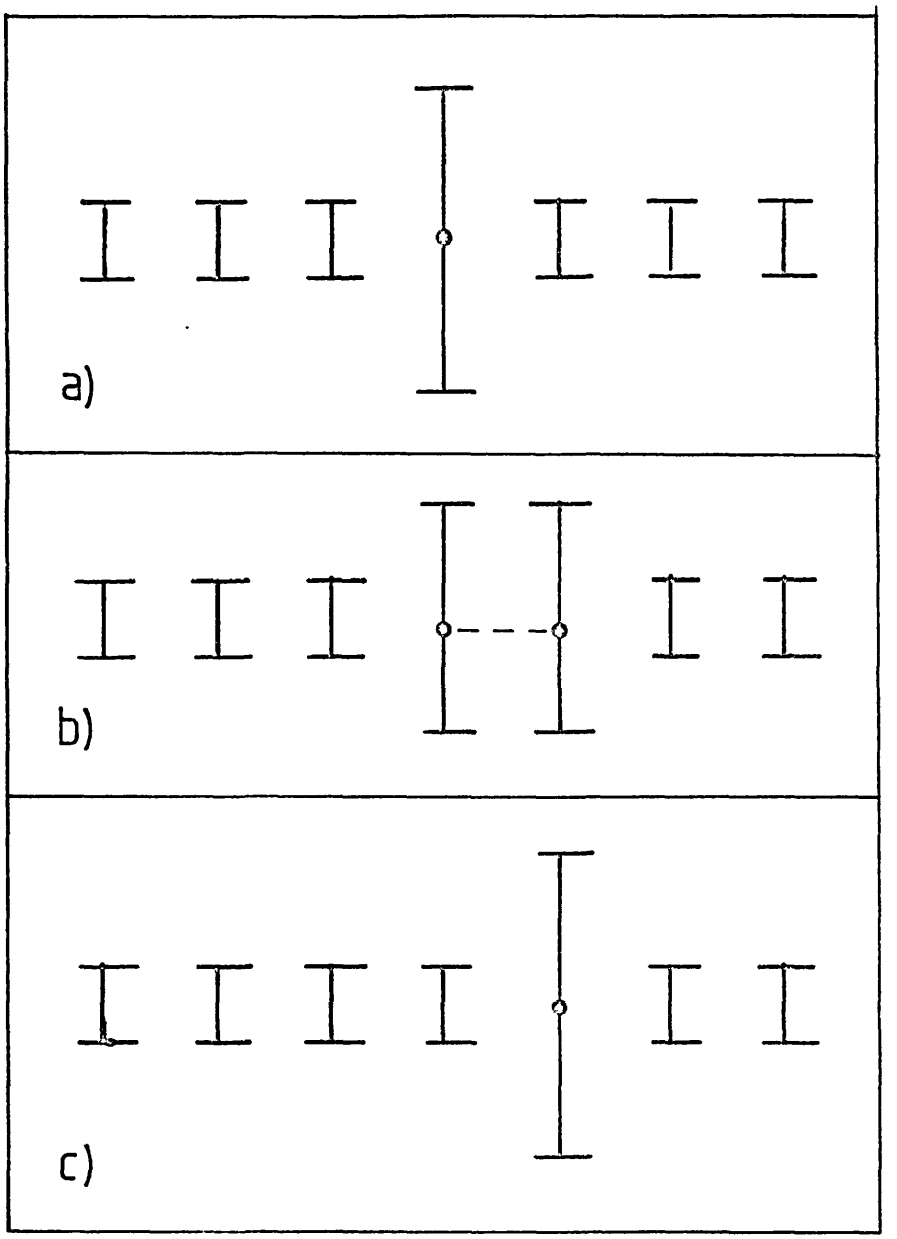

FIGURE 14 : Schematic diagram of the Molecular Crystal model of polaron propagation.

The jump probability can be written as the product of two terms; the probability for the occurrance of a coincidence event and the probability P_2 of charge transfer during this event. The total probability can be written

$$P = \frac{W_o}{2\pi} \exp\left\{-\frac{W}{kT}\right\} P_2 \qquad - 1.62$$

where $W_o/2\pi$ is an average phonon frequency, and W is the minimum energy necessary to obtain two equivalent sites. The hopping energy W is related to the small polaron binding energy E_b by

$$W = \frac{E_b}{2} \qquad - 1.63$$

In the adiabatic regime, where the carrier can follow the motion of the lattice, the probability of jumping during a coincidence is high, and one can set $P_2 = 1$. In the non-adiabatic regime, where the carrier is slow, one expects $P_2 << 1$. Holstein has derived the following expression for P_2 in this regime

$$P_2 = \frac{2\pi}{\hbar W_o} \left\{\frac{\pi}{WkT}\right\}^{\frac{1}{2}} J^2 \qquad - 1.64$$

where the electronic transfer integral J is a measure of the overlap of the wavefunctions.

Using this equation one obtains

$$\mu_c = \frac{ea^2}{kT} \frac{1}{\hbar} \left[\frac{\pi}{WkT}\right]^{\frac{1}{2}} J^2 \exp\left\{-\frac{W}{kT}\right\} \qquad - 1.65$$

for the conductivity mobility in the non-adiabatic regime. Thus the mobility will increase exponentially over a wide temperature range. This thermally activated behaviour is one of the essential features of small polaron transport. In the temperature range where kT becomes comparable with W, the pre-exponential term which varies as $T^{-3/2}$ will become dominant.

The calculation of the Hall mobility of the small polaron has proved to be a difficult theoretical problem. It has been found that the local geometry of the atoms is extremely important, and different arrangements can lead to different results. Freidman and Holstein (1963) found that in the non-adiabatic case

$$\mu_H = \frac{ea^2}{\hbar} J \left[\frac{\pi}{12kTW}\right]^{\frac{1}{2}} \exp\left\{\frac{-W}{kT}\right\} \qquad - 1.66$$

for a triangular lattice, and the sign of the Hall coefficient to be related to the number of nearest neighbours. Thus for the triangular lattice (two nearest neighbours) one finds a positive Hall coefficient for electrons, whereas for a square lattice (three nearest neighbours) the coefficient is negative! The above equation shows that the Hall mobility is thermally activated with an activation energy which is only one third of that associated with the conductivity mobility. Since the pre-exponent decreases with increasing temperature, the Hall mobility is expected to have a maximum at $kT = W/3$. Further, since $J >> kT$, the Hall mobility should be larger than the conductivity mobility.

Another transport property which has received special attention in the experimental studies of small polarons (see for example the review by Spear 1974) is the thermoelectric power S. For small polarons this is expected to have the form

$$S = -\frac{k}{e}\left\{\frac{E}{kT} + A\right\} \qquad - 1.67$$

(Nagels 1979) where E is the energy associated with the thermal generation of the carriers. The kinetic term A may be very small if there is no transfer of vibrational energy associated with a small polaron hop.

This chapter has summarised the main features of the theory of carrier transport in amorphous semiconductors, but has made no attempt to describe specific density of states models which have been proposed to explain the electrical properties of arsenic triselenide. This aspect will be treated in the next chapter, which also presents a summary of recent experimental results which are relevant to the present study.

CHAPTER 2

This chapter presents a review of the physical and electrical properties of arsenic triselenide. After an introductory section on the chalcogenide glasses in general, section 2.2 summarises what is known about the structure of As_2Se_3 prepared by different methods. The next section (2.3 to 2.6) summarise the most important recent work on the d.c. conductivity, thermopower and Hall effect (2.3), drift mobility (2.4), photoconductivity (2.5) and photo-induced absorption and ESR (2.6). Section 2.7 which concludes the chapter reviews the most important features of recent theoretical models of gap states with negative effective correlation energy.

2.1 THE CHALCOGENIDE GLASSES

Arsenic triselenide (As_2Se_3) is a member of a group of materials called the chalcogenide glasses. The chalcogens are the elements which make up group VI of the periodic table - sulphur (S), selenium (Se) and tellurium (Te). Within certain ranges of composition it is possible to form glasses by combining these elements with one or more of the elements As, Ge, Si, Tl, Pb, P, Sb and Bi among others. This glass forming tendency is thought to be due to the low co-ordination number of the chalcogens.

The terms 'glass', 'glassy' and 'vitreous' are often used synonymously for amorphous or non-crystalline. We shall, however, always reserve these words for the technical definition of a distinct thermodynamic phase. The existence of such a vitreous state, with a fairly well defined glass transition temperature (Tg), has been well documented for the chalcogenides, but not for the tetrahedrally bonded semiconductors such as Si or Ge. This is reflected in the ability to prepare the chalcogenide glasses from a semiconducting melt by rapid cooling (quenching) to temperatures below Tg. For semiconductors such as silicon, quenching from the melt (in this case metallic, with a different short range order from the desired semiconductor) cannot be achieved sufficiently quickly to freeze in an amorphous atomic arrangement, and polycrystallinity results (Brodsky(1979)). However, both the semiconducting chalcogenides and the tetrahedrally bonded semiconductors can be prepared in the form of amorphous thin films by various deposition methods such as thermal or electron beam evaporation, d.c. or r.f. sputtering, plasma decomposition of gases, chemical vapour deposition etc. (Mott and Davis (1979), Owen (1973)).

Of the binary glasses, arsenic triselenide, arsenic trisulphide and arsenic tritelluride have been the most extensively studied, and are often regarded as prototypes for the more complicated multicomponent chalcogenide glasses which have been studied in connection with the phenomenon of electrical switching (Fritsche (1974), Adler, Schur, Silver and Ovshinsky (1980)). It is also useful to study these binary glasses because

comparisons may be made with the properties of the corresponding layered structure crystals (Weiser (1979)).

In general, the chalcogenide glasses obey the so-called '8-N bonding rule' proposed by Mott (1969) according to which all electrons are taken up in bonds so that large changes of conductivity with small changes in composition do not occur. This was first established by the pioneering work of Kolomiets and co-workers which has been summarized by Kolomiets (1964).

In the glassy state, the chalcogen atoms will possess a well-defined co-ordination number. In the ground state the electronic configuration of the chalcogen is represented by s^2p^4. In the glasses of the type

$$A_2^{V} \quad B_3^{VI}$$

(where A = As,Sb; B = S, Se,Te) the structure will consist of a network showing (ideally) complete satisfaction of the two - and threefold bonding requirements of the B and A species. Each chalcogen atom will be bonded to two As atoms while each As atom is linked to three chalcogens. The chalcogen is thus twofold coordinated, and each atom will possess a nonbonding electron pair in a so-called lone pair orbital.

This 'ideal' network will of course contain structural defects as in any other crystalline or amorphous semiconductor because of its method of preparation. The position of the localised states deep in the mobility gap which will result from these defects is a difficult theoretical problem, and will be discussed in greater detail in section 2.7.

A summary of various properties of vitreous arsenic triselenide such as optical band gap, dielectric constant etc. may be found in table 1.

2.2 THE STRUCTURE OF ARSENIC TRISELENIDE

Arsenic triselenide crystallizes in the orpiment structure which consists of layers, which are a cross-linked structure of chains along

TABLE 1

Properties of Arsenic Triselenide

Density		-	4800 kg m^{-3}
Debye temperature		-	130K
Speed of sound		-	1.36 x 10^{3} m s^{-1}
Optical Band-gap	amorphous	-	1.8 eV
	crystalline	-	2.1 eV
Dielectric constant		-	11.2
Dielectric relaxation time (300K)		-	14 hours
Melting point		-	360°C
Glass transition temperature		-	187°C

the a-axis and helices along the c-axis.
These layers are stacked together and bonded by weak van der Waals' forces (see for example Weiser (1979)).

The structure of amorphous arsenic triselenide is not so well characterised. When arsenic triselenide is prepared in either a vitreous form (by quenching from the melt) or an amorphous form (by evaporation or r.f. sputtering), it will not possess the long range order observed in the crystal.

For any binary system A_x, $B_{(1-x)}$, analysis of the radial distribution function (RDF) from diffraction studies will be complicated by the difficulty of separating contributions from A-A, B-B and A-B bonds. A review of diffraction studies of the chalcogenide glasses has been given by Wright and Leadbetter (1976). In principle, EXAFS (extended X-ray fine structure) measurements should be capable of making the distinction between bond-types, but problems with the analysis have thus far not allowed conclusive results to be obtained (Mott and Davis 1979, p 445). For arsenic triselenide, most of our knowledge of the local atomic arrangement comes from NQR (nuclear quadrupole resonance) experiments and infra red and Raman spectroscopy.

Nemanich, Connell, Hayes and Street (1978) have studied the EXAFS and Raman spectra of arsenic triselenide prepared by evaporation onto substrates held near room temperature - and have studied the effect of annealing the samples near the glass transition temperature on these spectra. Their EXAFS results could not be unambiguously interpreted, but did seem to suggest 10 - 15% more homopolar bonding in the as-deposited films than in the crystal. The amount of homopolar bonding appeared to decrease with annealing, but did not disappear entirely even in bulk glass samples. It has been conjectured that this may be due to the presence of As_4Se_6 molecular units in the as-deposited films - analogous to the molecular ordering observed in As_2S_3, but to a much lesser extent due to the smaller electronegativity difference between As and Se (Apling, Leadbetter and Wright (1977)).

The structure of the bulk glass has been studied extensively

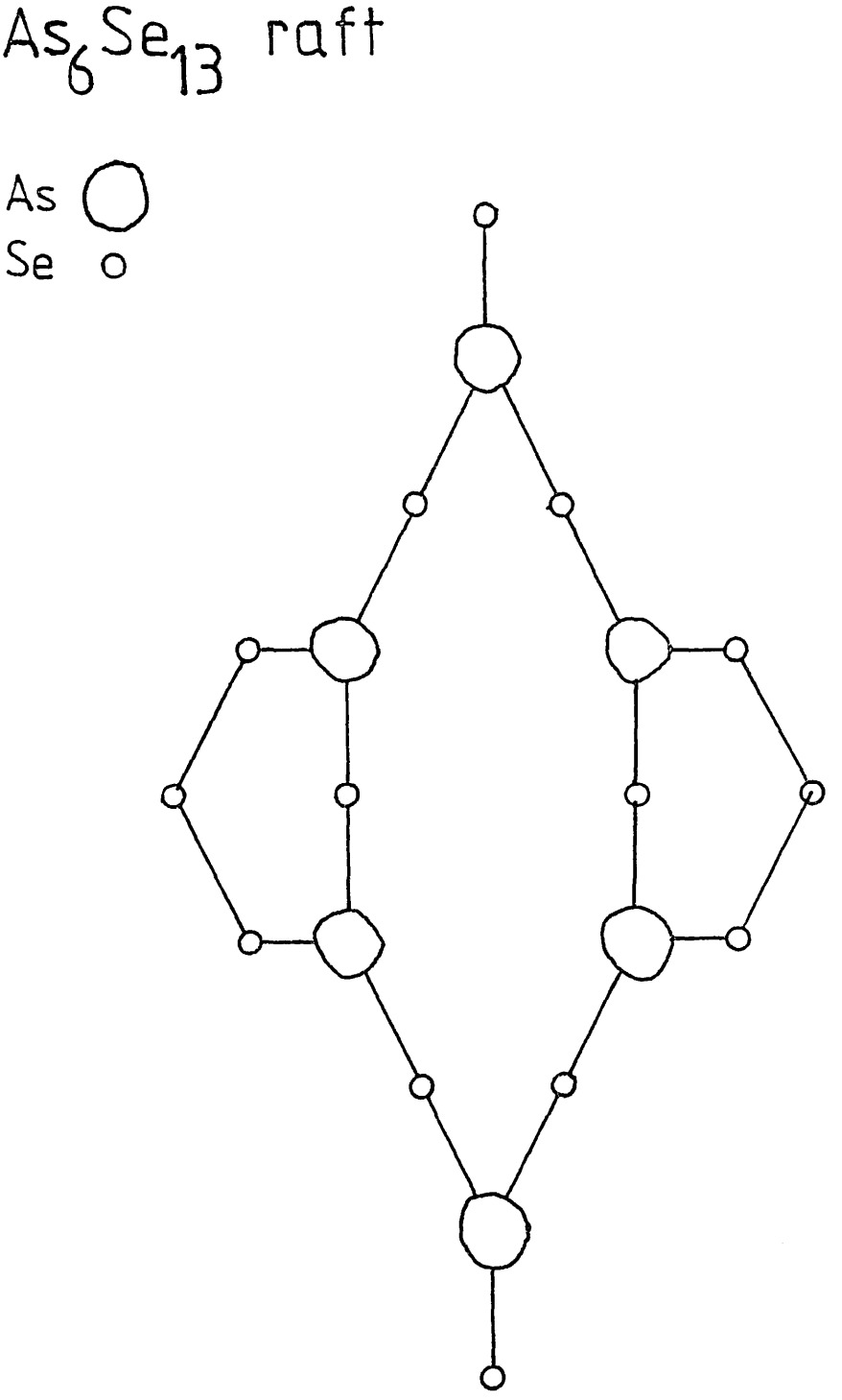

FIGURE 16 : One of the $As_6Se_{12}(\frac{1}{2}Se)_2$ rafts thought to occur in vitreous As_2Se_3 from I.R. absorption studies.

by Taylor, Bishop and Mitchell (1971). In these experiments, far infra red vibrational modes were observed in As_2Se_3 at temperatures above the glass transition temperature. The results showed that there were layered structural units present even above T_g. Thus as the glass is quenched one would expect a number of these 'rafts' to be frozen into the network, and provide a significant amount of medium range order. The experimental evidence in support of this model has been reviewed by Phillips (1979) and Szeftel (1981), who propose a structural model consisting of As_6Se_{13} rafts (shown in figure 16). In this model, vitreous arsenic triselenide is envisaged as a bundle of polymeric chains, containing these 'rafts' or puckered monomers. The model can thus account for the presence of Se-Se bonds and the presence of two non-equivalent As sites (Szeftel 1981), but would lead to a selenium rich glass. Phillips has suggested that this may be overcome by the ad-hoc introduction of a number of As_4Se_4 molecules situated in voids in the structure, but this is not supported by recent NQR measurements (Rubinstein and Taylor 1974).

We know of no published work on the structure of r.f. sputtered arsenic triselenide, although one may guess that the layered structures described in the previous section would only occur in films annealed near the glass transition temperature for long periods.

2.3 THE CONDUCTIVITY, THERMOPOWER AND HALL EFFECT

The temperature dependences of the d.c. conductivity, thermopower and Hall effect in amorphous As_2Se_3 observed in a number of previous investigations have been summarised in figures 17, 18 and 19 (these diagrams have been taken from a recent paper on the Hall effect by Mytilineou and Roilos (1978)). The thermopower indicates that undoped arsenic triselenide is p-type, while the Hall coefficient displays the anomalous behaviour described in chapter 1.

At high temperatues, the d.c. conductivity of vitreous As_2Se_3 obeys the relation

$$\sigma_1 = \sigma_o \exp\ (-\Delta E/kT)$$

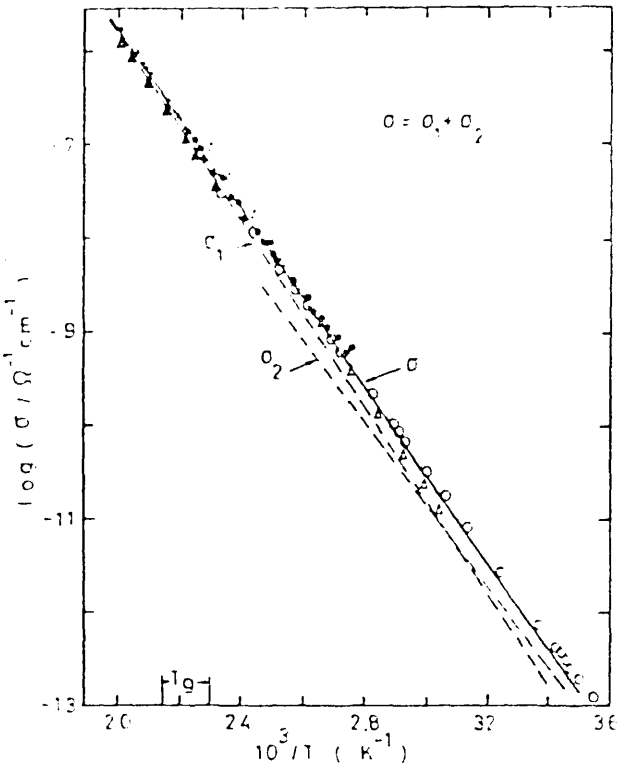

FIGURE 17

FIGURE 18

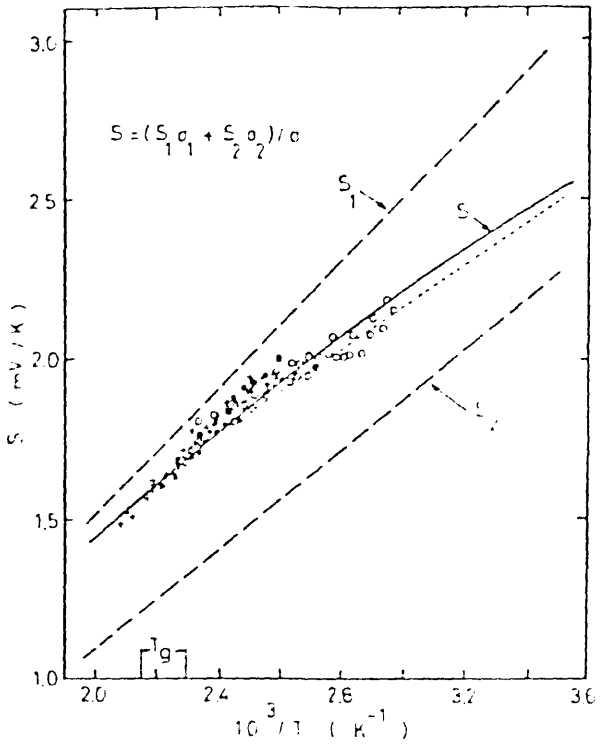

FIGURE 19

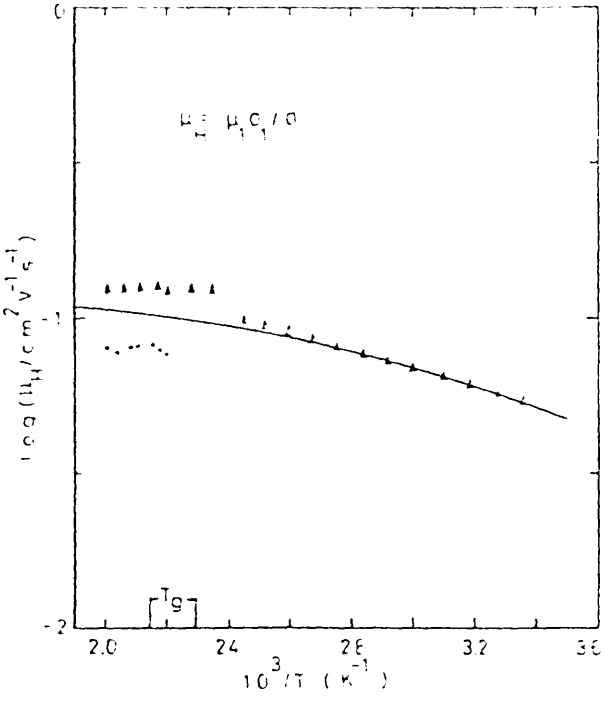

Temperature dependence of the (*a*) d.c. conductivity σ, (*b*) thermopower S, (*c*) Hall mobility μ_H for amorphous As_xSe_{1-x}. Data: + + +, Callaerts *et al.* (1972) and Nagels *et al.* (1971). – – –, Kolomiets and Raspopova (1972); ●, Hurst and Davis (1974); ○, Seager and Quinn (1975); ▲, Roilos and Mytilineou (1974); △, Kalffke and Wood (1977). Theoretical lines (continuous and dashed) as described in the text.

where ΔE = 0.95 eV, and $\sigma_o = 10^3 - 10^4\ \Omega^{-1}cm^{-1}$ (Edmond 1966). At lower temperatures (T < 300K), the graphs start to curve away from this straight line, as shown in figure 17. There have been two explanations which have been proposed to account for this curvature.

The first model is one which involves two 'conduction channels'. Marshall and Owen (1971, 1975), Nagels, Callaerts and Denayer (1974) and Mott and Davis (1979, p453) consider the high temperature results to be due to conduction at a mobility edge - because of the high value of the conductivity pre-exponent (as discussed in section 1.3 in the previous chapter). Using this model, the reduction in activation energy with decreasing temperature is thought to be due to the contribution made by another conduction mechanism - that of hopping conduction through a set of localised states far from the Fermi-level. Thus the total conductivity may be written as the sum of two terms (drawn as dotted lines in figure 17), corresponding to conduction in extended and localised states according to equations 1.14 and 1.41 respectively. A graph of $\ln(\sigma)$ versus 1/T will yield a straight line if $E_c - E_f$ is a linear function of T in the temperature range being studied. As discussed in chapter 1, the gradient of such a graph will be $E(0)/k$ and the intercept will be given by $\sigma_o \exp(\gamma/k)$.

At lower temperatures, the conductivity will be given by

$$\sigma_2 = \sigma_{hop} \exp\left\{\frac{-(E_f - E_x) + W}{kT}\right\}$$

as discussed in chapter 1. This will again lead to a straight line on a $\ln(\sigma)$ vergus 1/T graph (because the hopping activation energy W is only weakly temperature dependent), with an activation energy of $(E_f - E_x) + W$, and once again the slope and intercept will be affected by the temperature dependence of the optical band gap. The magnitude of the intercept in this region is difficult to calculate theoretically, but it is expected to be two to three orders of magnitude less than that expected for extended state conduction.

The thermopower expected on the basis of this model is the weighted sum of the contributions from extended states (S_1) and localised states (S_2)

$$S_1 = \frac{k}{e}\left\{\frac{E_f - E_v}{kT} - \frac{\gamma}{k} + A\right\}$$

$$S_2 = \frac{k}{e}\left\{\frac{E_f - E_x}{kT} - \frac{\gamma}{k} + A\right\}$$

such that

$$S_{TOT} = \frac{S_1\sigma_1 + S_2\sigma_2}{\sigma_1 + \sigma_2}$$

The constant A has been taken as unity and $\gamma = 5.51 \times 10^{-4}$ eV/K in the theoretical fit to the curve in figure 18.

At high temperatures, the activation energy for the thermopower should equal that for the conductivity - whereas at lower temperatures where hopping should predominate the conductivity activation energy should be greater by an amount equal to the hopping energy. Unfortunately, previous investigators were in conflict about whether the activation energies were the same at high temperatures or not (see Mytilineou and Roilos (1978) for a review of this problem). The behaviour expected on the basis of this model is shown as the solid lines in figures 17, 18 and 19 using the following values:-

$\sigma_o = 1.5 \times 10^4\ \Omega^{-1}\ cm^{-1}$ $\qquad$ $\sigma_{hop} = 200\ \Omega^{-1}cm^{-1}$

$E_f - E_v = 0.99eV$ $\qquad$ $W = 0.09$ eV $\qquad$ $E_f - E_x = 0.78$ eV

The other model which can explain most of the details of the results shown in figures 17, 18 and 19 is that of small polaron hopping. Seager, Emin and Quinn (1973), Seager and Quinn (1975) and Klaffke and Wood (1977) have argued that the graphs are continuously curved, and consequently are best explained by a small polaron model of conduction as described in section 1.6.4 of chapter 1.

According to this theory (as we saw in the previous chapter),

the conductivity should essentially be thermally activated, the activation energy being the sum of the energy required to generate the carriers plus a small polaron hopping energy W. The conductivity pre-exponent should be in the range $10 - 10^2\ \Omega^{-1}\ cm^{-1}$, which agrees with experiment if the temperature dependence of the band gap (and mobility edge) are taken into account. The thermopower for small polaron hopping should vary linearly with reciprocal temperature. The thermopower activation energy should yield the energy for carrier generation, so that

$$\Delta E_\sigma = \Delta E_s + W$$

And finally, the Hall coefficient for holes should be negative, and the Hall mobility should possess an activation energy of W/3.

It is clear that this second approach also provides a consistent physical basis for the essential features of these transport properties, and can therefore not be ruled out. To prove in a definite way the validity of either the two conduction channel model or the small polaron model, one would need to be able to perform these transport measurements at much lower temperatures. This is unlikely to be possible in undoped arsenic triselenide because of its extremely low conductivity, but may become feasible if doping can increase the conductivity appreciably. The lowest temperature at which conductivity measurements have been reported in the bulk glass is 250K by Hulls and McMillan (1974).

The temperature dependence of the d.c. conductivity in evaporated arsenic triselenide has been recently reported by Panasyuk, Manushevich, Goglidze and Provotorov (1980). These authors found a room temperature activation energy of 0.7eV decreasing to 0.31eV between 200K and 250K in samples freshly evaporated onto room temperature substrates. After annealing, these activation energies changed to 0.79eV and 0.31eV respectively.

We know of no previous report of conductivity measurements in arsenic triselenide prepared by r.f. sputtering, although Hauser

and Hutton (1976) and Marshall and Owen (1975) have investigated arsenic tritelluride prepared in this way.

The field dependence of the d.c. conductivity has been studied by De Wit and Crevecoeur (1972), Marshall and Miller (1974), Marshall, Fisher and Owen (1974), and Hurst and Davis (1974). All these investigations found that the conductivity varies as

$$\sigma = \sigma_o \quad \exp \left\{ \frac{F}{F_o} \right\}$$

up to fields of the order of 4×10^5 V/cm for various thicknesses of specimen from 5 microns to 1 mm. A remarkable feature of this result is the apparent absence of any ohmic region. Marshall et al. expressed their results in the form

$$\sigma\ (F) = \sigma\ (O) \quad \exp \{ ea\ F/kT \}$$

$$\mu_D(F) = \mu_D(O) \quad \exp \{ ea\ F/kT \}$$

and found that a (which decreases with increasing temperature) is the same for both the mobility and the d.c. conductivity.

No full explanation of these results has yet been given, although Mott and Street (1977) have indicated how these results may be explained in terms of their model of defect centres (described in detail in section 2.7). They argue that if the ratio between D^+, D^- and D^o centres is independent of the applied field, then the effect of the field on the conductivity and drift mobility should be the same - changing the equilibrium between the concentration of free holes and D centres. The rate of release of holes should be increased by some factor such as the Poole-Frenkel term $\exp(bF^{\frac{1}{2}}/kT)$, and the rate of recombination will be proportional to the free hole concentration (because of the large excess of D^- centres into which the holes can drop). However the Poole-Frenkel term, although fairly satisfactory at high fields, gives a term in $(1 + bF^{\frac{1}{2}}/kT)$ at low fields instead of the linear behaviour observed experimentally. They point out however, that the treatment due to Onsager (1938) can

yield the correct field dependence.

The Onsager theory, originally developed to explain the departure from ohmic behaviour in weak electrolytes or solid dielectrics, yields an expression for the probability that a pair of oppositely charged carriers will dissociate by Brownian motion in the presence of their Coulomb attraction and a static electric field F. The only variable parameter in this theory is thus the initial separation r. Although the expression for the probability of escape is complicated (Pai and Enck 1975, Pai 1975), it can be reduced to a convergent series in F. While giving high field results similar to the Poole-Frenkel analysis, this theory yields for low fields a quite different term $1 + b^2 F/(8k^2T^2)$. This is linear in F, and comparing with the observed form we find

$$ea(T) = b^2/8kT$$

which gives the observed variation with T and the correct order of magnitude. Of course, such a treatment neglects any change in, for example, the position of the mobility edge with field. The Onsager formulae should therefore reproduce the behaviour only approximately if the effect of the field on the mobility edge is important.

An exponential field dependence of the conductivity on the applied field is also to be expected for space-charge limited injection currents with a uniform distribution of traps near the Fermi-level. However, if this were the case in arsenic triselenide, non-ohmic conduction would depend on the sample thickness, whereas experiment shows a thickness independent conductivity (Marshall and Miller 1973).

2.4 DRIFT MOBILITY

Drift mobility experiments in arsenic triselenide are usually made using the time of flight or transient charge technique described in detail in chapter 3. Many investigations of the drift mobility in undoped arsenic triselenide have been reported in the last ten

years. These include the work of Marshall and Owen (1971), Pai and Scharfe (1972), Pfister (1974), Fisher, Marshall and Owen (1976), Pfister and Scher (1977, 1978), Kolomiets, Lebedev and Kasakova (1978), as well as the present work (Sharp, Marshall and Fortuna (1981) and Sharp and Marshall (1981). In all these investigations, only hole carrier pulses have ever been observed, even for very thin samples and high applied electric fields. The drift mobility of carriers in crystalline As_2Se_3 has been studied by Marshall (1977) - in this case only electron transits could be observed.

The experimental data from the above studies are summarised in figure 20. The data of Pfister et. al. were obtained from evaporated samples annealed near the glass transition temperature, whereas all the other data were for material prepared by quenching from the melt.

The measurements of Marshall and Owen were performed on very thin samples prepared by a bubble blowing technique (typically 1 - 5 microns thick). For this reason, the transit time of the carrier pulse in this investigation was much smaller than in the other studies. One can clearly see that this had the effect of reducing the observed drift mobility activation energy to about 0.43 eV, as opposed to the value of 0.6 - 0.65 eV observed in all the other investigations. Interestingly, the high temperature measurements of Kolomiets et.al. appear to have a similarly low activation energy.

It is well known that time of flight measurements of the mobility of hole carriers in arsenic triselenide films are complicated by a significant spreading of the carrier packet as it propagates through the sample (as we have described in detail in chapter 1, section 1.6). Scher and Montroll, whose work represented the first detailed analysis of such 'dispersive transport', showed that although the current transient in As_2Se_3 could appear featureless when displayed on linear axes (see figure 9), a 'break' or discontinuity of gradient should still be observed if the same pulse is displayed using logarithmic current and time axes. Their theory predicted that the gradients of such log (I) - log (t) graphs before and after the break should

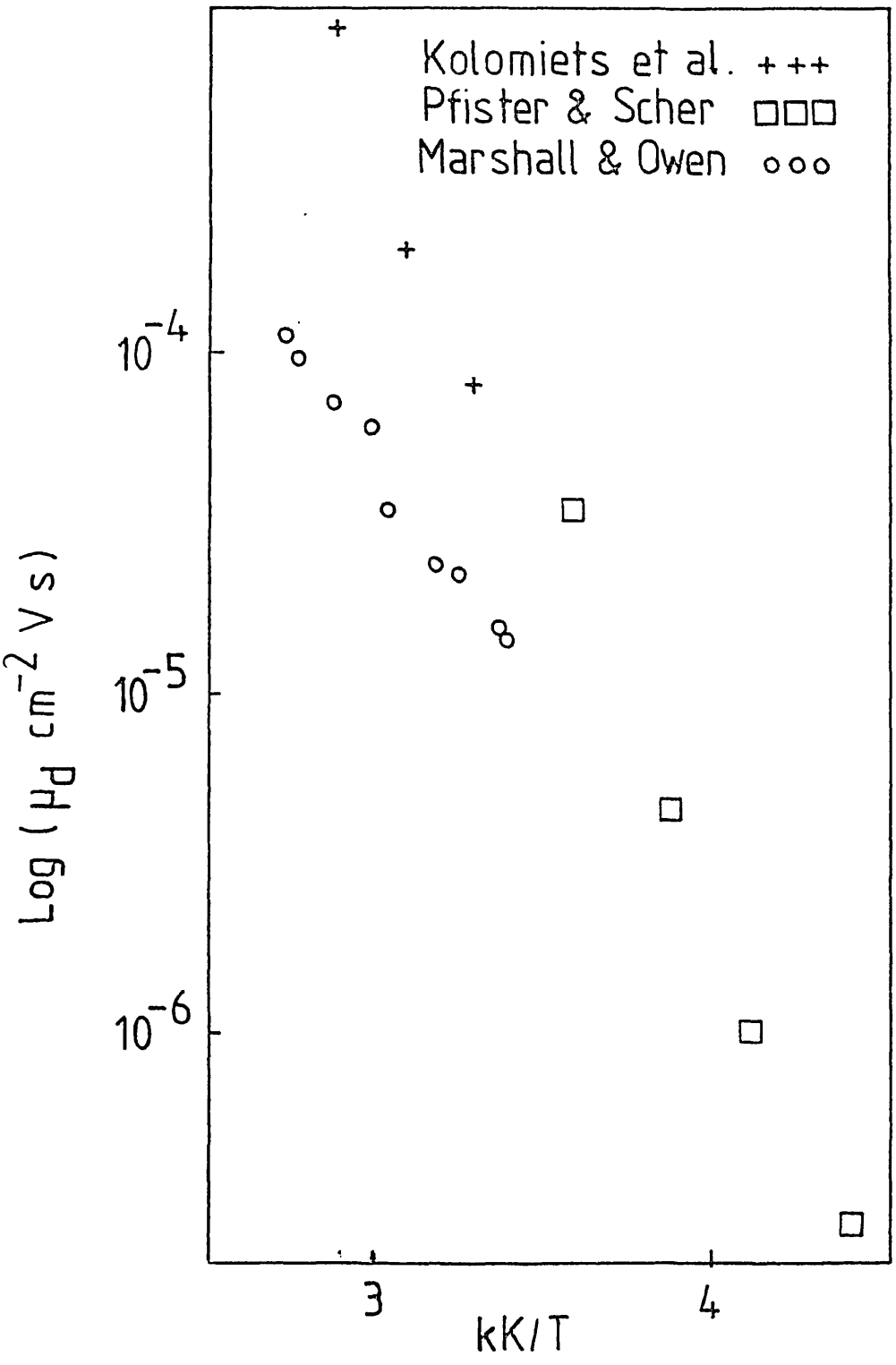
Kolomiets et al. +++
Pfister & Scher □□□
Marshall & Owen ooo
10^{-4}
10^{-5}
10^{-6}
Log (μ_d cm^{-2} V s)
3
4
kK/T

FIGURE 20

be - (1-α) and -(1+α) respectively where α, known as the dispersion parameter, is a measure of the degree of dispersion of the carrier packet.

This theory has been applied in detail by Pfister and Scher to the case of transit pulses in arsenic triselenide. These authors observed the value of α calculated from the gradient of the log (I) - log (t) graphs before and after the discontinuity of gradient to be equal (in other words, the gradients sum to two). In addition they found α to be insensitive to both the applied electric field and the specimen temperature.

As predicted by the hopping model of Scher and Montroll, these authors found the drift mobility to be <u>thickness</u> dependent such that

$$t_T \propto \left\{\frac{E}{L}\right\}^{-n}$$

where α may be found from n using

$$\alpha = \frac{1}{n}$$

Pfister and Scher did however find it difficult to explain their results on the basis of a pure hopping model, because the large drift mobility activation energy (0.6eV) could not be accounted for by a hopping energy alone. Similarly, a simple hopping model could not account for the small number of localised states (about $10^{16}cm^{-3}$) which are observed in photoinduced ESR and thermally stimulated depolarisation experiments - to get the required mobility by hopping alone would require about $10^{20}cm^{-3}$ localised states. They therefore considered either trap-limited band transport or trap-limited hopping to be more likely, and because they observed a temperature independent α, they concluded that trap-limited hopping was the most likely mechanism. This conclusion was supported by the pressure - dependence of the drift mobility and conductivity reported by Pfister (1974). It should however be pointed out that these measurements were made at room temperature, and that for films prepared in slightly different ways the transition from extended state conduction to hopping is

likely to occur at slightly different temperatures.

In contrast, Kolomiets, Lebedev and Kasakova (1978) observed a temperature dependence of the transit pulse shape in arsenic triselenide. It should be borne in mind that the method of sample preparation in these two studies differed significantly (although the method of preparation of the chalcogenide glasses seldom influences the electrical properties to a significant extent). The samples used by Pfister and Scher were prepared by evaporation of the bulk glass onto aluminium foil which was subsequently removed by flexing the foil, whereas Kolomiets et.al. used thin slices of arsenic triselenide cut from the bulk glass. The Kolomiets group actually observed a rather complicated variation of pulse shape with temperature - they saw dispersive behaviour below 280K and above 350K, but fairly well defined transits at intermediate temperatures.

The field dependence of the drift mobility in evaporated arsenic triselenide has recently been studied by Pfister (1977), who explained it on the basis of the CTRW theory of Scher and Montroll. He found that if an exponential field dependence for the probability of nearest neighbour hopping of

$$\exp \{epF/2kT\}$$

is introduced, one would expect a field dependence of the transit time of the form

$$t_T \propto L^{1/\alpha} (\sinh espF/2kT)^{-1/\alpha} \exp \{E_o/kT\}$$

where p is the average hopping distance in the real system, α is the dispersion parameter and E_o is the activiation energy at zero field.

This expression is similar to one derived recently by Funabishi and Rao (1976), who incorporated fluctuations in the potential barrier between sites in one dimension, giving

$$t_T \propto (\sinh \{esp\ F/2kT\})^{-1} \exp \{E_o/kT\}$$

where $s > 1$ is a function of the randomness of the barrier heights and applied fields. At sufficiently large fields, both this

treatment and the three dimensional treatment of Pfister approach a similar exponential field dependence where $s = 1/\alpha$.

Although Pfister's results exhibited such sinh behaviour for very thin samples (less than about 10 microns), for thicker samples it was very difficult to distinguish between this behaviour and the exponential behaviour reported by Marshall and Miller (1974).

The observation of drift mobility in a time of flight experiment implies that the contacts to the sample must have a 'blocking' or non-ohmic character. Paradoxically, the gold-As_2Se_3 contacts used in this study have previously been considered to show ohmic behaviour in steady-state electrical measurements (Hirst and Davis (1974)) but markedly non ohmic for transient time of flight studies. The nature of the gold-amorphous arsenic triselenide contact has been considered in detail by Abkowitz and Scher (1977) and Abkowitz and Scharfe (1977), who used the temporal response of the contact to step field excitation in the dark to probe the nature of the contact.

The idealised response to step excitation for a number of different cases is illustrated in figure 22, together with the typical response of a gold - As_2Se_3 contact for different time scales. The response of the contact appears qualitatively similar to the transient space-charge limited current (SCLC) depicted in curve d. Nevertheless, there are differences in the field and sample thickness dependence of both a) the time required for the dark current to reach a maximum value, and b) the magnitude of that value, which suggest that a small-signal approximation model is more appropriate.

These authors treated the problem as a convolution of the stochastic transport model of Scher and Montroll with a time dependent source of charge at the contact interface. They found that their results could be explained as follows. The time evolution of the current following the application of the field is initiated by the transit of a finite charge stored at the gold-a-As_2Se_3 interface. Under steady state conditions, the charge reservoir at this interface

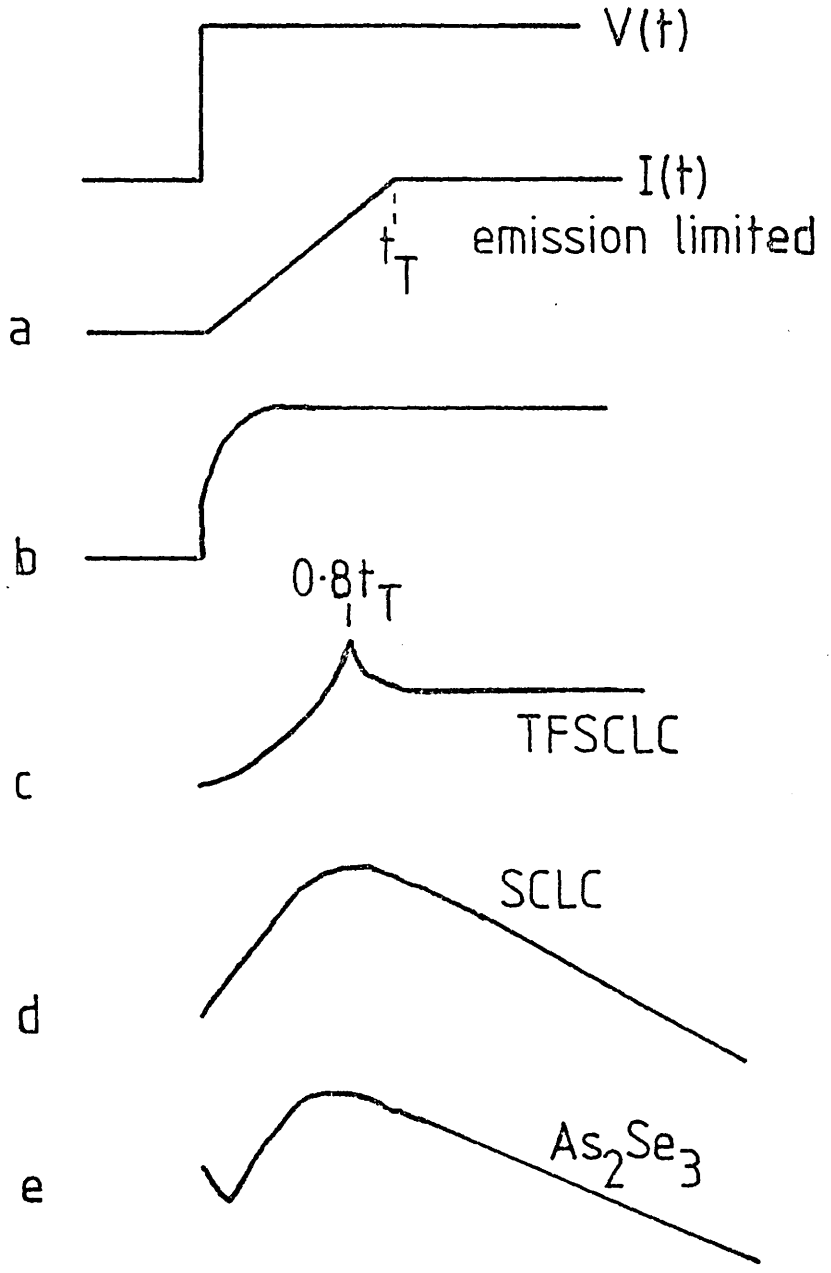
V(t)
I(t)
t_T
emission limited
a
b
$0{\cdot}8t_T$
TFSCLC
c
SCLC
d
As_2Se_3
e

FIGURE 22

becomes depleted, and the value of the current is determined by the rate carriers are emmitted from the contact. In other words, the contact may be considered a finite-reservoir emmission limited one.

2.5 PHOTOCONDUCTIVITY IN ARSENIC TRISELENIDE

Photoconductivity is the change in the electrical conductivity when a material is exposed to electromagnetic radiation, brought about by the generation of excess (non-equilibrium) carriers. That is

$$\Delta\sigma_{pc} = e(\Delta n \, \mu_e + \Delta p \, \mu_n)$$

Under steady state conditions, the excess carrier densities are equal to the generation rate multiplied by the average lifetime of the carrier. This lifetime is limited by recombination, which may occur in general through one of three competing processes:

1. Direct (band to band) recombination of a free electron and a free hole.

2. Capture of a free electron by a localised centre containing a bound hole, or vice versa.

3. Recombination of a bound hole and bound electron.

Studies of the photoconductivity of insulators and semiconductors have in the past been very successful in determining the recombination centre parameters in simple systems with one dominant recombination level. However, when several different defect centres act as trapping and/or recombination levels, the rate equation analysis can become extremely complicated. It is mainly for this reason that photoconductivity measurements in materials such as amorphous arsenic triselenide must be complimented

by other measurements, such as thermally stimulated depolarisation or drift mobility.

A large amount of work has been done in the past ten years on the photoconductivity of As_2Se_3, largely due to the interest in this material for xerographic applications. Photoconductivity in the chalcogenides has been studied by Main and Owen (1973), Main (1974), Simmons and Taylor (1972, 1974), Taylor and Simmons (1974) and Arnoldussen, Bube, Fagen and Holmberg (1974). More recently, the photoconductivity in the As:Se system has been investigated by Kitao, Ikeda, Hasegewa and Yamada (1978), Onari, Yamamoto, Kitahara and Arai (1980) and Petursson (1980, 1975).

When measured as a function of temperature, the photoconductivity of the chalcogenide glasses shows a typical behaviour shown in figure 23. At high temperatures, the photoconductivity is small compared to the dark conductivity, and increases exponentially as 1/T and linearly with the incident light intensity. At lower temperatures, the photoconductivity exhibits a maximum, and subsequently decreases exponentially with 1/T. In this regime, the photoconductivity is proportional to the square root of the incident light intensity. At still lower temperatures, the curves seem to level off to a constant value.

To explain these characteristics, Weiser, Fischer and Brodsky (1970) proposed a recombination model in which the electrical transport on either side of the maximum is of the same nature, but that the recombination kinetics change in character. For example, in an intrinsic crystalline semiconductor with only one type of recombination centre, if we assume charge neutrality (i.e. $n_o = p_o$ and $\Delta n = \Delta p$, we have

$$\frac{d(\Delta n)}{dt} = g - C_n N_r (n_o + \Delta n) - C_n n_o^2$$

where C_n is the capture coefficient (the capture cross-section times the average thermal velocity of the carriers). In the steady state $d(\Delta n)/dp = 0$, and $N_r = n_o + \Delta n$ so one gets

$$g = C_n (\Delta n^2 + 2n_o \Delta n)$$

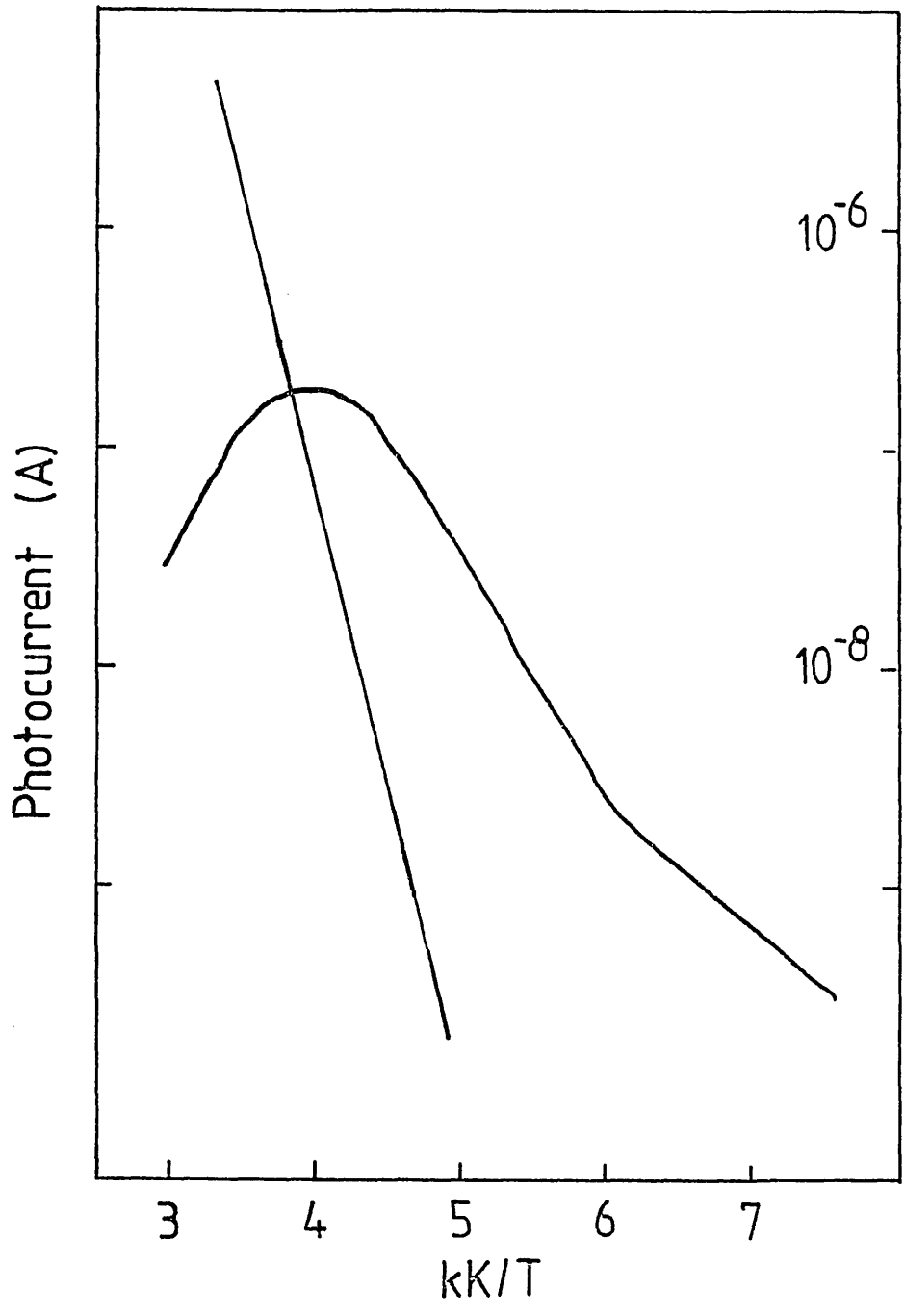

FIGURE 23

In the regime $n_o >> \Delta n$ (the monomolecular regime) this reduces to

$$\Delta n = {}^{g}/_{2C_n n_o}$$

and the photoconductivity will vary linearly with the excitation intensity. When $n_o << \Delta n$ (the bimolecular regime);

$$\Delta n = \left[{}^{g}/_{C_n} \right]^{\frac{1}{2}}$$

and the photocurrent is proportional to the square root of the light intensity.

The models which have been proposed to account for the photoconductivity described above may be classified into two main types:-

1. Models with fairly discrete trap levels (Main and Owen 1973, Main, 1974, Simmons and Taylor 1974, Taylor and Simmons, 1974 Fisher et al 1976).
2. Models with trapping centres distributed throughout the mobility gap (Weiser et al 1970, Arnoldussen et al 1974, Simmons and Taylor 1972).

All these models (summarised in detail by Petursson 1975) can account for the presence of a photoconductivity which behaves like the results shown in figure 23, although TSC (Street and Yoffa (1972) and electrical noise experiments (Main 1974) indicate the presence of fairly discrete trap levels in arsenic triselenide. Simmons and Taylor (1974) concluded that the discrete trap level model was the more appropriate for photoconductivity in As:Te:Si glasses. Main (1974) and Fisher et al (1976) considered the photoconductivity and transport properties of As_2Se_3, and concluded that the best fit to experimental data is obtained with band-localised recombination as the dominant mechanism. In this case, for the low intensity monomolecular region, we get

$$\Delta I_{ph} \propto \Delta p \propto g \exp \left\{ (E_{te} - E_f)/kT \right\}$$

and for the high intensity bimolecular region

$$\Delta I_{ph} \propto \Delta p \propto g^{\frac{1}{2}} \exp \left\{ -(E_{th} - E_v)/kT \right\}$$

where Δp is the density of excess holes, E_{te} the energy of the electron traps and E_{th} the energy of the hole traps. The values of the gradients in the two regimes yield $E_{te} - E_f = 0.37$ eV and $E_{th} - E_v = 0.66$ eV.

The work of Kitao et al (1978) and Onari et al (1980) has shown that shallow localised states within 0.4 eV of the valence band edge act as hole traps yielding a trap-limited drift mobility, whereas deeper traps operate as recombination centres and have a tendancy to accumulate carriers. They have also observed a strong dependence of the effect of light intensity with chopping frequency, namely the recombination kinetics are monomolecular at fast chopping frequencies but become bimolecular as the chopping frequency is reduced below $\sim$ 1 Hz. These authors explain this behaviour as follows - the time necessary for the process of thermal carrier generation from localised states in the gap may be longer than the time before recombination after the direct production of carriers by incident photons. The fast component may thus be due to direct recombination (which will be monomolecular because the density of the thermally generated electrons will be greater than the density of the photo-generated holes). The slow component would then correspond to the recombination of carriers from states deep in the mobility gap. Measurements of the critical chopping frequency as a function of incident photon energy appear to confirm this interpretation. A review of recombination in chalcogenide glasses has recently been given by Street (1976).

The transient photoconductivity can slso provide valuable information on localised states, and in particular Main (1974) has shown that a drift mobility may be derived from the transient rise of the photocurrent. In some cases it has been possible to observe three regimes of transient rise in a single sample of arsenic triselenide, corresponding to trap depths of 0.3eV, 0.44eV and 0.65eV. Unlike the time of flight technique however, the derivation of a mobility from the transient photoconductivity does not determine the

sign of the carriers. It is assumed that they refer to the trap-limited drift mobility of holes and this seems reasonable because of the consistency with TSC measurements.

In addition to the above investigations there have been a number of studies of the transient photoconductivity and photocurrent decay by Orenstein and Kastner (1979, 1981), Monroe, Orenstein and Kastner (1981), which are closely related to the mobility studies summarised in the previous section. In these experiments, a bulk sample of vitreous As_2Se_3 about 1mm thick equipped with coplanar graphite electrodes was used. The photoconductivity (PC) and photoinduced absorption (PA) in the samples were excited by a pulse from a dye laser - the photocurrent was detected as the voltage drop across a series resistor, while the PA was simultaneously monitored by measuring the transmission of a probe beam from a tungsten lamp. These experiments showed that the PC decays much more quickly than the PA for the same excitation pulse.

Orenstein and Kastner argued, however, that both effects were due to the same density of photoexcited carriers at all times after the laser pulse. This result is in conflict with recent measurements on thallium doped arsenic triselenide by Pfister, Liang, Morgan, Taylor, Friebele and Bishop (1978), who observed no correlation between PA or photoinduced ESR and drift mobility measurements.

To explain their measurements, Orenstein and Kastner developed a model similar to that of Tedje and Rose (which was described in section 1.5 on dispersive transport). They considered an exponential density of states in the mobility gap of As_2Se_3 similar to that sketched in figure 24. They assumed

1. The mobility decreased rapidly below the mobility edge, so that the motion of a bound carrier is limited by the rate of thermal release to extended states.
2. The capture cross-sections of all the localised states in the distribution are equal and independant of energy.

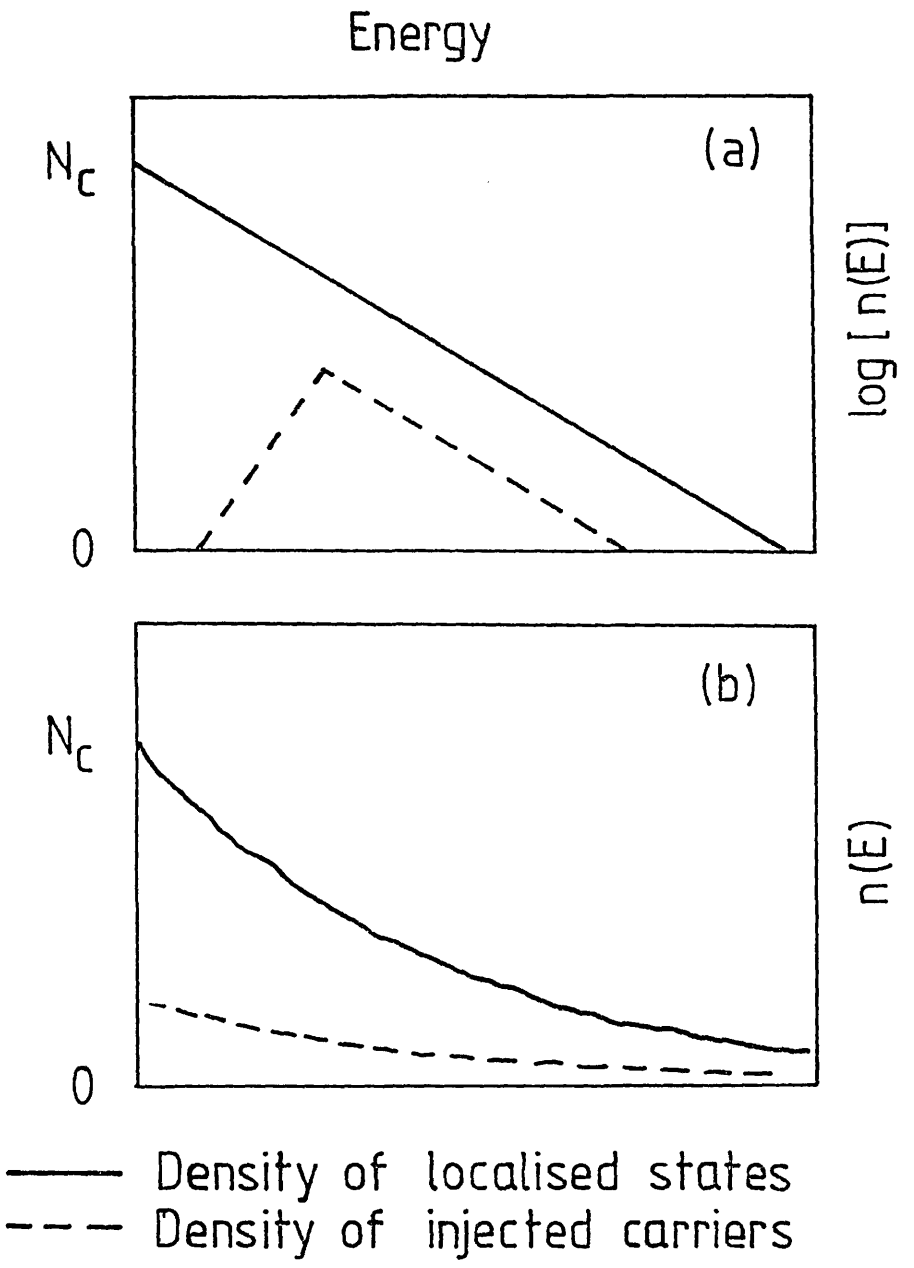
Energy
(a)
N_c
0
log [n(E)]
(b)
N_c
0
n(E)
Density of localised states
Density of injected carriers

FIGURE 24

As shown in section 1.5 of chapter 1, this model can reproduce the two straight-line regimes predicted by the Scher-Montroll analysis and observed in practice - although in PC measurements only the initial regime will be observed. The results of Orenstein and Kastner for vitreous arsenic triselenide were in substantial agreement with this work (Sharp and Marshall 1981) in that the gradient of the initial part of the log (I) - log (t) graph in vitreous material is temperature dependent. A full discussion of the similarities and differences between the present work and the results of Orenstein and Kastner appears in chapter 4.

2.6 PHOTOINDUCED EFFECTS

Arsenic triselenide displays a wealth of interesting phenomena which can be induced by disturbing equilibrium by optical excitation. Such effects include photoluminescence and photoluminescence fatigue, photoinduced absorption, photoinduced ESR, photodarkening and a number of photostructural changes. This section will present a brief review of the most important results from recent work on a number of these phenomena, and summarises the conclusions that may be drawn from such measurements about the nature of defect states in As_2Se_3.

2.6.1. Photoluminescence

Luminescence measurements in amorphous semiconductors (as in crystalline semiconductors) can yield much detailed information on localised states - information which cannot always be unambiguously deduced from transport measurements. For this reason luminescence measurements compliment transport measurements, and an understanding of luminescence mechanisms will contribute greatly towards a complete picture of the transport properties in a given material.

In luminescence experiments, carriers are excited by the absorption of light quanta with energies close to the width of the mobility gap. These non-equilibrium carriers will thermalise rapidly until

they are eventually captured by localised states in the mobility gap (recent studies by Fork et al (1981) indicate that the thermalisation time is less than 1 picosecond). When the carrier is captured, it must lose energy, and a proportion of this energy may be re-emitted as luminescence. Of course, not all the excitation energy will reappear as luminescence, and we must distinguish between radiative and non-radiative processes. The luminescence spectrum will give information about radiative processes only - the quantum efficiency will thus represent the fraction of electron-hole pairs which are captured by radiative centres.

Photoluminescence (PL) in arsenic chalcogenide glasses was first observed by the Kolomiets group in 1968. Since then PL in amorphous As_2Se_3 has been studied extensively by Kolomiets et al (1970, 1972), Street, Searle and Austin (1973, 1974), Street (1976), Cermogora, Mollot and Benoit a la Guillaume (1973, 1974, 1977), Mollot et al (1974, 1980), Kastner and Hudgens (1978) and Bishop and Mitchell (1973). The dominant feature in the luminescence spectrum is a broad band centred at about half the band gap energy. The luminescence is most efficient when excitation occurs with photons whose energy corresponds to the tail of the absorption edge. The PL spectrum of crystalline As_2Se_3 is very similar to that of the glass (Street, Searle and Austin (1973), Kolomiets (1970)), which suggests that the luminescence mechanisms and defect centres must be the same in both cases. The PL spectrum and excitation spectrum together with the absorption edge for amorphous and crystalline As_2Se_3 are shown in figure 25.

The PL intensity is a strong function of temperature, and increases by several orders of magnitude on cooling from room temperature to helium temperatures, reaching a maximum of 10 - 20%. In addition, the PL decays rapidly when the illumination is stopped (Street, Searle and Austin (1974)) - 95% of the signal decays within 1 ms, while the remainder decays with a time constant of 5 - 10 ms. Higashi and Kastner (1980) have shown that for times shorter than 1 ms after cessation of illumination, the total PL light decays as $t^{-0.89}$ over

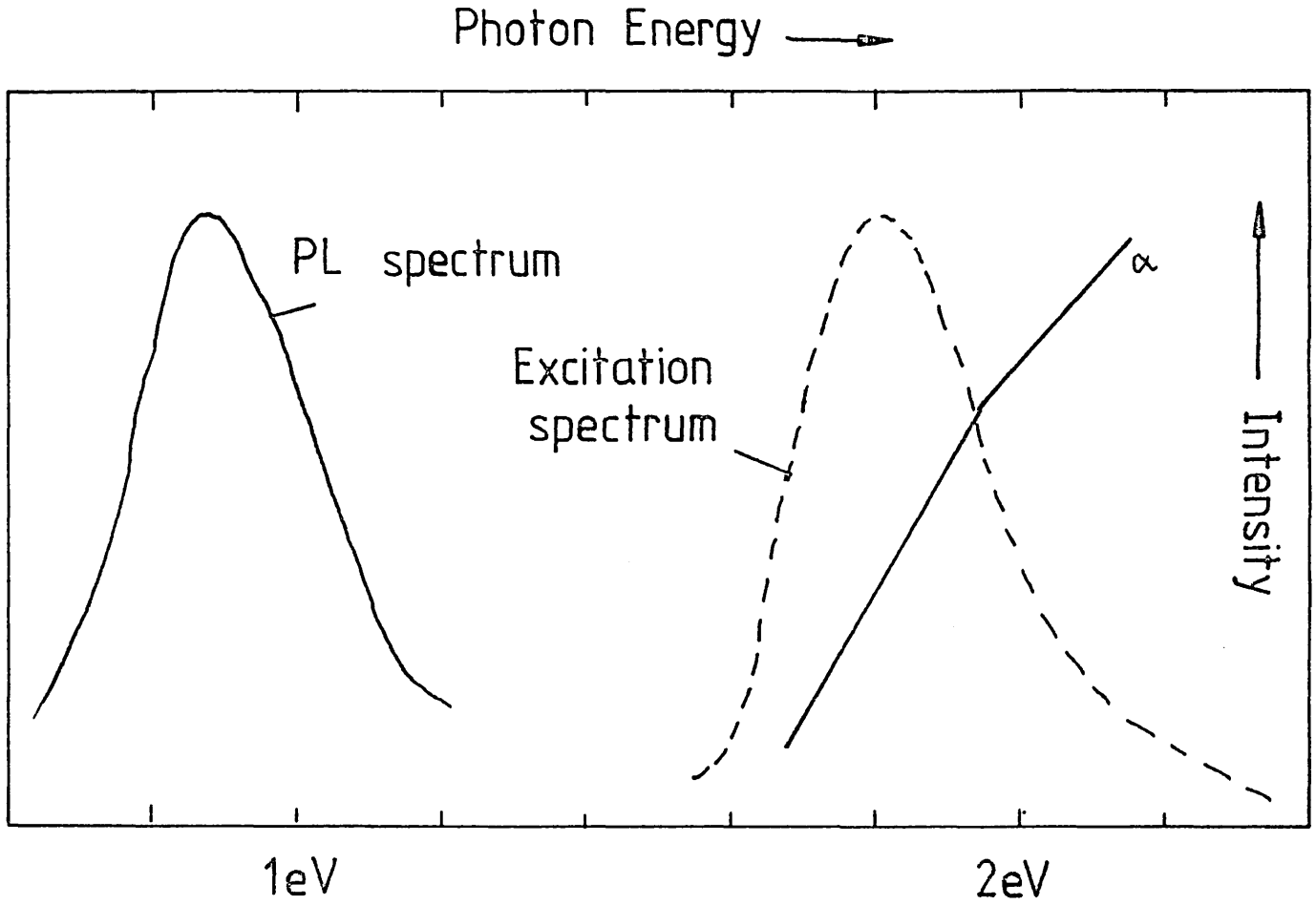
Photon Energy
PL spectrum
Excitation spectrum
α
Intensity
1eV
2eV

FIGURE 25

5 decades of time. The broad PL peak narrows dramatically with time, and its mean position shifts to lower energies.

Many of the photoinduced effects mentioned above can be explained if one introduces the concept of non-equilibrium optically induced defect states. The first indirect evidence for the existence of such states came from the property known as PL fatigue. This is simply a decay or fatigue of the PL efficiency with continuous excitation with band-gap photons (Street, Searle and Austin (1973), Cernagon et al (1973), Mollot et al (1974)). The PL fatigue has three interesting properties.

1. The rate of fatigue exhibits approximately the same dependence on excitation wavelength as the initial PL efficiency.
2. The fatigued condition is meta-stable i.e. if the excitation is interrupted and then resumed the PL intensity will not recover, but continues from the level it had reached before the illumination was switched off.
3. After fatiguing, excitation with photons of energy smaller than the band gap restores the PL efficiency.

This constituted the first evidence that the optically induced non equilibrium condition is also optically reversible and, as we shall see later, is one of the parallel properties which led to the identification at optically induced ESR centres as fatigued PL centres.

Mollot et al (1974) have carried out the most detailed studies of the PL fatigue, and have shown the fatigued PL intensity follows a t^{-b} dependence on the excitation time, where b depends on the excitation energy. These workers also performed annealing studies which established that the fatigued condition is stable below about 40K.

The implication of the result that PL efficiency can be restored by sub band gap illumination is that the PL fatigue is accompanied by the appearance of an optically induced absorption in the normally transparent below gap spectral region of the glass. This was first demonstrated by Bishop, Strom and Guenzer (1974) who showed that this absorption extended from the vicinity of the mid gap PL band up to the band edge. The application of more intense light within the induced absorption band bleaches or restores the transparency as it

restores the PL efficiency (Bishop, Strom and Taylor 1977). Fatiguing and associated effects have not been observed in crystalline As_2Se_3 (Street et. al. 1974).

2.6.2 Photoinduced ESR

Bishop, Strom and Taylor (1977 a & b) observed that band-gap light excitation of amorphous As_2Se_3 produces an ESR spectrum which was not present in the dark at low temperatures (in addition to the PL and fatiguing effects noted above). This effect has not been observed in crystalline As_2Se_3. This optically induced paramagnetism persists after illumination has ceased, and can be bleached by sub-band gap light in the same way and at the same rate that the optical absorption is bleached. This behaviour has also been investigated by Biegelson and Street (1980), and Pfister, Liang, Morgan, Taylor, Friebele and Bishop (1978). Optically detected magnetic resonance has been observed both in amorphous and crystalline As_2Se_3 by Depinna, Cavenett, Austin and Searle (1980).

There is some evidence for two superimposed resonance features in the induced ESR spectrum of amorphous As_2Se_3. The first is a fairly narrow central resonance which has been interpreted as arising from a centre consisting of an electron missing from a non-bonding chalcogen p orbital. The second feature is a broad resonance believed to be associated with an As - centre resonance broadened by a large hyperfine interaction. This indicates that there may be two types of optically induced centres in vitreous As_2Se_3 - one localised on arsenic atoms and one associated with chalcogenide atoms. The width of the arsenic resonance provides evidence that the centre is localised on a single As atom (Bishop, Strom and Taylor (1976)). Computer simulation has shown that it is possible to exclude the possibility thatthis ESR centre is localised on more than three As sites.

The first estimates of the density of optically induced spins deduced from the ESR spectra of Se, As and As_2Se_3 indicated values which 'saturated' at densities of about $10^{17}cm^{-3}$, if the excitation was continued for long periods (Bishop, Strom and Taylor (1977)). This saturation behaviour was taken to indicate a specific concentration

of defect or other structural feature (such as a dangling bond) which determined the density of optically induced paramagnetic centres, and was in substantial agreement with the density of radiative recombination centres estimated from PL studies (Kastner and Hudgens (1978)). Recently, however, Biegelson and Street (1980) and Mollot et al (1980) have observed induced spin densities larger than $10^{20}cm^{-3}$ in certain chalcogenide glasses after prolonged illumination.

Biegelson and Street have attempted to resolve this paradox by suggesting that there are two distinct mechanisms for inducing defect centres, which are characterised by a fast and a slow rate of defect creation. Their interpretation of the fast rate is exactly that of Bishop, Strom and Taylor- namely, that the photoexcited carriers are trapped at existing defects. If the spin density N_s is represented by the product of the density of centres N_t and the fraction f that are singly occupied - N_t will be constant while f increases, and one will get fairly rapid saturation. As before, one may think of the bleaching effect as the thermal or optical detrapping of those centres. Since f reaches saturation in such a short time, the slow increase of N_s observed at long lines was interpreted by these authors as a slow light induced increase in the defect density N_t. Biegelson and Street therefore concluded that prolonged illumination caused reversible structural damage which introduces specific defects into the glass.

This interpretation is supported by the fact that the shape of the ESR resonances for low densities and high densities are different. However, the general similarity of the g values and line widths suggests that the defects are generically related. Biegelson and Street concluded that these slowly induced effects were a manifestation of the same physical mechanism that gives other reversible photo structural effects (reviewed by Tanaka (1980)). Evidence for this assertion is that in each case similar light exposures are involved, the effects anneal in the same temperature range (150K as opposed to 50K for the native centres), and the slow photoinduced defects are always accompanied by photodarkening.

There are several reasons for believing that the native centres responsible for photoinduced ESR, PL fatigue and optically induced absorption are related. All these processes exhibit a similar temperature dependence. This temperature dependence implies a broad distribution of defect densities and thermal release rates. All the phenomena exhibit similar annealing behaviour, etc. The repeated parallels in the behaviour of these phenomena suggest the obvious hypothesis that during the PL fatigue process diamagnetic radiative recombination centres are converted to paramagnetic centres which are radiatively inactive. Bishop, Strom and Taylor (1977) have shown that the compositional dependence of the above effects can be understood on the same basis, providing a more stringest test of the hypothesis. The data suggests that a defect or structural anomally associated with the presence of As is involved in both processes.

The interpretation of these PL and fatiguing mechanisms and the nature of the optically induced paramagnetic centres is very complicated, and has been reviewed by Street (1976), Fisher (1979), Davis (1979), Kastner and Hudgens (1978) and Biegelson and Street (1980). A number of models have been proposed to account for the experimental data, the most important of which involve defects with negative effective correlation energy which will be described in section 2.7.

The luminescence spectrum in As_2Se_3 peaks at an energy close to half the band gap energy. Street et al (1974) first proposed that this could be due to a strong electron-phonon interaction. If the photoexcited carriers are captured by localised 'traps' before recombination, in the presence of strong electron-phonon coupling the network may deform or relax around an occupied site, thereby lowering the total energy. This leads to a Stokes' shift of the luminescence band with respect to the absorption edge - evidence for this comes from the lack of optical absorption in the luminescence region.

Three basic models have been proposed to account for the results discussed above:-

1. Mott, Davis and Street (1975) have proposed a model in which the unit responsible for radiative recombination is a defect level which is charged in the ground state.

2. Hudgens and Kastner (1978) have proposed that the radiative PL centres are composed of defect pairs (called valence-alternation pairs or VAPs) such as a four-fold coordinated arsenic atom together with a one-fold coordinated selenium atom, and are consequently electrically neutral.

3. Emin (1980) has proposed a small polaron model for photoinduced effects.

None of these models explains all the observations (Kastner 1980), but some have greater drawbacks than others. In particular, the polaron model cannot explain the proportionality between the excitation spectrum and the inverse of the absorption co-efficient. A more serious criticism is that at longer times, the PL peak shifts to higher energies using this model.

The model of Mott, Davis and Street comes closer to an adequate description of the observations. These authors propose that after photoionisation from a negative centre (the D^-), the electron is trapped in a band tail state, and the energy shift of the PL peak occurs due to thermalisation in the band tail. Although fatigue, and the existence of photoinduced ESR and absorption are explained quite naturally using this model in terms of the conversion of D^- (and perhaps D^+) states into metastable D^o centres, the doping experiments of Pfister et.al. (1978) indicate that defect pairs may account better for the independence of PL on doping. Even with the defect pair model however (discussed in more detail later in the chapter) there are discrepancies evident - for example, crystalline As_2Se_3 shows photo absorption with a spectrum very similar to that of amorphous material, but shows no photoinduced ESR or PL fatigue at all (Kastner 1980, Bishop, Shanabrook, Strom and Taylor 1981).

Fisher (1979) has proposed a compromise between the small polaron and valence alternation pair models discussed above. He points out that the band structure of crystalline As_2Se_3 (shown in figure 26) is unlike that of selenium in that there is no separate lone-pair band at the top of the valence band due to the ionicity of the As-Se bond. This separate band is thus unlikely to occur in the amorphous case either. A consequence of this band structure is that incident light may break bonds by transitions from bonding to antibonding states (leading to the photostructural effects mentioned earlier). On this

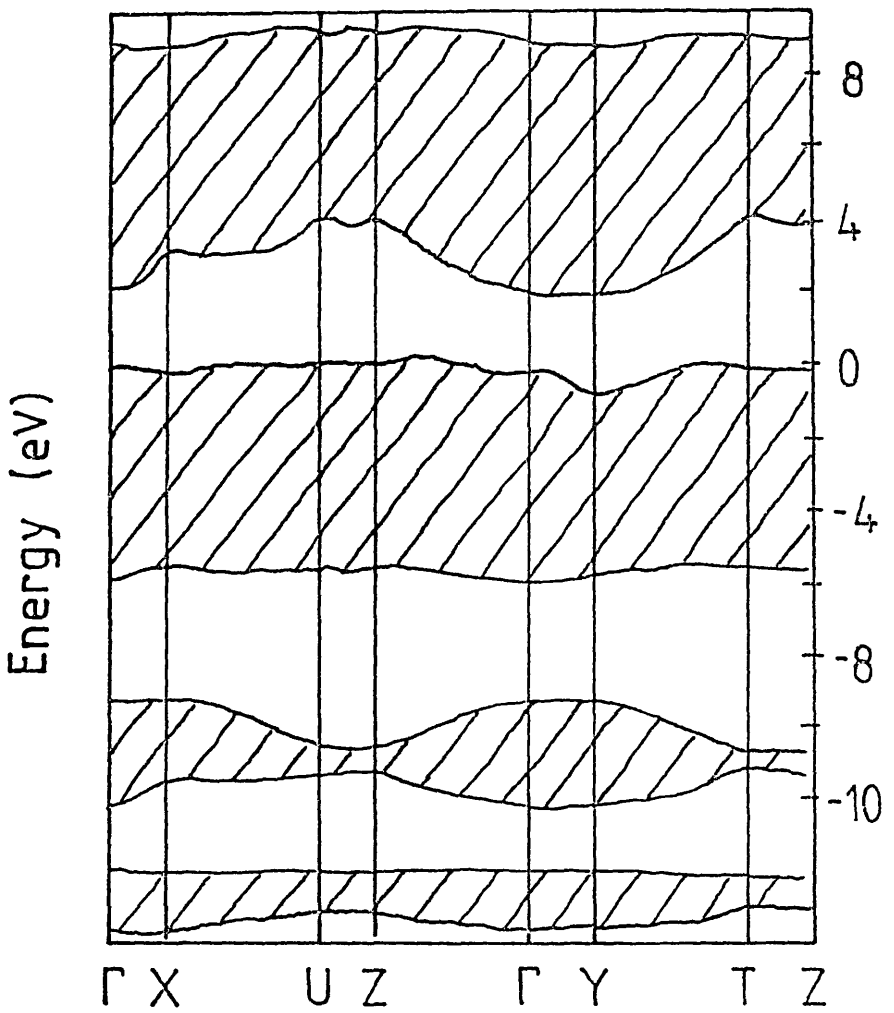

FIGURE 26 : Energy bands of crystalline As_2Se_3 after Weiser et al..

basis the defect and polaron models may be reconciled, since a photo-induced broken bond can be considered as an extreme case of electron-lattice coupling of a fundamental excitation.

It must be remembered that experiments such as photoluminescence only yield information about radiative centres, and the PL efficiency of about 10% implies that 90% of the relaxation processes are non-radiative. These non-radiative processes could dominate the transport properties in some cases, although Mott and Stoneham (1977) have shown that non-radiative and radiative recombination can occur at the same centre.

2.7 DEFECT MODELS

The diamagnetic ground state which is a characteristic of most well annealed glasses led Anderson (1975) to suggest that band-tail states may be doubly occupied: the repulsive Coulomb energy being overcome by strong bond distortion (negative effective correlation energy). As a result, a gap opens up seperating doubly occupied negatively charged bonding states from empty positively charged anti-bonding states. Since the two electron states are spin-paired, this concept accounted for the striking absence of paramagnetic centres (Argawal (1973)), and also for the apparent experimental contradiction that the Fermi-level is pinned, yet variable-range hopping is not observed. This contradiction was difficult to rationalise with the earlier Cohen, Fritsche and Ovshinsky (1969) model of overlapping one electron band-tail states.

A different approach based on Anderson's concept of a negative effective correlation energy was proposed by Mott, Davis and Street (1975) and Mott and Street (1977). Rather than put two electrons onto normal (though distorted) bonds, MDS suggested that the charged two electron states could derive from bonding defects. They considered a defect which can have three different charge states, denoted by D^+, D^o and D^-. The negatively charged defect D^- is a dangling bond associated with an undercoordinated atom - for example an Se atom bonded to one other atom, or an As atom bonded to two

others. When an electron is removed forming a D^{o} defect, there will be a weak bond to a nearby fully coordinated chalcogen atom. However this bond is not as strong as when a second electron is removed, for then both lone-pair electrons are used in bonding, and the formerly singly coordinated chalcogen atom becomes essentially three-fold coordinated - the D^{+} centre. In addition it is assumed that the reaction

$$2D^{o} \rightarrow D^{+} + D^{-}$$

is exothermic. This implies that the Coulombic repulsive energy between the two electrons is more than compensated by the lattice energy gained. This is what is meant by a negative effective correlation energy (or Hubbard U) for the defect.

In the ground state of the system, all the states are therefore either positively or negatively charged, and free spins such as the D^{o} will only occur under excitation. The electronic levels of the dangling bonds are largely determined by the lattice distortions, and the level applicable to a particular experiment depends on whether an optical or thermal process is involved (because the former will occur before the lattice has had time to relax). The model thus accounts for the absence of ESR signals and paramagnetism; the absence of optical absorption at energies below the band gap energy also follows. The electron-phonon coupling in the model is the essential feature required to explain the Stokes' shift observed in luminescence measurements. Moreover, the model predicts that the Fermi-level is pinned near the centre of the gap (Adler and Yoffa (1976)), which is consistent with transport and photoconductivity measurements.

Since all the above phenomena are related to either one or both defects, one expects on the basis of this model that there should be a strong correlation between the electrical and optical properties of the chalcogenide glasses. Kastner, Adler and Fritsche (Kastner et al 1975, 1977, 1978, 1979, 1980) have proposed a slightly different model based on chemical bond arguments. They point out that a single dangling bond is energetically unfavourable, and propose instead the concept of valence alternation pairs (VAPs) which result, for example when a pair of normally two fold coordinated chalcogen atoms combine to form one singly coordinated and one three-fold coordinated atom.

It is suggested that these states are unstable towards charge transfer and that the former would normally be negatively charged, and the latter positively charged. One expects a distribution of intersite distances ranging from non interacting isolated pairs to the nearest neighbour bound pair or intimate valence alternation pair (IVAP). Kastner et al. attribute the photoluminescence to recombination of excited interacting defect pairs, so that because the transport active traps are associated with single defects, the strong correlation between optical and transport measurements as predicted by MDS is not expected.

Neither of the above models is restricted to the amorphous state, and should therefore be equally aplicable to crystalline chalcogenides. In As_2Se_3 crystals, sets of traps 0.49 eV, 0.58 eV and 0.72 eV above the valence band mobility edge have been observed (Kolomiets (1969)). These energies correspond roughly to those observed in the glass if one takes account of the difference in optical band gap.

Although one cannot deny the existence of defects in a real amorphous solid any more than one can in a crystalline solid, an explanation of the experimentally observed properties exclusively in terms of defects is not in the spirit of the original Anderson model. Ngai and Taylor (1978) have suggested that the configurational entropy characteristic of an amorphous solid makes possible the formation of abnormal bonding configurations not present in the corresponding crystal. The specific defect states suggested by MDS and KAF represent only a small subset of the possible localised states in a glass. In addition to states which can be obtained from broken and rearranged bonds within the normal bonding configuration, these authors predict a large number of abnormal bonding configurations associated with highly distorted sites lying deep in the gap to which the application of normal bond energetics is questionable.

Perhaps the most striking feature of the abnormal bonding picture is that there exists an astonishingly large number of distinct deep gap states possible in a simple binary glass. In As_2Se_3 for example, one can construct 10 pairs of sites involving only Se atoms, 8 involving only As atoms, and 18 involving pairs of abnormal As-Se sites. Certainly some of these sites will be less energetically favourable than others, but it is not obvious which ones these will be because

one may not be able to invoke arguments involving normal bonding energetics for abnormal sites.

A second important feature of the abnormal bonding description is that a great number of diamagnetic gap states are (in theory) capable of yielding metastable paramagnetic sites with properties matching those inferred from photoinduced ESR measurements.

CHAPTER 3

In this chapter the experimental techniques and equipment used in this investigation are described in detail. Sections 3.1 to 3.4 describe the methods of preparation of vitreous, evaporated and sputtered As_2Se_3. The analysis of sample composition is then discussed in section 3.5. Sections 3.6 and 3.7 describe the apparatus and techniques employed to measure the d.c conductivity and drift mobility. The chapter ends with a section describing the apparatus used for optical absorption measurements.

3.1 PREPARATION OF THE BULK GLASS

The samples used in this study were prepared from bulk glass starting material. The glass was prepared in batch weights of approximately 60g by melting 5N purity elemental arsenic and selenium in an evacuated sealed tube of fused silica. The silica tube was carefully cleaned prior to being weighed and filled with the arsenic and selenium. This was achieved using an ultrasonic bath in which a strong detergent solution had been placed. After 20 minutes the tube was removed from the ultrasonic bath and rinsed in isopropyl alcohol for several minutes. The tube was then placed in an oven at a temperature of 100°C for 2 hours to dry. During weighing of the constituents disposable gloves were worn to avoid contamination of the outer surface of the tube (which may lead to significant errors). As far as possible, large lumps of selenium and arsenic were used in preferance to powder to reduce the effects of surface adsorption of atmospheric gasses. It was estimated that errors during the weighing process should not result in stoichiometric variations greater than

$$As_2 \pm 0.0002 \qquad Se_3 \pm 0.0003$$

After weighing, the silica tube was connected to a rotary vacuum pump, and the internal pressure slowly reduced to below 50 millitorr. The bottom section of the tube was then heated gently using a bunsen burner to accelerate outgassing of any adsorbed gasses. When such outgassing was judged to be complete, the tube was allowed to cool under continuous evacuation. The tube was sealed by directing a finely focussed flame from an oxy-hydrogen torch onto the neck of the tube. This process is aided by the tendency of the neck of the tube to collapse inwards as the silica softens.

After sealing the silica tubes they were taken to the Electrical Engineering faculty of Dundee University, where they were heated in a rocking furnace at 800°C for approximately four hours. The author is grateful to Dr J T Edmond of Dundee

University for performing this part of the preparation. After continuous agitation in the rocking furnace for about four hours, the tube was removed and placed in a container packed with glass fibre. This allows the tube to cool whilst avoiding excessive thermal shock.

The ingots of glassy arsenic triselenide thus prepared were removed from the silica tube by scribing the tube with a diamond stylus and giving it a sharp tap. This usually resulted in a clean break, after which the arsenic triselenide could be easily removed.

The compositions of the ingots were checked using X-ray fluorescence. The ingots were always found to be stoichiometric to within the experimental error involved using this technique (approximately 0.3 % for a 40g sample).

3.2 THE PREPARATION OF VITREOUS SPECIMENS

Thin samples of vitreous arsenic triselenide (typically 30 - 100 microns thick) were prepared using a 'compression' technique similar to that of Marshall (1971). A small pellet of the bulk glass was placed between two freshly cleaved mica plates approximately 5cm square. This assembly was then heated gently in a bunsen flame until the glass began to soften. The pellet and mica were then transfered to a brass plate held at a temperature close to T_g. A second plate was then placed on top of the first, and pressure immediately applied to 'squash' the pellet of arsenic triselenide. The arsenic triselenide will then flow into a a large thin layer between the two mica sheets.

Unfortunately, differential contraction of the vitreous layer and the mica plates can cause cracking of the arsenic triselenide film at this stage. With practice, however, it is possible to obtain sufficiently large samples possessing high quality surfaces and a thickness variation of less than about 15% over 1 cm^2.

Samples were equipped with thin, semitransparent gold electrodes evaporated onto the top and bottom surfaces to form the 'sandwich' configuration shown in figure 27 . Electrical contact was made to

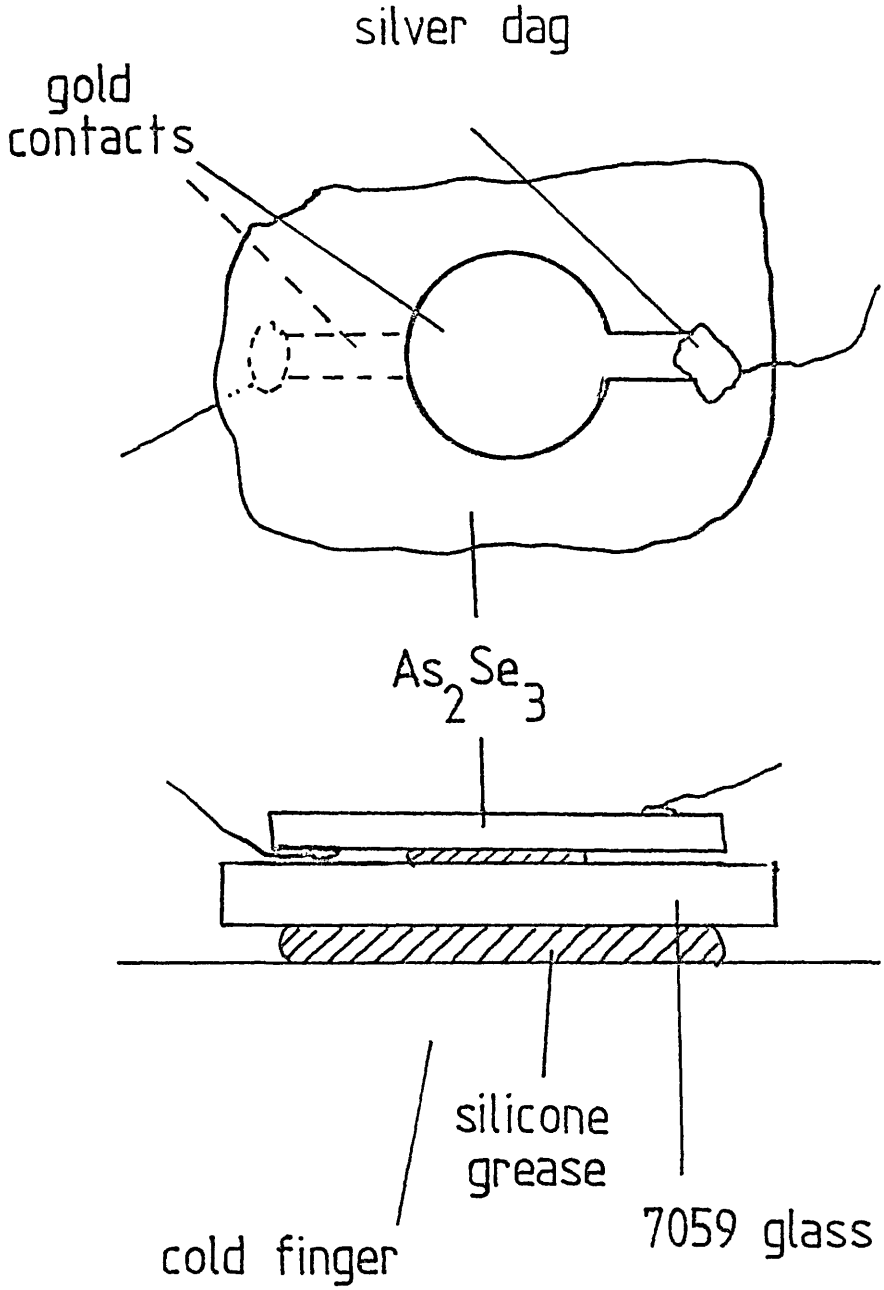

FIGURE 27 : Sandwich cell configuration (top) and contact to coldfinger (bottom).

the electrodes by means of thin aluminium wire of diameter 50 microns. This wire was dipped into silver dag, then brought into contact with the narrowest part of each electrode (as shown in the figure). The silver suspension must be kept as far away as possible from the region of overlap of the electrodes because silver diffuses fairly rapidly through arsenic triselenide even at room temperature (Freeman et al. (1969)).

Sample thickness was determined after the conductivity and mobility measurements had been completed. Two methods were employed, the choice between them depended on the sample thickness. For fairly thick samples (> 50 microns) a micrometer screw gauge capable of measuring thicknesses to an accuracy of $\pm$ 3 microns was used. For thinner samples where a more accurate method is desirable, a Taylor Hobson 'taly-surf' was employed. This machine uses a diamond stylus which travels over the surface of a specimen and can measure thickness changes very accurately. Unsupported films must therefore be attached firmly to a substrate for measurements to be performed using this machine. This was accomplishedby breaking the sample into small fragments which were then pressed onto a damp microscope slide. After the slide was allowed to dry, these fragments adhered quite well to the glass, and thickness measurements which agreed well with those performed using the micrometer screw gauge were obtained. Each sample was measured several times, and an average value taken when calculating the conductivity and drift mobility.

3.3 PREPARATION OF EVAPORATED FILMS

Thin samples of evaporated arsenic triselenide were prepared by evaporating the bulk galss onto aluminium foil which was subsequently removed by flexing. The evaporation was performed in a large evacuated bell jar. The glass to be evaporated was placed in a small pyrex beaker or silica crucible which was then placed on the titanium boat in the chamber. The chamber was evacuated to a pressure of less than 10^{-6} Torr using a diffusion pump prior to the evaporation. The

foil was placed about 8 cm above the crucible containing the bulk glass, and was sheilded from the source by a brass paddle which could be swiveled out of the way by means of a lever on the outside of the chamber. The brass paddle was used to prevent deposition of evaporated material whilst the source was heating up or cooling down. No attempt was made to control the temperature of the aluminium foil during deposition - the foil was always at room temperature prior to the start of all the deposition runs.

Although stoichiometric As_2Se_3 glass was used as a starting material, the evaporated film will not necessarily have the same composition due to differing evaporation rates of different species. The actual composition obtained cannot be easily predicted in advance as it is likely to be a complicated function of heating rate, chamber geometry and so forth. The compositions of the evaporated films used in this study determined by X-ray fluorescence were found to be one to two percent arsenic rich. This figure must of course be considered as an average value because the actual sample composition may vary with thickness through the specimen.

The thickness of the evaporated films was measured in the same way as we have described in the previous section on vitreous samples. Similarly, semitransparent gold electrodes were evaporated onto the films and electrical contact made in exactly the same way as for vitreous films. Once again thin aluminium wire was used to minimise the conduction of heat to the sample.

3.4 PREPARATION OF R.F. SPUTTERED FILMS

3.4.1 The Sputtering Process

In 1955, Wehner suggested that the problems associated with the d.c. sputtering of insulators could be overcome by the application of a high frequency potential to a metal base underneath the insulator. Seven years later, Anderson, Mayer and Wehner (1962) reported that they had put the idea into practice, and had sputtered diamond and sapphire.

Nowadays, r.f. sputtering is commonly used in the semiconductor industry to etch or deposit a wide range of insulating and conducting materials. A schematic diagram of the essential features of an r.f. sputtering system is shown in figure 28. The dielectric target which is to be sputtered is positioned so that it forms a boundary of a plasma. A radio frequency voltage is applied to the metal backing electrode, which induces an r.f. voltage on the front of the target due to capacitive coupling through the target.

The operation of an r.f. sputtering machine depends on the electrons and positive ions in the plasma having different mobilities. In general, the mobility of electrons in the plasma will be greater than that of the positive ions. This means that more electrons will be attracted to the front surface of the target during the positive half cycle than positive ions during the negative half cycle. The resultant electron current will cause the dielectric surface to aquire an increasing negative bias voltage during succesive cycles until a stage is reached when the substrate surface is positive with respect to the normal wall potential for a short period of the r.f. cycle. During this time, enough electrons are attracted to the surface to neutralise the positive ion charge accumulated during the rest of the cycle (see for example Jackson (1970)). The bias potential is close to half the value of the peak to peak r.f. voltage appearing on the target surface. The ions are accelerated essentially by the bias voltage rather than the r.f. potential, and bombard the target with energies of the order of V_B electron volts (where V_B is the bias voltage). Sputtering is generally performed using ions with an energy of a few keV, thus r.f. voltages of a few keV are required. The drop in bias voltage experienced during each half cycle is a function of the r.f. frequency. For the frequency used in this study (13.56 MHz), this drop in bias voltage should be less than 100V.

The sputtering mechanism is still not completely understood, although there have been several reviews in the literature (see for example Jackson (1970)). Studies of the sputtering of single crystal and polycrystalline conductors have shown that the sputtering process can be considered to be largely due to the transfer of momentum from the bombarding ion to the ejected particle. In general the sputter-

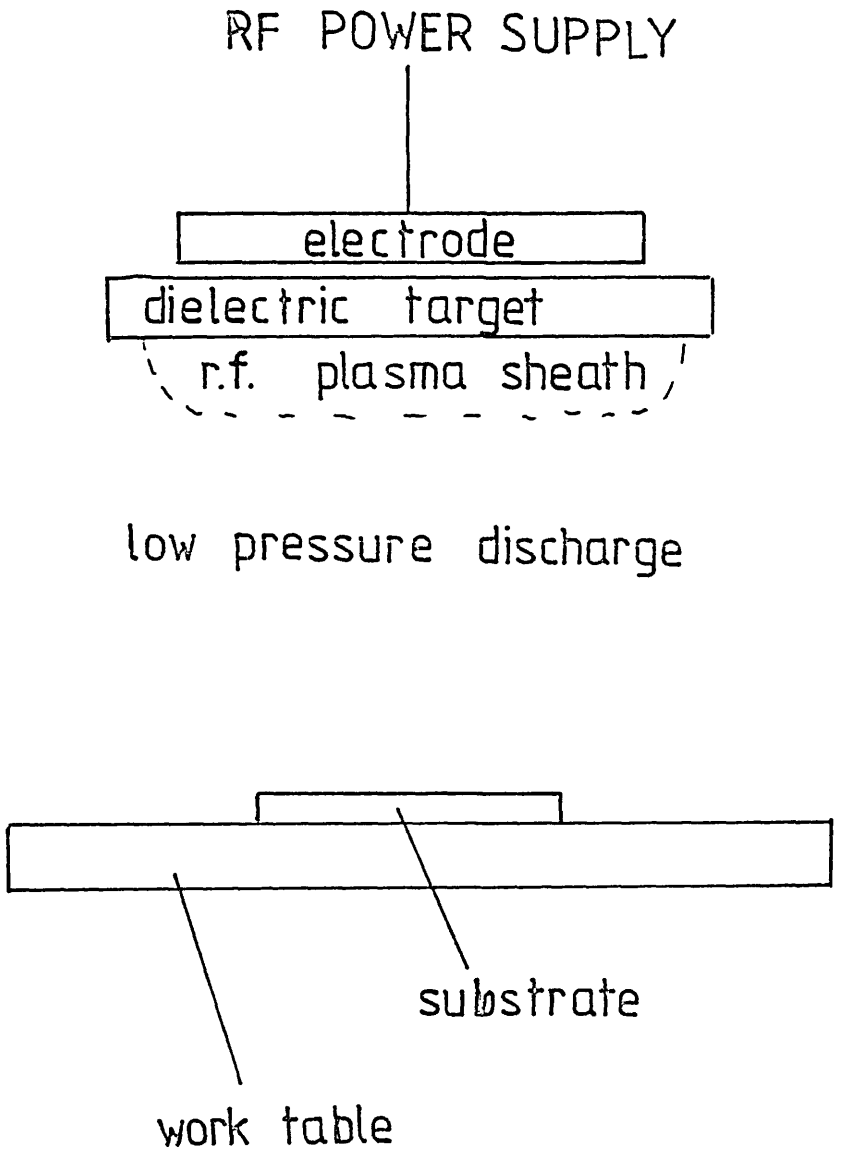

FIGURE 28 : Schematic diagram of sputtering apparatus.

ing yield (that is the number of target atoms emitted per bombarding ion) increases with increasing positive ion energy from 0 - 10 keV; it often varies approximately linearly with bombarding ion energies of between 100 and 1000 eV, but is usually independent of bombarding ion current density.

3.4.2 The Nordiko Sputtering System

Schematic diagrams of the Nordiko sputtering unit used to deposit sputtered undoped and doped samples of arsenic triselenide appear in figures 29 and 30 . A 'sputter-up' type of system was chosen which has the targets set below the substrates. The main advantages with this arrangement are firstly that powdered targets may be easily used, and secondly that flakes of material from the target will not fall onto the substrates and cause pinholes in the deposited films. The system had three seperate target assemblies which could be rotated into place without breaking vacuum. Initially a powdered arsenic triselenide target was used, but for several reasons it was decided to abandon this in favour of a bulk glass target. There were three main problems with the powdered target. Firstly, it was felt that atmospheric gasses would be more easily absorbed in such a target due to the very large surface area. Secondly, a powdered target is much less efficient at dissipating heat produced at the surface of the target. Thus to avoid surface melting a low power density was required which reduced the deposition rate and caused increased deviations from stoichiometry. Lastly, it proved very difficult to judge when the target was wearing thin. For these reasons a solid target was used for all the samples reported in this study.

The solid target was fabricated in the following way. A stainless steel base 8mm thick was placed on a heater taken from a small diffusion pump. Pellets of the bulk glass were placed on this base, and the whole system placed in a bell jar containing nitrogen gas at slightly less than atmospheric pressure. The steel disc was then heated to just above the glass transition temperature, and the molten As_2Se_3 allowed to flow until it covered

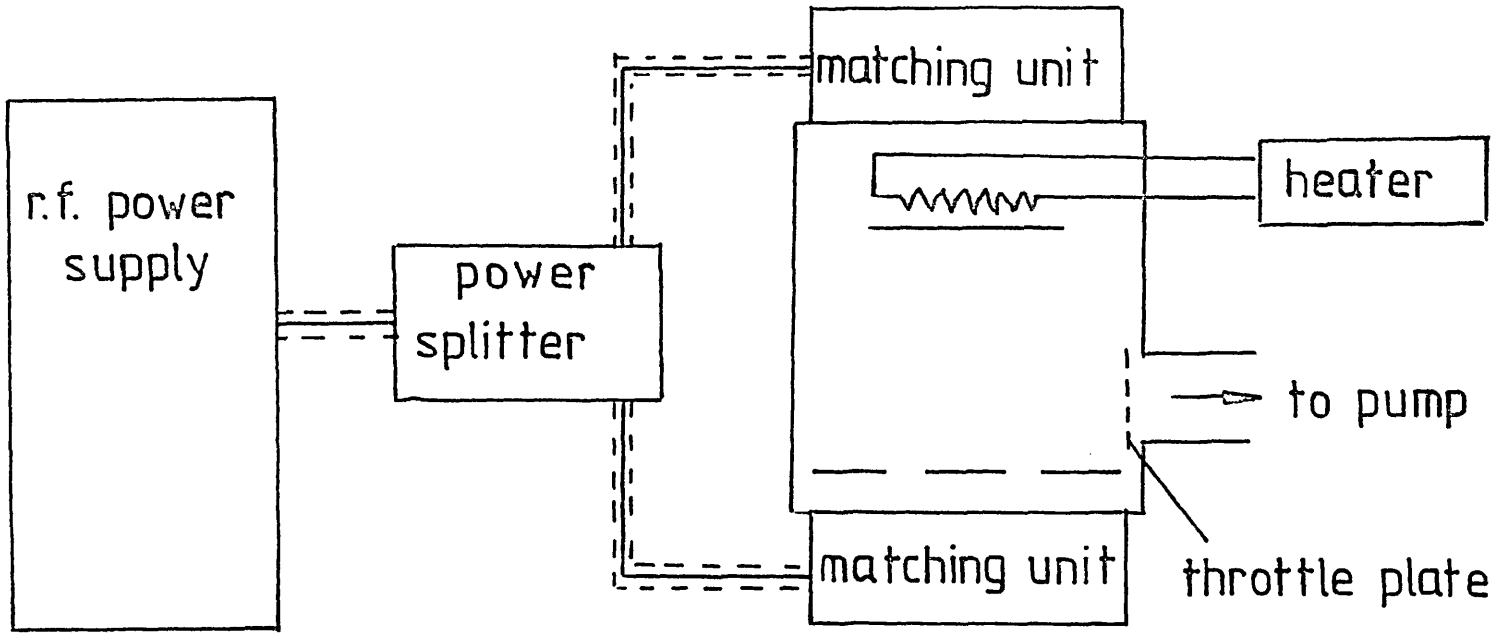

FIGURE 29 : Schematic diagram of Nordiko sputtering system.

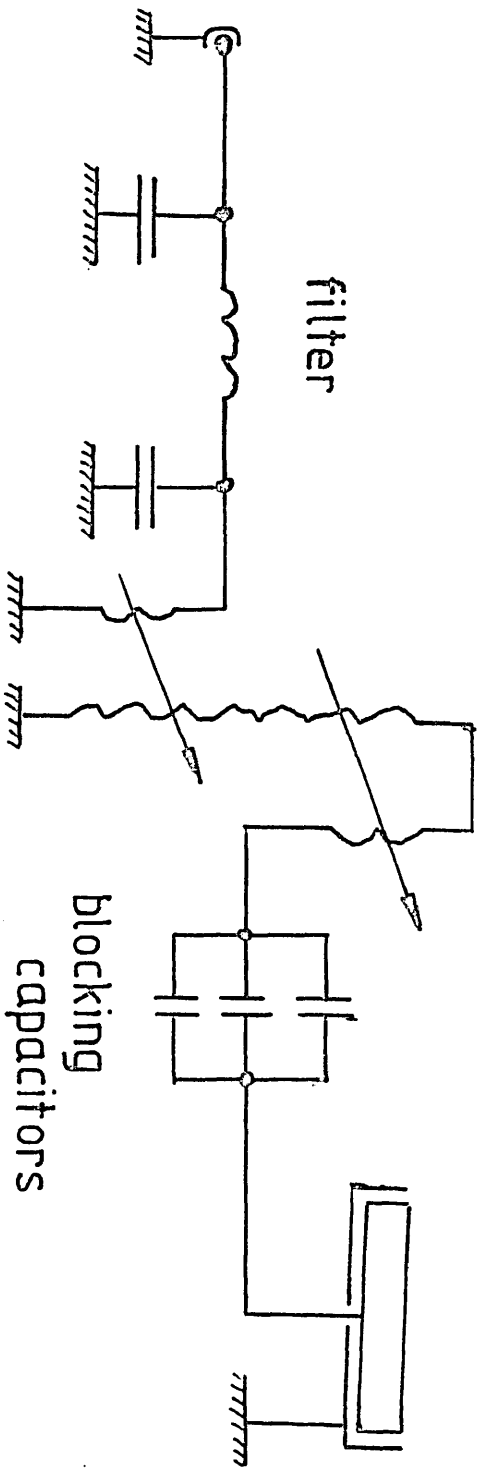

FIGURE 30 : Circuit diagram of matching units.

the base to a depth of about 5mm. The target was then allowed to cool in the nitrogen atmosphere before being removed and placed in the sputtering system. Using such a target power densities of up to 0.7 W cm^{-2} could be used without significant surface melting - resulting in deposition rates of the order of 2 microns per hour, and deviations from stoichiometry of less than 2%.

Several different substrate arrangements were used to give both supported and unsupported films. Unsupported films were obtained by sputtering onto thin aluminium foil which was subsequently removed by flexing. This method could produce samples thicker than about 20μm - for thinner films the aluminium had to be removed by dissolving in HCl. Supported films were deposited onto Corning 7059 glass substrates 25mm x 12mm x 0.8mm. Two different substrate holders were used, depending upon whether undoped or doped arsenic triselenide was being deposited. The two holders are sketched in figure 31 .

The arsenic triselenide samples investigated in this study were all produced using bias sputter deposition. In this arrangement the r.f. power is split between the target and substrate so that sputter etching of the deposited film occurs during deposition. This technique has the advantage of removing most of the gas trapped from the plasma in the deposited film, leading to films with more repeatable characteristics which are closer to those of the bulk target. For all the samples prepared for this study the power was split in the ratio 5:1 between the target and substrate respectively. This yielded typical bias voltages of 900 - 1100 V.

Samples of arsenic triselenide doped with small amounts of copper and nickel were produced by co-sputtering the dopant with the glass. This was achieved by placing a small amount of copper or nickel wire on the top surface of the arsenic triselenide target near one side. This produced a graduation in the impurity concentration in the film adhering to the surface of the substrates - the heaviest doping occuring directly above the position of the wire. Of course, this method is likely to contaminate the surface of the bulk target. For this reason the target was sputtered for a couple of hours between dopant changes (in addition to the time normally allowed to sputter clean

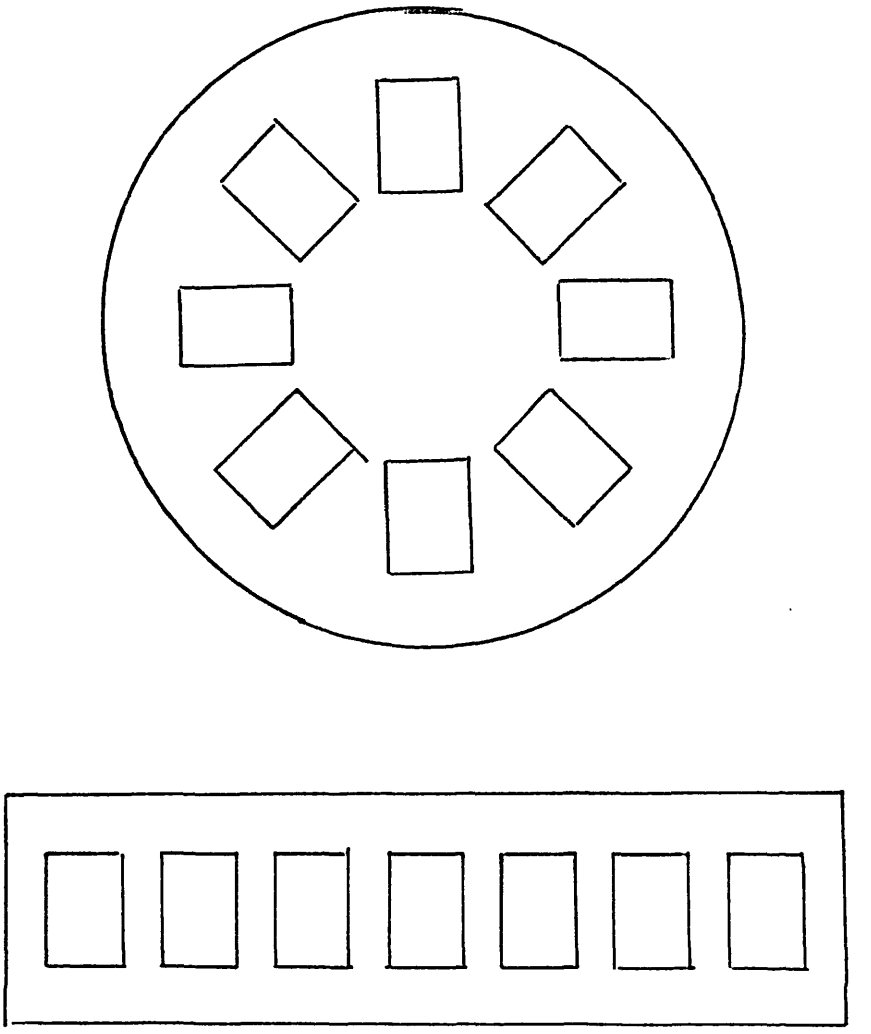

FIGURE 31 : Sketch of sample holder used for undoped depositions (top) and for doped depositions (bottom).

the surface of the target prior to a deposition run). The substrate electrode assembly could be water-cooled or heated. Films of undoped arsenic triselenide were deposited both at room temperature and at temperatures near the glass transition. The temperature of the substrate was measured using a copper-constantan thermocouple screwed onto the substrate electrode but seperated from it by a PTFE washer. The voltage across the thermocouple was measured using a Keithley DVM. Unfortunately the presence of r.f. power was found to effect the reading on the DVM - for this reason the rig was usually allowed to pump down overnight while the temperature stabilised, and this temperature noted before the discharge was struck. The temperature was also noted after the deposition run had been completed, and the higher of the two readings taken as the maximum temperature of the film during deposition.

The gas used for the plasma was high purity 'zero-grade' argon supplied by BOC. All the gas line piping was constructed from copper to reduce the effects of adsorbed gasses which can be present in plastic tubing. The stainless steel vacuum chamber was pumped by a large (600 l s^{-1}) diffusion pump backed by a powerful rotary pump and fitted with a water cooled baffle. The argon pressure in the chamber could be controlled upstream of the chamber by a sensitive needle valve or downstream of the chamber using a 'throttle plate' which impeded the flow of gas into the diffusion pump and thus reduced the effective pumping speed. The gas pressure was measured using a Hastings thermocouple gauge, which could be read to an accuracy of $\pm$ 0.2 millitorr in the pressure range 5 - 20 millitorr. Unfortunately the reading on this gauge could also be effected by the presence of the r.f. discharge - it was therefore assumed that the true pressure during deposition corresponded to the pressure which this gauge read immediately after the discharge was switched off. The chamber was always pumped down for several hours before each run commenced.

3.5 ANALYSIS OF SAMPLE COMPOSITION

The composition of the bulk glass and undoped deposited films of arsenic tri-selenide was measured using X-ray fluorescence spectroscopy. This technique is fast and non-destructive but requires a fairly large sample size. The as-deposited films were removed from the aluminium foil substrate and placed on a thin mylar film. The analysis was performed in a Telsec series 300 machine equipped with a ^{238}Pu X-ray source. Seperate filters were used to measure the arsenic and selenium counts seperately. The calibration was checked before each determination using a 100g sample of the bulk glass of known stoichiometry The author is grateful to Mr J Higgins of Dundee College of Technology Physics Department who performed the analysis.

Typical results from such analyses are displayed in table 2. The ratio's represent an average composition for several grams of material. Variations in sample composition with depth cannot be detected using this technique, a method such as scanning Auger Microanalysis would be required to give a depth profile of possible compositional variations.

The copper and nickel concentrations present in doped films were determined by energy dispersive X-ray analysis techniques using a scanning electron microscope. In this technique a focussed electron beam impinges on the sample surface stimulating atoms near the surface to emit characteristic X-rays which are then energy analysed. As the penetration depth and beam diameter are both of the order of 1 micron, and because the characteristic X-rays have a range of several microns in solids, this technique yields an average concentration for a volume of about $10^{-12}cm^3$. Absolute measurements of concentration are difficult using EDX techniques, but because it is possible to simultaneously detect a spectrum of X-ray energies atomic ratios may be determined to an accuracy of about 1%. The author wishes to express his gratitude to Mr J Patel of the Materials Characterisation Department at the GEC Research Laboratories, Hirst Research Centre who performed the SEM-EDX analysis.

TABLE 2

MATERIAL	ATOMIC % As	ATOMIC % Se
	(±0.3)	(±0.3)
Bulk Glass	40.0	60.0
Evaporated Films	41.2	58.8
R.F.Sputtered Films	38.6	61.4

3.6 D.C. CONDUCTIVITY MEASUREMENTS

D.c. conductivity measurements on semiconductors are normally preformed using either 4 point probe methods or Van der Pauw structures (Van der Pauw (1958)). Such techniques are, however, notoriously unreliable when applied to materials with high resistivities (Abkowitz and Scher (1977)). The d.c. conductivity measurements in this study were therefore performed on the same bulk 'sandwich-cell' samples used for the drift mobility measurements.

The samples were mounted on a cold finger (shown schematically in figure 27) and placed in an evacuated chamber. Contact to the evaporated gold contacts on the sample was made using thin aluminium wire to minimise heat conduction from the surroundings (the method has been described in section 3.2). The sample was placed on a glass slide using a small amount of silicone grease to provide good thermal contact between sample and slide (and slide and cold finger). Care was taken to ensure that stray light could not reach the sample during measurements. The sample was placed in a light tight box sealed with insulating tape, and no transparent components were used in the fabrication of the vacuum chamber. The temperature of the sample was sensed by a copper-constantan thermocouple imbedded in the cold finger directly under the sample. This configuration may cause a slight discrepancy between the actual and measured temperature of the sample which will be observed as hysteresis - a difference in the measured conductivity between heating and cooling cycles. In practice this effect was found to be slight, corresponding to a temperature differance of less than 0.5 K. All the results quoted in later chapters are an average of the conductivity obtained for heating and cooling cycles.

The voltage across the sample was maintained by a Fluke 415B power supply which is capable of providing 0 - 3000 V $\pm$ 0.1 %. The current flowing through the sample was measured using a Keithley 610C solid state electrometer in the 'fast' mode.
The electrometer was always switched on several hours before measurements were made to minimise possible drift during cooling cycles.

The conductivity of doped As_2Se_3 films was measured using gap

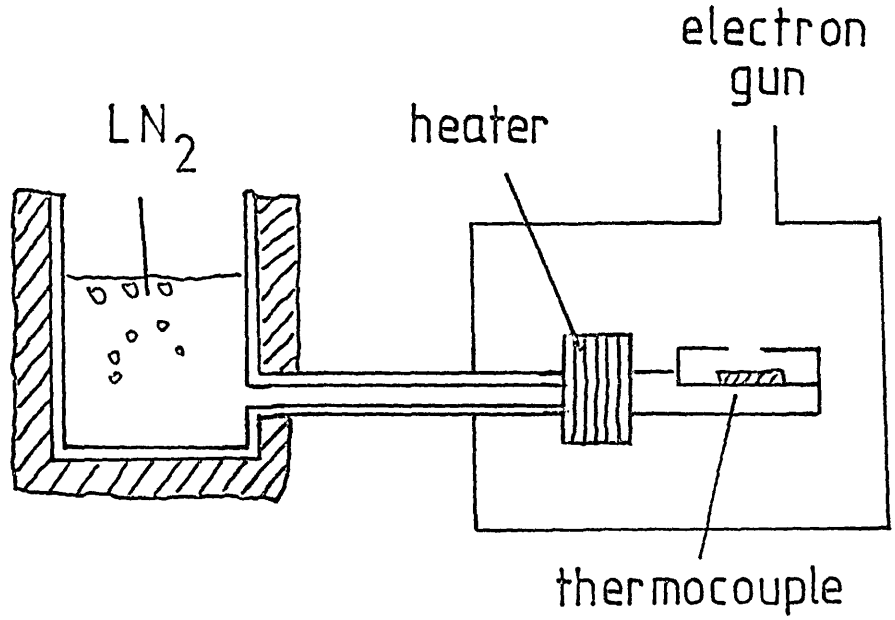

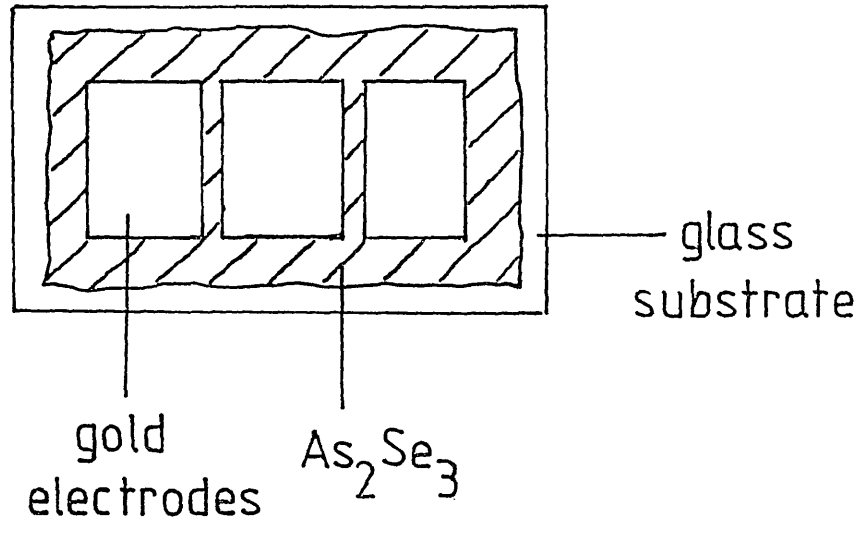

FIGURE 33 : Schematic diagram of cold finger and heater arrangement (top). Below is a diagram of the gap cell configuration used for measurements on supported films.

cell samples, the structure of which is illustrated in figure 33. This was mainly due to the lower deposition rates encountered when sputtering these glasses which made the fabrication of unsupported films impractical.

3.7 DRIFT MOBILITY MEASUREMENTS

This section is in two parts. In the first part the apparatus involved is described, while the second subsection discusses the techniques which were employed to minimise space-charge and contact effects.

3.7.1 Drift Mobility Apparatus

The measurement of drift mobility by the time-of-flight or transient charge technique provides a physically direct method of transport measurement which is particularly suited to the combination of high specimen resistivity and low carrier mobility found in amorphous arsenic triselenide. The technique has been reviewed in detail by Spear (1969), Martini, Mayer and Zanio (1972) and Dolezalek (1976). The technique essentially involves detecting the drift through the semiconductor of a sheet of excess carriers generated near one electrode by a pulse of electrons, a strongly absorbed light flash, or some other excitation. The technique is more fully described in the next subsection.

In this investigation both electron beam and light flash excitation were employed. Light flash excitation offers the advantage that no high voltage electronics or complex vacuum systems are necessary, and presents the possibility of the examination of spectral response effects by simply scanning the photon energy. The major drawback with such a system, however, is that the chosen wavelength must be very strongly absorbed to ensure that excess carriers are only generated in a thin layer near one surface of the specimen. If weakly absorbed light is used electron-hole pairs may be produced throughout the bulk of the semiconductor.

In contrast, using a focussed beam of electrons the penetration depth may be accurately controlled simply by varying the accelerating potential of the electron gun.

The arrangement used for light flash excitation i n this study is shown schematically in figure 34 . The short flash of light was generated by a spark discharge across a narrow air gap in a light tight box. The light pulse was transmitted to the sample via a light pipe fitted with black plastic cladding . The sample was kept in an Oxford Instruments cryostat in which its temperature could be controlled between 77K and room temperature. The temperature was sensed by a platinum resistance thermometer.

The transient current produced by the drift of carriers through the sample was measured as the voltage drop across a series resistance. This voltage drop was captured using a Datalab DL905 transient recorder, which stores the signal digitally as 1024 points, each of which may have a value from 0 to 255. A Nascom microcomputer was used to retrieve the information from the transient recorder and transfer the data to the College's DEC 20 mainframe computer for storage and analysis. The author is grateful to Lindsay Arcari and Henry Fortuna who wrote the Nascom monitor program which transferred the data to the DEC. All the other programs used were developed by the author.

The equipment required for electron beam excitation was much more complex, and the arrangement used is illustrated in figure 35. Specimens were mounted in a holder which was in thermal contact with a cold finger - the temperature of this finger could be controlled over a wide range by pouring liquid nitrogen into the reservoir and/or by heating the cold finger using the coils between the reservoir and the sample holder. The sample holder projected into an evacuated electron gun, the pulsed operation of which was controlled by the H.T. electronics section which was at a positive potential of several kilovolts relative to the sample holder while the gun was operating. Overall control of the experiment was effected by the L.T. electronics section, which provided triggering for the electron gun, changed the applied electric field, focussed the electron gun by means of a Helmholtz coil, and dealt with control of the sample temperature.

The electron gun system used in this investigation was similar to

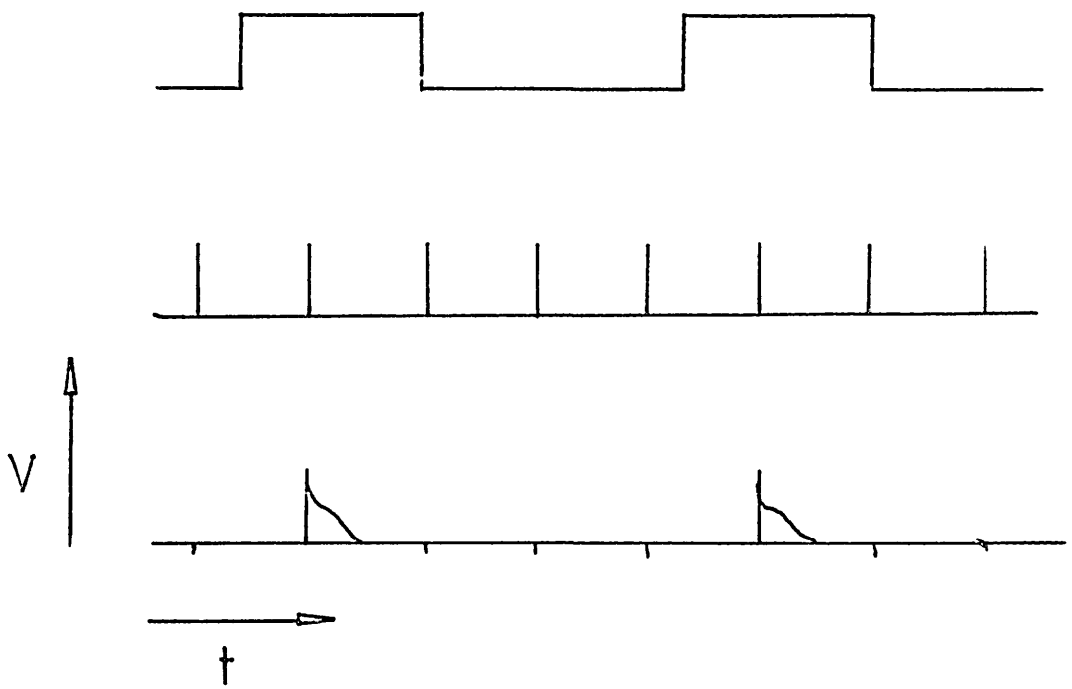

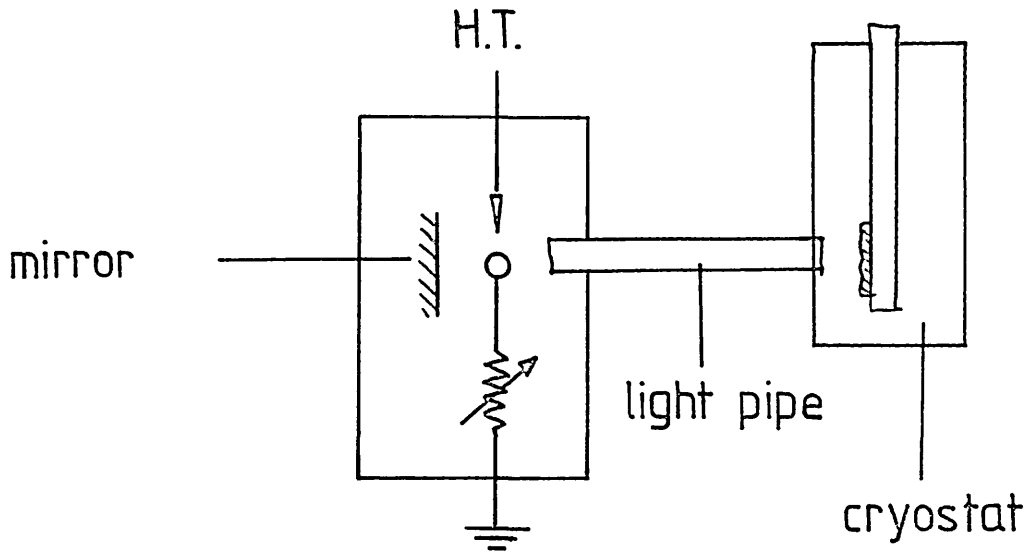

FIGURE 34 : Diagram showing timing relationship between field, excitation pulse and transit pulse (top). Lower diagram shows the spark-gap system used for light flash excitation.

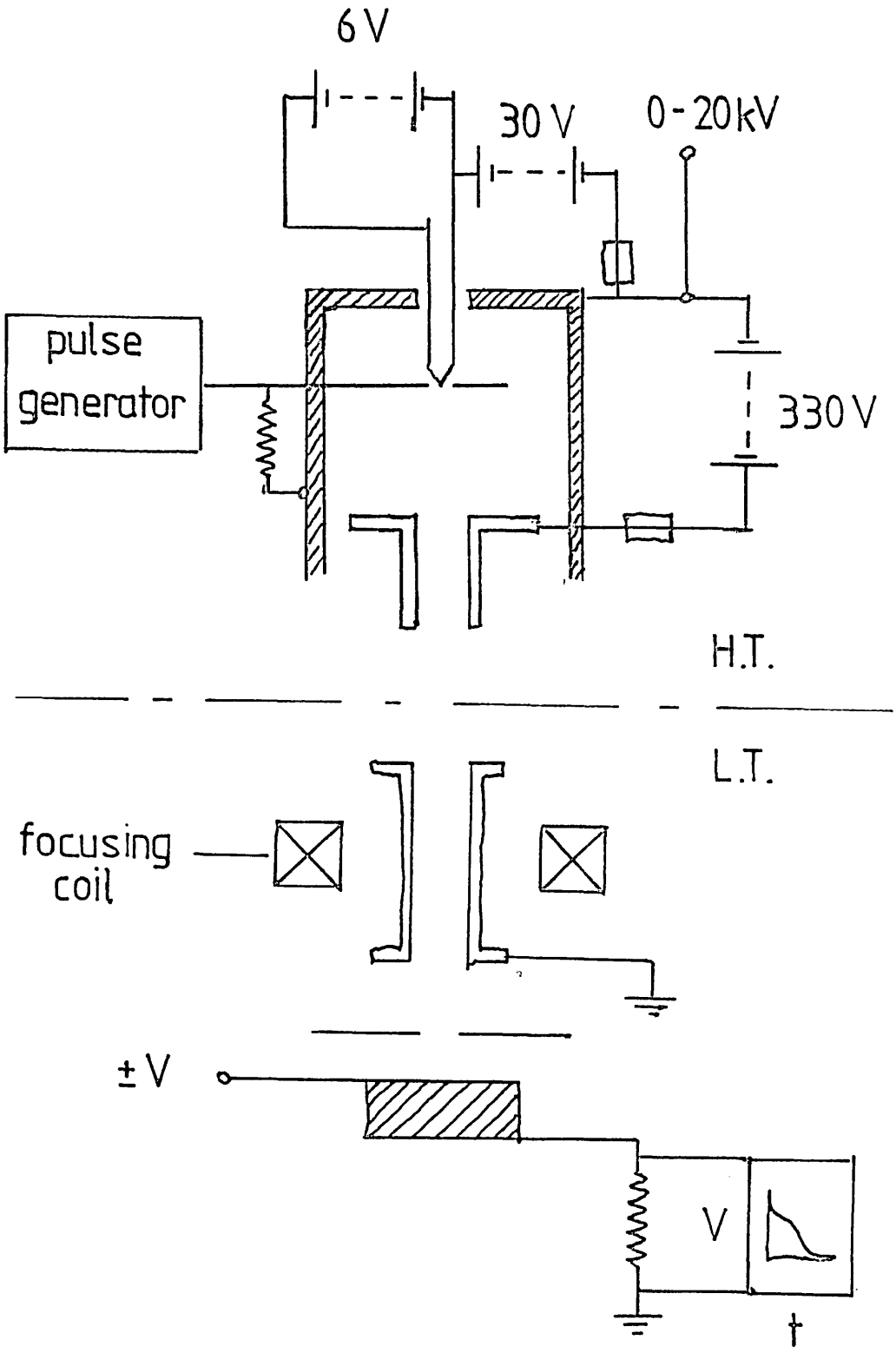

FIGURE 35 : Schematic diagram of the electron gun system.

the tetrode arrangement described by Marshall (1971), and is shown in figure 35 . The cathode was a directly heated tungsten wire which was powered by a 6 volt audio frequency supply. The position of the filament with respect to the modulating grid could be adjusted both vertically and horizontally such that the filament could be accurately positioned in the immersion field of the grid system. The cathode was held in the off state by an adjustable positive bias (normally about 30V) relative to the casing of the H.T. section of the gun. A selected 75 ohm non-inductive resistor was connected between the grid lead and the casing to provide correct termination of the drive pulses. Due to this resistor, the grid was normally at the casing potential so that its negative bias with respect to the cathode held the gun in the off state. A sufficiently large positive pulse on the grid thus served to switch the beam on. The anode grid, situated below the modulation grid, was held at a potential of about 300 volts which helped to stabalise the operation of the gun. With this arrangement the beam current is almost independent of the accelerating voltage over the range 0 to 20kV. The electron beam was focussed by means of two adjustable magnetic coils powered by a Farnell L.T. supply. The coils also allowed control of the beam position relative to the sample.

The electron gun accelerating potential was supplied by a Brandenburg 276A generator. The H.T. electronics section of the equipment was surrounded by a plastic box to provide insulation, while the metal beam line to the sample chamber was seperated from the H.T. by nylon insulation. The electron gun was usually operated at an accelerating potential of 8 - 9kV, which corresponds to a penetration depth in As_2Se_3 of less than 0.3 μm. The high voltage fast pulse generator was designed and built by J.M. Marshall along the lines described by Spear (1969). The essence of this unit was a T-shaped brass tube fitted with 75 ohm BNC sockets on the end of each arm. The vertical section of the tube housed a mercury wetted contact relay driven by an externally wound coil (as described by Marshall (1971)). Longer pulses were produced using a thyristor based circuit. The pulse length could be chosen to be 50ns, 500ns, 5μs, 500μs, 5ms - in addition the gun could be driven continuously to facilitate beam positioning and focussing.

The L.T. control electronics controlled the triggering of the electron gun and detection system, and the field across the specimen. The time relationship between the applied field and bombarding electron pulses is illustrated schematically in figure 34 .

3.7.2 The Time-of-flight Technique

The principle underlying drift mobility measurements on insulating specimens is illustrated in figure 36 . A sample in the form of a thin platelet, thickness d, is equipped with electrodes on the top and bottom. The top electrode is connected to a steady or pulsed source of potential V_a with respect to ground. The bottom electrode is returned to ground via the resistor R which is normally much smaller than the specimen resistance. Excess carriers are generated by photon or electron beam excitation near the top electrode. It is essential that the duration of the excitation pulse be much shorter than the transit time t_T of the carriers across the sample, and that the absorption depth of the excitation (δ) be kept much smaller than the specimen thickness. The electric field will then draw a sheet of charge carriers of one sign across the sample. If there are no traps in the specimen, and if a fraction N of the carriers escape recombination between x = 0 and $x = \delta$, the drifting sheet of charge at x = x' will modify the applied field $E_a = V_a/d$ such that (Spear (1969)):

$$E_1(x') = E_a - \frac{4\pi Ne}{\varepsilon A} (1 - x'/d) \qquad -3.1$$

$$E_2(x') = E_a + \frac{4\pi Ne}{\varepsilon A} \left(\frac{x'}{d}\right) \qquad -3.2$$

where ε is the dielectric constant of the solid.

Thus the drifting carriers alter the field within the specimen. However, if N is kept sufficiently small so that the self field $4\pi Ne/\varepsilon A$ is much less than E_a, it is a good approximation to take the internal field as V_a/d. It must be remembered that this description of carrier transport applies to a low conductivity solid in which the

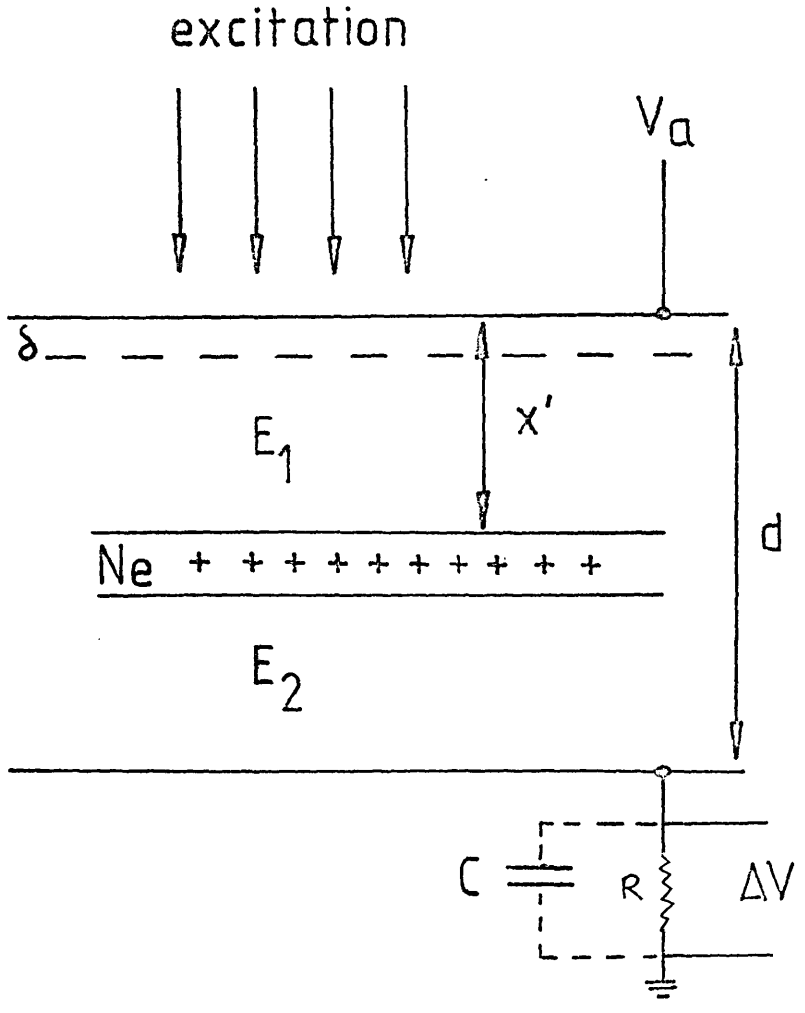

FIGURE 36: Schematic diagram of time-of-flight drift mobility experiment.

dielectric relaxation time is very much longer than the transit time. In this respect the situation is fundamentally different from standard Haynes - Schockley mobility measurements on the drift of minority carriers in an extrinsic semiconductor, in which the condition of local space charge neutrality must pertain during the transit. The highly resistive sample therefore has an advantage over the semiconductor in this respect, because drift mobility measurements on both types of carrier are possible (in principle) simply by reversing the polarity of the applied electric field.

There are two ways in which the transit time of the carriers may be determined. The first relies on charge integration when the CR time constant of the system is much longer than the transit time. The capacitance C is the total capacity across R and includes the sample capacitance and the leads and input to the detection system. As the excess carriers drift across the specimen, the changing fields E_1 and E_2 will cause a redistribution of charge on the electrodes. For the bottom electrode this is

$$q = Nex'/d \ .$$

The potential developing across R is then

$$V(t) = Nevt/Cd$$

during $0 < t < t_T$, where $v = d/t$ denotes the drift velocity. For $t > t_T$ V remains constant and equal to Ne/C if $t \ll CR$. The typical pulse shape from which t_T may be obtained is shown in figure 37 (here we have neglected the effects of trapping and/or dispersive transport). The linear rising edge implies that N remains constant during the transit, and will become curved if N changes due to appreciable interaction with deep traps.

Alternatively, if we reduce R so that $CR \ll t_T$, the transit time may be measured from the duration of the current pulse produced by the drifting charges. The current flowing during the transit is

$$I = Nev/d$$

Therefore

$$V = RNev/d$$

for $0 < t < t_T$, and $V = 0$ when $t > t_T$. This case is illustrated in figure 37 .

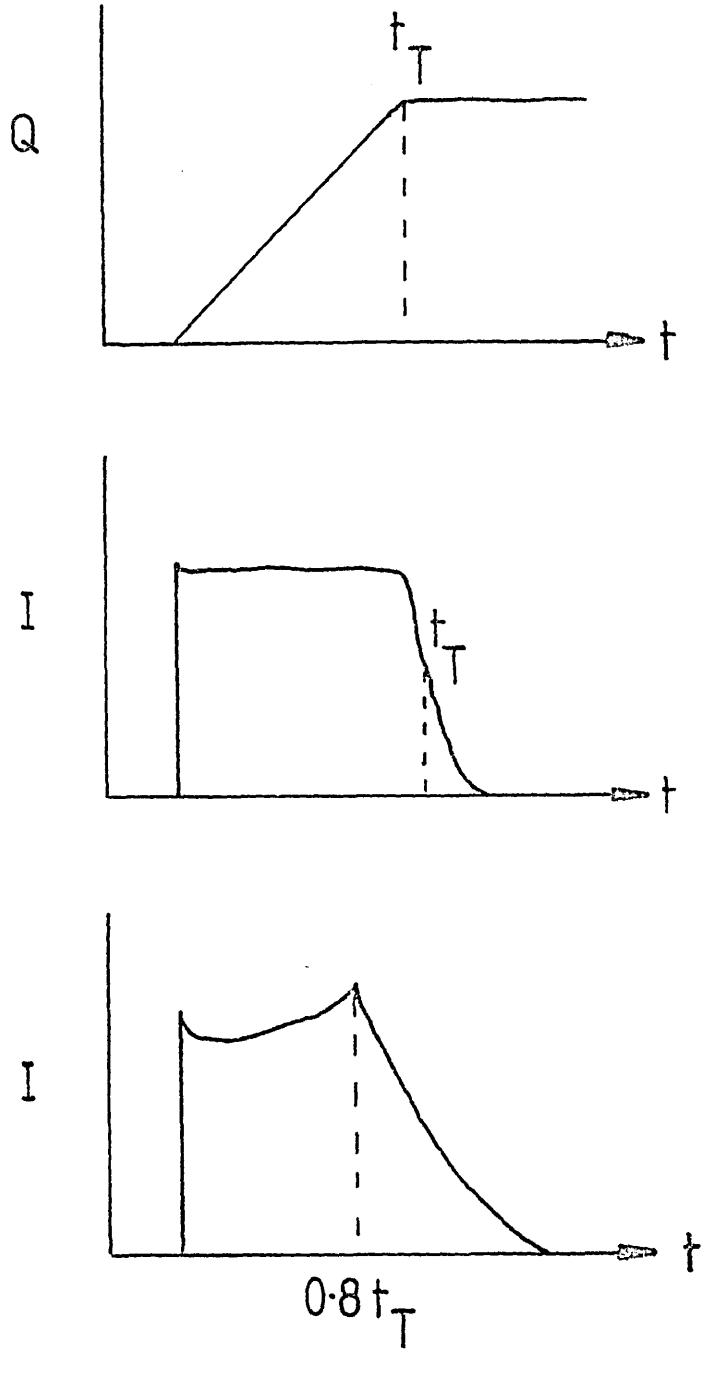

FIGURE 37: Transit pulses observed in a time-of-flight mobility experiment. Top-charge integration transient. Centre-idealized current transient. Bottom-current transient with space charge perturbation.

Carrier transit times for a vitreous As_2Se_3 sample 50 μm thick are typically hundreds of microseconds at room temperature and low applied electric fields so that detector rise times are not critical and large values of R may be used. For this reason all our drift mobility measurements were made using the current pulse mode, which has several advantages if deep traps are present.

Once the transit time has been measured, the drift mobility may be obtained from

$$\mu_d = d/E_a t_T.$$

The safest procedure is to determine t_T over as wide a range of applied fields as possible. A graph of $1/t_T$ versus E_a should be a straight line, and the mobility may be obtained from the gradient. This line will not however pass through the origin if a trapped surface charge layer builds up near the top electrode. Obviously such a technique cannot be used if a field dependent mobilitymay be present.

The time-of-flight technique relies on a well defined pulse of generated carriers, and any effect which broadens the sheet of carriers is to be avoided if possible. This applies particularly to the injection of excess charge from the electrodes during the generation and transit of the carriers. In an extreme case, the position of the transit time may be totally obscured if this occurs. Ideally therefore, the top electrode should be 'blocking' to the charge carrier under investigation and 'extracting' to that of the opposite sign. In fact the observation of a well defined transit pulse is usually taken to imply that the top electrode is at least partly blocking in character. Unfortunately, such contacts usually impede the extraction of carriers of the opposite sign. This tends to produce polarisation effects which must be carefully minimised using techniques which we will describe in the next section.

3.7.3 Minimisation of Space-charge and Contact Effects

There are two kinds of space-charge effects which are of importance in drift mobility experiments. The first is concerned with the presence of deep trapping centres in the volume of the sample (particularly near the surface), whilst the second effect is due to the space-charge associated with the carriers themselves.

In the first case, the gradual build-up of charge in deep traps during sucessive transits will modify the internal field, so that the assumption of an essentially uniform field is no longer valid. Experimentally, one observes slow polarisation effects in which the transit pulses diminish in size during the first few transits after the field is switched on. Occasionally the signal disappears completely, and it must be concluded that the resultant field has become very small in part or all of the specimen.

To eliminate effects of this kind two precautions are essential. Firstly, the density of generated carriers must be kept as low as is consistent with the sensitivity of the detection apparatus. Secondly space-charge neutralisation techniques must be employed. A simple but effective neutralisation technique employed throughout this study to minimise such effects involves running the excitation pulses at a frequency of a few Hertz while both top and bottom electrodes are earthed. The presence of an internal charge distribution, particularly near the top surface, is then indicated by the appearance of a reverse signal caused by the displacement of generated carriers in the space-charge field. This signal will decrease as the trapped charges are removed by recombination, and normally disappears after a few seconds. The external field is then applied across the specimen, but is removed as soon as the transit has been recorded. The sequence of excitation pulses, field pulses and observed signals is shown in figure 34 . This technique has been used by Spear and co-workers with considerable sucess in their work on the rare gas solids, where surface polarisation presents a particular problem. In the experimental set-up used throughout this study the excitation and field pulses were enabled using logic circuits present in an Advance Instruments PG52 pulse generator. The field pulse was produced from a Fluke 415B H.T. supply using a mercury wetted relay gated by the output of the PG52.

The second effect is caused by the space charge of the drifting carriers themselves. If the number of carriers is increased to the point where the self field is of the order of the applied field, equations 3.1 and 3.2 show that the fields behind and in front of the drifting charge sheet will be very different, and marked changes will occur in the observed signal shape. Figure 37 shows a typical electron transit pulse in the current mode when $4\pi Ne/\varepsilon A = \frac{1}{2}E_a$, and is taken from the review by Spear (1969). The most obvious feature is the cusp at $0.81t_T$. The physical reason for this pulse shape is as follows: electrons near the leading edge of the carrier packet experience a higher field, and will 'run away' from the slower moving carriers. The current will thus increase until the extraction of the faster carriers causes it to drop beyond the cusp. Thus the cusp can provide a useful feature for the accurate measurement of the transit time if N is kept reasonably constant during the experiment. However, the larger the number of generated carriers, the more important effective space-charge neutralisation between excitation pulses becomes.

The important role that contacts may play in conductivity and drift mobility measurements is well appreciated in crystalline semiconductor research, but has recieved relatively little attention in characterising the electrical properties of amorphous solids. Ideally, the contact used for d.c. measurements should be ohmic, such that the d.c. current flowing through the sample for a fixed external field is determined solely by the bulk transport parameters of the specimen. Usually ohmic contacts are difficult to fabricate, but by using 4-point probe or Van der Pauw techniques (Van der Pauw (1958) non-ohmicity of contacts may be circumvented. However, for insulating solids or specimens with appreciable surface conductivity these methods may lead to erroneous results and it is better to rely on bulk measurements made performed on thin samples in the 'sandwich-cell' configuration (Seager, Emin and Quinn (1973)).

Unfortunately, although ohmic contacts are desirable for conductivity measurements, as discussed earlier they must be avoided for drift mobility measurements. In this investigation thin evaporated gold electrodes were used throughout for both conductivity and drift mobility measurements. The contacts were thus similar to those recently investigated by Abkowitz and Scher (1977) and Abkowitz and Scharfe (1977). These authors employed step-function excitation and observed the

resultant current transient. Their work showed that the time evolution of the current following the application of the field was initiated by the transit of a finite charge stored at the Au/As_2Se_3 interface. Under steady state conditions, these authors suggest that the charge reservoir at the interface becomes depleted so that the value of the current is determined by the rate at which carriers are emitted from the contact. Such a 'finite reservoir emission-limited' contact would help to explain the dual nature of evaporated gold contacts on arsenic triselenide - the contacts appear ohmic in conductivity measurements, but exhibit blocking behaviour during drift mobility measurements.

3.8 OPTICAL ABSORPTION MEASUREMENTS

Optical absorption measurements were performed on thin (0.7 - 2 micron) doped and undoped films of r.f. sputtered arsenic tri-selenide deposited on Corning 7059 glass substrates 0.9mm thick. The measurements were made on a Pye-Unicam SP6 visible and U.V. spectrophotometer in transmission mode. The measurements were simply to give information about possible changes in the optical band gap with sample doping; for this reason absolute measurements were not attempted. Losses due to reflection and so forth were estimated by averaging a number of readings taken at long wave lengths (greater than 900nm) and taking this average as an estimate of the maximum transmitted intensity (Io). The absorption coefficient α was calculated from:-

$$\alpha = {}^{1}/_{t} \ln ({}^{I}/Io)$$

Where t is the sample thickness and I is the measured intensity.

To get a value for the optical band gap from optical absorption data involves a number of assumptions, the most important of which are:-

a. The matrix elements for the electronic transitions are constant over the range of photon energies of interest.

b The $\underline{k}$ conservation selection rule is relaxed in amorphous materials.

Under the further assumption of parabolic bands (Petursson (1975), Mott and Davis (1979) p 288) one may derive the relation:-

$$\alpha(\nu) = \frac{\text{const.}\ (h\nu - E_0)^2}{h\nu}$$

This relation may also be derived for linear band tails using slightly different arguments (Mott and Davis loc. cit.). The constant E_0 may be used to define the optical gap from the intercept of a graph of $(\alpha h\nu)^{\frac{1}{2}}$ versus $h\nu$, although it does not imply a zero in the density of states at this point. Such a quadratic relation between $\alpha h\nu$ and $h\nu$ has been observed for arsenic tri-selenide prepared in a number of ways (Petursson (1975)), and in arsenic selenide doped with Ag (Ishikawa et al, (1980)), Cu (Kitao et al, (1981)) and Ni (Averyanov et al, (1980)).

CHAPTER 4

This chapter presents a summary of the experimental results obtained from d.c. conductivity and drift mobility measurements on undoped vitreous arsenic triselenide prepared by quenching from the melt. Section 4.1 contains the conductivity results, while section 4.2 contains the drift mobility results. These results are discussed in detail in sections 4.3 and 4.4.

4.1 D.C. CONDUCTIVITY RESULTS

The temperature dependence of the d.c. conductivity of a 58 micron thick unsupported arsenic triselenide sample is shown in figure 38 for several different values of applied electric field. Figure 39 illustrates typical results for a somewhat thicker sample (130 microns). At low applied electric fields, the graph of log σ versus 1/T is to a good approximation a straight line. The gradient of the line corresponding to a field of 8.6×10^3 V cm^{-1} corresponds ot an activation energy of 0.92 $\pm$ 0.01 eV. The gradients were calculated using a least squares fit where each point could be assigned a different weight depending upon the estimated experimental error involved. The error quoted corresponds to the standard deviation of the gradient calculated in this way. Note that at this field the current was too low to detect below about 270 K.

The measured activation energy was found to depend upon the value of the applied electric field in the manner shown in figure 40. The activation energy decreased linearly with increasing field above 10^5 V cm^{-1}, but more slowly below this value. An extrapolation of these high field values to zero applied field yields an activation energy of 0.98 eV, whereas a typical low field value would be 0.93 eV.

The field dependence of the conductivity was measured at several different temperatures. Typical results are presented in figures 41, 42 and 43 , which show log σ versus E, log σ versus log E and log I_D versus log E, where I_D is the dark current.

These results are consistent with previous measurements reported by Marshall and Miller (1973) and Marshall, Fisher and Owen (1974), and show an exponential dependence of the conductivity on the applied electric field. Such a field dependence is sometimes found in the case of space-charge injection currents in a sample with a uniform distribution of traps near the Fermi level. This is not thought to be the correct explanation in this case however because the conductivity was found to be thickness independent, in contrast to the predictions of the SCLC theory. A fuller discussion of this appears in section 4.4.

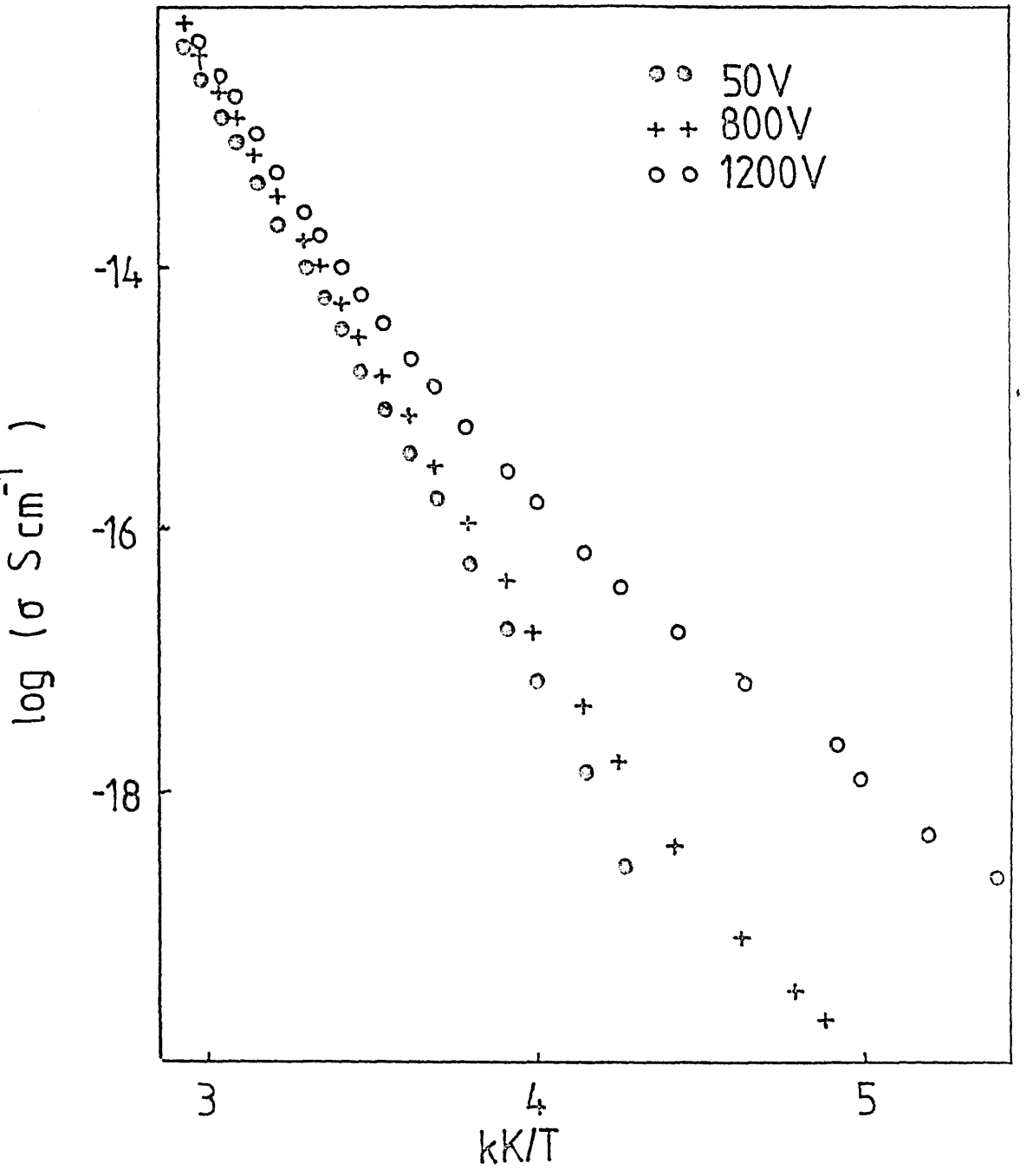

FIGURE 38 : Graph of the logarithm of the conductivity versus inverse temperature for a 58 micron thick vitreous As_2Se_3 film.

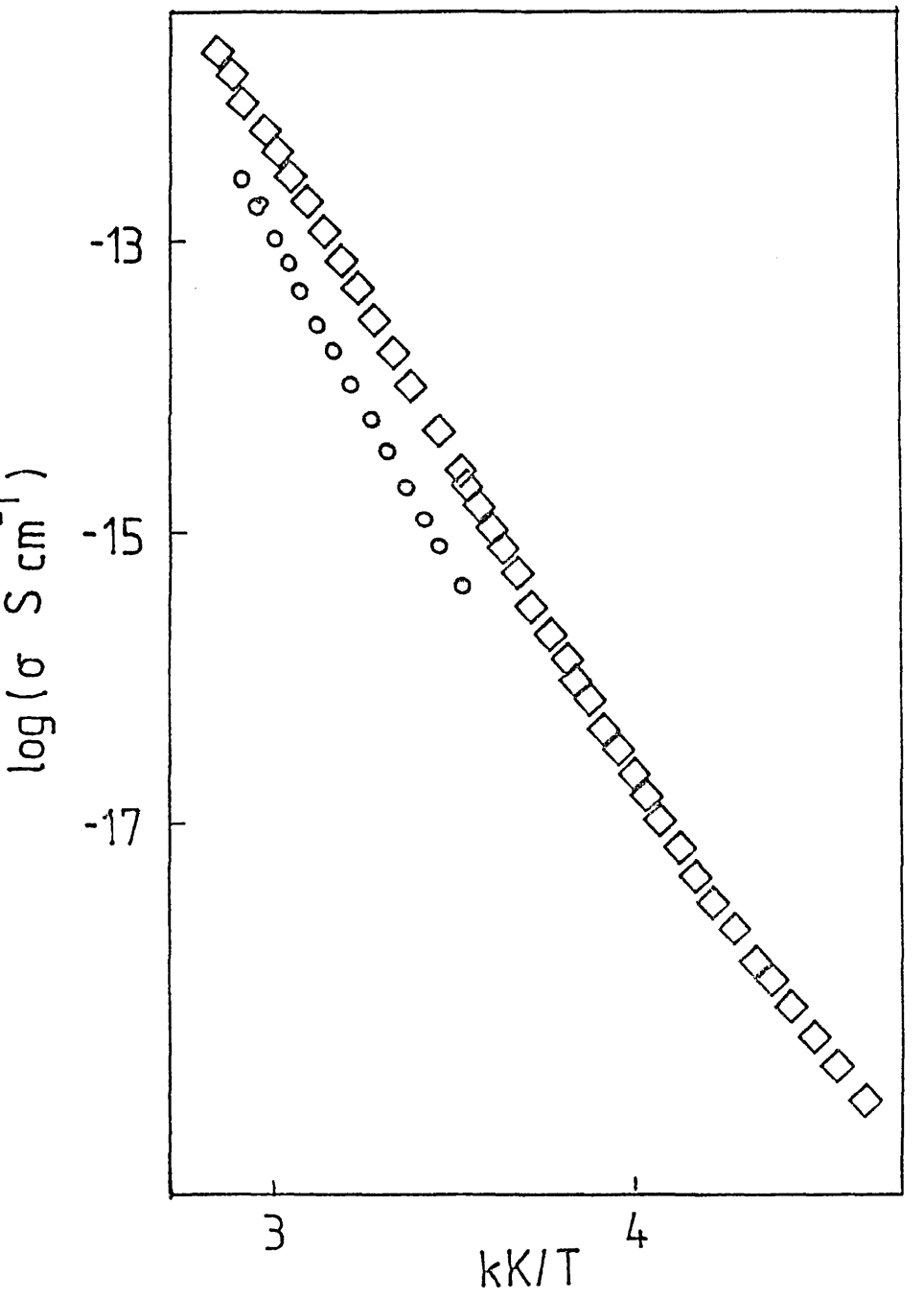

FIGURE 1 : Ion conductivity versus inverse temperature for a 140 micron thick vitreous As_2Se_3 film. Open circles represent a field of 5.6×10^3 V cm^{-1}, squares to a field of 5.6×10^4 V cm^{-1}.

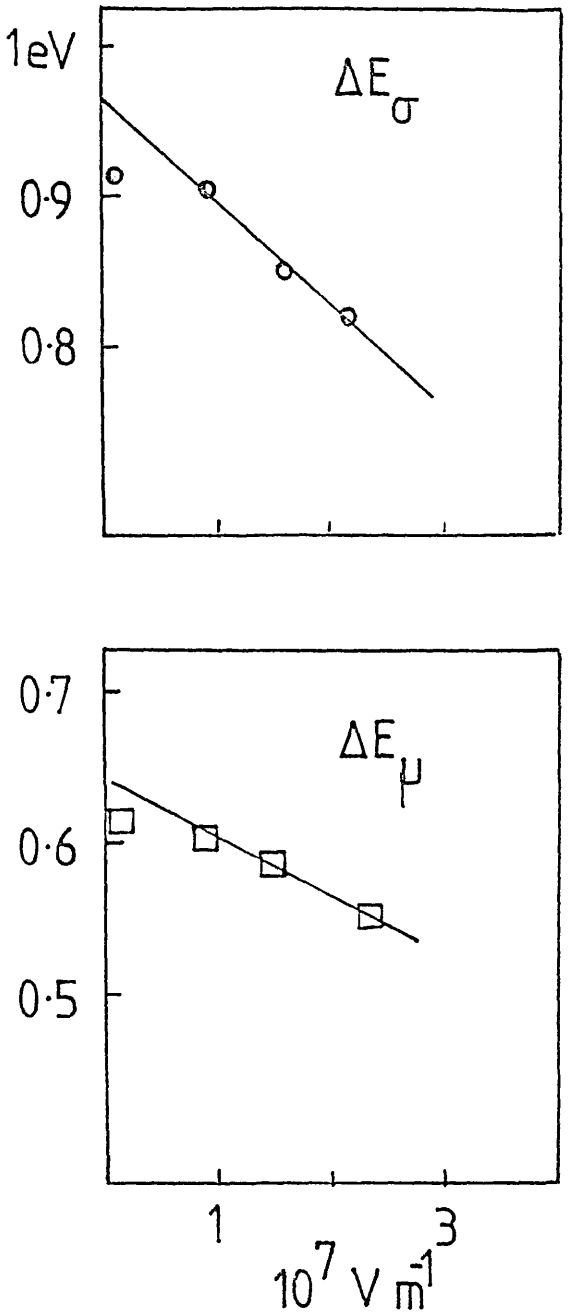

FIGURE 40 : Electric field dependence of the conductivity and mobility activation energies.

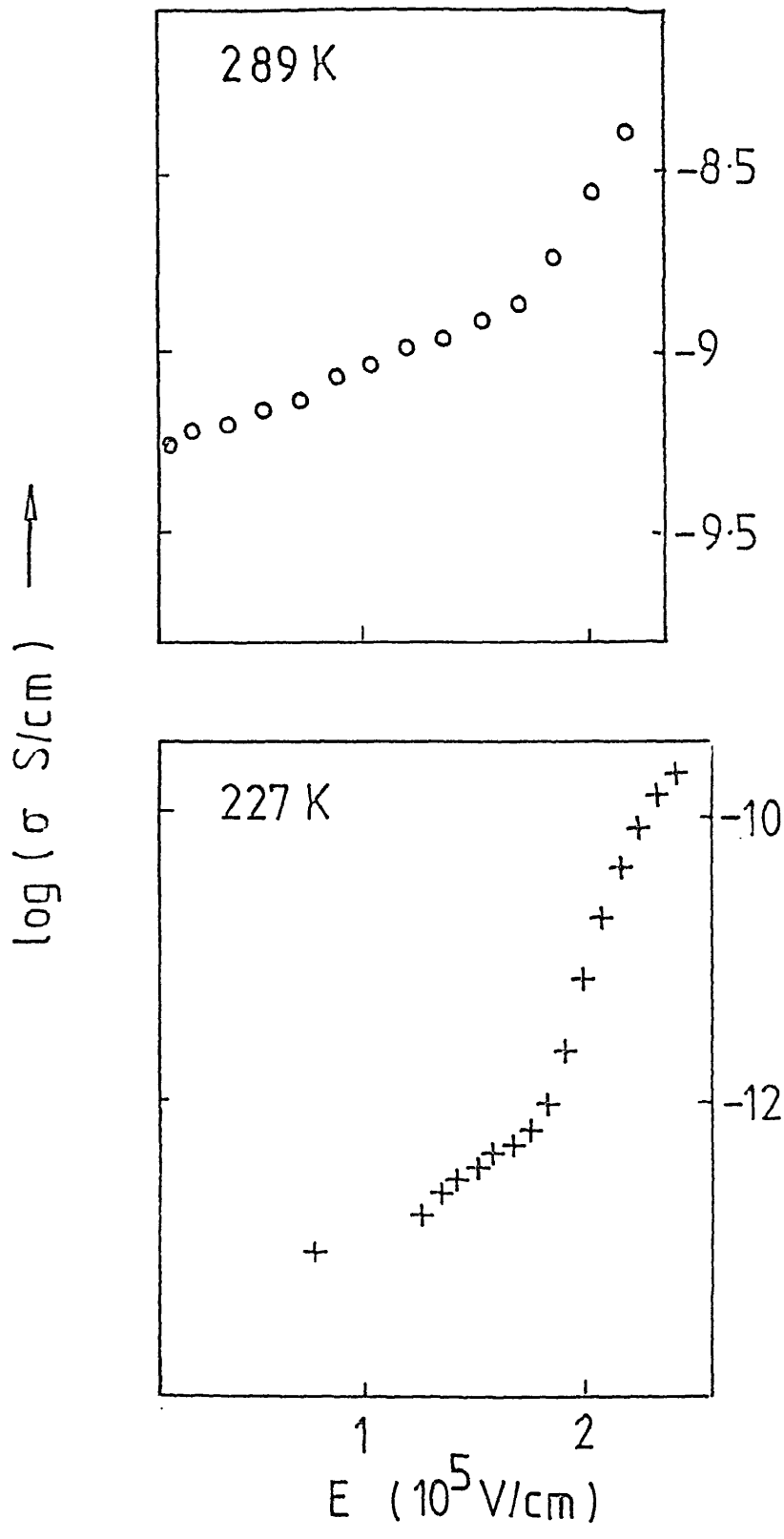

FIGURE 41 : Electric field dependence of the d.c. conductivity in a 58 micron thick vitreous As_xSe_y film.

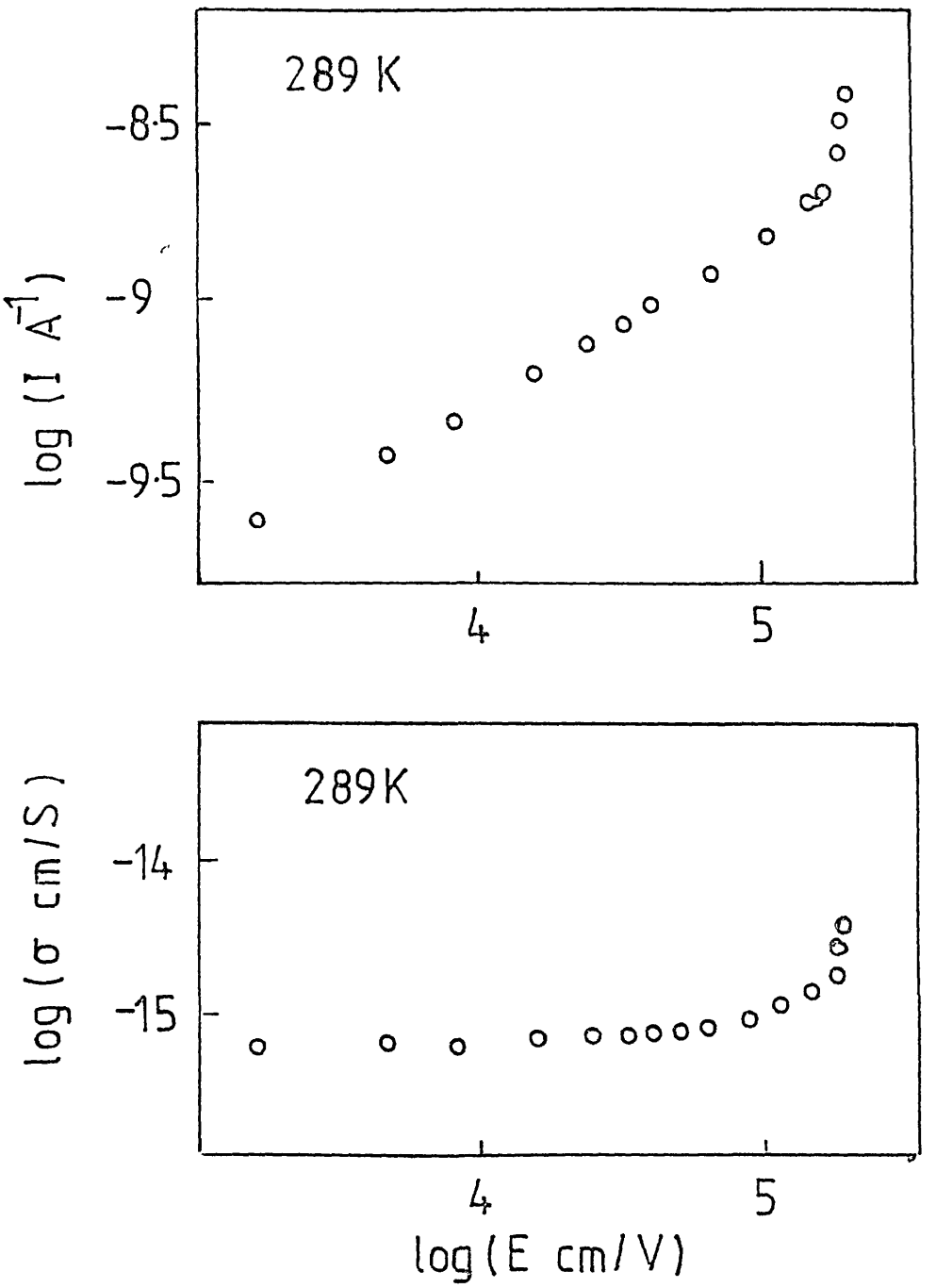

FIGURE 47 : Electric field dependence of the dark current and conductivity in a 58 micron thick vitreous film at 289 K.

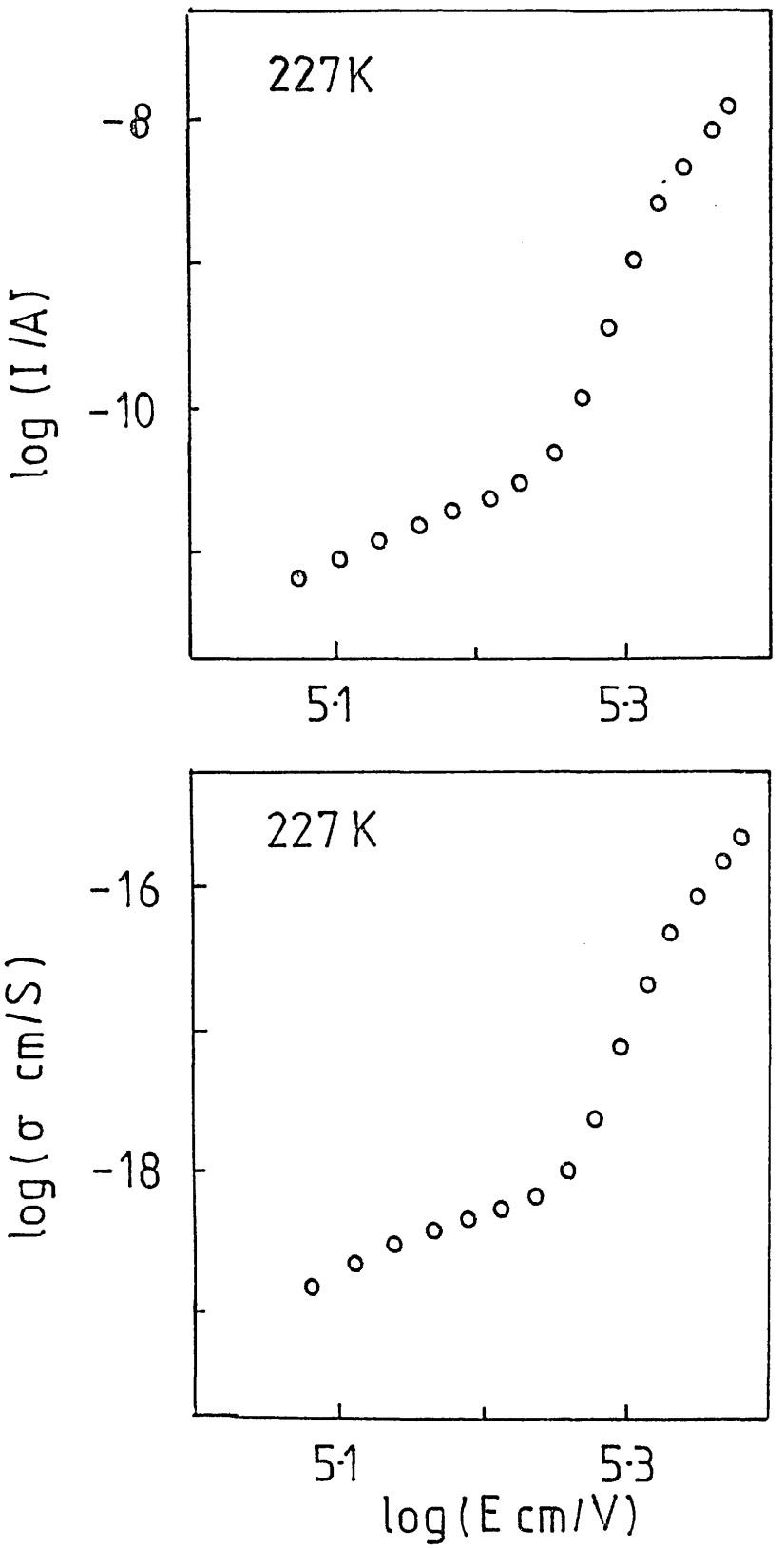

FIGURE 43 : Electric field dependence of the dark current and d.c. conductivity in a 58 micron thick vitreous film at 227 K.

The temperature dependence of the d.c. conductivity at higher applied fields (as shown in figure 38) is very interesting. As the temperature is lowered, the activation energy decreases significantly. Previous investigations of the conductivity of vitreous arsenic triselenide have concentrated on the temperature range from 240 K to the glass transition temperature. This study therefore represents an extension to significantly lower temperatures - down to 160 K. During this investigation temperatures above 360 K were not employed in order to minimise any possible diffusion of gold from the contact areas into the bulk of the sample. The lowest temperatures attained in this study were determined by experimental considerations. For example with 1200 V across a 50 micron thick sample equipped with contacts of area $4mm^2$, the current flowing at 160 K would be of the order of 10^{-13} amp. The detection of such small currents would be impossible in a material which did not posses a remarkably low level of electrical noise (Main (1973)). Indeed at such low current levels small movements near the apparatus must be avoided to minimise induced currents. It is also necessary to fasten all cables securely to the worktop or walls of the laboratory to minimise sudden movements.

In the low temperature high field regime, there appeared to be evidence for three regions with different activation energies - 0.9 eV above 270 K, 0.6 eV between 270 K and 235 K, and 0.35 eV below 235 K. A computer analysis of these results was performed to find out if the data could be described by the sum of a number of exponential functions (as predicted by the mobility edge model of chapter 1), or whether they could better be described as a continuous curve (as predicted by the small polaron model of conduction). It was Halpern (1977) who first pointed out that a careful computer analysis of experimental d.c. conductivity results might be able to distinguish between the two rival models of conduction in As_2Se_3.

The computer analysis was performed using a large FORTRAN program developed by Provencher (1976). The program is designed to analyse data composed of random noise, plus an unknown constant baseline, plus a sum of exponential decay functions. The algorithm on which the program is based involves the solution of a Fredholm integral equation of the first kind in the eigenfunctions of the kernel. The program is completely automatic in that the only information required are the experimental

points themselves, and so no potentially biased initial estimates of either the number of exponential functions present or of their amplitudes and decay constants are necessary. These parameters and their standard deviations are decided with a linear hypothesis test corrected approximately for non-linearity.

The program was run on Dundee College of Technology's DEC 2050 computer, and was comprehensively tested before use. The optimum initial weighting of the data was determined using simulated data with amplitudes and decay constants close to those expected for the genuine data.

Figure 44 shows the same data points as on the graph in figure 38 for an electric field of 2.1×10^5 V cm^{-1}. The dotted lines are the exponential functions which were calculated by the computer program to give the best fit to the experimental points, whilst the solid line represents the sum of these three exponentials. The boxes drawn round the data points simply indicate the expected experimental error present for each point. The best fit was found to be

$$\sigma = 100\ (\pm 50)\ \exp[-1.05(\pm 0.03) \times 10^4/T]$$

$$+ 2 \times 10^{-5 \pm 0.5}\ \exp[-5.9(\pm 0.4) \times 10^3/T]$$

$$+ 2 \times 10^{-10 \pm 1.5}\ \exp[-3.5(\pm 0.1) \times 10^{-3}/T]$$

which corresponds to three exponential components with activation energies of 0.91 ± 0.03 eV, 0.51 ± 0.05 eV and 0.3 ± 0.1 eV.

The program did not find a three component fit for all the data points for a given sample - it tended to treat the low temperature points as a constant baseline. Unfortunately, when the program was altered to look for solutions with a baseline of zero the analysis failed. Hence the analysis showed evidence for only two components with activation energies of 0.91 eV and 0.51 eV. Interestingly, when only the 15 or 20 lowest temperature data points were analysed by themselves the data was resolved into two components with activation energies of 0.51 eV and 0.3 eV. It is felt that these conflicting analyses were due to the limited number of data points used for the analysis - typically 50 to 60 points would be analysed at a time. With this number of data points the establishment of a third exponential component would be problematical even with small experimental error in each point. It is felt that in subsequent studies 150 to 200 data points should be analysed if three components are expected

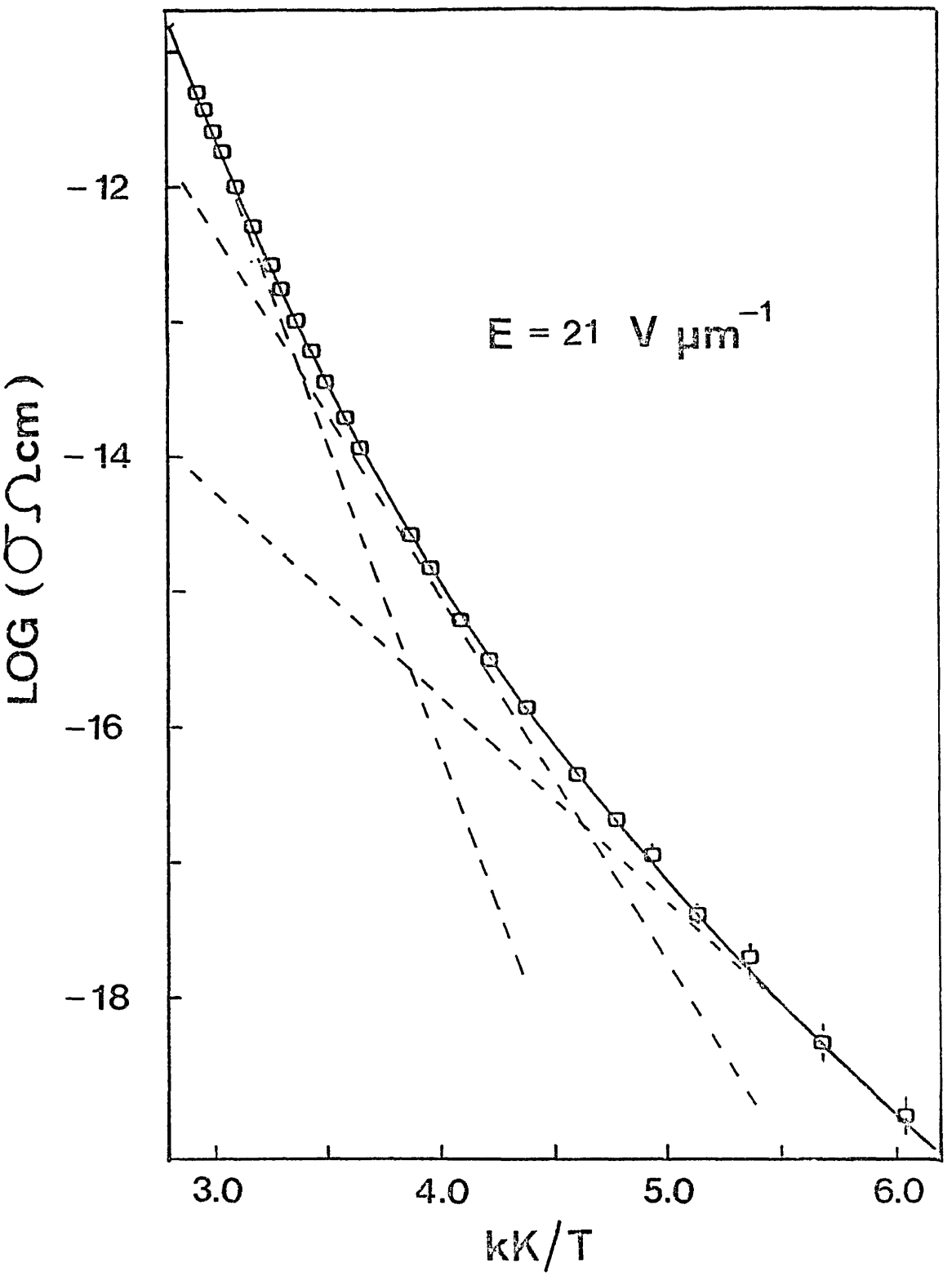

FIGURE 44 : Computer fit of three exponentials to the conductivity data, as described in the text.

The experimental data were also analysed to see if there was any evidence for variable range hopping conduction (viz. $T^{-\frac{1}{4}}$ behaviour) in the experimentally accessible temperature range. In every case however, the analysis failed. This would appear to indicate that variable range hopping does not occur in vitreous arsenic triselenide at temperatures above 160K.

4.2 DRIFT MOBILITY MEASUREMENTS

The temperature dependence of the hole drift mobility in a 58 μm thick unsupported film of vitreous arsenic triselenide at two different applied electric fields is shown in figure 45. The sample from which these measurements were taken was the same sample as that used for the data shown in figure 38 in the previous section. The activation energy observed for different samples above 300K was always within about 5% of the value for this sample, although the pre-exponent varied by about a factor of two. On the same figure are summarised some results from previous investigations by Kolomiets et al. (1978), Pfister (1977), and Marshall and Owen (1971). The drift mobility was calculated from the break-point in log (I) - log (t) graphs as described in chapter 1. The drift mobility activation energy was found to depend on the applied electric field as shown in figure 40. At an applied electric field of 14 V μm^{-1} the measured activation energy was 0.58 $\pm$ 0.02 eV, which may be extrapolated to give a zero-field activation energy of 0.63 $\pm$ 0.03 eV above 300K. This activation energy was observed to decrease to about 0.50 $\pm$ 0.03 eV (zero field) between 300 and 270K. An abrupt change in this activation energy to about 0.15 $\pm$ 0.05 eV was observed below 265K, although there were not enough data points at these low temperatures to determine this activation energy accurately.

Measurements of the hole drift mobility in these samples became progressively more difficult as the temperature was lowered. This is illustrated quite well by figures 46 to 48 which display the shape of the transit pulse on both linear and logarithmic current and time axes at several different temperatures. The transit pulses get more dispersive as the temperature decreases. In addition, the amount of charge in transit across the sample decreases until the point where

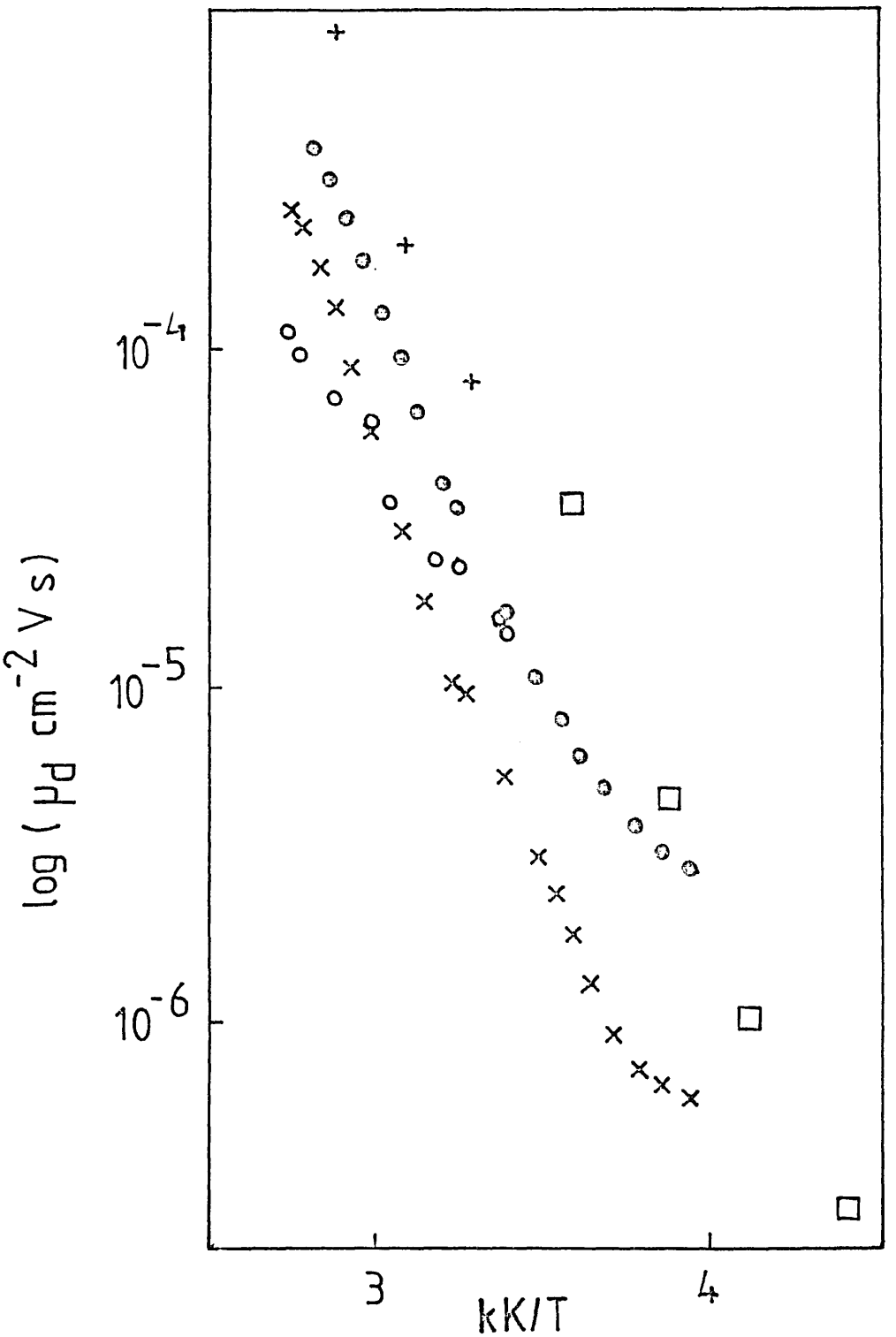

FIGURE 45 : Log of the hole drift mobility versus 1/T for a 58 micron thick vitreous film (x - 1×10^4 V cm^{-1}, ● - 1.4×10^4 V cm^{-1}). Other data as in figure 20.

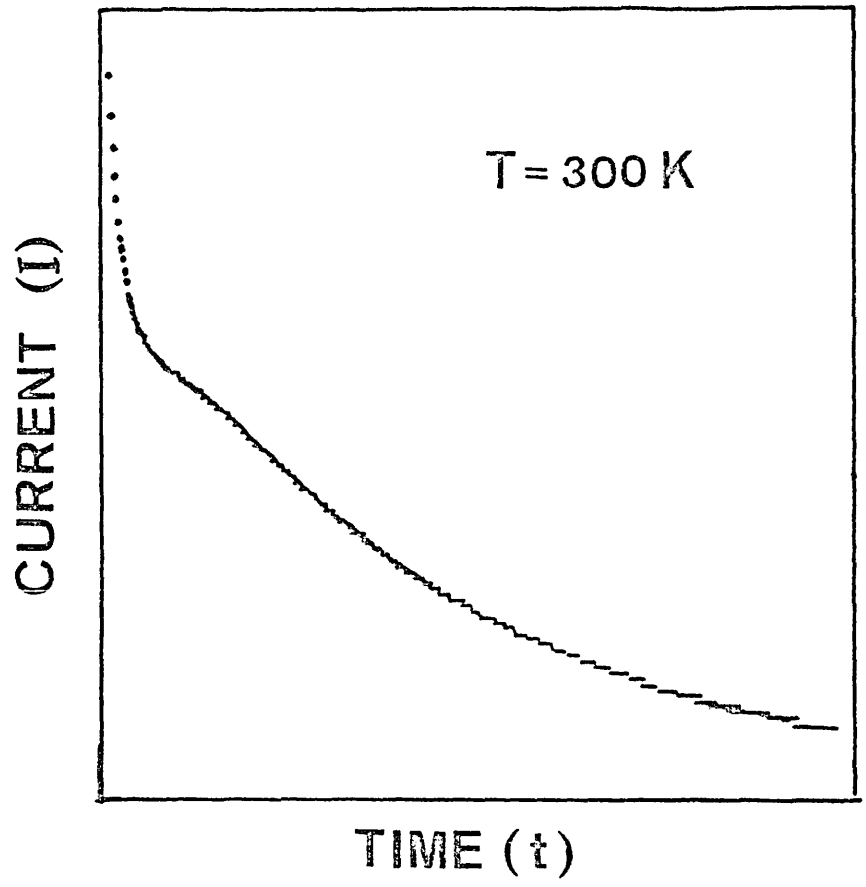

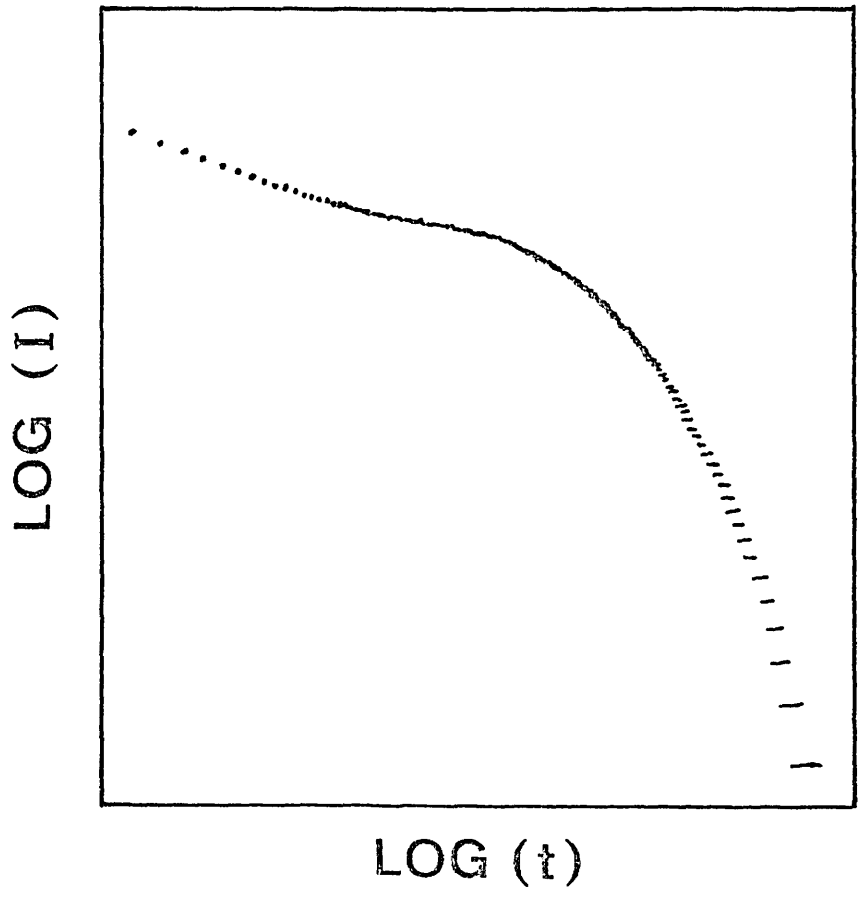

FIGURE 46

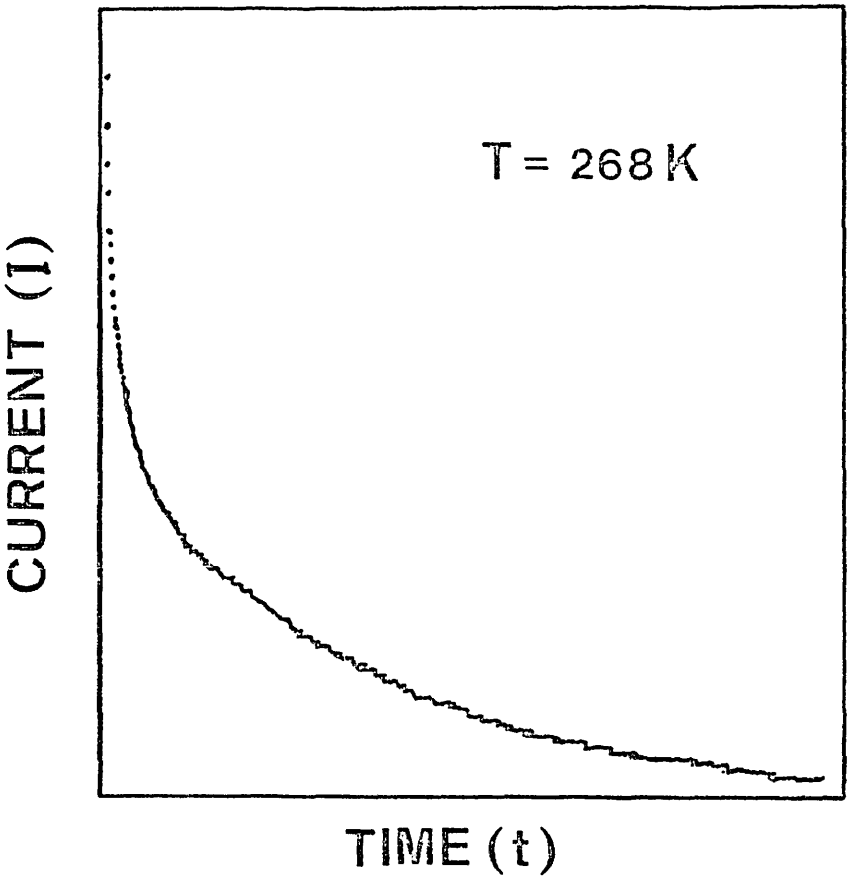

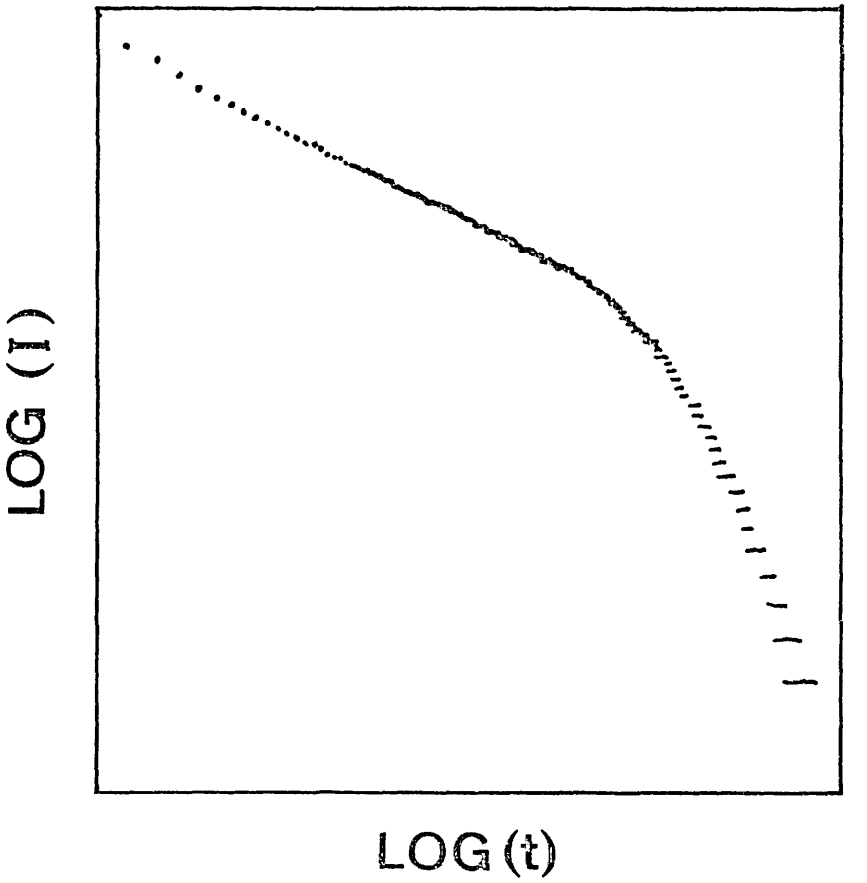

FIGURE 47

FIGURE 4B

the change in gradient of the log (I) - log (t) graphs disappears into the background electrical noise.

As a cross check, the magnitude of the mobility and its activation energy calculated from the position of the change of gradient of log (I) - log (t) graphs was compared with the values obtained by measuring the position of the end of the plateaux region observed in relatively undispersive transits above 300 K displayed on linear axes. In all cases where this was possible the calculated activation energies were the same within experimental error, although the magnitude of the mobility was always found to be about 50% larger when the plateaux method was used.

The electric field dependence of the drift mobility was measured for fields up to 3×10^6 V cm^{-1} at several different temperatures, and the results are displayed in figure 49.

No electron transits were observed in any of the vitreous As_2Se_3 samples used in this study. This is in agreement with all previous investigations reported in the literature, but is still puzzling.

4.3 DISCUSSION OF RESULTS

Electronic transport in vitreous arsenic triselenide has been explained on the basis of three models. These models, which have been discussed in detail in the first two chapters are

a. trap-limited band motion
b. trap-limited hopping conduction
c. small polaron hopping conduction.

In this section our experimental results will be analysed primarily in terms of a trap-limited band motion model. This model was chosen because of the simple way in which it can explain most of the experimental results summarised in chapter two and in the first two sections of this chapter. The model was also chosen because it can be used to calculate trap densities of levels in the mobility gap which may then be compared with those calculated from other experiments such as photoconductivity, photoluminescence and photo-induced

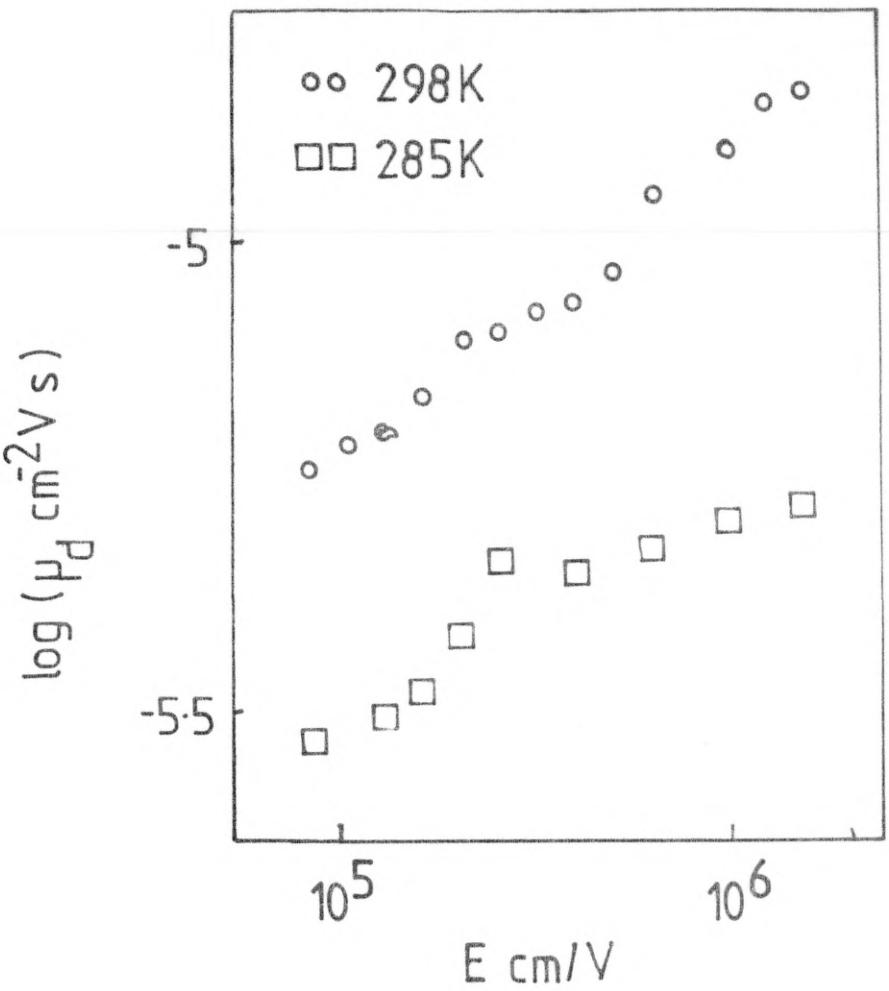

FIGURE 49 : Field dependence of the drift mobility in a 58 micron thick vitreous film.

ESR. After the results have been analysed in terms of this model, the arguments for and against the other two models will be reviewed.

4.3.1 The Trap-limited Band Motion Model

The low field d.c. conductivity data presented in section 4.1 obeys the relationship

$$\sigma = \sigma_o \exp \{-\Delta E/kT\}$$

with values of the pre-exponent in the range 600 - 800 $\Omega^{-1}cm^{-1}$. This behaviour is in good agreement with previous measurements reported by Fisher, Marshall and Owen (1976), Hulls and McMillan (1974) and Edmond (1968). Our value for the pre-exponent is between that quoted by Fisher et al. (300 - 500 $\Omega^{-1}cm^{-1}$) and that quoted by the other authors (3000 - 4000 $\Omega^{-1}cm^{-1}$). This discrepancy could possibly be due to a temperature dilation of the mobility gap similar to that of the optical band gap (Main (1974)), because the measurements of Hulls and McMillan and Edmond were performed at much higher temperatures than those of this study or that of Fisher, Marshall and Owen. Alternatively, the discrepancy could be caused by a slight shift in the position of the Fermi level with temperature.

The magnitude of σ_o suggests that carrier transport occurs through extended states at temperatures above 300K rather than by a process of thermally activated hopping between localised states in the mobility gap. It was shown in chapter one that with a slight temperature dependence of the mobility gap the conductivity pre-exponent may be expressed

$$\sigma_o = \sigma_{min} \exp \{\gamma/2k\} \simeq 700\ \Omega^{-1}cm^{-1}$$

where the temperature dependence of the band gap is given by

$$E_c - E_v = E(0) - \gamma T$$

Main (1974) has shown that γ is in the range 4.5 - 6.0 x 10^{-4} eV K^{-1}, and thus σ_{min} must lie in the range 20 - 70 $\Omega^{-1}cm^{-1}$. This value is two to three orders of magnitude greater than one would expect to observe for hopping conduction, although the value is consistent with the mechanism of small polaron hopping.

It was shown in section 4.2 that the hole drift mobility at low applied fields was thermally activated, with an activation energy of about 0.6 eV above 300K. Such behaviour may occur for a number of transport mechanisms including trap-limited band motion, trap-limited hopping conduction, thermally activated hopping or small polaron hopping conduction. It is felt that thermally activated hopping at a single trap level is the least likely of these processes because of the large conductivity pre-exponent encountered, and because of the large hopping energy required (0.6 eV). For hopping in a single trap level far from the Fermi level, the mobility pre-exponent will be of the form

$$\mu_o = \frac{\nu e R^2}{6kT} \exp\{-2\alpha R\}$$

where ν is a characteristic phonon frequency for hops of length R, α is the localisation parameter of the centres, and T is the temperature. For nearest neighbour hopping far from the Fermi level the term $\nu \exp\{-2\alpha R\}$ cannot be higher than about 10^{13} Hz, which sets an upper limit on μ_o of 0.1 $cm^2V^{-1}s^{-1}$. This must be compared with the experimentally determined value of 10^3 - 10^5 $cm^2V^{-1}s^{-1}$ found in section 4.2. It must be stressed, however, that this value of pre-exponent is compatible with small polaron hopping or trap-limited hopping (Street and Gill (1966)).

Recent studies of hopping conduction in disordered systems have suggested that for the above term $\nu \exp\{-2\alpha R\}$ to be of the order of 10^{13}Hz in the variable range hopping regime, phonon frequencies of the order of 10^{16} - 10^{22} Hz have to be postulated because of the effect of the exponential factor $-2\alpha R$. Although such unphysically large values of phonon frequency indicate that the theoretical model may be breaking down in the variable range hopping regime, there is no evidence to suggest that similarly high phonon frequencies are to be expected in the nearest neighbour hopping regime at higher temperatures, where it is difficult to imagine a carrier hopping faster than a phonon.

To get meaningful quantitative estimates of the density of trap and transport states in the multiple trapping model from measurements of the d.c. conductivity and drift mobility, it is necessary to make

the assumption that the carriers responsible for the mobility and conductivity move through the same conduction path through the solid. This is an important assumption, and one which may only really be justified by observing how well the trap densities calculated on the basis of this model compare with other estimates from different experiments. One implication of the assumption is that changes in the mobility and conductivity activation energies should occur at roughly the same temperature in the same sample. Our results were encouraging in this respect, because several of the samples studied showed such a change in both activation energies at about 250 - 270K. Another encouraging feature of the results was the similar field dependence of the hole drift mobility and d.c. conductivity. The field dependence of bothquantities should be the same if the number of carriers is not effected by the applied field, and the carriers move through the same conduction path. Unfortunately, however, carriers moving through different paths may exhibit the same field dependence of the mobility and conductivity. One of the best examples of this behaviour is that of vitreous selenium - in this material the hole and electron mobilities have the same field dependence.

When considering the question of possible conduction paths, it must be remembered that the drift mobility and d.c. conductivity are of necessity measured under different experimental conditions. In particular, because of the need for a heated filament or light source to produce excess carriers, drift mobility measurements must be performed whilst the sample is being illuminated with photons of energy greater than the optical band gap of the material. This is in contrast to measurements of the d.c. conductivity, where steps are taken to exclude all light from the chamber. Such illumination may effect the density of defect states in the mobility gap of As_2Se_3 (as observed for example in photoinduced ESR experiments and the phenomenon of photodarkening), and thus affect the dominant conduction path at a given temperature. One would expect such effects to be more serious at larger photon fluxes and at lower temperatures when there will be a lower recombination rate and reduced annealing of photoinduced defects (such behaviour has recently been reported by Kasakova et al.). Figure 50 shows how the d.c. conductivity was effected by the presence of light from the electron gun filament for

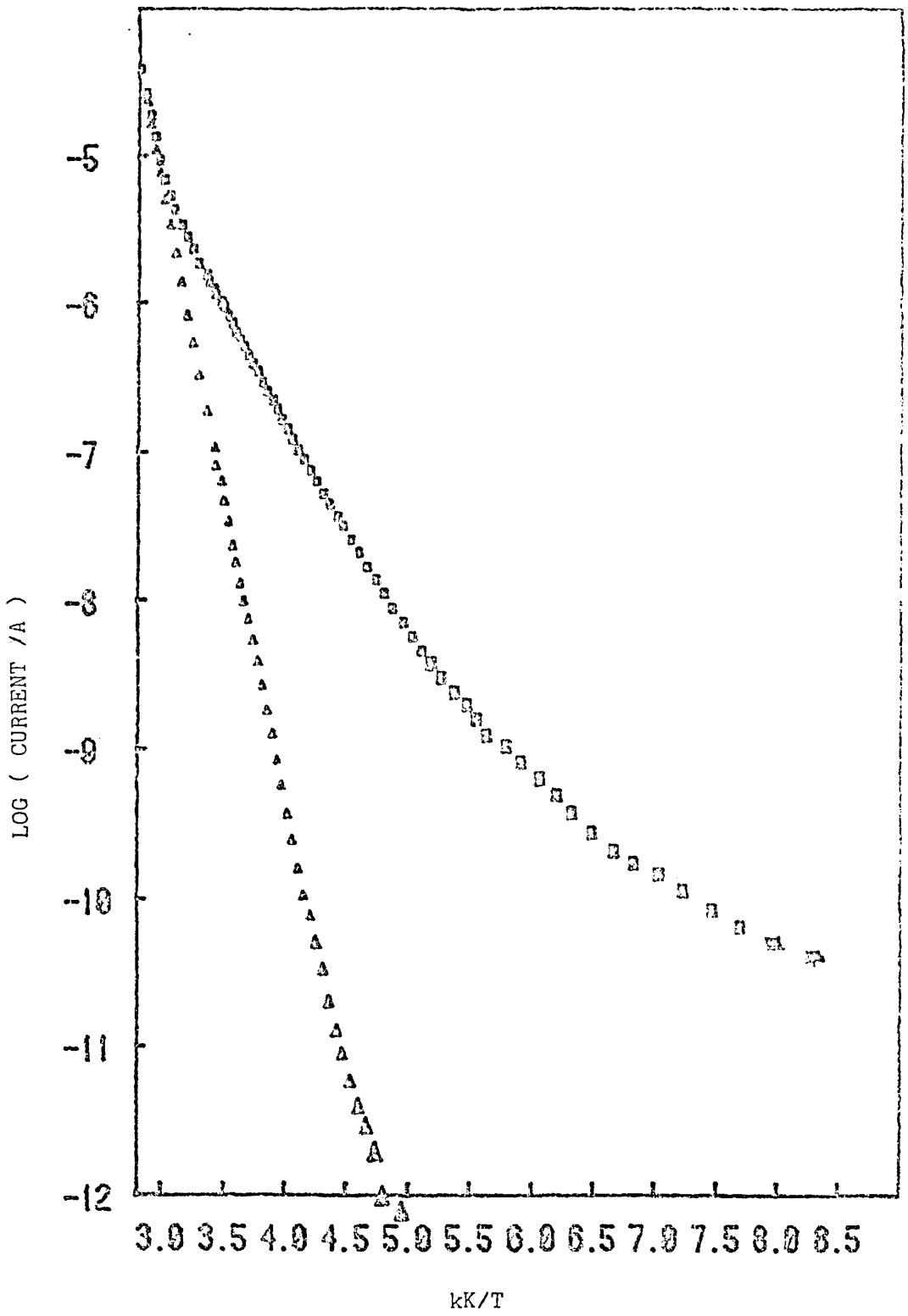

FIGURE 50: Effect of electron gun filament on the conductivity - squares show photocurrent and triangles dark current.

various temperatures.

For the case of carrier motion at a mobility edge (periodically interupted by trapping in localised states within the mobility gap a number of expressions for the mobility may be derived, the exact form of which depend on the particular energy distribution of the localised states involved. The simplest case, in which the localised states may be considered as a well defined trap level located E_t above the valence band mobility edge, leads to an expression for the hole drift mobility of the form

$$\mu_d = \mu_o \, N_v/N_t \, \exp \{-E_t/kT\}$$

as previously described, where N_v is the effective density of states at the valence band mobility edge and N_t is the density of trapping centres. Therefore, when this mechanism is applicable it is possible to determine the trap density from combined conductivity and mobility measurements, since $\sigma_o = N_v e \mu_o$ if we assume that the conduction is by hole carriers only. Thus

$$N_t = \frac{\sigma}{e\mu_d} \exp \{(E_\sigma - E_t)/kT\}$$

A graph of log (σ/μ_d) versus 1/T should therefore be a straight line if such a conduction mechanism is involved. Such a graph has been drawn for our 14 V μm^{-1} results, and is displayed in figure 51 . A value for N_t may be obtained from the intercept on the 1/T = 0 axis of an extrapolation of the high temperature results. This yields a value of N_t of $7 \pm 3 \times 10^{15}$ cm^{-3} uncorrected for temperature dilation of the mobility gap (or $2 \pm 1 \times 10^{15}$ cm^{-3} if a temperature dependence of the trap depth of about 30% of that for the entire optical gap is taken into account. This in turn implies a value for N_v of 1.5×10^{19} cm^{-3} (5×10^{18} cm^{-3} corrected) if one assumes μ_o is approximately 5 $cm^2 V^{-1} s^{-1}$ at the mobility edge with a mobility pre-exponent of 10^4. These values are similar to those calculated by Fisher, Marshall and Owen (1976), who deduced a trap density of $4 \times 10^{15} cm^{-3}$ corrected for temperature dilation of the band gap.

At temperatures lower than about 300K, the graph of log (σ/μ_d) versus 1/T exhibits a different activation energy from that observed at higher temperatures. The activation energy decreases from -0.27 eV

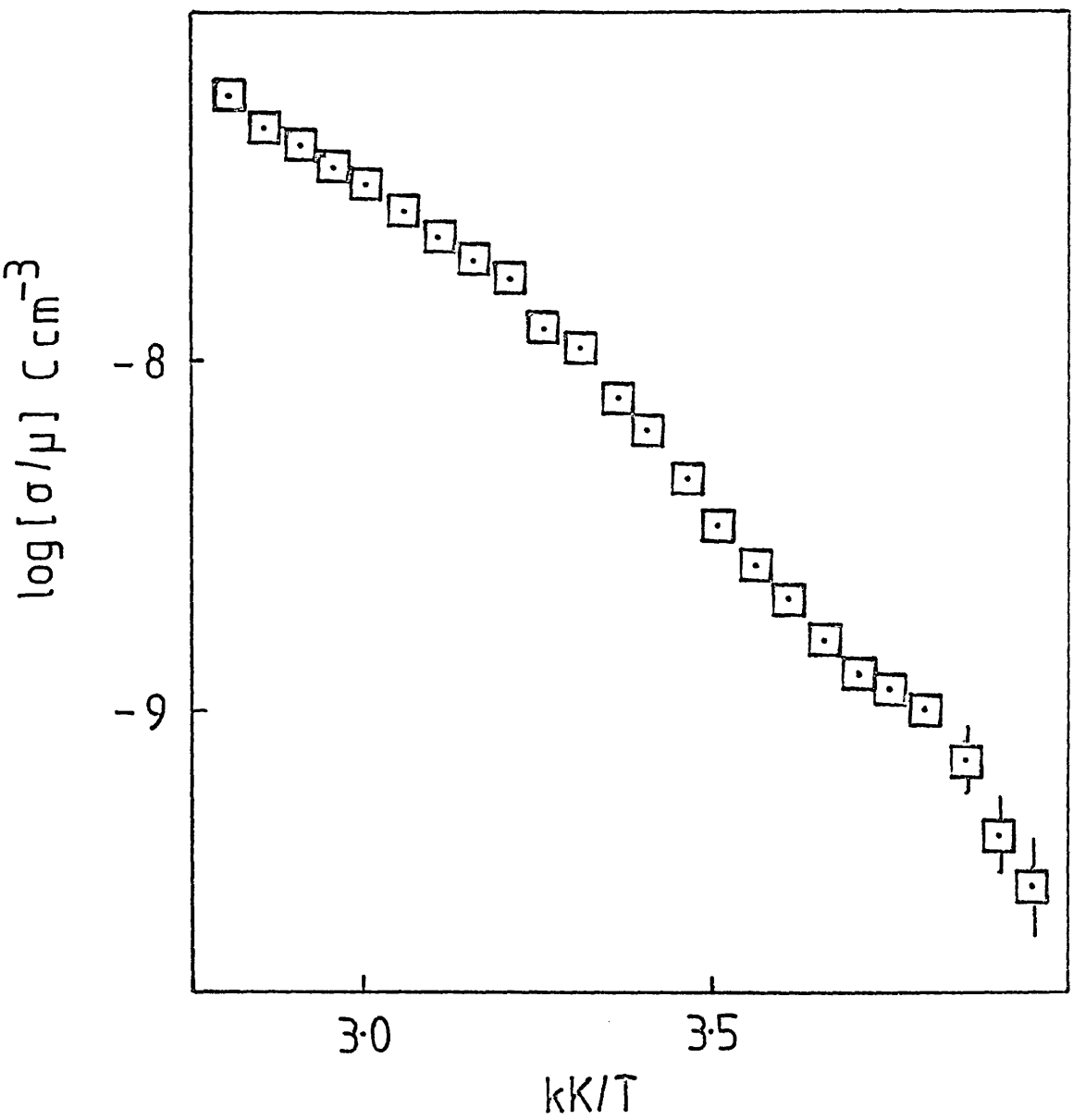

FIGURE 51 : Graph of log (σ/μ_d) versus inverse temperature for the 58 micron thick vitreous film at 1.4 x 10^5 V cm^{-1}.

above 300 K to - 0.46 eV below 300K. In the trap limited band motion model, the activation energy of this graph represents the depth of the mobility controlling traps from the Fermi level. It would thus appear that the mobility controlling traps move further from the Fermi level as the temperature is lowered. Such behaviour is surprising, but can be understood if one considers the constraint imposed by the release rate from deep traps becoming important at these temperatures.

It was shown in chapter one that the condition for a trap level to be observed in a drift mobility experiment was that the average release time from the set of traps had to be shorter than the transit time (or at least of a similar magnitude). In other words

$$\nu_{ph}\, t_T \exp\{-\Delta E/kT\} > 1 \qquad (1.26)$$

where ν_{ph} is the phonon attempt to escape frequency, t_T is the transit time and ΔE is the trap depth. The thicker the sample or the lower the applied field, the longer the transit time, and the lower the temperature at which a given trap level will be observable (if one neglects a possible field dependence of the release rate). One would thus expect a trap level to become difficult to observe below a critical temperature (T_{crit}) such that

$$\nu_{ph}\, t_T \exp\{-\Delta E/kT_{crit}\} = 1$$

For our results, ΔE = 0.6 eV, t_T = 11 ms at 1.4 x 10^7 V/m, and T_{crit} is about 300K. It therefore follows that ν_{ph} = 1.1 x 10^{12} Hz. The possible error in this value for the phonon frequency comes mainly from the uncertainty in T_{crit}, which if this is estimated to be ± 10K should be of the order of 50%. This value of phonon frequency is indeed close to the maximum normally assumed in calculations of 10^{12} - 10^{13} Hz. From these values of N_v and ν_{ph} one may calculate a capture coefficient if one assumes microscopic reversibility. Then

$$\nu_{ph} = b_{0.6}\, N_v$$

where $b_{0.6}$ is the capture coefficient of the traps 0.6 eV from the valence band mobility edge, which is equal to the product of the capture cross-section and the thermal velocity of the carriers. Thus for these traps $b_{0.6}$ = 1.1 x 10^{-7} cm^3/s at 300K, which yields a cap-

ture cross-section of 10^{-14} - 10^{-15} for hole effective masses of from one to fifteen electron masses respectively (if one assumes the thermal velocity to vary with temperature in the normal way).

The measurement of $b_{0.6}/\mu_o = 2.2 \times 10^{-8}$ cm V provides a measure of the capture radius of the traps. In highly disordered material where the mean free path of the carrier approaches the interatomic spacing, the carrier motion becomes diffusive - the so-called random phase regime. In this case the usual explanation of trapping in terms of a capture cross-section and a thermal velocity may break down. Instead, from the solution of the diffusion equation one finds (Chandrasekar (1943))

$$b = 4\pi R_o D = 4\pi R_o kT\mu_o/e$$

where D is the diffusion coefficient, and R_o is the trapping radius. Our result gives a value of R_o of 6 Å. This value for R_o is large, but is typical of traps which have a strong electron-phonon coupling (Henry and Lang (1977)). On would expect these traps to have a large electron-phonon coupling because of the large Stokes' shift observed in this material (Street (1976)).

Our value for the quantity b/μ_o is within 70% of the value recently calculated by Orenstein, Kastner and Vaninov (1982) for the recombination radius of these traps from transient photoconductivity experiments. This agreement is remarkable for capture cross-section measurements, for which 'order of magnitude' agreement is often difficult to achieve. This agreement is encouraging, and gives added confidence to the approximations used in the calculation.

Thus the position of the discontinuity in gradient of a $\log(\sigma/\mu)$ versus 1/T graph may be used to find the phonon attempt-to-escape frequency and hence the capture radius of the mobility controlling traps. It is anticipated that by using several specimens of different thicknesses a fairly accurate value for the phonon frequency could be obtained from the gradient of a t_T versus T_{crit} graph. Further information on the temperature dependence of the capture radius could be obtained from the careful study of several samples of different thicknesses, although the amount of data required would be very large. The agreement between our value of the capture radius and Orenstein et al.'s value for the recombination radius

would seem to indicate that any field dependence of the release rate or capture coefficient must be small, because transient photoconductivity measurements are performed at very low fields whereas our time of flight measurements were performed at 1.4×10^7 V/m.

In chapter one it was shown that one of the conditions for the observation of dispersive transport in the multiple trapping model was that the solid should posses a set of traps which will be visited on average only once during the transit of the carrier pulse. This condition will be automatically satisfied if the release time is of the order of the transit time. Thus the observation of a discontinuity of gradient in log (I) versus 1/T graphs is to be expected if dispersive transport is observed. This implies that the capture coefficient of a particular trap level may only be calculated from time-of flight data when dispersive transport is present.

The above explanation of our drift mobility results can also be used to explain some puzzling behaviour reported by Kolomiets, Lebedev and Kasakova (1978). In their experiments on drift mobility in arsenic triselenide, these authors observed dispersive current transients between 290K and 320K, normal gaussian spreading of the carrier packet between 320K and 360K, and dispersive transport again above 360K. In these experiments the mobility activation energy changed from 0.28 eV above 360K to about 0.4 eV below 360K. One can explain these results by assuming that the release time from the traps 0.4 eV above the valence band mobility edge becomes comparable to the transit time below about 320K. Above 360K the mobility controlling traps are 0.28 eV above the valence band, but as the temperature approaches 360K the release time from these traps becomes comparable to the transit time giving dispersive transport once again. Thus one will observe two regimes where dispersive transport is observed - just above 360K when trapping occurs in the 0.28eV traps, and at below 320K where the trapping occurs in the 0.4 eV level.

Although the above argument shows how the mobility controlling traps observed in a time-of-flight experiment may appear to move further from the Fermi level as the temperature is lowered. one may still make the assumption that the transport states through which conduction takes place are the same for both the mobility and con-

ductivity measurements. The only difference will be a reduction in the apparent depth of the trapping level. Thus the model used by Sharp, Marshall and Fortuna to explain some of the above data is still applicable. This model is illustrated schematically in figure 52. In this model it is assumed that there are three fairly distinct trap levels in the mobility gap of As_2Se_3 located 0.3 eV, 0.4 eV and 0.6 eV above the valence band mobility edge. The model is not fundamentally new, and has been used by Marshall and Owen (1971), Fisher, Marshall and Owen (1976) and Main (1974) to explain thermally stimulated current, electrical noise and transient photoconductivity data.

At high temperatures, one expects to observe trap limited band motion. The carriers will move through extended states close to the valence band mobility edge, with occasional trapping in and release from the trap levels in the mobility gap and in the band tails. The large value of the conductivity pre-exponent in this regime is the main reason for preferring this transport mechanism to one of the variants on hopping conduction. The activation energy of the drift mobility indicates that the mobility controlling traps are 0.63eV above the valence band mobility edge in this regime, whilst the activation energy of the d.c. conductivity (0.93 eV) indicates that the Fermi level is close to the centre of the optical gap and is 'pinned' (i.e. insensitive to temperature). At higher temperatures than those used in this study it is anticipated that one may observe trapping in levels closer to the valence band edge. Indeed the mobility data displayed in figure 45 indicates that the activation energy began to decrease at about 350K.

As the temperature is reduced, the conduction path will move into the localised valence band tail states. The temperature at which this transition occurs will depend on the exact details of the density of states in the band tails, and is likely to be strongly dependent on the method of preparation of the material and its thermal history. As the conduction path moves up through the band tails, the conductivity and drift mobility activation energies should decrease. This appears to happen for our samples between 330K and 300K. As described above, we then expect the mobility controlling traps to move from the 0.63eV level to the 0.43 eV level. A fairly clear change in the drift mobility activation energy from about 0.5 eV to 0.4 eV occurs at this

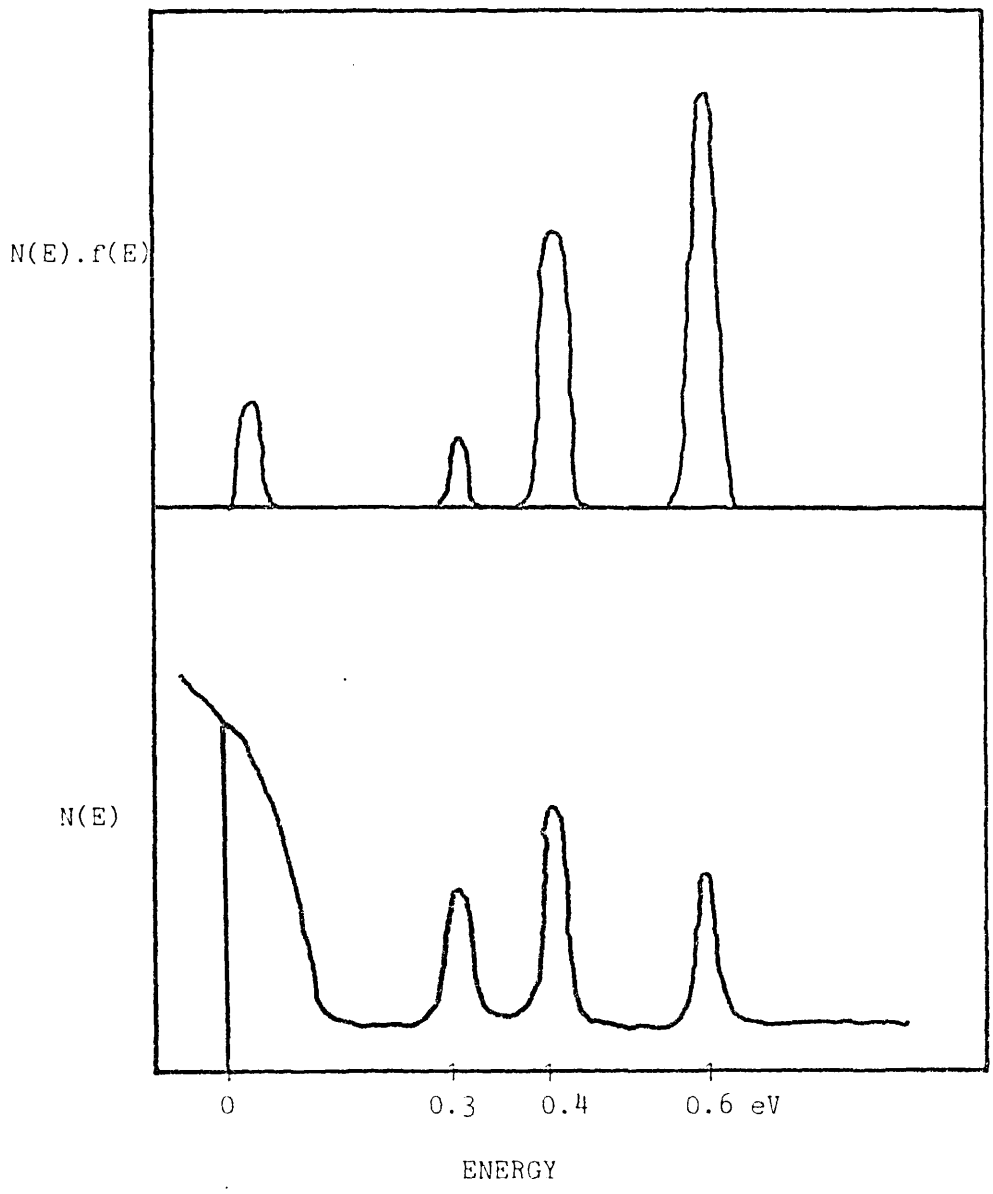

FIGURE 52 : Schematic diagram of model with three sets of traps 0.3, 0.4 and 0.6 eV above the valence band mobility edge.

point, although there is no such obvious change in the conductivity activation energy.

As the temperature is reduced further from 300K to 265K, the activation energy of the d.c. conductivity decreases to 0.51 ± 0.06 eV. This observation is consistent with the conduction path moving directly into the 0.43 eV trap level (i.e. missing out the 0.3 eV level completely). As these are the mobility controlling traps for this combination of temperature, applied field and sample thickness, one would expect the drift mobility activation energy to to fall to that expected for hopping conduction. This indeed was observed below about 265K, which gives good support to the model. Unfortunately the transit pulse was difficult to observe at much lower temperatures, so that a value for this hopping energy cannot be calculated accurately. The value from the gradient of the drift mobility graph would seem to indicate a hopping energy of the order of 0.1eV.

Below 230K, the activation energy of the d.c. conductivity falls to 0.3 ± 0.1 eV. This is consistent with the conduction path moving into the trap level 0.63 eV above the valence band mobility edge. As pointed out by Sharp, Marshall and Fortuna (1981), one would expect hopping in a particular trap level to predominate when the average time for thermal release to the band becomes greater than the average hopping time between sites. Then

$$\nu_{ph}^{-1} \exp\{\Delta E/kT\} > \nu_{ph}^{-1} \exp\{2\alpha R\} \exp\{\omega/kT\}$$

Assuming the phonon frequencies cancel and the density of traps in the 0.63 eV level is 2×10^{15} cm^{-3} we have

$$2\alpha R = (\Delta E - \omega)/kT$$

where R is about 100 nm and T is 230K. If we take the hopping energy to be 0.1 eV, this implies a value of $1/\alpha$ of 6 nm. An increase in the hopping enery to 0.2 eV would decrease this value to about 4 nm, while a decrease in the hopping energy would indicate a larger value for the reciprocal of the localisation parameter α.

It is possible to give a rough estimate of the density of states in the 0.43 eV trap level in a similar way. From our vitreous results this may be calculated to be about 4×10^{16} cm^{-3}, using a hopping energy of 0.1 eV and a similar value of the localisation parameter.

This value is about two orders of magnitude greater than TSC or transient photoconductivity measurements have indicated. This may be explained quite easily if the two trap levels have a different localisation parameter. If a $1/\alpha$ of 1nm was substituted into the above calculation, the density of traps 0.43 eV above the valence band would become $10^{18} cm^{-3}$ in agreement with other experiments. It would thus appear that these traps may be more localised than the traps in the 0.63 eV level, as suggested by Sharp, Marshall and Fortuna (1981).

In the above analysis, the mobility activation energy has been taken to provide a measure of the depth to which the fastest few percent of carriers have equilibrated during the transit. This depth is related to the free carrier capture process rather than to that of trapped carrier release - and thus is normally temperature independent (see for example Marshall and Allan (1979)).

However, as pointed out by Schmidlin (1977, 1981) it is possible for the capture process itself to be activated. If this were the case in our samples the depth of equilibration would change with temperature. As suggested by Sharp and Marshall (1981), the fact that α_i is insensitive to temperature for evaporated As_2Se_3 may indicate that at least in this material there are a number of traps such that $\Delta_i = \alpha E_i$, where Δ_i is a possible activation energy for a capture event and E_i is the trap depth. Such a temperature dependence of the capture cross section of deep traps has recently been observed in a-Si by Okushi et al. (1983)

4.3.2 Temperature Dependence of Dispersion

Perhaps the most interesting observation during the drift mobility experiments was that the pulse shape changed significantly with temperature, in marked contrast to the behaviour reported by Pfister and Scher (1978). This discrepancy may be due at least in part to differing methods of sample preperation. These authors used evaporated samples annealed near T_g, whereas the above results were for the bulk glass. This explanation is consistent with our work on evaporated samples discussed in the next chapter - here we observed a less pronounced temperature dependence.

Typical current transients from a pulse of hole carriers passing through a 58μm As_2Se_3 film are shown in figures 46 to 48 for various

temperatures. The upper portions of each diagram show the pulse displayed on linear current and time axes, whereas the lower portions show the same pulse displayed on logarithmic axes). There is clearly an increase in the amount of transit pulse dispersion as the specimen temperature is lowered, although changing the applied field did not significantly change the dispersion at a given temperature. These results have been reported in the paper by Sharp and Marshall (1981). In contrast, the degree of dispersion observed in evaporated specimens changed much less with temperature. This is illustrated in figure 53 , which shows the dispersion parameter α_i (calculated from the initial slope of the log(I) log(t) graphs) as a function of temperature for both vitreous and evaporated films.

For vitreous films, there is a clear linear temperature dependence of α_i for temperatures below about 300K. If this behaviour is considered to be associated with a characteristic temperature T_o such that $\alpha_i = T/T_o$, then T_o= 330K for vitreous films. This temperature is very close to the temperature at which the $\log(\sigma/\mu_d)$ vs. 1/T graph showed a discontinuity in gradient - indicating that there may be a connection between the kink and the onset of anomalously dispersive transport. In evaporated samples, the temperature dependence of α_i was much less marked, and its increase with increasing temperature was slow. This implies that T_o must be much higher in evaporated films, possibly of the order of 600K.

Orenstein and Kastner (1981) recently speculated that there were inconsistencies in the temperature dependence of the dispersion parameter deduced from time-of-flight and transient photocurrent experiments. They observed a linear temperature dependence of α_i, with a value for T_o of 550K for vitreous films and argued that because this behaviour was different to that observed by Pfister and Scher (who used a time of flight method in samples prepared by evaporation which were subsequently annealed at T_g) the difference must be due to the different methods of measurement. Our results indicate that differences in the method of sample preparation can account for these differences.

Although the value of α_f calculated from the final slope of log(I) log(t) graphs was difficult to measure with accuracy, the measurements which were performed indicated that α_i and α_f for vitreous As_2Se_3 behaved in a similar way to that observed in a

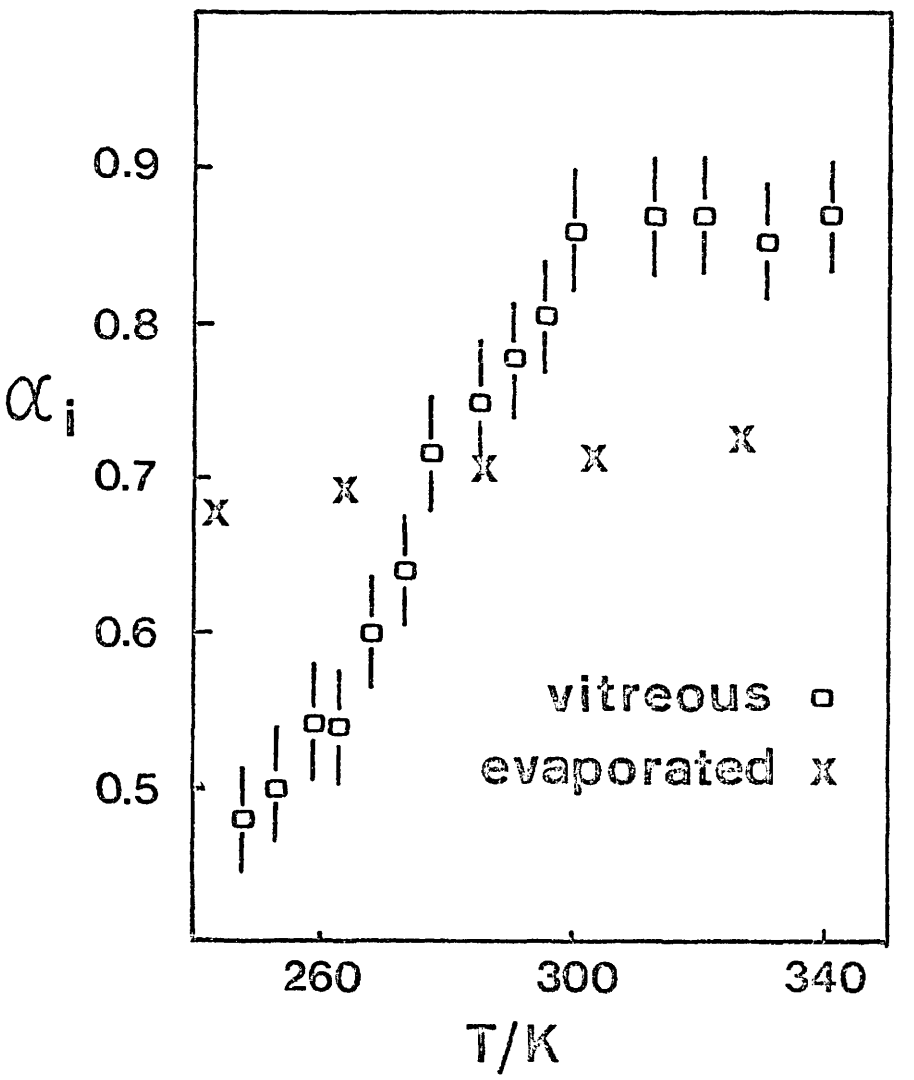

FIGURE 53 : Dispersion parameter calculated from the initial slopes of log (I) log (t) graphs for vitreous and evaporated films.

number of other materials. Results for vitreous As_2Se_3, selenium, PVK and 3BrPVK are illustrated in figure 54, taken from the paper by Marshall and Sharp (1979). As can be seen from this figure α_f is always less than α_i at the lowest temperatures studied, but increases with temperature faster than α_i - thus becoming greater than α_i at higher temperatures (indeed becoming greater than unity in some cases). This behaviour may have important consequences for the diagnosis of transport mechanisms in these materials, as will be explained below.

As we saw in chapter one, Tiedje and Rose (1980) and Orenstein and Kastner (1981) have analysed dispersive transport in terms of carrier thermalisation in an exponential tail of localised states such that

$$N(E) = N_c \exp(-E/kT_o).$$

Using this value for N(E) and assuming that the tail of states can be seperated into 'trapping' and 'transport' states above and below a critical energy E_c which moves further from the mobility edge with time, leads to a power-law waiting time distribution

$$\Psi(t) = t^{-(1+\alpha)}.$$

For an arbitrary $\Psi(t)$ it is difficult to calculate the current as a function of time (I(t)), but for this particular case the analysis of Scher and Montroll will apply because the waiting time distribution is identical. The only significant difference between this model and that of Scher and Montroll is that in this case $\alpha = T/T_o$. It is clear, therefore, that an exponential tail of localised states will give an I(t) similar to that predicted by Scher and Montroll. Orenstein and Kastner went further, however, and suggested that because the experimental current transients observed in As_2Se_3 were similar to those predicted by Scher and Montroll, and because $\alpha=T/T_o$ there must be exponential tails present in the mobility gap of As_2Se_3. This conclusion is not justified on the basis of the above results because it is not clear what other localised state distributions could give rise to similar current transients, and because there are significant differences between the behaviour predicted by Scher and Montroll and that observed in actual films (for example, the value of $\alpha_i \neq \alpha_f$ for As_2Se_3 or any other material). Certainly the Gaussian

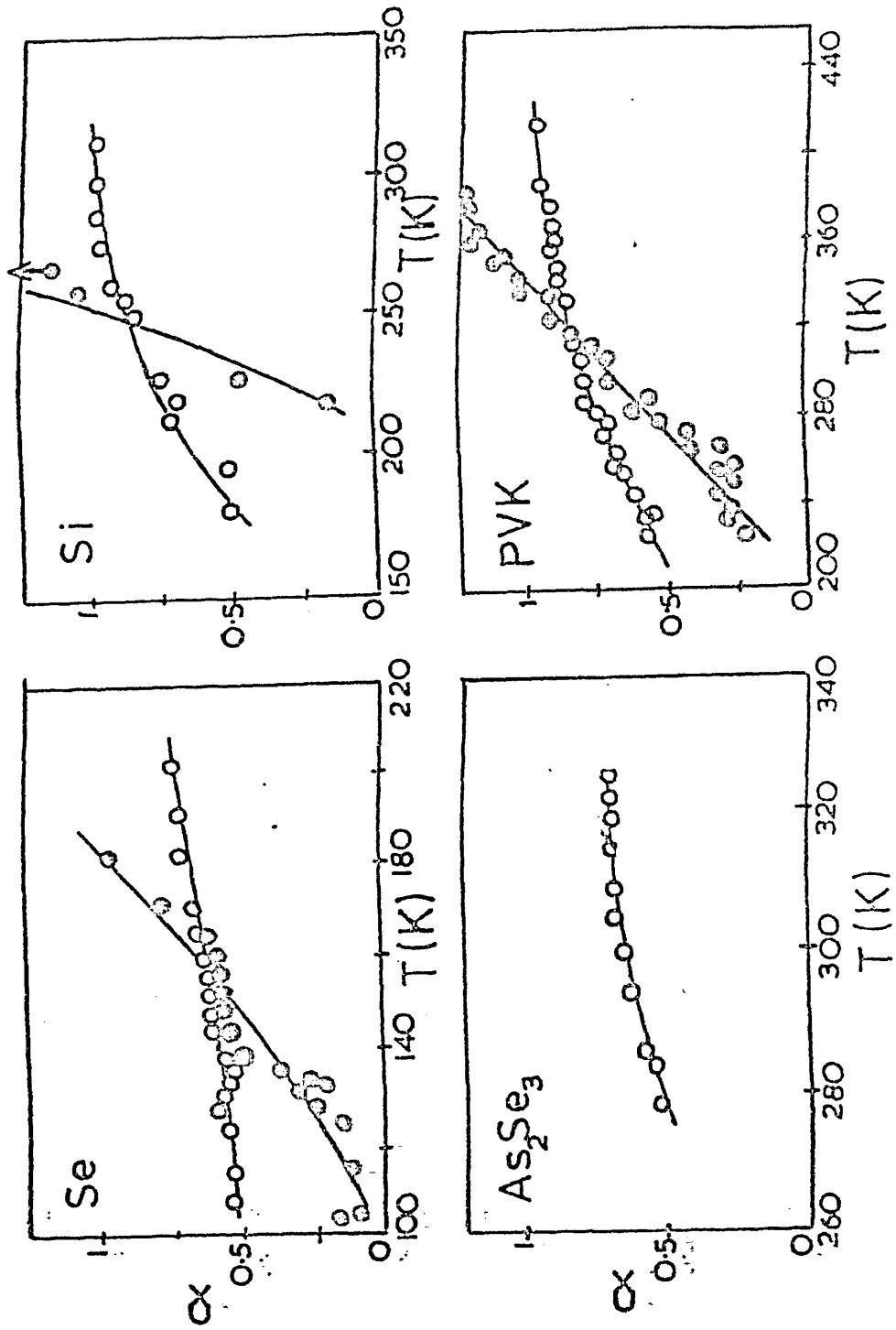

FIGURE 54 : Values of the dispersion parameter as a function of temperature for a number of materials (after Marshall and Sharp).

distribution of localised states used by Marshall (1977) gave very similar current transients to the experimentally observed ones.

The position has recently been clarified by Marshall, Michiel and Adriaenssens (1983) and Michiel, Adriaenssens and Marshall (to be published). These authors have shown how a variety of trap distributions can be used to calculate waiting time distributions from which the corresponding current transient shape may be deduced. The main conclusions of this work were

a). The observation of a linear temperature dependence of α does not exclusively imply an exponential tail of traps.

b). The observation of $\alpha_f > \alpha_i$ is not consistent with the presence of an exponential tail of traps.

c). The observed relationship between α_f and α_i is consistent with a fairly well defined peak in N(E).

Most of the above analyses have concentrated on the initial region of the time-of-flight current transient or on the transient decay of the photocurrent for coplanar samples (which should give equivalent results). In future studies it would be desirable to look in greater detail at the final regime of the current transient. This was not possible in the present study due to a lack of resolution in the transient recorder used for data capture. In this machine the pulse height is stored as a series of numbers in the range 0 to 255, which meant that only two decades of current could be accurately analysed. If this resolution could be increased by several decades, the determination of the density of states in the gap could become simpler. This is because at long times I(t) becomes equivalent to the waiting time distribution $\psi(t)$. As the main body of the pulse goes through the sample deep lying traps will become populated. For such deep traps the release time will be longer than the mean transit time, so that after the current pulse has passed I(t) will be determined solely by the distribution of release times - which is just $\psi(t)$. Thus the latter portion of the transit pulse could give a fairly accurate picture of the density of states deep in the mobility gap.

4.4 ELECTRIC FIELD DEPENDENCE

4.4.1 D.c. Conductivity

The increase in d.c. conductivity with applied electric field illustrated in figures 41 to 43 is very similar to that observed in previous studies (DeWit and Crevecoeur (1972), Marshall and Miller (1974), Hurst and Davis (1974) and Marshall, Fisher and Owen (1974)). The conductivity was found to increase with applied field according to the relationship

$$\sigma(E) = \sigma(0) \exp \{ e\, a(T)\, E / kT \}$$

where $\sigma(0)$ and $\sigma(E)$ are the conductivity with no field and with a field E applied respectively. This behaviour is similar to that of the drift mobility described in the next subsection. The parameter a(T), which decreases with increasing temperature is the same for both the mobility and conductivity - it has the dimensions of length but does not necessarily correspond to any physical length. This sort of behaviour has been observed in a wide variety of chalcogenide glasses for thicknesses from 5 microns to 1 mm and for electric fields up to about 4×10^5 V cm^{-1}. A remarkable feature of the results is the absence of an ohmic region (Marshall and Miller (1974)).

Although Marshall and Miller attempted to analyse this behaviour in a number of different ways - in terms of space-charge injection, field assisted release from shallow traps, tunneling or field dependence of the trapping probability etc. - they found that none of the usual sources for an electric field dependence of the conductivity could account for this behaviour. A sucessful explanation of these results has yet to be given, although a model using the properties of defects with a negative effective correlation energy can provide a qualitative explanation.

In this model, proposed by Street and Mott (1977), it is argued thatif the ratio between D^+, D^o and D^- centres is independent of the applied field then the effect of the field on the conductivity and mobility should be the same - changing the equilibrium between the concentration of free holes and D centres. The rate of the release of the carriers should be increased by some factor such as the

Poole-Frenkel term $\exp(bE^{\frac{1}{2}}/kT)$, and the rate of recombination will be proportional to the free hole concentration (because of the large excess of D^- centres into which the holes can drop). Unfortunately, the Poole-Frenkel term, whilst satisfactory at high fields yields a term in $(1 + bE^{\frac{1}{2}}/kT)$ at low fields, instead of the linear behaviour observed experimentally. However, a treatment due to Onsager (1938) can yield the correct field dependence.

The Onsager theory, originally developed to explain the departure from ohmic behaviour observed in weak electrolytes or solid dielectrics, yields an expression for the probability that a pair of oppositely charged carriers will dissociate by diffusive or Brownian motion in the presence of their Coulomb attraction and a static electric field E. The only variable parameter in the theory is the initial seperation r. Although the expression for the probability of escape is complicated (see for example Pai (1975), Pai and Enck (1975)), it can be reduced to a convergent series in E. While giving high field results similar to the Poole-Frenkel analysis this theory yields for low fields a quite different term $(1 + b^2E/(8k^2T^2))$. This <u>is</u> linear in E, and comparing with the observed form we find

$$e\, a(T) = b^2/8kT$$

which gives the observed variation with temperature and the correct order of magnitude. Such a treatment neglects any variation of the position of the mobility edge with field, and should therefore only approximate the behaviour if this variation is significant.

4.4.2 Drift Mobility

The increase in drift mobility with applied electric field may also be expressed in the form

$$\mu(E) = \mu(0) \exp \{ e\, a(T)\, E/kT \}$$

where $\mu(0)$ and $\mu(E)$ are the mobilities with no field and with a field E respectively.

The field dependence of the drift mobility in evaporated As_2Se_3

has been discussed in detail by Pfister (1977). Using the CTRW theory of Scher and Montroll with a field dependent hopping probability of exp (e p E/2kT), he showed that a field dependence of the transit time of the form

$$t_T \propto L^{1/\alpha} \left(\sinh\{epE/2kT\} \right)^{-1/\alpha} \exp\{E(0)/kT\}$$

is to be expected where p is the average hopping distan ce in the real system, α is the dispersion parameter, and E(0) is the activation energy at zero field.

This expression is similar to one derived by Funabishi and Rao (1976), who incorporated fluctuations in the potential barrier between sites in one dimension, giving

$$t_T \propto \left(\sinh\{espE/2kT\} \right)^{-1} \exp\{E(0)/kT\}$$

where $s \sim 1$ is a function of the randomness of the barrier heights and applied fields. At sufficiently large fields both treatments approach an exponential field dependence.

Although Pfister's results exhibited sinh behaviour for very thin samples, it is very difficult to distinguish between sinh and exponential field dependences for films of thickness greater than about 10 microns. As our results are all for samples much thicker than this it is difficult to distinguish between the models. The fact that the Scher and Montroll model more closely resembles the behaviour observed in evaporated As_2Se_3 (Sharp and Marshall (1981)) suggests that one should be wary about applying the analysis to vitreous material.

CHAPTER 5

This chapter presents a summary of the experimental results obtained from d.c. conductivity and drift mobility measurements on undoped arsenic triselenide prepared by thermal evaporation and r.f. sputtering. Section 5.1 contains the conductivity results, section 5.2 the drift mobility results, and section 5.3 a discussion of these results in terms of a three trap level model.

5.1. D.C. CONDUCTIVITY

The temperature depedence of the d.c. current in a 63 μm thick unsupported arsenic tri-selenide sample prepared by thermal evaporation is shown in figure 55 for applied electric fields of $1.59 \times 10^4 Vcm^{-1}$ and $1.59 \times 10^5 Vcm^{-1}$. The two lines drawn through the low field data have activation energies of $0.84 \pm 0.01eV$ above 277K, and $0.72 \pm 0.01eV$ below 277K. The high field data shows similar behaviour, with the activation energy decreasing to about 0.51 ± 0.01 eV below 235K. This sample was prepared by thermal evaporation onto an aluminimum foil held at close to room temperature, and subsequently equipped with evaporated gold electrodes. No thermal annealing of the film was performed prior to these measurements, but the film was allowed to relax in the dark at room temperature for a few days. The d.c. current on a log scale will behave in exactly the same way as the d.c. conductivity - it is used in this figure to increase the seperation between the 100V and 1000V data points. Using an electrode area of $0.125cm^2$ the low field data gives a pre-exponent of $20-70\Omega^{-1}cm^{-1}$.

The temperature dependence of the d.c. current in a 14.5 μm thick film of arsenic tri-selenide prepared by r.f. sputtering is displayed in figure 56. The deposition parameters for this film were as follows:

Power Split	3:1
Argon Pressure	17mT
d.c. bias	700V
Total power	50W
Time	18 hours
Substrate temperature	315K

This graph shows a distinct discontinuity in gradient at about 310-320K. Above this temperature the activation energy (at a field of $1.93 \times 10^5 Vcm^{-1}$) is $0.91 \pm 0.01eV$, decreasing to $0.79 \pm 0.01eV$ at lower temperatures. The pre-exponent of the high temperature conductivity result is of the order of 2000-5000 S cm^{-1}, which is

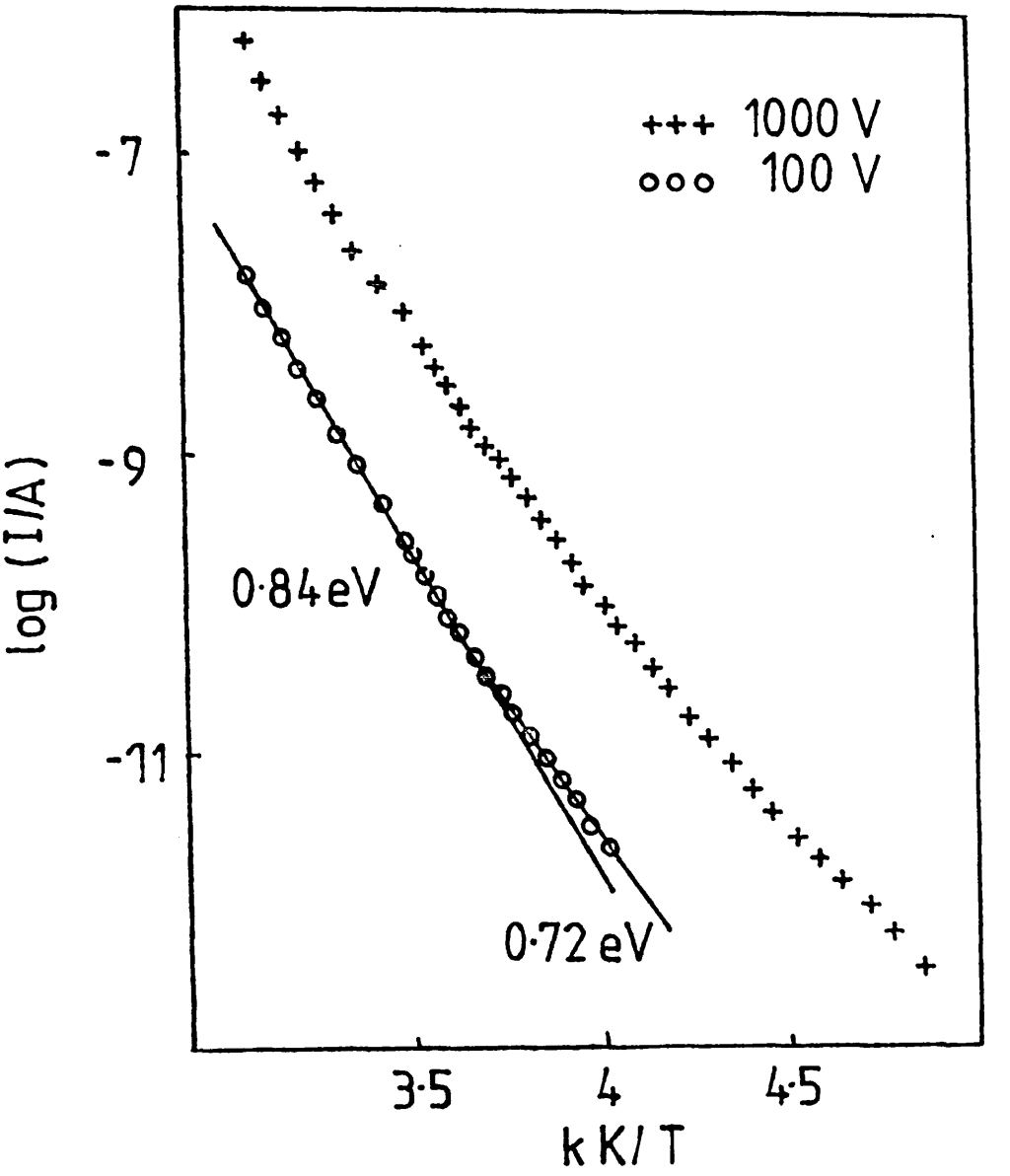

Figure 55 : Dark current in 63 μm evaporated film

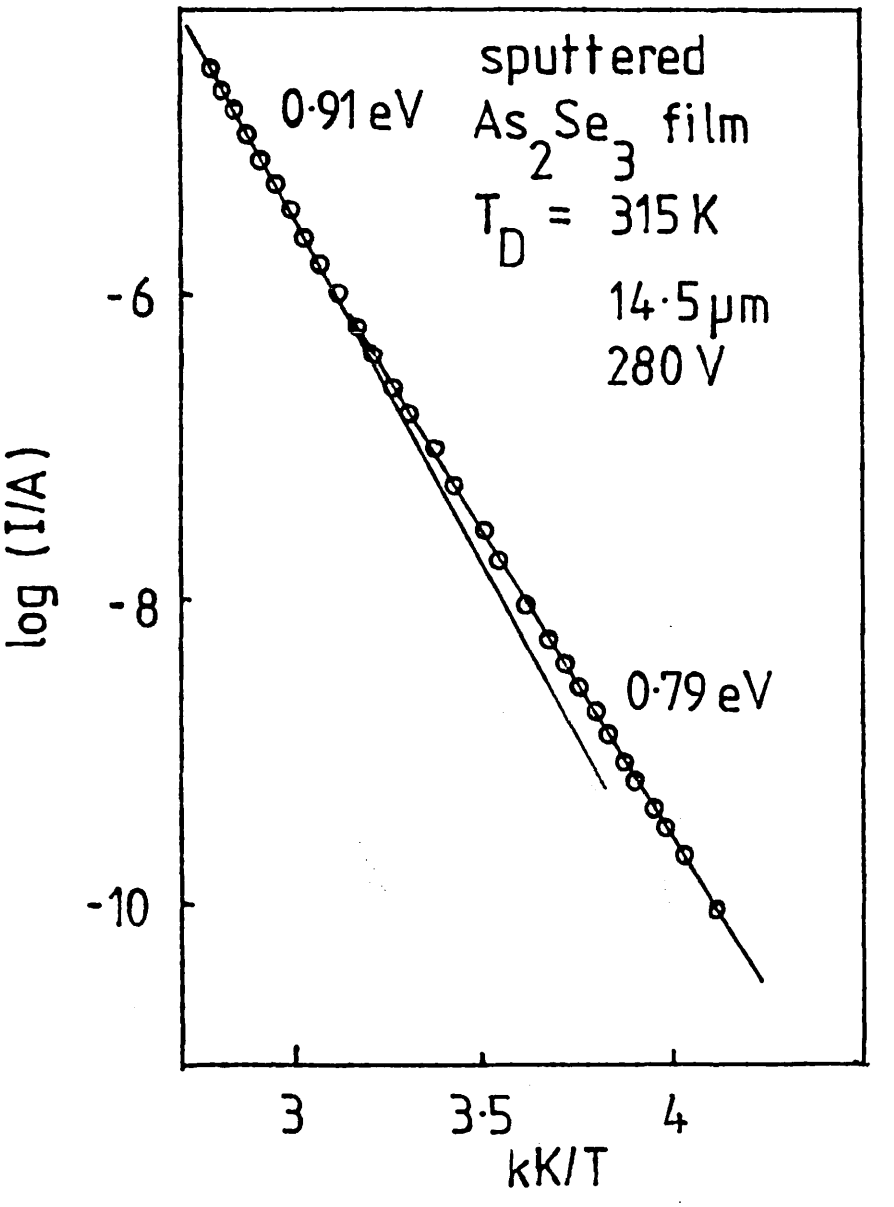
sputtered
0·91 eV
As2Se3 film
TD = 315 K
14·5 μm
280 V
-6
-8
-10
log (I/A)
0·79 eV
3
3·5
4
kK/T

Figure 56.

more similar to the values obtained for vitreous As_2Se_3 than for the evaporated material in figure 55 . The lower temperature data (with 0.79eV activation energy) yield a conductivity pre-exponent of 70 - 120 S cm^{-1}. All these pre-exponents have not been corrected for temperature dilation of the mobility gap. Similar behaviour is shown for a thicker sputtered film in figure 57. This film was 130 μm thick, and unlike the previous sample, was deposited near Tg. The deposition parameters were as follows.

Power Split	5:1
Argon Pressure	18 mT
d.c. dias	860V
Total power	50W
Reflected power	2W
Time	8 hours
Substrate temperature	420K

In the next figure (figure 58) similar results are plotted for a 130 μm thick sample deposited at near room temperature with similar deposition conditions. Figure 59 shows the results for a 71 μm thick film sputtered at 420K again with similar deposition conditions.

All these films (evaporated and sputtered) were deposited onto aluminium foil. This foil was subsequently removed by flexing. In addition to these unsupported films, films were deposited onto CORNING 7059 glass substrates. To get 'sandwich' type cells using this technique requires gold electrodes to be evaporated onto the glass slides before the arsenic tri-selenide is depositied

Using such a supported film, the d.c. conductivity of a 3 μm thick film was measured. The data from this thin sample are displayed in figure 60 along with data from a thicker sputtered film and a vitreous film for comparison. The electric field dependence of the conductivity in sputtered films is shown in figures 61 and 62.

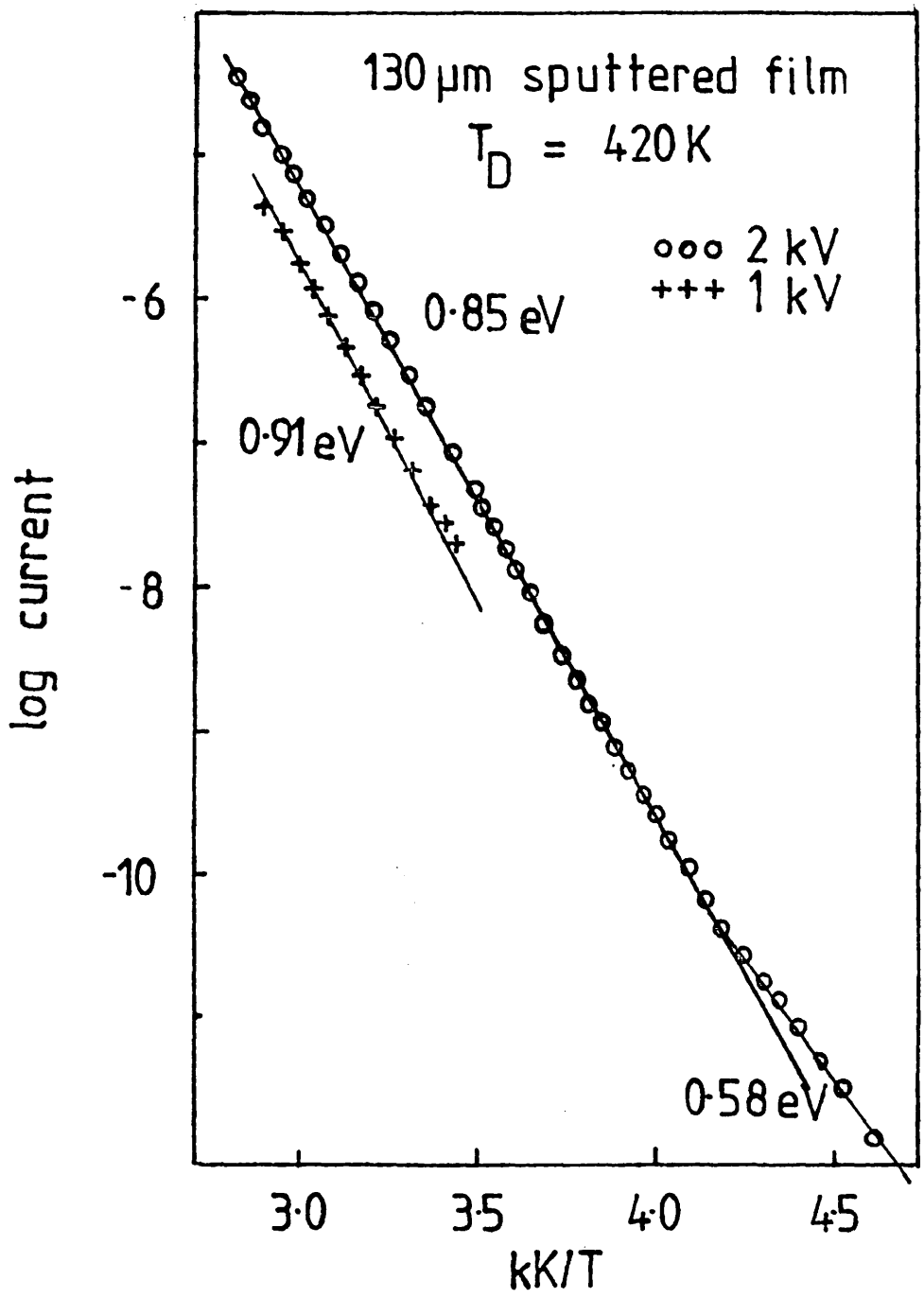
130 μm sputtered film
T_D = 420 K
ooo 2 kV
+++ 1 kV
0·85 eV
0·91 eV
0·58 eV
log current
-6
-8
-10
3·0
3·5
4·0
4·5
kK/T

Figure 57

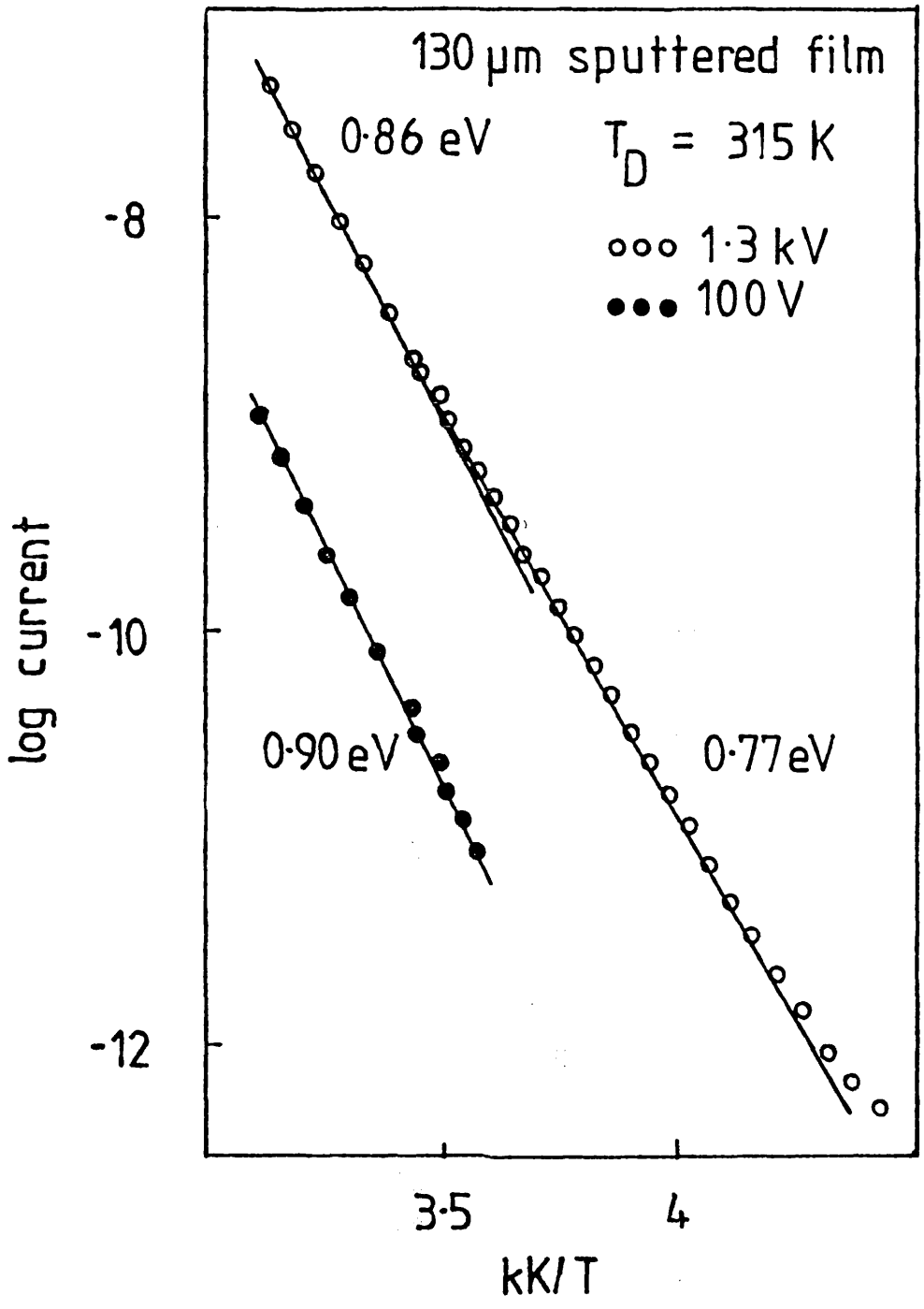
130 μm sputtered film
0·86 eV
T_D = 315 K
ooo 1·3 kV
●●● 100 V
-8
-10
-12
log current
0·90 eV
0·77 eV
3·5
4
kK/T

Figure 58

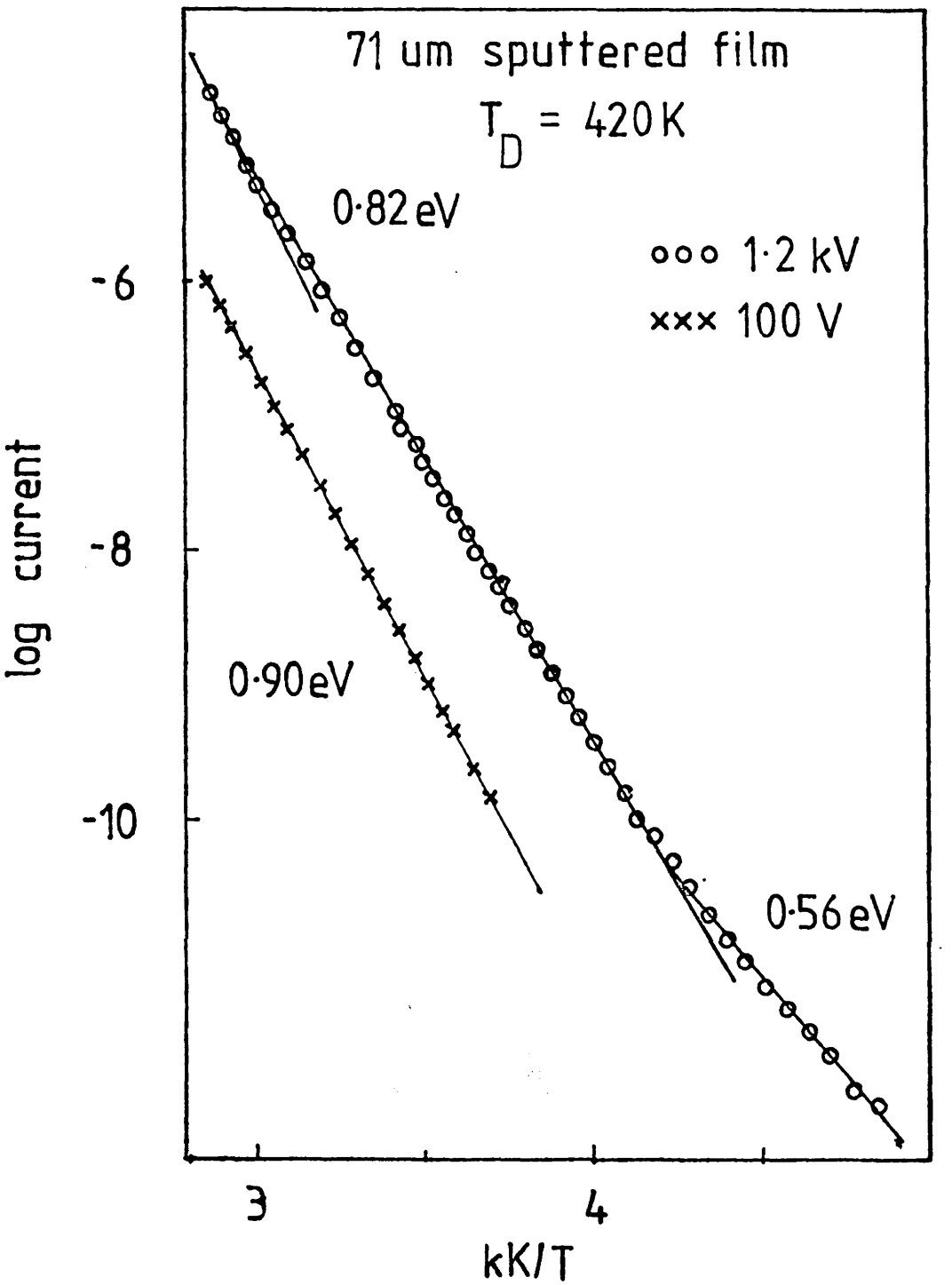
71 um sputtered film
T_D = 420 K
0·82 eV
ooo 1·2 kV
xxx 100 V
-6
-8
-10
log current
0·90 eV
0·56 eV
3
4
kK/T

Figure 59

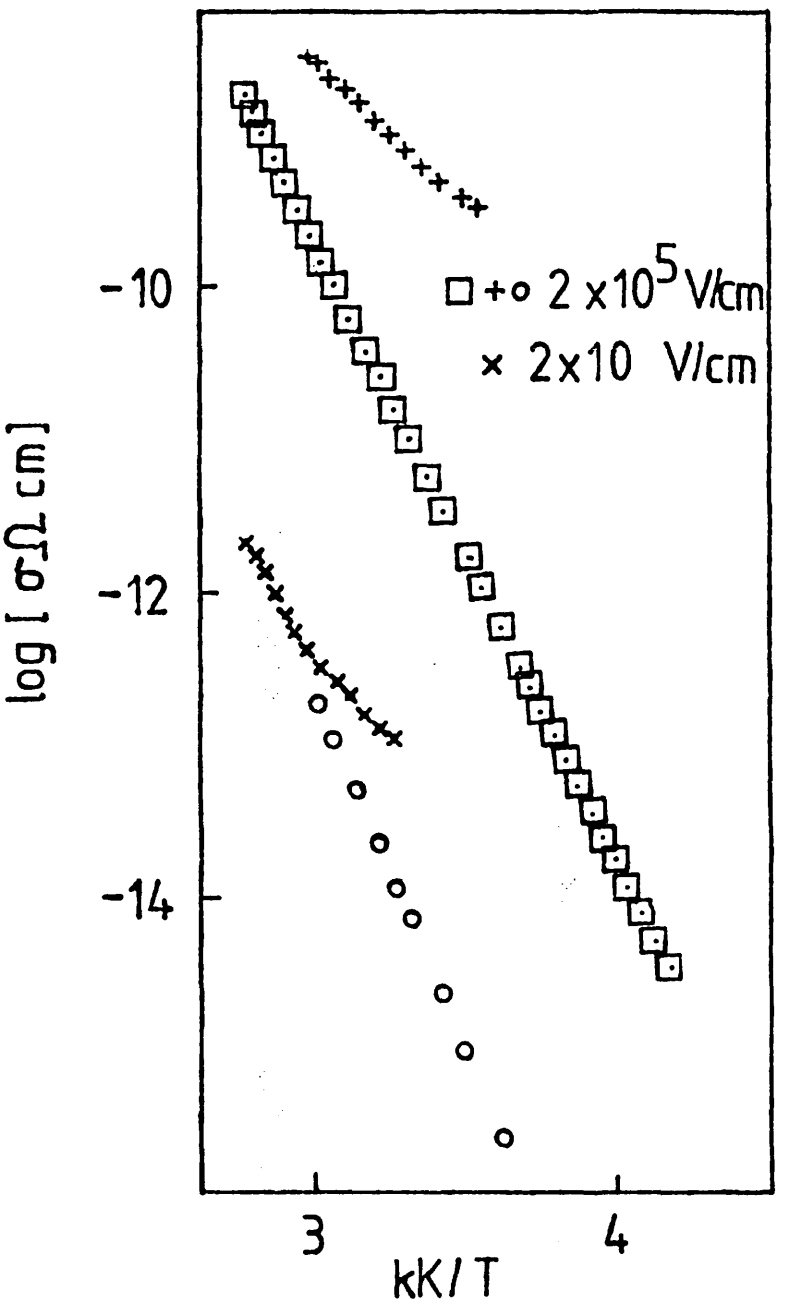

Figure 60 □ 130 µm sputtered film
+ × 3 µm " "
o 58 µm vitreous film

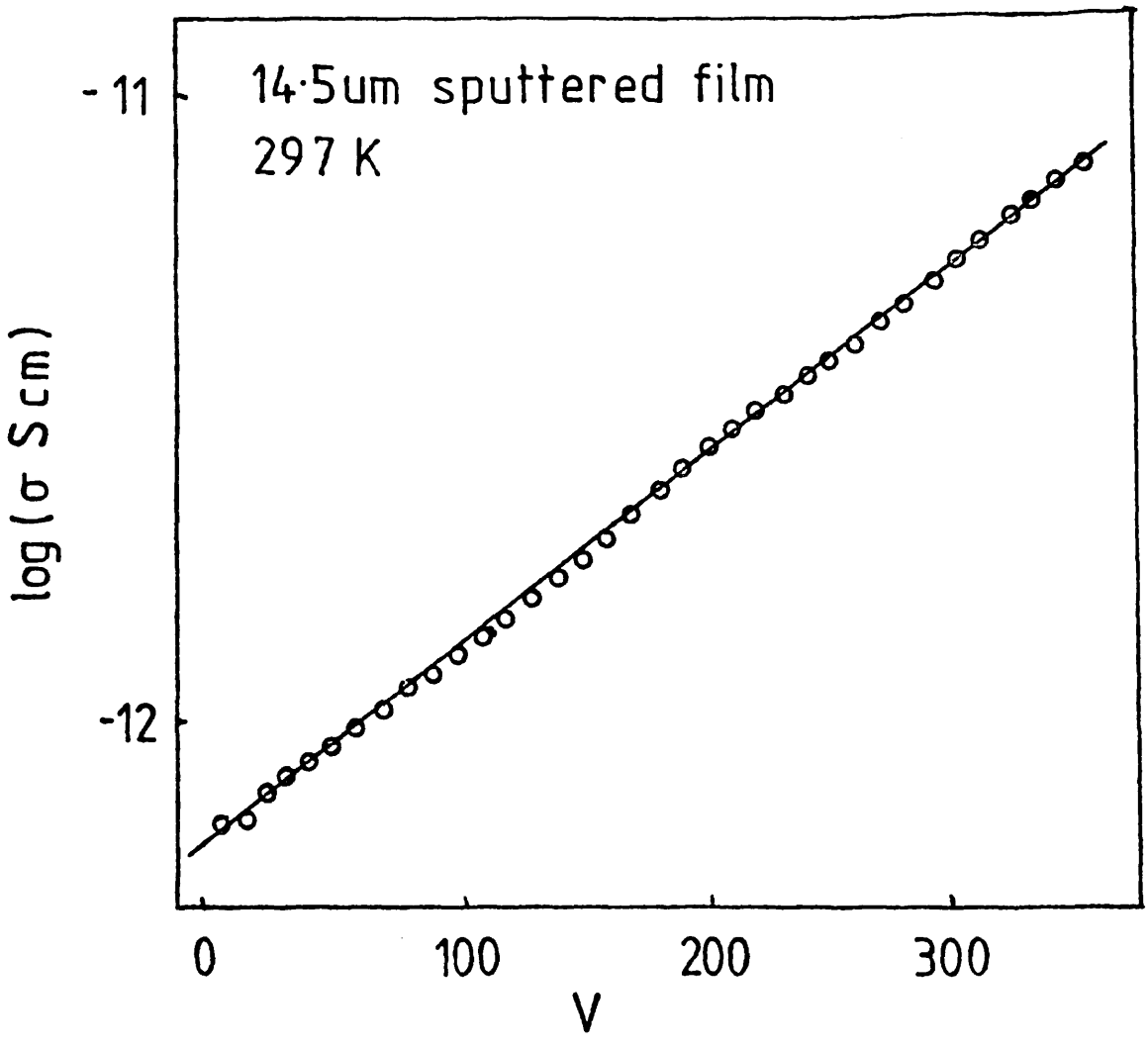

Figure 61

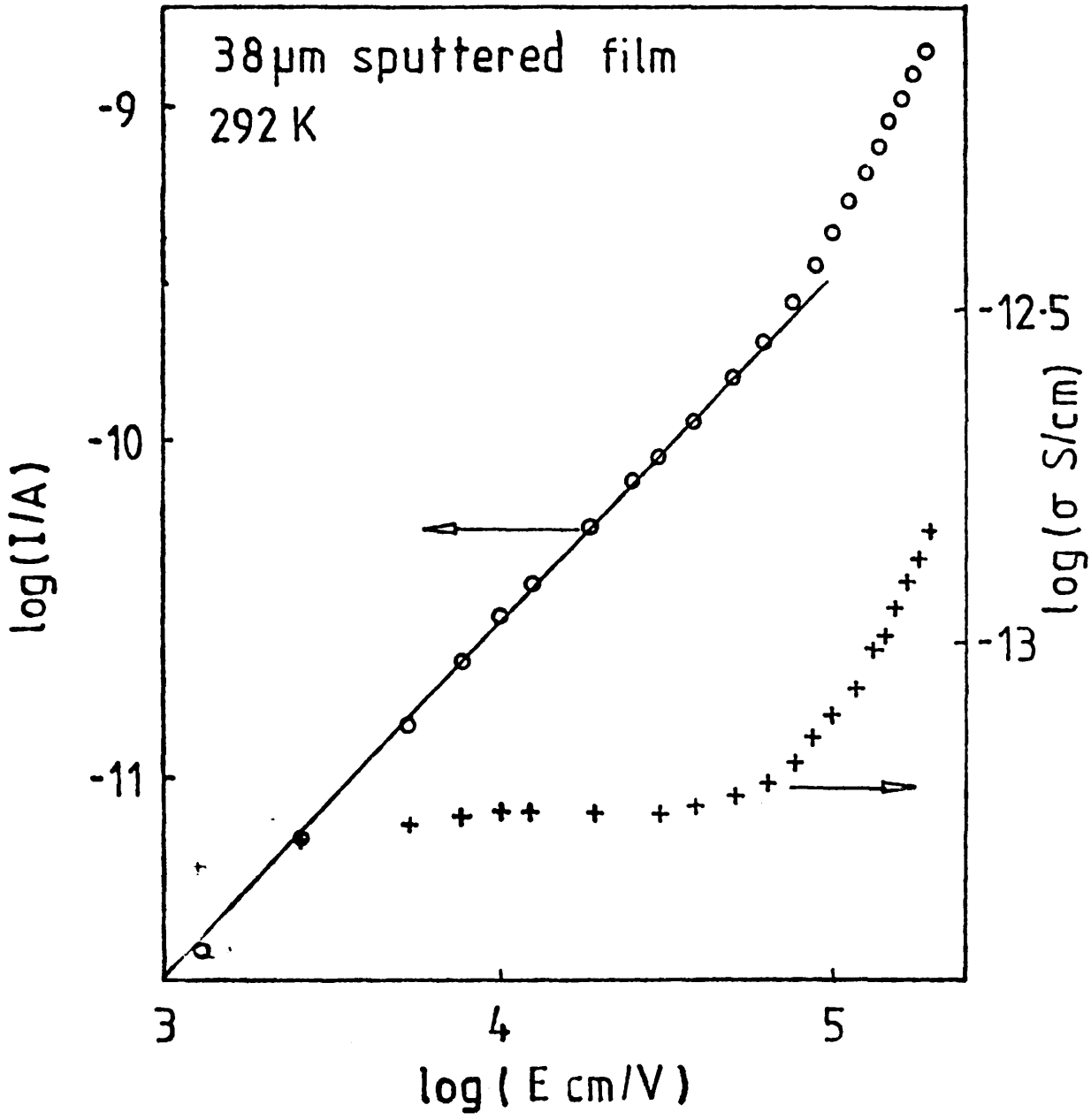
38 µm sputtered film
292 K
-9
-10
-11
log(I/A)
-12·5
-13
log(σ S/cm)
3
4
5
log (E cm/V)

Figure 62

5.2. DRIFT MOBILITY

The temperature dependence of the hole transit time in a 63 μm thick evaporated As_2 Se_3 specimen is displayed in figure 63 . This data was obtained from the same sample used for the d.c. conductivity measurements presented in the previous section. The transit time has been plotted rather than the drift mobility to make the curves for different applied fields more distinct. Above about 295K, the activation energy observed was high - about 0.65 ± 0.03eV. At lower temperatures and fields the activation energy was observed to decrease to 0.42 ± 0.03eV. At higher fields ($1.26 \times 10^5 Vcm^{-1}$) two regions become evident. Between 295K and 250K the activation energy decreased to $0.40eV\pm0.02eV$ and below 250K, the activation energy again decreased to $0.24eV\pm0.02eV$. The electric field dependence of the drift mobility in evaporated As_2 Se_3 at 295K is displayed in figure 64 . The 500V low temperature data had an extapolated mobility pre-exponent of the order of $0.1\text{-}1cm^2V^{-1}s^{-1}$. The extapolated pre-exponent for the higher temperature ($\Delta E \sim 0.4eV$) data is approximately 2 orders of magnitude larger.

It proved extremely difficult to observe transit pulses in r.f. sputtered material. Many samples were investigated, but in only two cases were transit pulses observed. In these two samples, the observed transits behaved unlike those observed in As_2 Se_3 prepared by other methods. Firstly, and most surprisingly, electron transits were observed in both samples. This is the first time to our knowledge that electron transits have been observed in arsenic tri-selenide prepared by any method. Secondly the observed magnitude of current transients decreased fairly rapidly with time, so that one had at most a couple of hours to observe the transits before they became submerged in background noise. For this reason it was only possible to ensure that the transit pulse behaved correctly with field, and take a few measurements before the pulses became too small to observe. The results for a 130μm thick sputtered sample are summarized in the table overleaf:

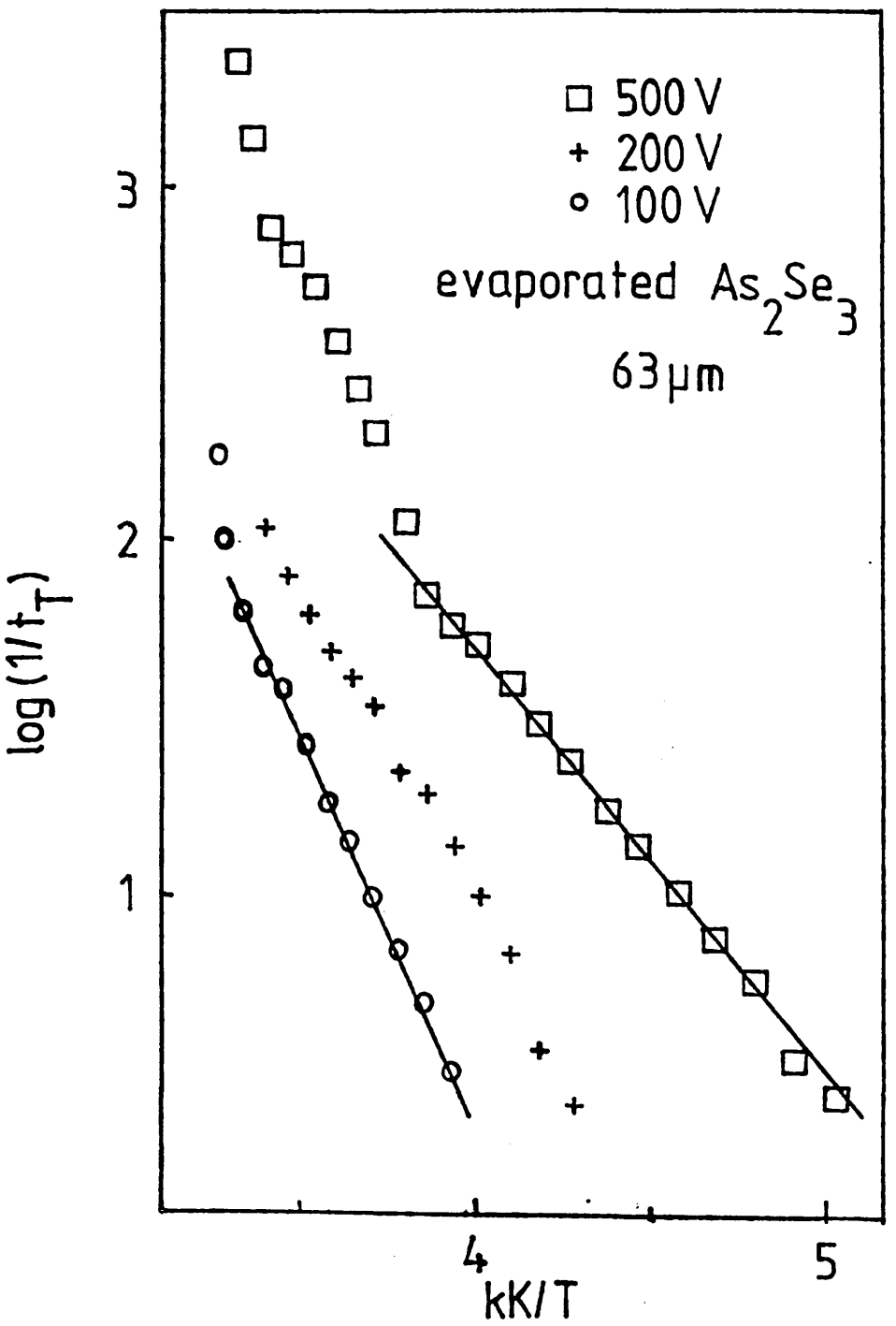

Figure 63

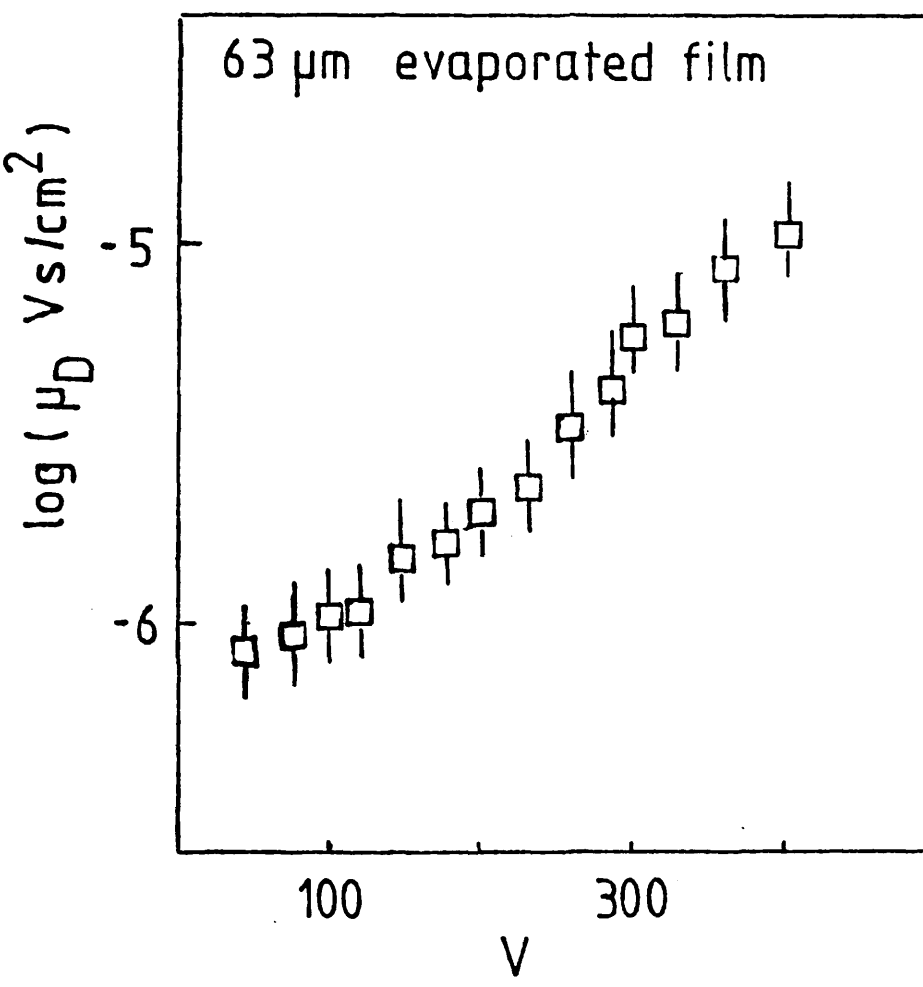

Figure 64

V	t_T	μd
Hole transits at 298K		
500	2ms	1.9×10^{-4} cm^2 V^{-1} s^{-1}
1000	1ms	
Electron transits at 298K		
500	600μs	6×10^{-4} cm^2 V^{-1} s^{-1}
1000	300μs	

The hole mobility is the same order of magnitude as that observed for the evaporated specimen at similar fields and temperatures.

In the r.f. sputtered samples, the absence of mobility pulse must indicate either:

1. Lack of carrier generation,
2. Lack of carrier seperation - geminate recombination or trapping near the surface,

or

3. Carrier trapping and recombination in the bulk sample.

Some r.f. sputtered samples were equipped with artificially blocking contacts to see if this behaviour might be due to contact effects. The method of preparation was similar to that described by Pfister and Scher (1977). Lexan (a polycarbonate resin made by General Electric Inc. of the USA) was dissolved in 1.2, dichloro ethane, and the arsenic tri-selenide samples dipped in the solution. This produces a thin film of lexan (10 - 100nm) on the sample surface which blocks possible charge injection from the gold electrodes subsequently evaporated. Unfortunately this treatment did not appear to improve the visibility of transit pulses.

5.3. DISCUSSION

5.3.1. Evaporated Arsenic Tri-selenide

The results presented in the previous two sections for evaporated As_2 Se_3 although different in detail from those presented in

Chapter 4 for vitreous material may be explained using a similar model of fairly discrete sets of traps in the mobility gap. The conductivity pre-exponent was observed to be an order of magnitude smaller than that for vitreous material, which may indicate that the conduction path has started to move into the localized band tail states in the temperature range investigated in this sample. As discussed in Chapter 4, the mobility pre-exponent for nearest neighbour hopping far from the Fermi level is expected to be of the form

$$\mu_o = \frac{\nu e R^2}{6kT} \exp -(2 \alpha R)$$

which sets an upper limit on μ_o of approximately $0.1 cm^2 V^{-1} s^{-1}$ for such a conduction mechanism. The low temperature high field data for the evaporated sample in figure 55 has such a pre-exponent for data below about 250K, but is significantly larger at higher temperatures.

Once again, to get meaningful quantitative estimates of the density of trap states one must make the assumption that the carriers involved in the conductivity and drift mobility measurements move in the same conduction paths. This point was discussed in detail in the previous chapter. Even if this is not the case, however the model can explain all the salient features of the behaviour in the previous two sections qualitatively.

At high temperatures, the activation energy of the drift mobility indicates hole trapping in a set of deep states at least 0.65eV above the valence band mobility edge. Optical absorption data indicates that the optical band gap of $As_2 Se_3$ does not change significantly with preperation methods (Petursson 1975) so that if the Fermi level is pinned, one would expect a d.c. conductivity activation energy of 0.91eV as in vitreous material. As seen in figure 55 , between 350-300K the conductivity activation energy is of the order of 0.84eV at low fields. Such an activation energy is consistent with band-tail state hopping conduction in tails of approximately 0.1eV in extent. Then the activation energy would be (0.91 - 0.1)+w = 0.81eV+w, and w (the hopping energy) would be of order 1/3 of the trap level width (0.03 - 0.04 eV).

The reduction of the drift mobility activation energy below 300K to 0.42eV could be explained in two ways. Firstly, it could be due to the conduction path rising into a defect level about 0.23eV above the valence band resulting in a trap-limited hopping conduction mechanism with hopping in this level and trapping in the 0.65eV deep level. This would yield a conductivity activation energy of (0.91 - 0.23+w) or 0.72eV (the observed activation energy) with a hopping energy of 0.04eV. This is good agreement between model and experiment. The change in activation energies occurs at approx. 295 $\pm$ 5K for the drift mobility and 280 $\pm$ 5K for the d.c. conductivity which would seem to indicate that the carriers move in a similar conduction path in both experiments. Secondly, it might be due to experimental factors effecting which trap is observed during the transits at lower temperatures - the mobility controlling traps moving into a trap level 0.4eV above the valence band mobility edge (as was discussed for the vitreous material in Chapter 4). To help to clarify the possibility, a graph of log ($\sigma/\mu d$) versus 1/T was drawn and is shown in figure 65. The high temperature regime shows an activation energy of about 0.23eV corresponding to the difference between the conductivity and drift mobility activation energies. The extrapolated pre-exponent for this data of about 1$\pm$0.5 indicates a high density of traps ($2\text{-}8\times10^{19}cm^{-3}$) uncorrected for temperature dilation of the optical band gap ($5\times10^{18}\text{-}2\times10^{19}$, if a temperature dependence of the trap depth of about 30% of that of the optical band gap is considered). As the mobility pre-exponent is equal to μ_o Nv/Nt, if one takes μ_o to be about $5cm^2V^{-1}s^{-1}$, one gets a value of Nv of at least $3\times10^{20}cm^{-3}$ which is an order of magnitude greater than that calculated for the vitreous results.

The activation energy of the log ($\sigma/\mu d$) versus 1/T graph corresponds to the depth of the mobility controlling traps from the Fermi level, and so the high temperature results show that the mobility is controlled by traps about 0.61eV above the valence band mobility edge. Unfortunately high field d.c. conductivity and drift mobility data at lower temperatures at the same field were not possible for this sample. However, if one assumes the 1000V d.c. conductivity behaviour to be an approximation to what would happen at 500V then the activation energy of log ($\sigma/\mu d$) would remain at about 0.27eV (0.51-0.24eV).

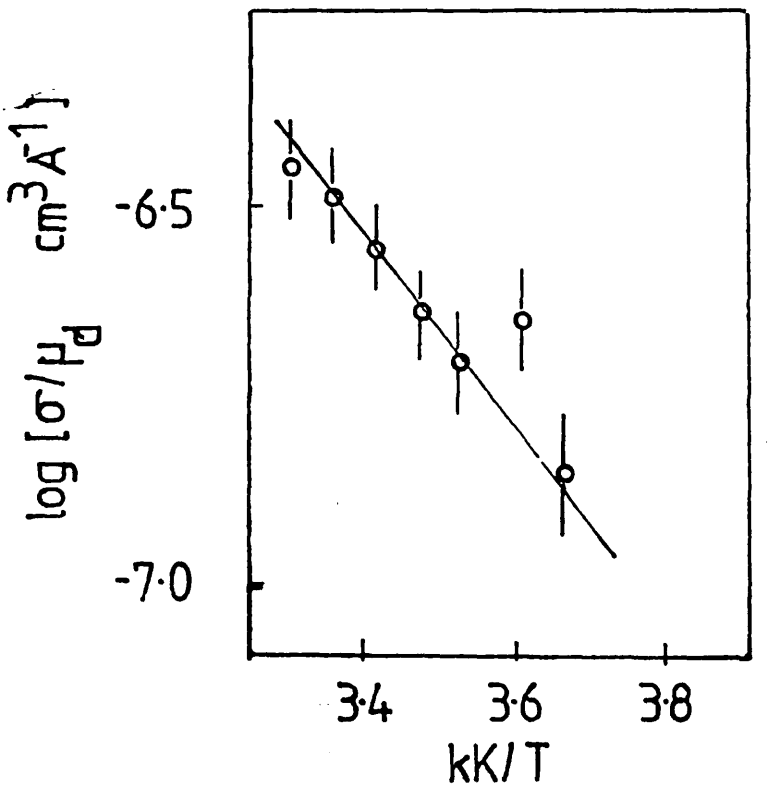

Figure 65

It seems likely, therefore, that the mobility controlling traps 0.65eV above the valence band mobility edge remain dominant for all the experimentally observable regimes. Thus the reduction of activation energy of the drift mobility with temperature is probably due to the conduction path moving into sets of localized states closer to the Fermi level. Below 250K, the conductivity activation energy becomes 0.51eV and the mobility activation energy 0.26eV. This can be explained quite naturally by the conduction path moving into a trap level 0.41eV above the valence band mobility edge. This model is similar to that described by Sharp, Marshall and Fortuna (1981). With a few additional assumptions it is now possible to calculate a value for the degree of localization of the traps 0.41eV above the valence band mobility edge. We must assume (as mentioned in Sharp et al 1981) that hopping through the 0.41eV trap level will become important when the average time for thermal release to the band becomes greater than the expected hopping time between sites. Mathematically, when

$$\nu ph^{-1} \exp(\Delta E/kT) \geq \nu ph^{-1} \exp(2R/Ro + w/kT)$$

where ΔE is the depth of the traps (0.41eV in this case), w is the hopping energy (0.02eV) T is 250K for the transition, $R = (N_{0.41})^{-1/3}$ (where we expect $N_{0.41}$ to be at least $5x10^{18}cm^{-3}$), and $R_o = 1/\alpha$ is a measure of the localization of the wavefunction which should behave as

$$\Psi = k \exp(-\alpha R)$$

(Mott & Davis (1979) p 29).

Substituting these values, one finds a maximum for R_0 of about 1.7nm so that R/R_0 is approximately 10. It is useful to compare this value of localisation parameter with the values used in Monte Carlo simulation of hopping (e.g. Marshall(1978) Marshall and Sharp (1980). In these studies, localization parameters of the order of 3-10 were used. Clearly hopping through a lattice of such sites could not by itself produce the anomalously dispersive transport observed : a trap-limited conduction mechanism must be present.

The temperature dependence of the dispersion parameter calculated from log (I) log (t) plots was discussed briefly in the previous chapter, and by Sharp and Marshall (1981). It was observed that the value of α for evaporated films increased more slowly with temperature than for vitreous films, so that if one defined a critical temperature such that $\alpha=T/To$, To would be of the order of 600K for the evaporated specimens as compared to 330K for vitreous specimens. A comparison of the measured values of α in an evaporated film has been made with the values predicted by the Monte Carlo computer simulation model of Marshall (1977). In this model, carriers interact with a set of traps which have an energy distribution approximated by a Gaussian function. Using this model, a value of α of 0.7 (typical for the evaporated films) corresponds to a trap level distribution with a width of order 3kT or 0.07eV at 270K. As kT varies linearly with T, the trap level width would appear to increase from 0.05eV at 200K to 0.09eV at 300K. Such behaviour may indicate that the trap distribution is not truly Gaussian, but the behaviour of α_i and α_f do appear to indicate a trap limited transport model is appropriate with significant structure in the density of states in the mobility gap (Michiel et al (1983)).

5.3.2. R.F. Sputtered $As_2 Se_3$

The d.c. conductivity by itself cannot yield much information on the transport mechanism in a given material. However, because a few transit pulses were observed in drift mobility studies, and because the behaviour of the d.c. conductivity was similar to that for the evaporated and vitreous material, some tentative explanations can be put forward.

At high temparatures (above about 330K) the activation energy of 0.91eV and the pre-exponent of 2000-5000 S cm^{-1} indicate behaviour similar to that of the vitreous material. One suspects that the conduction path is in the extended states just below the mobility edge. As the temperature is lowered, the activation energy falls to 0.77-0.79eV for materials sputtered at room temperature. This, coupled with the pre-exponent falling to 70-120 S cm^{-1} is similar to the behaviour observed in evaporated samples, and may indicate the

onset of hopping in the band tail states. These states would have to extend about 0.2eV into the mobility gap to produce a reduction in the activation energy of this order.

Material sputtered at near the glass transition temperature exhibits a smaller reduction in activation energy-it changes from 0.91eV to approximately 0.84eV. This would appear to indicate a reduction in depth of the band tail states so that they only extend for 0.10-0.12eV into the mobility gap - very similar behaviour to that observed for the vitreous samples of the previous section. All the sputtered materials show a further reduction in activation energy at about 240K to a value of 0.56-0.58eV. This behaviour is again similar to that observed in our vitreous samples, and could indicate the onset of hopping in a wide trap level 0.4eV above the valence band mobility edge. The position of this change of gradient does not seem to be sensitive to the temperature at which the material was deposited.

As mentioned in section 5.2., the most interesting features of our attempts to measure the drift mobility in r.f. sputtered material was the observation of electron transits. Initially it was thought that what was observed was hole transits generated near the back electrode by a reflection of the exciation light flash. However, masking the back of the sample with black insulating tape had no effect, and the magnitude of the drift mobility was not the same as for hole carriers. It was therefore concludes that genuine electron transits were being observed in a $As_2 Se_3$ for the first time.

The rapid decay of observable transit pulses with time is puzzling. As previously mentioned, the absence of transit pulses implies either:

1. Ohmic Contacts
2. Lack of carrier generation
3. Surface trapping or germinate recombination

or

4. Carrier recombination as the pulse travels through the sample.

Explanations 1 and 2 cannot account for the fact that transits were sometimes observed, but decayed quickly. It is also difficult to imagine why the carrier generation rate should be different for

sputtered material when the optical properties are so similar (Petursson (1975)). Similarly surface or bulk trapped charge is unlikely to be responsible, as one would observe inconsistancies during the temperature cycling involved during d.c. conductivity measurements at low temperatures. Thus by a process of elimination we come to the conclusion that there must be a higher density of recombination centres in As_2Se_3 prepared by r.f. sputtering. All the transit pulses observed were in material deposited at near room temperature, and the decay of transit pulses with time would seem to indicate that the number of active recombination centres increases with annealing at or above room temperature - implying that as-deposited r.f. sputtered films may be structurally unstable if the defects are structural in origin. Further, because the behaviour is so different from that observed in material fabricated using other methods, it would appear that the film relaxes to a structure different in detail from evaporated or vitreous films. For example there may be no As_6Se_{12} rafts and a higher density of dangling bonds. We know of no previous work on the structure of As_2Se_3 prepared by r.f. sputtering. Such a study would provide significant insight to why these films behave so differently .

If such rapid recombination is due to localised states in the mobility gap, one would expect to observe an increase in optical absorption at low photon energies; 1.4 eV if the states are located 0.4 eV from the valence or conduction band edges. In our limited work on the optical absorption of sputtered films a feature was observed at photon energies of about 1.4 eV, but this proved difficult to seperate from possible interference effects for the sample thickness ranges investigated. More work would be required using techniques such as transient photoconductivity and photoluminescence to be able to explain the above results unambiguously.

CHAPTER 6

This chapter presents a summary of the experimental results obtained on samples of arsenic triselenide doped by co-sputtering copper or nickel. Section 6.1 contains the results for nickel doping, and section 6.2 the results for copper doping. These results are discussed in section 6.3.

6.1 NICKEL DOPED ARSENIC TRISELENIDE

The d.c. conductivity of three samples of r.f. sputtered As_2Se_3 doped with different amounts of nickel by co-sputtering is illustrated in figure 66. All these samples were produced during the same deposition run, so that any differences in the properties should be due solely to differing Ni concentrations in the films. The as-deposited samples were equipped with evaporated gold electrodes on the top surface to form 'gap - cell' structures (as shown in figure 33 in chapter 3). The gap seperation was 140 microns and the electrode length 9.5 mm in each case. The thickness, nickel concentration and conductivity activation energies of a number of samples from this run are summarised in table 3 overleaf.

An interesting feature of these results is the change in activation energy which occurs in each sample at approximately the same temperature - 300 K. The conductivity pre-exponent for the high temperature results in each case is of the order of 10^{-2} S cm^{-1}, indicating that hopping conduction is the likely transport mechanism in both regimes.

Typical results for the field dependence of the d.c. conductivity in a moderately nickel doped sample are illustrated in figure 67 at both 327 K and 232 K. In this figure log(I) has been plotted versus log(E).

The optical absorption measurement results are plotted in figure 68 for several samples with different nickel concentrations. In this figure $(\alpha h\nu)^{\frac{1}{2}}$ has been plotted as a function of photon energy, as described earlier in section 3.8. This yields a value for the optical band gap E_{opt}. The values of E_{opt} have been calculated for a number of samples with differing Ni concentrations, and the results are summarised in table 4 overleaf.

The sample numbers refer to the position of the substrate with respect to the nickel wire on the arsenic triselenide target. Samples 6 and 7 were directly above the wire, and consequently have the highest nickel concentrations; sample 1 was the farthest from the dopant source, and thus contained the least amount of nickel. The samples used for the conductivity and optical absorption measurements

TABLE 3

SAMPLE	THICKNESS	ACTIVATION ENERGIES	Ni CONC.
6	5.5μm	0.3leV, 0.23eV	1.5%
5	7 μm	0.36eV, 0.26eV	1.4%
3	6.5μm	0.42eV, o.34eV	1.0%

TABLE 4

SAMPLE	EXPECTED Ni CONCENTRATION	Eopt (±0.0lev)
Undoped	0	1.77eV
1	0.4%	1.75eV
2	0.8%	1.72eV
3	1.0%	1.7leV
4	1.2%	1.68eV
5	1.4%	1.63eV
6	1.5%	1.6leV
7	1.5%	1.6leV

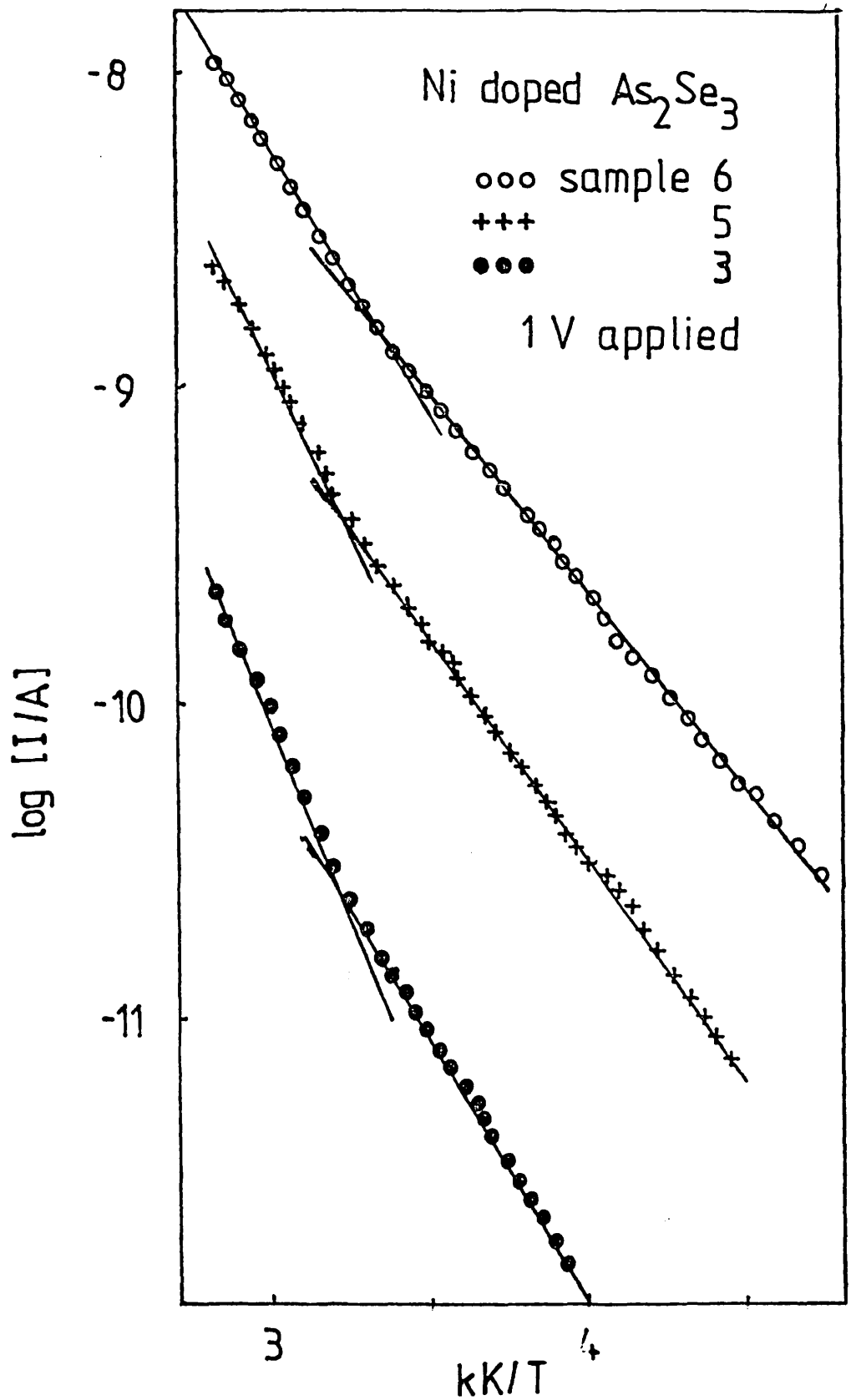
Ni doped As_2Se_3
ooo sample 6
+++ 5
●●● 3
1 V applied
-8
-9
-10
-11
log [I/A]
3
4
kK/T

Figure 66

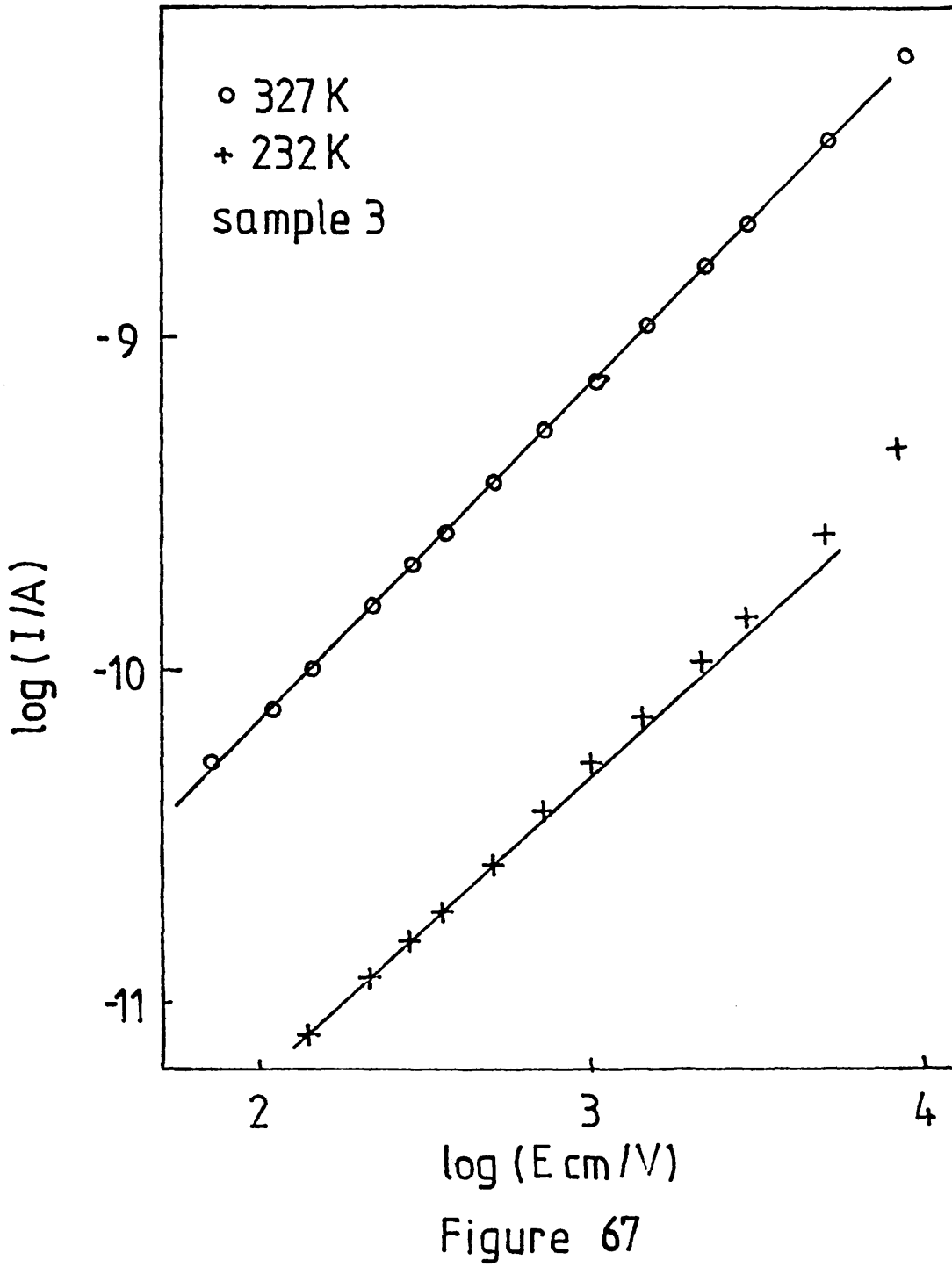

Figure 67

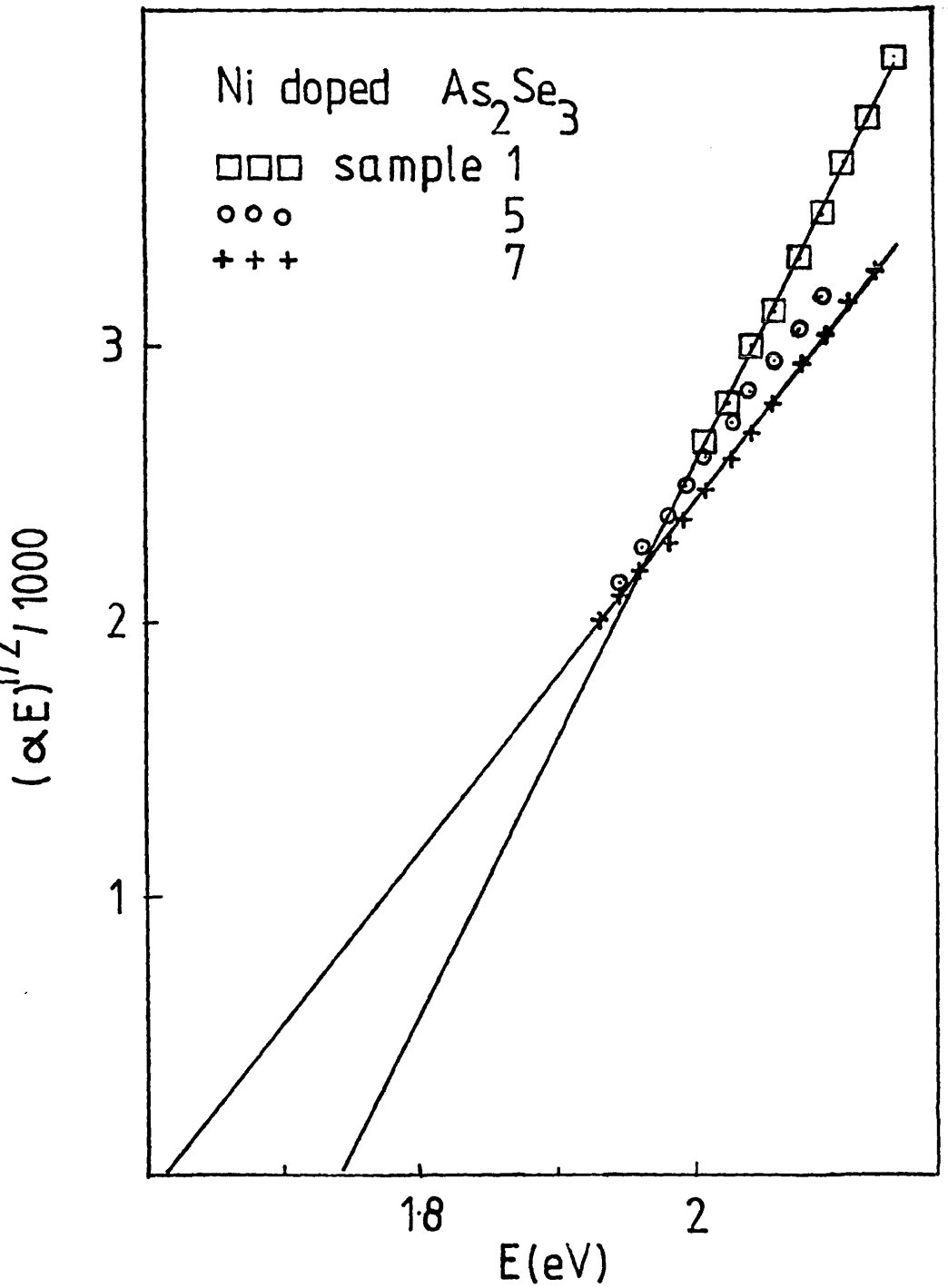

Figure 68

were not the same, but every effort was made to keep the deposition parameters the same in each case so that both measurements would be performed on similar material. The thinner optical absorption samples were deposited a few hours before the thicker conductivity specimens - once again to keep the dopant concentrations in the the two sets of samples as similar as possible. The sample composition measurements were performed on the actual samples used for the conductivity measurements. The measurements were taken as close as practicable to the position of the gap between the electrodes.

6.2 COPPER DOPED ARSENIC TRISELENIDE

The d.c. conductivity of two samples of r.f. sputtered As_2 Se_3 doped with different amounts of copper by co-sputtering is illustrated in figure 69. Once again, both these samples were produced during the same deposition run, so that any difference in properties should be attributable to different concentrations. The electrode size and spacing were the same as reported for the samples doped with nickel.

The graph of log (I) versus $^1/T$ for the heavily doped sample (7) is interesting in that there is no obvious straight line region at temperatures below 300K. The two sets of results displayed in figure 69 were not taken at the same field. The results for sample 7 were taken at an applied voltage of IV, where as those for sample 2 were taken at 400V.

The results of optical absorption measurements on a series of specimens with different copper concentrations are displayed in figure 70. Once again $(\alpha h\nu)^{\frac{1}{2}}$ has been plotted versus $h\nu$ to give values of the optical band gap which are summarized in table 5.

TABLE 5

SAMPLE	EXPECTED Cu CONCENTRATION	Eopt (±0.01eV)
Undoped	0	1.77eV
1	0.2%	1.73eV
2	0.3%	1.71eV
3	0.3%	1.70eV
4	0.4%	1.68eV
5	0.5%	1.67eV
6	0.6%	1.65eV
7	0.6%	1.64eV

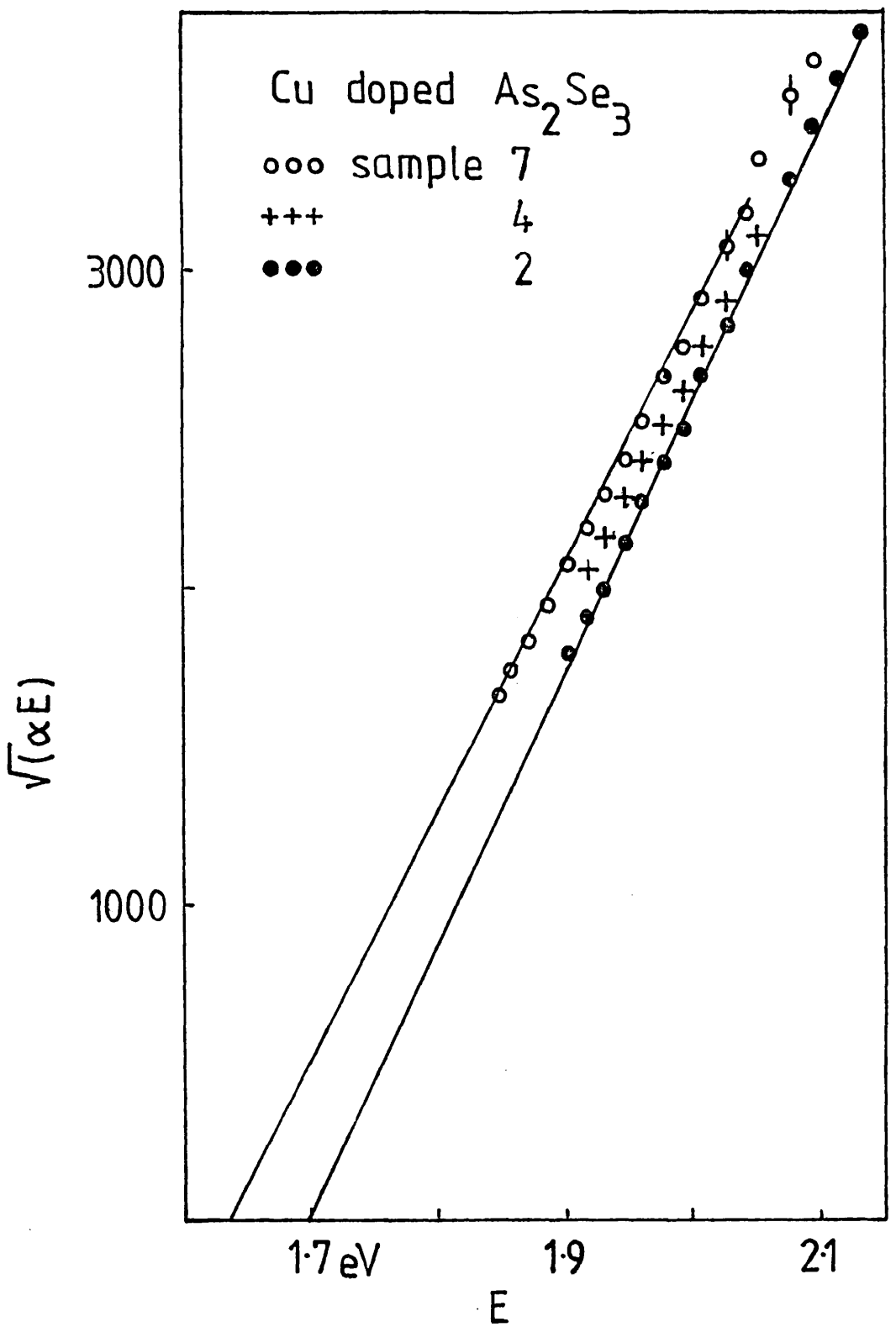
Cu doped As_2Se_3
ooo sample 7
+++ 4
●●● 2
3000
1000
$\sqrt{(\alpha E)}$
1·7 eV
1·9
2·1
E

Figure 70

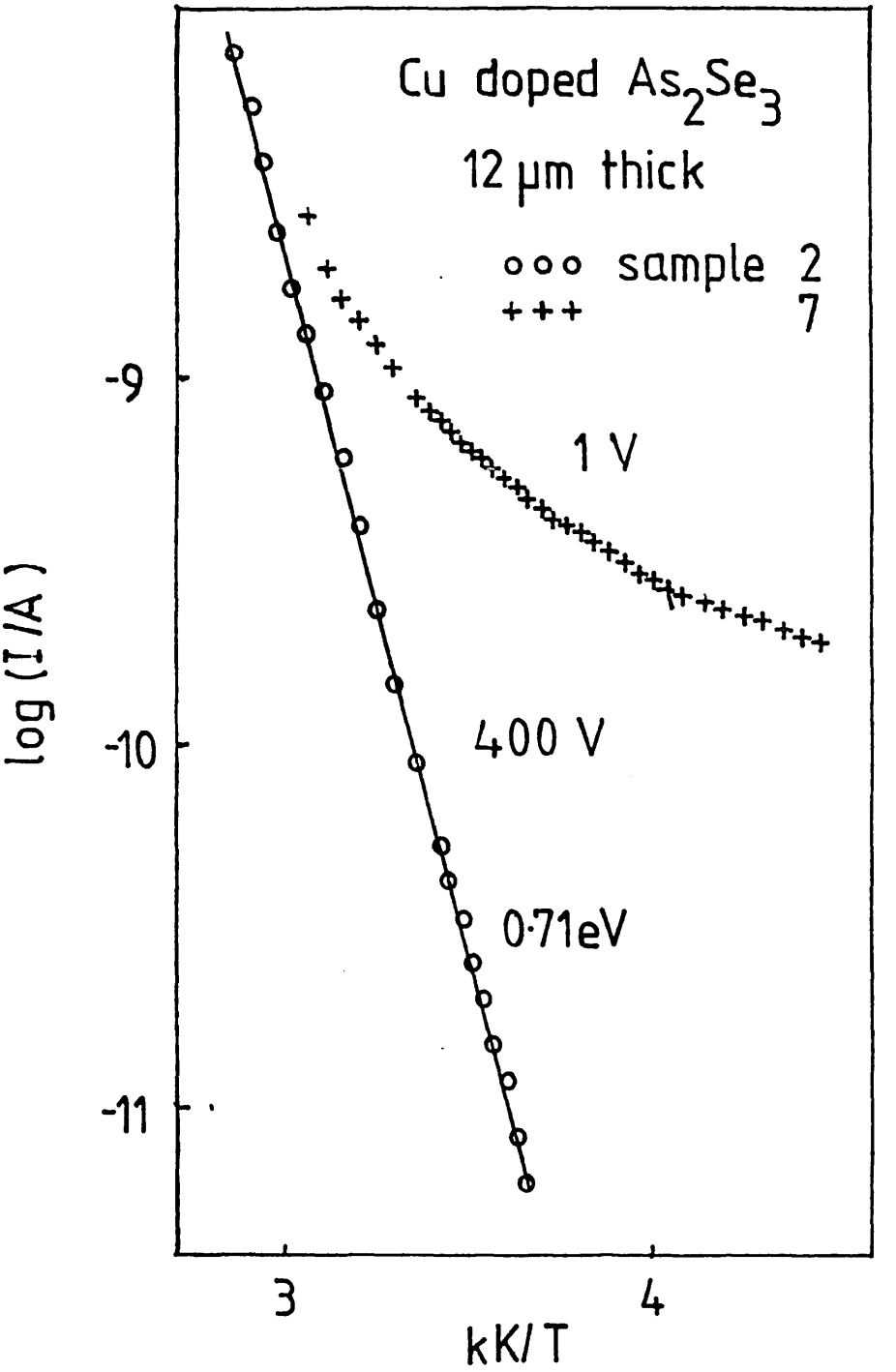
Cu doped As_2Se_3
12 μm thick
ooo sample 2
+++ 7
1 V
400 V
0·71eV
log (I/A)
-9
-10
-11
3
4
kK/T

Figure 69

6.3 DISCUSSION

A number of investigations into the effects of impurities in arsenic triselenide have been published in recent years. Impurities in the bulk glass have been studied by Danilov and Mosli (1964), Edmond (1968), Kolomiets, Rukhyadev and Shilo (1971), Shimakawa et al. (1978), Kitao et al. (1981), Vaninov, Orestein and Kastner (1982) and Seregin et al. (1982). Impurities in evaporated films have been studied by Liang, Bienenstock and Bates (1974), Pfister et al. (1978), Pfister and Taylor (1980) and Pfister and Morgan (1980); whilst doping by co-sputtering has been studied by Flasck et al. (1977), Ovshinsky (1977) and Averyanov et al. (1980). The most relevant to the present study are the papers by Kitao et al. on the effect of copper doping on the conductivity and optical band gap of vitreous As_2 Se_3, and the paper by Averyanov et al., on the doping of r.f. sputtered As_2 Se_3 by co-sputtering nickel. The other papers deal with dopants not used in the present study, or with lower concentrations of dopants.

The introduction of Ni increases the d.c. conductivity observed in our samples of sputtered As_2 Se_3 by up to 4 orders of magnitude, and decreases the conductivity activation energy from 0.92eV to 0.31eV. However, the optical band gap changes by less than 10% for the same concentration of dopant. This indicates that either the Fermi level has been shifted significantly, or a large increase in gap states leading to hopping conduction far from the mobility edge has occured. Because the high temperature conductivity activation energy changes progressively with impurity concentration, it would appear that a change in the position of the Fermi - level is more likely. If the addition of nickel increased the density of a trap level in the mobility gap, it is difficult to see why it would also change the position of the trap level for higher concentrations. The Fermi - level shift is assumed to be towards the valence band because Averyanov et al. performed thermo power

measurements on their specimens in the composition range 0-5.4 at % and found them to be p-type.

If these changes in the d.c. conductivity are mainly due to a shift in the Fermi - level, what transport mechanism would give rise to the results displayed in figure 66? As mentioned in section 6.1, the d.c. conductivity pre-exponents indicate that hopping conduction is likely in both temperature regions, and because the transition from one activation energy to another occurs at approximately the same temperature in each sample it is reasonable to suppose that the same trap levels are involved - the only difference being the position of the Fermi level. If we assume that there are three trap levels at 0.3, 0.42 and 0.63eV above the valence mobility edge (the model used to explain the undoped results) there are three possibilities:-

a. Hopping occurs in the 0.3eV trap level at high temperatures and in the 0.42eV trap level at lower temperatures. The activation energies in table 3 would then indicate that the Fermi - level had shifted to about 0.6eV above the mobility edge for the heaviest Ni doping, or 0.7eV above E_v for the lightest doped samples. This would be consistent with the Fermi - level moving through a trap level about 3kT wide centred 0.65eV above E_v.

b. Hopping occurs in valence band tail states about 0.2eV in extent at high temperatures, with hopping occuring in the 0.3eV trap level at lower temperatures. The activation energies in the table would then indicate a shift in the Fermi - level to 0.5eV above E_v for the highest Ni concentrations and 0.6eV for the lowest impurity concentrations.

c. The nickel dopant introduces an acceptor type trap level into the mobility gap close to the valence band edge. This

must occur if the Fermi - level shifts, but one would require other measurements to be made on the same samples (such as drift mobility or transient photoconductivity and photoluminescene) to find out the position of such a trap level.

Our data for nickel doped As_2 Se_3 is similar to that reported by Averyanov et al., but markedly different from the behaviour reported by Pfister and Morgan. This is probably due to the different methods of sample preparation used. Both Averyanov et al. and the present work studied r.f. sputtered films deposited below 350K, whereas Pfister and Morgan studied films evaporated onto substrates held near T_g. Pfister and Morgan concluded from their results that adding Ni or Cu to As_2 Se_3 did not shift the Fermi - level significantly or introduce any levels closer to the valence band mobility edge. Clearly the impurity atoms in such evaporated films annealed near Tg are not electrically active in the same was as in films deposited at lower temperatures.

Our results for the d.c. conductivity in Ni doped films are also fundamentally different from the results reported by Flasck et al. (1977) for a complicated STAG glass. These authors observed variable range hopping (ie $\sigma \propto T^{-\frac{1}{4}}$) in doped films with Ni concentrations in the range 7-11%. None of our films exhibited such behaviour, but of course none were so highly doped.

The behaviour of the films doped with copper is similar to that reported by Kitao et al. (1980). Sample 2 behaves exactly the way one would expect from these authors work if the copper concentration was 2%. Kitao et al. did however study only bulk glass samples in the concentration range up to 4 at % Cu. This is probably why these workers did not observe the curvature associated with our heavily doped sample 7. This behaviour looks superficially similar to that expected in the variable-range hopping regime (ie $T^{-\frac{1}{4}}$ behaviour), but if the data is plotted versus $T^{-\frac{1}{4}}$ a straight line does not result.

Unfortunately time did not permit a more detailed study of the effects of copper doping in the low-concentration regime. Kitao et al. (1981) observed interesting behaviour below Cu impurity concentrations of 0.5 at %. For small concentrations of copper they observed the conductivity activation energy to increase with increasing Cu content, and the conductivity at 323K to decrease by almost an order of magnitude for a 0.1 at % copper concentration. This behaviour is what would be expected from the work of Pfister and Morgan (1981) who observed an increase in the hole transit time in time of fight measurements, and attributed this to the formation of localized states just above the Fermi level. Pfister and Morgan did not, however notice any significant change in the d.c. conductivity activation energy, or decrease in the magnitude of the conductivity.

CHAPTER 7

This chapter summarises the main conclusions of the thesis. Section 7.1 compares the behaviour observed in undoped films prepared by different methods, whilst section 7.2 summarises the results for doped samples. Section 7.3 attempts to interpret the observed trap levels in terms of recent defect models.

7.1 UNDOPED ARSENIC TRISELENIDE

Measurements have been reported on the d.c. conductivity and carrier drift mobility in arsenic triselenide prepared from the melt, by thermal evaporation, and by r.f. sputtering.

The results for vitreous films were explained on the basis of a model using two trap levels in the mobility gap. At high temperatures unipolar hole conduction was thought to occur in extended states below the valence band mobility edge. As the temperature is reduced, the conduction path moves slowly up through the defect levels in the mobility gap. First through a 'tail' of states approximately 0.1eV in extent, then through a trap level 0.43eV above the valence band mobility edge, and finally into a trap level 0.63eV above the valence band mobility edge. The density of states in each trap level calculated from these results is summarised in table 6 over leaf.

The unusual behaviour of the graph of log ($\sigma/\mu d$) versus $^1/T$ led to the hypothesis that one of the trap levels involved in the transport process had an activated capture cross-section. A new analysis based on this assumption was used to calculate the capture cross section of the traps 0.6eV above the valence band at 300K. The capture coefficient calculated in this way agreed well with recent calculations based on the transient photo conductivity in vitreous As_2 Se_3 published by Orenstein, Kastner and Vaninov (1982).

The results for evaporated films were explained using a similar model. The main differences between the two cases were:-

TABLE 6

Vitreous As_2 Se_3

Band tails		0.43eV traps	0.63eV traps
Temperature Corrected density	$10^{19}\ cm^{-3}$	$4x10^{16}\ cm^{-3}$ - $10^{18}\ cm^{-3}$	$2x10^{15}\ cm^{-3}$
Localization parameter (Ro)		6nm - 1nm	6nm
Trapping radius at 300k			6A
Capture coefficient $b/\mu o$			$2.2x10^{-8}$ cm V

TABLE 7

Evaporated As_2 Se_3

	Band Tails	0.41eV traps	0.65eV traps
Temperature corrected density	$3x10^{20}$	$>5x10^{18}$	$5x10^{18}$
Localization parameter (Ro)		2nm	

1. At high temperatures the conduction mechanism in evaporated films was thought to be hopping conduction in band tails 0.1eV in extent.

2. At lower temperatures the conduction path appears to first rise into a trap level 0.23eV above Ev and than move into a trap level 0.41eV above Ev.

3. The density of localised states in the band tails and in the trap levels are at least an order of magnitude larger than in the case of vitreous material (see table 7).

The transit pulse in time-of-flight mobility measurements on both vitreous and evaporated films displayed anomalous dispersion. The variation of this dispersion with temperature was different in both cases, however. In vitreous films the dispersion increased rapidly with decreasing temperature - possibly due to the activated carrier trapping mentioned above. In evaporated specimens, however, the variation with temperature was much less marked.

The results for undoped films of arsenic triselenide prepared by r.f. sputtering differed significantly from the results obtained on films prepared by other methods in that drift mobility pulses were difficult to observe. In some samples, however, electron transits were observed for the first time - exhibiting a room temperature drift mobility a factor of three higher than for holes. The drift mobility pulses decayed rapidly with time, possibly due to the formation of recombination centres in the bulk of the sample.

The d.c. conductivity in sputtered films deposited at room temperature and at 420 K behaved in a similar way to that observed in vitreous material. At high temperatures extended state conduction appears to be most likely, with hopping in the band tail states becoming

important at lower temperatures. The extent of the localised band tail states appeared to depend upon the deposition temperature. At 420K the tails were calculated to extend 0.1eV into the mobility gap, whereas for a deposition temperature of 330K the tails appeared to extend for up to 0.2eV.

7.2 DOPED ARSENIC TRISELENIDE

An apparent shift in the position of the Fermi-level with heavy nickel and copper doping was observed. This resulted in conductivity increases of up to 4 orders of magnitude, with a change in the optical band gap deduced from optical absorption measurements of less than 10%. For nickel doping the conductivity activation energy decreased to 0.31eV at high temperatures and 0.23eV at low temperatures for Ni concentration of 1.5 at %. This indicates a Fermi level shift of at least 0.3eV towards the valence band mobility edge. No variable range hopping was observed at the temperatures used in this study.

7.3 INTERPRETATION OF TRAP LEVELS

In this section an attempt is made to compare the trap depths determined experimentally in As_2 Se_3 with the expected positions of defect levels predicted on the basis of the defect models described in Chapter 2.

To recapitulate the model: the defects can have three different charge states D^+, D^- and D^o. It is assumed that they posses a

negative effective correlation energy so that the energy gained from lattice relaxation overcomes the Coulamb replusive energy, and so that reaction $2D^{o} \rightarrow D^{+} + D^{-}$ is exothermic.

The D^{-} centre is a dangling bond associated with an under co-ordinated atom, whilst the D^{+} centre can be considered an over co-ordinated atom.

The energy level diagram for these defects has been proposed by Street and Mott (1975), and is shown diagramatically in figure 71. The D^{-} and D^{+} defects act as shallow acceptors and donors for trapping processes but, having trapped their respective carriers, they distort to become D^{o}s with activation energies enhanced by W^{-} and W^{+} respectively. The Fermi-level will be pinned midway between the two D^{o}s, even if the concentration of D^{+} and D^{-} centres differs quite widely (Adler and Yoffa (1976)).

In this model the activation energy for the drift mobility will be the energy required to take a hole from a D^{o} centre to the valence band. We denote this energy by W_1 and our data suggest this should be of order 0.63eV. If we now consider the energy evolved during the reaction $D^{-} + D^{+} \rightarrow 2D^{o}$ to be 2E, then at high temperatures the activation energy of the conductivity should be $W_1 + E$. Thus E is about 0.3eV.

It is now possible to calculate the hopping energies to be expected for:-

a. The movement of an electron or hole allowing a D^{o} centre to exchange with D^{+} and D^{-} centres.

b. Charge transport due to exchange of D^{+} and D^{-}.

For the first process one expects a hopping activation energy of about $\frac{1}{4}$ of the Stokes' shift, or about 0.2eV. Such a small energy would allow unactivated hopping of polaron type at sufficiently low temperatures with an activation energy equal to E (o.3eV), provided the concentration of defects is great enough to allow tunneling from one defect to another (Mott and Davis (1979) p489). In contrast the hopping energy for the exchange

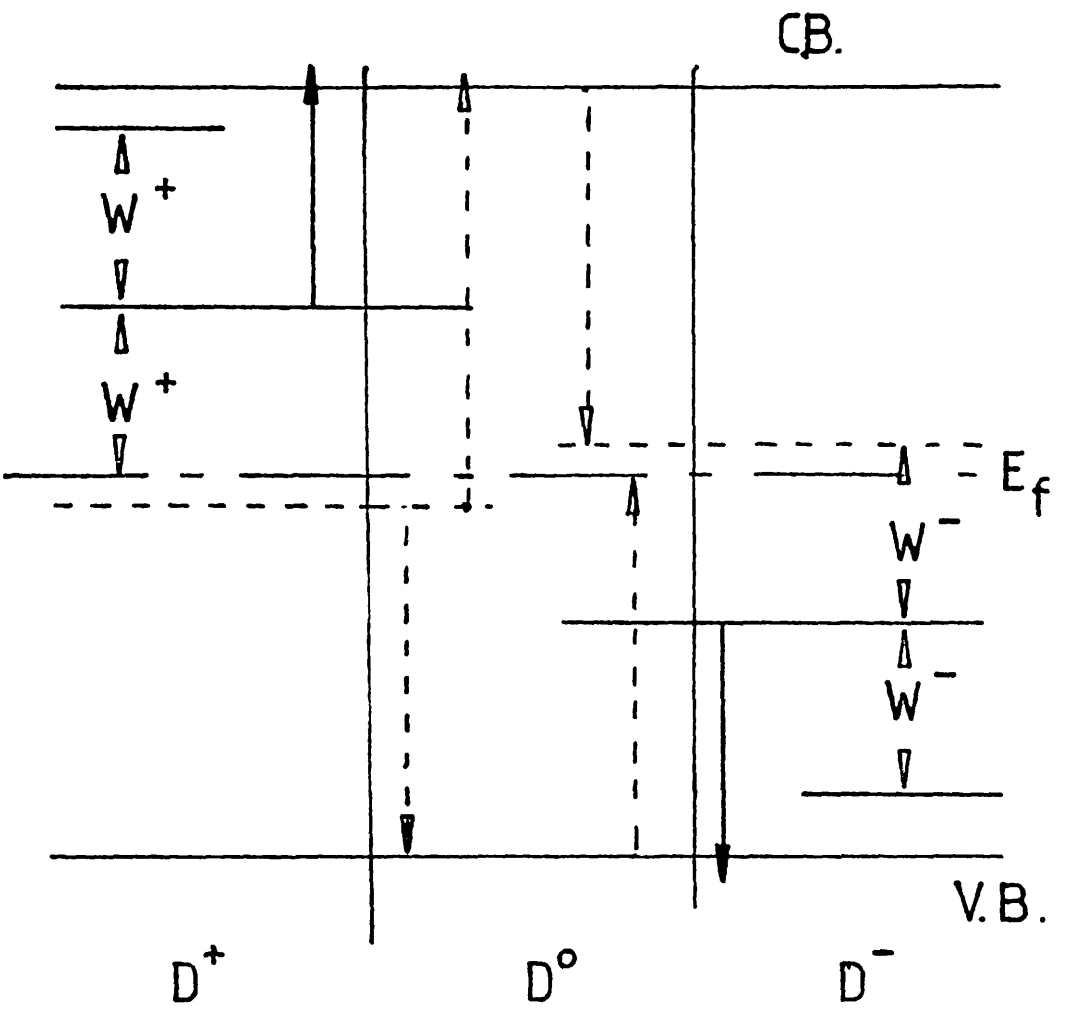

FIGURE 71.

Energy levels associated with D^+, D^o, and D^- according to Street and Mott (1975). Transitions associated with thermal excitation of an electron trapped at D^+ and a hole trapped at D^- to the conduction band (C.B.) and valence band (V.B.), respectively, are denoted by solid arrows. Optical transitions are denoted by dotted arrows: luminescence (downward facing arrows), absorption (upward facing arrows).

of D^+ and D^- (motion of a bipolaran) should be about four times as large, or about 1.2eV. The bipolaran should therefore be practically immobile below the glass transition temperature. It is doubtful whether this model can be applied in detail to the transport data. Trapping of a hole carrier may be followed by a number of process such as (Street (1978)):-

1. its release
2. electron capture ($D^0 + e \rightarrow D^-$)
3. capture of a second hole ($D^0 + h \rightarrow D^+$)
4. the release of an electron ($D^0 \rightarrow D^+ + e$).

To obtain a better understanding of the possible structural origin of states in the gap it is necessary to develop a realistic theoretical treatment. Although a difficult problem, recent attempts to cope with the problem have shed some light on the defect's possible electronic structure (Joannapoulos (1980), Vanderbilt and Joannopoulos (1981), Stys and Foigel (1979)).

Although defects in Se and a - Si : H have recieved much more attention than those in As_2 Se_3, it has been shown that many defects in As_2 Se_3 that are structurally quite similar to those in Se can, in fact, have very different electronic structure. Further, like-atom bond defects can give rise to states in the gap even although the defect atoms may have their normal bonding co-ordination satisfied.

The approach used for these calculations is one using chemical pseudopotentials. The defects were modelled by replacing Se atoms with As atoms and vice versa in crystalline As_2 Se_3. Figure 72 shows the energies of defect states in As_2 Se_3 for a variety of defect configurations. The gap states in panel 4 arise from the As dangling bond and an As - As bonding state. The dangling bond state is however rather sensitive to neighbouring atoms - in panel 5 for example it is shifted in energy because of strong interaction with a Se non-bonding orbital. Panel 7

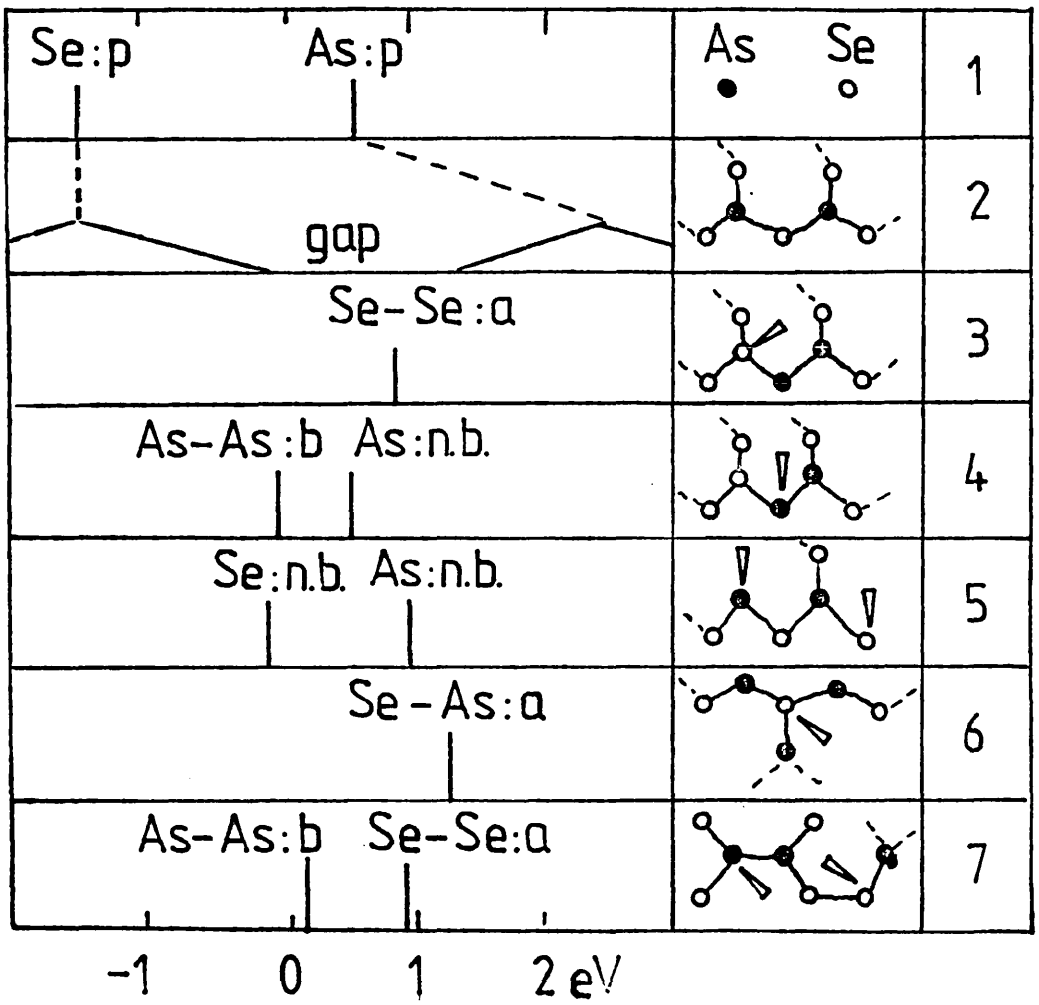
Se:p
As:p
As
Se
1
gap
2
Se-Se:a
3
As-As:b
As:n.b.
4
Se:n.b.
As:n.b.
5
Se-As:a
6
As-As:b
Se-Se:a
7
-1
0
1
2 eV

Figure 72

shows that localized levels will occur even in normal bonding situations. On the basis of this model, the trap levels at 0.6eV could be due to an As dangling bond or the exchange of a carrier from the Se - Se anti-bonding state of panel 3 to an As - As bonding state (as in panel 4). The trap levels at 0.3eV and 0.4eV could be due to the movement of a carrier from the Se - Se anti-bonding state to an As dangling bond.

REFERENCES

Many references are to papers presented at international conferences. With the exception of those for which the proceedings have been published in a journal, they are referred to under the name of the place at which the meeting took place. The following list gives the full references of the relevant proceedings.

1. Proceedings of the 5th International Conference on Amorphous and Liquid Semiconductors, held in Garmisch-Partenkirchen (1973),eds J Stuke and W Brenig, Taylor and Francis, London (1974),(ref: Garmisch (1974)).

2. Proceedings of the 7th International Conference on Amorphous and Liquid Semiconductors, held in Edinburgh (1977) ed W E Spear, Center for Industrial Consultancy and Liason, University of Edinburgh (ref: Edinburgh (1977)).

3. Proceedings of the 9th International Conference on Amorphous and Liquid Semiconductors, held in Grenoble (1981), ed A Deneuville, to be published in J. de Physique.

4. Proceedings of the 13th Session of the Scottish Universities Summer School in Physics. Electronic and Structural Properties of Amorphous Semiconductors, held

in Aberdeen (1972), eds P G LeComber and J Mort, Academic Press (1973), (ref: Aberdeen (1973)).

5. Proceedings of the 19th Scottish Universities Summer School in Physics, held in St. Andrews in 1978, and edited by D P Tunstall and L Friedman. (ref: St. Andrews (1978)).

In addition, there are several books which contain chapters written by different authors in the nature of review articles. When we wish to quote an article from one of these books, the following references will be used.

1. PHOTOCONDUCTIVITY AND RELATED PHENOMENA, eds J Mort and D M Pai, Elsevier (1976), (ref: Mort and Pai (1976)).

2. AMORPHOUS AND LIQUID SEMICONDUCTORS, ed J Tauc, Plenum Press New York (1974),(ref: Tauc (1974)).

3. AMORPHOUS SEMICONDUCTORS - Topics in Applied Physics, volume 36. Editor M H Brodsky, Springer-Verlag (1979), (ref: Brodsky (1979)).

1. ABKOWITZ M - in 'The Physics of Selenium and Tellurium' eds. E. Gerlach and P. Grosse (Springer Series in Solid-State Sciences, vol.13, 1979) p210.

2. ABKOWITZ M and ENCK R - J. Non-cryst. Solids 35-36, (1980) p831.

3. ABKOWITZ M and PAI D M - Phys. Rev. Lett. 38, 1412, (1977)

4. ABKOWITZ M and SCHARFE M E - Solid State Comm. 23, 305 (1977).

5. --------- , ------- - Edinburgh (1977) p 585.

6. ABKOWITZ M and SCHER H - Phil. Mag. 35, 1585 (1977).

7. ADAMS A R, GIBBONS D J and SPEAR W E - Solid State Commun. 2, 387 (1964).

8. ADLER D - J. Non-cryst. Solids 35-36, (1980) p819.

9. ADLER D and YOFFA E J - Phys. Rev. Letts. 36 1197 (1976).

10. AGARWAL S C - Phys. Rev. B 7 685 (1973).

11. ALASTI H, HIGASHI G S and KASTNER M - Phil. Mag. B 39 195 (1979).

12. AMBEGOAKER, HALPERIN and LANGER - Phys. Rev. B4, 2612, (1971).

13. ANDERSON P W - Phys. Rev. 109, 1492 (1958)

14. ANDERSON P W - Phys. Rev. Letts. 36, 953 (1975)

15. ANDERSON G S, MAYER W N and WEHNER G K - J. Appl. Phys. 33, 2991 (1962).

16. APLING A J and LEADBETTER A J - Garmisch (1973) p457

17. ARNOLDUSSEN T C and BUBE R H - J. Appl. Phys. 43, 1798 (1972)

18. -------, -----, FAGEN E A and HOLMBERG S - J. Appl. Phys. 43, 1798 (1972)

19. ARNOLDUSSEN T C, MENEZES C A, NAKAGAWA Y and BUBE R H - Phys. Rev. B 9, 3377 (1974).

20. AUSTIN I G and MOTT N F - Adv. Phys. 18, 41 (1969)

21. AVERYANOV V L, KOLOMIETS B T, LYUBIN V M and PRIKHODKO O Yu - Sov. Phys. Tech. Lett. 6, 249 (1980).

22. ----------, ---------, ------, ---------- - Grenoble (1981).

23. BAGLEY B G - Solid State Commun. 8, 345 (1970)

24. BAILEY K E, JOINER B A, SHERRILL P L and THOMPSON J C - Garmisch (1974) p767.

25. BERKES J S, ING S W, HILLEGAS W J - J. Appl. Phys. 42, 4908 (1971).

26. BIEGELSON K and STREET R A - Phys. Rev. Lett 44, 803 (1980).

27. BISHOP S G, and MITCHELL D L - Phys. Rev. B 8, 5696 (1973).

28. BISHOP S G - Garmisch (1974) p 997.

29. BISHOP S G and SCHEVCHIK N F - Solid State Commun. 15, 629 (1974).

30. ---------- ---------- - Phys. Rev B 12, 1567 (1975).

31. -------, SHANABROOK B V, STROM and TAYLOR - Grenoble (1981).

32. ------- , STROM U and GUENZER C S - Garmisch (1974) p963

33. -------, ------, and TAYLOR P C - Phys. Rev. Letts. 34, 1346 (1975).

34. -------, ------, -------- - Phys. Rev. B 15, 2278 (1977).

35. -------, ------, -------- - Garmisch (1974) p 963.

36. ------, -----, ------ - Edinburgh (1977) p 595.

37. BLOCH F - Z. Physik, 52, 555 (1928).

38. BOTILA T and ALDEA M L - J. Non-cryst. Solids 35-36, (1980) p1079.

39. BOTILA T, VANCU, LAZARESCU, VESCAN, GRIONID, ST. SLADARU - Thin Solid Films 12, 223 (1972).

40. -----, SLADARU ST, CROITORU N - Garmisch (1974) p 799.

41. BRODSKY M H - Edinburgh (1977) p 881.

42. BUBE R H, DUSSEL, HO, MILLER - J. Appl. Phys. 37, 21 (1966).

43. BURMAN and HIRSCH J - J. Non-cryst. Solids 35-36, (1980) p 987.

44. BUTCHER P N - Phil. Mag. 37, 653 (1978).

45. BUTCHER P N and CLARK J D - Phil. Mag. B 43, 1029 (1981).

46. CALLAERTS R, NAGELS P and DENAYER M - Phys. Lett. 38A, 15 (1972).

47. CERNOGORA J, MOLLOT F, BENOIT A LA GUILLAUME C - Phys. Stat. Solidi A15, 401 (1973).

48. CHANDRASEKHAR - Rev. Mod. Phys. 15, 1 (1943).

49. CHEN I - Phys. Rev. B 8, 1440 (1973).

50. COHEN M H - J. Non-cryst. Solids 4, 391 (1970).

51. COHEN M H, FRITSCHE H and OVSHINSKY S R - Phys. Rev. Lett. 23, 1065 (1969).

52. COHEN J D, LANG D V, BEAN J C and HARBISON J P - J. Non-cryst. Solids 35-36, (1980) p581.

53. CONNEL G A N - in Brodsky (1979) p73.

54. CLARK J D and BUTCHER P N - Phil. Mag. B 43, 1017 (1981).

55. DANILOV A V and MOSLI M E - Sov. Phys. - Solid State 5, 1472 (1964).

56. DAVIS E A - Aberdeen (1973) p425.

57. DAVIS E A - in Brodsky (1979) p41.

58. DEMBOVSKII and VAIPOLIN - Sov. Phys. Solid State 6, 1388 (1964).

59. de NEUFVILLE - in Optical Properties of Solids, New Developments. edited by Seraphim (N. Holland, Amsterdam 1974) Chapter 95

60. DEPINNA S P, CAVENETT B C, AUSTIN I G, SEARLE T M - J. Non-cryst. Solids 35-36, (1980), p933.

61. de WIT and CREVECOEUR - J Non-Cryst. Solids 8-10, 787 (1972)

62. DOLEZALEK - Mort and Pai (1976) p 27.

63. DOW J D and REDFIELD D - Phys. Rev. B 1, 3358 (1970)

64. ------- ---------- - Phys. Rev. B 5, 594 (1972)

65. ECONOMOU E N, COHEN M H, FREED K F, KIRKPATRICK E S - in Tauc (1974) p101

66. ECONOMOU E N, NGAI K L and REINECKE T L - Linear and Non-linear Electron Transport in Solids, ed Devreese and Van Doren (New York - Plenum 1976) p 595.

67. --------, ----, ---------- - Edinburgh (1979) p296.

68. EDMOND J T - J. Non-Cryst. Solids 1, 39 (1968)

69. ELLIOT S R - Phil. Mag B 36, 1291 (1977)

70. ------- - Phil. Mag B 37, 135, 553 (1978)

71. ------- - Edinburgh (1977), p637

72. ------- - J. Non-cryst. Solids 35-36, (1980), p 855.

73. EMIN D - Adv. Phys. 22, 57 (1973)

74. ------ - Adv. Phys. 24, 305 (1975)

75. ------ - Aberdeen (1973) p261

76. ------ - Phil. Mag. B 35, 1188 (1977)

77. ------ - Phys. Rev. Letts. 32, 303 (1974)

78. ------ - Edinburgh (1977) p249

79. ------ - Edinburgh (1977) p261.

80. ------ - J. Non-cryst. Solids 35-36, (1980) p 969.

81. ------, HOLSTEIN T - Ann. Phys. (N. Y.) 53, 439 (1969)

82. ------, SEAGER C H and QUINN R K - Phys. Rev. Lett. 28, 813 (1972)

83. ENCK R and PFISTER G - Mort and Pai (1976) p 215.

84. FEINLEIB J, de NEUFVILLE J, MOSS S C, OVSHINSKY S R - Appl. Phys. Lett 18, 254 (1971).

85. FISHER F D, MARSHALL J M and OWEN A E - Phil. Mag. 33, 261 (1976)

86. FISHER R - Phys. Rev. B 5, 3087 (1972).

87. ------ - Brodsky (1979), p 159.

88. FLASCK R, IZU M, SAPRU K, ANDERSON T, OVSHINSKY S R, FRITSCHE H - Edinburgh (1977) p524

89. FLEMING R J - J. Appl. Phys. 50, 8075 (1979).

90. FORK R L, SHANK C V, GLASS A M, MIGUS A, BOSCH M A, SHAH J - J. Non-cryst. Solids 35-36, (1980) p963.

91. FREEMAN L A et al - Thin Solid Films 3, p367 (1969).

92. FRIEDMAN L - J. Non-Cryst. Solids 6, 329 (1971)

93. -------- - Aberdeen (1973) p363

94. -------- - St. Andrews (1978) p239 .

95. -------- and HOLSTEIN T - Ann. Phys. 21, 494 (1963)

96. -------- and POLLAK M - Phil. Mag 38, 173 (1978)

97. FRITSCHE H - Edinburgh (1977) p3

98. ---------- - Aberdeen (1973) p55

99. ---------- - Tauc (1974) p221

100. ----------, GACZI P J, KASTNER M - Phil. Mag. B 37, 593 (1978)

101. ----------, KASTNER M - Phil. Mag. B 37, 285 (1978)

102. FROHLICH H - Proc. R. Soc. A 188, 521 (1947)

103. -------- and SEWELL G - Proc. phys. Soc. 74, 643 (1959).

104. FRYE R C and ADLER D - Phys. Rev. Lett. 46, 1027 (1981).

105. FUNABBASHI K and RAO B N - J. Chem. Phys. 64, 1561 (1976)

106. GILL W D - Garmisch (1974) p901

107. GILL W D - Mort and Pai (1976) p 303.

108. GREEN and RADJY - Phil. Mag. 39, 65 (1979)

109. HALPERIN B I - Phil. Mag. 34, 331 (1976).

110. ---------- - Phil. Mag. 37, 423 (1978)

111. HALPERN V - Edinburgh (1977) p 276.

112. HARRISON W A - Phys. Rev. Lett. 37, 312 (1976).

113. HARTKE J L - Phys. Rev. 125, 1177 (1962)

114. HAUSER J J - Phys. Rev. Lett. 44, p1534 (1980).

115. HAUSER J J and HUTTON R S - Phys. Rev. Lett. 37, 868 (1976)

116. ------- and ------ - J. Non-cryst. Solids 35-36, (1980) p889.

117. -------, DISALVO F J, HUTTON R S - Phil. Mag. B 35, 1557 (1977)

118. HECHT K - Z. Phys. 77, 235 (1932).

119. HENRY C H and LANG D V - Phys. Rev. B15, 989 (1977).

120. HIRSCH J - J. Phys. C 12, 321 (1979).

121. HOLSTEIN T - Ann. Phys. 8, 343 (1959)

122. --------- and FRIEDMAN L - Phys. Rev. 165, 1019 (1968)

123. HUBBARD J - Proc. R. Soc. A 277, 237 (1964)

124. HULLS K and McMILLAN P W - J. Non-cryst. Solids 15, 357 (1974).

125. HUNTER S H, BIENENSTOCK A and HAYES T M - Edinburgh (1977) p 78.

126. HURST C H and DAVIS E A - Garmisch (1973) p349

127. --------- ------- - J. Non-Cryst. Solids 16, 343 355 (1974)

128. IOFFE A F - Bull. Acad. Sci. (USSR), 15, 477 (1951).

129. IOFFE A F and REGEL A R - Prog. Semicond. 4, 237 (1960)

130. JACKSON G N - Thin Solid Films 5, 209 (1970)

131. JELLISON G E and BISHOP S G - Phys. Rev. B 19, 6418 (1979)

132. JESZKA J K, ZIELINSKI M and KRYSZEWSKI M - J. Non-Cryst. Solids 37, 149 (1980).

133. JOANNOPOULOS J D - J. Non-cryst. Solids 35-36, (1980) p781.

134. JOHNSON, BARTELINK, GOLD, GIBBONS - J. Appl. Phys. 50, 4828 (1979)

135. JONSCHER A K - Phil. Mag. B 38, 587 (1978)

136. KASTNER M - Phil. Mag. 37, 127 (1978)

137. KASTNER M - J. Non-cryst. Solids 35-36, (1980) p 807.

138. -------- - Edinburgh (1977) p504

139. --------- - J. Non-Cryst. Solids 31, p223 (1979).

140. -------, ADLER D, FRITSCHE H - Phys. Rev. Letts. 37, 1504 (1975)

141. ------- and FRITSCHE H - Phil. Mag. 37, 199 (1978)

142. ------- and HUDGENS S J - Phil. Mag. 37, 665 (1978)

143. KITAO M, IKEDA H, HASEGAWA H and YAMADA S - Phys. Stat. Solidi A 45, 107 (1978).

144. KIVELSON S and GELATT C D - Phys. Rev. B 19, 5160 (1979)

145. -------- ------ - Phys. Rev. B 20, 4167 (1979).

146. KLAFFKE and WOOD - in Proc. 4th Internat. Conf. on Non-Cryst. Solids (1977, Trans Tech), ed Fritschat.

147. KOLOMIETS B T - Phys. Stat. Solidi 7, 359, 713 (1964).

148. KOLOMIETS B T - Proc. 9th Internat. Conf on the Physics of Semiconductors, held in Leningrad, published by Nauka (1969), p 1259.

149. ---------- - Garmisch (1974) p 189.

150. KOLOMIETS B T, LEBEDEV E A, KASAKOVA L P - Sov. Phys. Semicond. 12, 1049 (1978)

151. ---------, --------- - Sov. Phys. Solid State 8,905 (1966)

152. ---------, LJUBIN V M, AVERJANOV V L - Mat. Res. Bull. 5, 655 (1970)

153. ---------, MASETS T F - J. Non-Cryst. Solids 1, 112 (1969)

154. ---------, ------- - J. Non-cryst. Solids 3, 46 (1970).

155. ---------, ---------, EFENDIEV S M - Sov. Phys. Semicond. 4, 934 (1970)

156. ---------, ---------, ----------, ANDRIESH A M - Sov. Phys. Semicond. 4, 45 (1970)

157. ---------, RUKHYLADEV Y V, SHILO V P - J. Non-Cryst. Solids 5, 402 (1971)

158. ---------, ----------, ------, VASSILYEV V A - Garmisch (1974) p939

159. ---------, et al Sov. Phys. Semicond 12 (1978) no 7

160. KRAMER B and WEAIRE D - in Brodsky (1979) p9.

161. KUNUGI M et al - Zairyo 18, 807 (1969).

162. LANG D V - J. Appl. Phys. 45, 3023 (1974)

163. LANG D V and HENRY C H - Phys. Rev. Lett. 35, 1525 (1975).

164. LEZAL D, TRKAL V, SRB I, DOKOUPIL S, SMID V, ROSICKA V - Phys. Stat. Solids a12, k39 (1972)

165. LIANG K S, BIENENSTOCK A, BATES C W - Phys. Rev. B 10, 1528 (1974)

166. LICCIARDELLO D C and STEIN D L - J. Phys. C, 13, L391 (1980).

167. ----------, ----- and HALDANE F D M - Phil. Mag. (B), 43, 189 (1981).

168. LUCOVSKY G - Garmisch (1974) p1099

169. MAHAN G D and BUBE R H - J. Non-Cryst. Solids 24, 29 (1977)

170. MAIN C - PhD Thesis (1974) University of Edinburgh.

171. ----- and OWEN A E - Aberdeen (1973).

172. MARSHALL J M - Phil. Mag. 36, 959 (1977)

173. MARSHALL J M - Phil. Mag. B 38, 335 (1978).

174. MARSHALL J M - PhD Thesis (unpublished), University of Edinburgh 1971.

175. MARSHALL J M - Edinburgh (1977) p542.

176. -------, Phil. Mag. B 43, 401 (1981).

177. --------- - J. Phys. C 10, 1283 (1977).

178. --------, FISHER F D, OWEN A E - Garmisch (1974) p1305

179. --------, MAIN C, OWEN A E - J. Non-Cryst. Solids 8-10, 760 (1972)

180. --------, MILLER G R - Phil. Mag. 27, 1151 (1973)

181. --------, OWEN A E - Phil. Mag. 24, 1281 (1971)

182. --------, ----- - Phil. Mag. 31, 1341 (1975)

183. --------, ----- - Phil. Mag. 33, 457 (1976)

184. -------- and SHARP A C - J. Non-cryst. Solids 35-36, (1980) p 99.

185. MARIANI E, TRNOVCOVA V, LEZAL D - Phys. Stat. Solids a16, K51 (1973)

186. MARTINI, MAYER and ZANIO - Applied Solid State Science vol 3. Academic Press (1972) ed Wolfe.

187. MELNYK - J. Non-cryst. Solids 35-36, (1980) p837.

188. MIKLA V I, SEMAK D G and KIKINESHI A A - Ukr. Fiz. Zh. (U.S.S.R.) 25, 2021 (1980).

189. MILLER A and ABRAHAMS S - Phys. Rev. 120, 745 (1960).

190. MOLLOT F, CERNOGORA J, BENOIT a la GUILLAUME C - Phys. Stat. Sol. A21, 281 (1974).

191. MONROE D, ORENSTEIN J and KASTNER M - Grenoble (1981).

192. MOORE A R - App. Phys. Lett. 31, 762 (1977)

193. MORT J - Aberdeen (1973) p439

194. MORT J - Adv. Phys. 29, 367 (1980).

195. MOTT N F - Metal-Insulator Transitions (Taylor and Francis 1974).

196. ------ - Adv. Phys. 16, 49 (1967)

197. ------ - Phil. Mag. 19, 835 (1969)

198. ------ - Phil. Mag. 22, 7 (1970)

199. ------ - Aberdeen (1973) p1

200. ------ - Rev. Mod. Phys. 50, 203 (1978).

201. ------ and DAVIS E A - Electronic Processes in Non-crystalline Semiconductors. 2nd edition (Oxford University Press, 1979).

202. ------, ------ and STREET R A - Phil. Mag. 32, 961 (1975).

203. ------, PEPPER M, POLLITT S, WALLIS R H, ADKINS C J - Proc. R. Soc. A 345, 169 (1975).

204. ------ and STONEHAM A M - J. Phys. C 10, 3391 (1977).

205. ------ and STREET R A - Phil. Mag. 36, 33 (1977).

206. ------ and TWOSE W D - Adv. Phys. 10, 107 (1961).

207. MYTILINEOU E and ROILOS M - Phil. Mag. 37, 387 (1978).

208. ---------- and DAVIS E A - J. Non-cryst. Solids 35-36, (1980) p 883.

209. NAGELS P - Brodsky p113, (1979).

210. NAGELS P, COLSON, VAN GOOL - Edinburgh (1977) p546.

211. NAGELS P, CALLAERTS R and DENAYER M - Garmisch (1974) p 867.

212. NEMANISCH R J, STREET R A, CONNELL - Phys. Rev. B 18, 6915 (1979)

213. ----------, -------, --------, HAYES -Phys. Rev. B 18, 6900 (1979).

214. NGAI K L and TAYLOR P C - Phil. Mag. 37, 175 (1978).

215. NOOLANDI J - Phys. Rev. B 16, 4468 and 4474 (1977).

216. ---------- - Edinburgh (1977) p224.

217. ----------, HONG - Chem. Phys. Lett. 58, 575 (1978).

218. ONARI S, YAMAMOTO K, KITAHARA T and ARAI T - Japanese Journal of Appl. Phys. 19, 1083 (1980).

219. ONSAGER L - Phys. Rev. 54, 554 (1938).

220. ORENSTEIN J and KASTNER M - Phys. Rev. Lett. 23, 161 (1979).

221. ORENSTEIN J and KASTNER M - Phys. Rev. Lett. 46, 1421 (1981).

222. ---------, --------- and MONROE D - J. Non-cryst. Solids 35-36, (1980) p951.

223. OVAGHAR B M, POHLMANN B, SCHIRMACHER W - Phil. Mag. B 41, 46 (1980).

224. OVSHINSKY S R - Edinburgh (1977) p519.

225. --------- and ADLER D - Contemp. Phys. 50, p109 (1978).

226. --------- and SAPRU K - Garmisch (1974) p 447.

227. OWEN A E and MARSHALL J M - Edinburgh (1977) p524.

228. OWEN A E and SPEAR W E - Phys. Chem. Glasses 17, 174 (1976).

229. PAI D M - J. Appl. Phys. 46, 5122 (1975)

230. PAI D M and ENCK R C - Phys. Rev. B 11, 5163 (1975)

231. ---- and SCHARFE M E - J. Non-Cryst. Solids 8-10, 752 (1972)

232. PANASYUK L M, MANUSHEVICH G N, GOGLIDZE and POROTOROV V L - Sov. Phys. Semicond. 14, 34 (1980).

233. PETURSSON J - J. Non-cryst. Solids 35-36, (1980) p977.

234. PFISTER G - Edinburgh (1977) p765

235. PFISTER G - Phys. Rev. Lett. 33, 1474 (1974).

236. -------, - Phil. Mag. B 36, 1147 (1977).

237. -------, - Phys. Rev. B 16, 3676 (1978).

238. ------- and GRIFFETHS - Phys. Rev. Lett. 40, (1979).

239. -------, LIANG K S, MORGAN M, TAYLOR P C, FRIEBELE E J, BISHOP S G - Phys. Rev. Lett. 41, 1318 (1978).

240. -------, MELNYK A R and SCHARFE M E - Solid State Commun. 21, 907 (1977).

241. ------- and MORGAN M - Phil. Mag. B 41, 191 (1980).

242. ------- -------- - Phil. Mag. B 41, 209 (1980).

243. ------- and SCHER H - Phys. Rev. B 15, 2062 (1977).

244. ------- --- ------- - Adv. Phys. 27, 747 (1978).

245. ------- and TAYLOR - J. Non-cryst. Solids 35-36, (1980) p 793.

246. PHILLIPS J C - J. Non-cryst. Solids 35-36, (1980) p 1159.

247. -------- - J. Non-cryst. Solids 34, 153 (1979).

248. POLLAK M - Edinburgh (1977) p 219.

249. POLLAK M - J. Non-cryst. Solids 35-36, (1980) p83.

250. ------ - Phil. Mag. 36, 1157 (1977).

251. ------ - St. Andrews (1978) p95.

252. ------ and GEBALLE T H - Phys. Rev. 122, 1742 (1961).

253. PROVENCHER S W - J. Chem. Phys. 64, 2772 (1976).

254. RAMANI, GIRIDNAR, SINGH, RAO - Phil. Mag. B 39, 385 (1979).

255. REEHAL and THOMAS - Phil. Mag. 39, 321 (1979).

256. ROBERTS G G - Aberdeen (1973) p 409

257. ROBERTS G G, APSLEY N and MUNN R W - Phys. Rep. 60, p59 (1980).

258. ROBERTSON J - Phil.Mag. B 41, 177 (1980).

259. RUBENSTEIN M and TAYLOR P C - Phys. Rev. B9, 4258 (1974).

260. RYVKIN - Photoelectric Effects in Semiconductors, published by Consultants Bureau, New York 1964.

261. SAYERS D E - Edinburgh (1977) p 61.

262. SEAGER C H, EMIN D, QUINN R K - Phys. Rev. B 8, 4746 (1973).

263. ------ and QUINN R K - J. Non-Cryst. Solids 17, 386 (1975)

264. SCHARFE M E - Phys. Rev. B 2, 5025 (1970).

265. SCHER H - Mort and Pai (1976) p 71.

266. SCHER H and LAX M - Phys. Rev. B 7, 4502 and 4491 (1973).

267. ------, and MONTROLL E W - Phys. Rev. B 12, 2455 (1975).

268. SCHMID A P - J. Appl. Phys. 39, 3141 (1968).

269. SCHMIDLIN F W - Phys. Rev. B 16, 2562 (1977).

270. SCHMIDLIN F W - Solid State Commun. 22, 451 (1977).

271. --------- - Mort and Pai (1976) p 421.

272. -------- - Phil. Mag. 41, p535 (1980).

273. SCHOTTMILLER J, TABAK M, LUCOVESKY G, WARD A - J. Non-Cryst. Solids 4, 80 (1970).

274. SEKI H - Garmisch (1974) p1015

275. SEMAK D G, CHEPUR D V, ZOLOTAREV V F - Sov. Phys. Solid State 9, 966 (1967).

276. SHAH J and BRIDENBAUGH P M - Solid State Commun. 34, 101 (1980).

277. SHARP A C and MARSHALL J M - J. Phys. C 14, L761 (1981).

278. SHARP A C, MARSHALL J M and FORTUNA H S - Grenoble (1981).

279. SHIMAKAWA K, NITTA S, MORI M - Phys. Rev. B 18, 4348 (1978).

280. SHIMAKAWA K - Grenoble (1981).

281. SILVER M - Edinburgh (1977) p 214

282. ------- and SHAW M P - Mort and Pai (1976) p1.

283. ------ and COHEN L - Phys. Rev. B 15, 3276 (1977).

284. SIMMONS J G and TAYLOR G W - J. Non-Cryst. Solids 8-10, 947 (1972).

285. -------- and -------- - J. Phys. C 7, 3051 (1974).

286. SOGA, KUNUGI, OTA - J. Phys. Chem. Solids 34, 2143 (1973).

287. SPEAR W E - Proc. phys. Soc B 70, 669 (1957)

288. ----- - Proc. phys. Soc. 76, 826 (1960)

289. ----- - Adv. Phys. 23, 523 (1974)

290. ----- - Garmisch (1974) p 1

291. ----- -Adv. Phys. 26, 811 (1977)

292. ----- - J. Non-Cryst. Solids 1, 197 (1969)

293. ----- and LeCOMBER P G - Solid State Commun. 17, 1193 (1975).

294. SPICER W E - Garmisch (1974) p499.

295. SMITH, COWLAM, SHAMAH - Phil. Mag. B 39, 111 (1979).

296. STREET G B and GILL W D - J. Phys. Chem. Solids 28, 1517 (1967).

297. STREET R A - Adv. Phys. 25, 397 (1976).

298. STREET R A - Phil. Mag. 38, 191 (1978).

299. ------ - Phys. Rev. B 17, 3984 (1978)

300. ------ and YOFFE A D - Thin Solid Films 11, 161 (1972)

301. STROM U and TAYLOR P C - Garmisch (1974) p 375

302. STYS L E, FOIGEL M G - Sov. Phys. Semicond. 13, 1220 (1980).

303. SZEFTEL J - Phil. Mag. (B), 43, 549 (1981).

304. TANAKA K - J. Non-cryst. Solids 35-36, (1980) p 1023.

305. TAYLOR G W and SIMMONS J G - J. Phys. C 7, 3067 (1974).

306. TAYLOR P C, BISHOP S G, MITCHELL - Phys. Rev. Lett. 27, 414 (1971).

307. TEDJE T and ROSE A - Solid State Commun. 37, 49, (1981).

308. THOULESS D J - Phys. Rep. 13C, 93 (1974).

309. -------- - St. Andrews (1978) p 61.

310. TREACY D J, STROM U, KLEIN P B, TAYLOR P C, MARTIN T P - J. Non-cryst. Solids 35-36, (1980) p1035.

311. VAN DER PAUW - Phillips Res. Bull. 13, p1 (1958).

312. WALLACE A, OWEN A E, ROBERTSON J M - Phil. Mag. 38, 57 (1978).

313. ------, SEARLE T M, AUSTIN I G - J. Phys. C 6, 1830 (1973).

314. WEISER G - in 'The Physics of Selenium and Tellurium' eds. E. Gerlach and P. Grosse (Springer Series in Solid-State Sciences, vol.13 (1979)) p230.

315. WEISER K, FISHER R and BRODSKY M H - Proc. 10th Internat. Conf. Physics of Semiconductors (U.S. Atomic Energy Commission, Oak Ridge, 1970) p667.

316. WEHNER - Electronics and Electron Physics 7, 253 (1955).

317. WEINSTEIN B A - Phil. Mag. 41, 235 (1980).

318. --------, ZALLEN R and SLADE M L - J. Non-cryst. Solids 35-36, (1980) p 1255.

319. WEISZ, COBAS, TESTER and MANY - J. Appl. Phys. 39, 2296 (1968).

320. WRIGHT A C - Adv. Struct. Res. Meth. 5, p1 (1974).

321. WRIGHT A C and LEADBETTER A J - Phys. Chem. Glasses 17, 121 (1976).

322. ZACHARIASEN W H - J. Am. Chem. Soc. 54, 3841 (1932).

323. ZELLER R C and POHL R O - Phys. Rev. B 4, 2029 (1971).

324. ZIEGEL V V and ORLOVA G M - Zh Prikl Khim 46, 721 (1973).

325. ZHDAN A G, LUSHNIKOV N A - Sov. Phys. Semicond. 13, 585 (1979).

326. ZVYAGIN I P - Phys. Status Solidi B95, 227 (1979).

327. ---------- - Phys. Status Solidi B98, K159 (1980).

RECENT REFERENCES

These papers have been cited in the text, but were published too late to be included with the other references.

1 KASAKOVA L P, TOTH L and TAGUYRDZHANOV M A -
Phys. stat. sol. (a) 71, K 107 (1982).

2 MARSHALL J M, MICHIEL H and ADRIAENSSENS G J -
Phil. Mag. B 47, 211 (1983)

3 MICHIEL M, ADRIAENSSENS G J, and MARSHALL J M -
to be published (1983)

4 OKUSHI H, TAKAHAMA T, TOKUMARU Y, KYAMASAKI S, OHEDA H and TANAKA K -
Phys. Rev B27, 5184 (1983)

5 ORENSTEIN J, KASTNER M and VANINOV V -
Phil. Mag B46, 23 (1982)

6 SEREGIN P, REGEL A , ANDREEV A A and NASREDINOV F S -
Phys. stat. sol. (a) 74, 373 (1982)

7 VANINOV V, ORENSTEIN J and KASTNER M -
Phil. Mag B45, 399 (1982)

APPENDIX

Papers published on the work described in this thesis.

The published papers cited below have been removed from the e-thesis due to copyright restrictions:

Marshall, J.M. and Sharp, A.C. (1980) Carrier mobility and transit pulse dispersion for the mechanisms of activated and unactivated hopping in disordered semiconductors. In: *Journal of Non-Crystalline Solids,* 35-36(Part 1), pp.99-104

A. Sharp, J. Marshall, H. Fortuna. Transport properties of amorphous As2Se3. In: *Journal de Physique Colloques*, 1981, 42(C4), pp.C4-159-C4-162

Sharp, A.C. and Marshall, J.M. (1981) Temperature-dependent dispersive transport in a-As2Se3. In: *Journal of Physics C: Solid State Physics*, 14, pp.L761-L765